The Synthesis and Characterisation of Novel Low Molecular Weight Gelators and their Applications in Electrospinning to Develop Biocompatible Materials and Tissue Scaffolds

A thesis submitted to Maynooth University in fulfilment of the requirements for the degree of

Doctor of Philosophy

by

Jessica Ramos Ondono, B.Sc.

Chemistry Department,

Maynooth University,

Maynooth,

Co.Kildare,

Ireland.

March 2018

Research Supervisor: Dr Trinidad Velasco-Torrijos

Head of Department: Dr Jennifer McManus

Table of Contents

To my family, Gavin, Juan, Ana and Carlos.

Thanks for everything.

Gracias por todo.

Acknowledgements

I would like to thank my supervisor Dr. Trinidad Velasco Torrijos for her constant support, encouragement and enthusiasm. The amazing connection between us made this journey easier. As a mentor, friend and a supervisor I could not have had better.

I would also like to thank Maynooth University for awarding the John and Pat Hume scholarship to complete the PhD. Without this valuable contribution completing this journey would have been distinctly more difficult.

In no particular order I would like to thank the following people:

Thank you to the heads of the chemistry department past and present, Dr. John Stephens and Dr. Jennifer McManus for all their assistance. To all the academic staff who have helped me during the PhD, in particular Dr. Denise Rooney for her collaboration on our paper as well as her brilliant ideas and better interpretation of IR data. I would like to also sincerely thank Dr. Ramon Moreira Martinez and Dr. Santiago Arufe for teaching me the rheological techniques which allowed me accurately test my LMWGs in Santiago de Compostela University.

A special thanks to all the technical and administrative staff in the Chemistry department. To Ria, Barbara, Ollie, Ken, Anne, Orla, Walter, Donna and Carol, thank you for all your help and being so accommodating with all my requests. A special thank you to Noel, for fixing, helping and minding Ria (the cat). You helped make my ideas about electrospinning and DSC a reality!. I will miss working with you on a daily basis!

Outside of Maynooth, thanks to B. Twamley for the x-ray crystal structures; to W. Reddington and A. Erxleben for performing the XPD samples and the D. Kelly group for growing the hMSCs on my tissue scaffolds.

To all members of the TVT research group past and present, Roisin, Lorna, Gama, Andrew (you are my "UrbanDictionary"), Harlei (the best person to take over my bench and fumehood) and Matthew (Uuuuuhhhh…).

Special thanks to my "Pressexpress" girls, Karen, Michelle D and Caroline and to my Irish twin Justine. We have a lot of great memories together. You made my four years

Declaration

I hereby certify that this thesis has not been submitted before, in whole or in part, to this or any other university for any degree and is, except where otherwise stated, the original work of the author.

Signed: _____ Date: _____

Abstract

The work described in this thesis reports the design, synthesis and characterisation of novel compounds capable of acting as Low Molecular Weight Gelators (LMGWs). This class of compounds form self-assembled fibrous networks which entrap the solvent and form gels. These materials have received considerable attention in recent years due to a variety of applications that range from environmental to biomedical fields. Amphiphilic lipoamino acids, squaramides and carbohydrates are useful starting materials to synthesise LMWGs because they provide functional groups that can form the intermolecular interactions necessary for the formation of supramolecular self-assembled structures.

Chapter 2 describes the synthesis and characterisation of amphiphilic derivatives of L-serine and their evaluation as LMWGs. This study shows how structural features, such as the functional groups in the side chain, or the length of the hydrocarbon chains affect their ability to form gels. These compounds were found to effect selective gelation of aliphatic or aromatic solvents. The lipoamino acids were also tested as phase selective gelators of organic solvents in biphasic aqueous mixtures. In addition, these compounds were used for the removal of aromatic pollutants from water.

Chapter 3 describes the synthesis and characterisation of glycolipid derivatives of galactosyl, L and D/L (racemic) aspartic acid. Two families of glycolipids (*O*-linked and *N*-linked) were evaluated as LMWGs. It was found that structural features such as the chirality of the aspartic acid core or the nature of the glycosidic bond strongly affect the gelation ability and selectivity of these compounds.

Chapter 4 describes the synthesis and characterisation of LMWGs from galactosylated amphiphilic squaramides. These compounds were found to be excellent gelators of mixtures of EtOH:H_2O (1:1) and represent the first example of a glycosylated squaramide supramolecular gelator.

Finally, Chapter 5 describes the application of the LMWGs discussed in previous chapters for the formation of PCL blended electrospun materials. The conditions to form electrospun fibres were optimised and their morphology and hydrophilic / hydrophobic character evaluated. In addition, preliminary studies determining the suitability of these materials as drug delivery systems and tissue scaffolds were carried out by our collaborators.

Abbreviations

A

A = Aggregates

Ac = Acetyl

Aq = Aqueous

AS = Stearic acid

Asp. acid = Aspartic acid

Atm = Atmospheric pressure

ATR = Attenuated Total Reflection

ΔH = Enthalpy

B

B.V. = Betamethasone Valerate

Boc = *t*-butyloxycarbonyl

C

°C = Degrees Celsius

CA = Contact Angle

Cbz = Benzyloxycarbonyl

$CDCl_3$ = Deuterated chloroform

CDMT = 2-Chloro-4,6-dimethoxy-1,3,5-triazine

CGC = Critical Gelation Concentration

$CHCl_3$ = Chloroform

C_nAsp = *N*-acyl-L-aspartic acid

COSY = Correlation spectroscopy

D

D_2-DCM = Deuterated Dichloromethane

D_3-MeCN = Deuterated Acetonitrile

D_5-Pyr = Deuterated Pyridine

D_8-Toluene = Deuterated Toluene

Da = Dalton

DCC = Dicyclohexylcarbodiimide

DCM = Dichloromethane

DEPT = Distortionless enhancement by polarization transfer

DIC = *N,N'*-Diisopropylcarbodiimide

DMF = Dimethylformamide

DMSO = Dimethylsulfoxide

DMTMM = 4-(4,6-Dimethoxy-1,3,5-triazin-2-yl)-4-methylmorpholin-4-ium chloride

DSC = Differential Scanning Calorimetry

E

e.g. = Exempli gratia (Latin for "for example")

ECM= Extracellular matrix

Equiv = Equivalents

ESCA = Electron Spectroscopy for Chemical Analysis

Et_2O = Diethyl ether

EtOAc = Ethyl acetate

EtOH = Ethanol

F

F.A. = Fusidic Acid

FDA = Food and Drug Administration

Fmoc = 9-Fluorenylmethoxycarbonyl

FT-IR = Fourier Transform Infrared Spectroscopy

G

G' = Storage modulus

G'' = Loss modulus

Ga = Gauge

GalNAc-aa = *N*-acetyl-galactosamine-appended amino acid

H

h = Hours

HAS = 12-hydroxystearic acid

HFIP = 1,1,1,3,3,3-hexafluoro-2-propanol

HLB = Hydrophilic-Lipophilic Balance

HMBC = Heteronuclear Multiple Bond Correlation

hMSCs = Human bone-Marrow Stem Cells

HOBt = Hydroxybenzotriazole

HPLC = High Performance Liquid Chromatography

HR-MS = High Resolution Mass Spectroscopy

HSQC = Heteronuclear Single Quantum Coherence

I

I = Insoluble

i.e = Id est (Latin for "that is")

in = Inch

IR = Infrared spectroscopy

IVRT = In Vitro Release Testing

J

J/g = Joule per gram

K

K = Kelvin

keV = Kiloelectron volt

kV = kilovolt

L

LMWGs = Low Molecular Weight Gelators

LMWHs = Low Molecular-mass Weight Hydrogelators

LMWOGs = Low Molecular-mass Weight Organogelators

LVER = Linear Viscoelastic Regime

M

mbar = Millibar

MeCN = Acetronitile

MeOH = Methanol

MFs = Microfibres

mg = Milligram

Min = Minutes

mL = Millilitre

mm = Millimetres

MO = Methyl Orange

mp = Melting point

MS = Molecular sieves

MU = Maynooth University

µm = micrometer

N

NEt$_3$ = Triethylamine

nm = Nanometre

NMM = *N*-methylmorpholine

NMR = Nuclear Magnetic Resonance

O

OAc = Acetoxy group

OG = Opaque gel

OH = Hydroxy group

P

PCL = Polycaprolactone

Pd = Palladium

Pd/C = Palladium on activated charcoal

Pet. ether = Petroleum ether

PG = Partial gelation

PGA = Polyglicolide

PLA = Polylactic acid

PLGA = Poly(lactic-co-glycolic)acid

PS = Partial soluble

Pyr = Pyridine

R

RhB = Rhodamine B

rt = Room temperature

S

S = Soluble

SAFIN = Self-Assembled Fibrillary Network

SAOS = Small Amplitude Oscillatory Shear

SAXS = Small-Angle X-ray Scattering

sec = Seconds

SEM = Scanning Electron Microscope

soln. = Solution

T

Tanδ = Loss tangent

TBTU = *O*-(Benzotriazol-1-yl)-*N,N,N',N'*-tetramethyluronium tetrafluoroborate

TEM = Transmission Electron Microscope

TFA = Trifluoroacetic Acid

TFE = Trifluoroethanol

T_g = Glass Transition Temperature

TG = Transparent gel

T_{gs} = Gel-sol Transition Temperature

THF = Tetrahydrofuran

TLC = Thin Layer Chromatography

T_m = Transition Melting Temperature

TMS = Trimethylsilyl

TOF = Time Of Flight

Tol. = Toluene

U

UFs = Ultrafine Fibres

UHV = Ultra-High Vacuum

UV-Vis = Ultraviolet-Visible Spectroscopy

V

VOC = Volatile Organic Compounds

vs = Versus

W

w/v = Weight per Volume

WAXS = Wide-Angle X-ray Scattering

X

XPS = X-Ray Photoelectron Spectroscopy

Chapter 1

Introduction

1.1. Gels

As Jordan Lloyd said in 1926 "A gel is easier to recognise than to define". In recent years, there has been ample discussion concerning gels' definition, characterisation, properties, design, applications and classification. Generally, gels can be considered as a solid-like viscoelastic material, formed by a major component, the solvent (typically 99 % by weight of the gel), and a minor component, the gelator (remaining 1 %). The gelator forms a solid-like microfibrillar network that percolates the solvent and avoids its fluxion due to capillary forces.[1] Although more extensive classifications have been reported,[2] for the purposes of this thesis gels can be classified into two different groups: "Supramolecular gels" or "polymer gels". Traditionally, this classification depended on the nature of the interactions that lead to the formation of the fibrous matrix. However, in recent years, the classification has been extended to their constitution, origin, type of cross-linking, mechanical properties, nature of the solid component [colloidal, molecular (supramolecular), and polymer (macromolecular)] or the nature of the liquid component (organogel, alcogel, hydrogel, polymer liquid gel, oleogel, ionic liquid gel) and so forth.[3-5] The most relevant categorisation for the work presented in this thesis is shown in the following diagram which follows the traditional gel classification (Figure 1.1.).
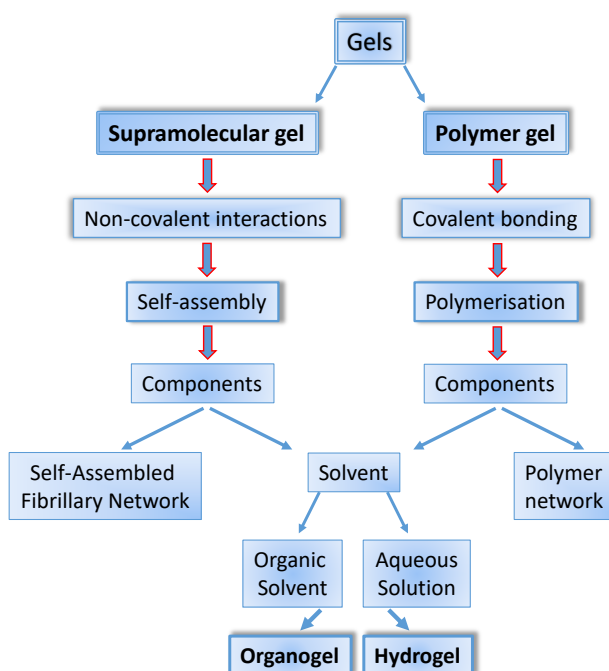
Figure 1.1. Classification of gels by nature of interactions.

1.2. Supramolecular Gelators

Supramolecular gelators, often called Low Molecular Weight Gelators (LMWGs), are small molecules (< 3000 Da, however, the borderline is indistinct) which can self-assemble through non-covalent interactions (H-bonding, π - π stacking, electrostatic interactions and van der Waals forces) into structured three-dimensional networks.[6,7] Those fibrous networks are capable of entrapping solvent molecules in a matrix, which prevents them from free-flow. This matrix is a consequence of self-aggregation of the small gelator molecules to form entangled Self-Assembled Fibrillary Networks, also known as SAFINs (Figure 1.2.). Since these networks concern weak interactions, they lead for the most part to the formation of thermally reversible gels. This means they can be transformed reversibly into 'liquid – solid' states by heating-cooling cycles without modification of the gel properties.

Dissolved gelator

1-D aggregation

Supramolecular gel

Self-Assembled
Fibrilar network
(SEM image of a xerogel)
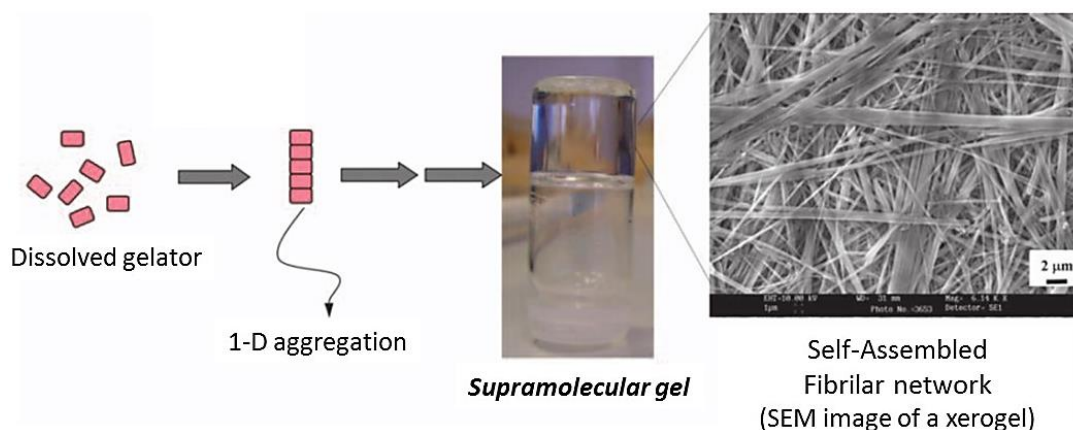
Figure 1.2. Schematic representation of the self-assembly process that produces supramolecular gels.[1]

LMWGs can be classified as LMWOGs (Low Molecular Weight Organogelators) when an organic solvent is the fluid component or LMWHGs (Low Molecular Weight Hydrogelators) when an aqueous solvent, usually water,[2] is the fluid component. Although LMWGs were reported in the early 19th century,[8] the supramolecular nature of these materials was poorly understood and they were largely neglected until the late 20th century. Currently, there is much interest in studying LMWGs not only to understand their fundamental supramolecular structures, but also to explore their potential technological applications as versatile "smart materials".[9,10] Numerous applications of gels in fields as diverse as sensor development,[11] optoelectronics,[12,13]

waste management,[14,15] drug delivery and tissue engineering[16] have been found. The properties of these systems and their ability to respond to external stimuli strongly depend on the structural features of the molecular species that will trigger the assembly process.[17-19] Supramolecular gels are usually prepared by increasing the solubility of the gelator in an appropriate solvent using heat and then cooling the resulting supersaturated solution to room temperature (rt). Upon cooling, the molecules start to condense and three situations are possible (Figure 1.3.): (1) a highly ordered aggregation which results in the formation of crystals; (2) a random aggregation which results in an amorphous precipitate or (3) an aggregation process intermediate between these two, which yields a gel. The process of gelation involves self-assembly of the gelator molecules to form long, polymer-like fibrous aggregates, which get entangled during the aggregation process forming a matrix that traps the solvent mainly due to surface tension. This process prevents the flow of solvent under gravity and the mass appears like a solid.[5]
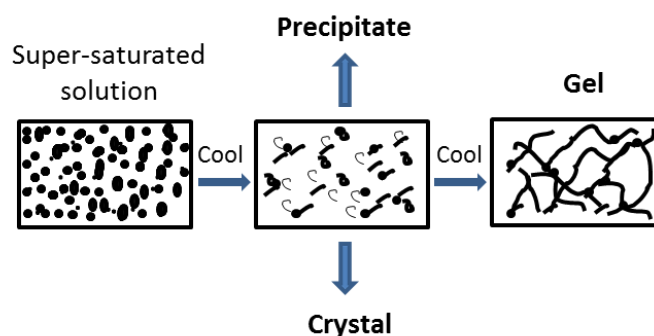
Figure 1.3. Schematic representation of the gelation process. Figure adapted from Neralagatta M. S. *et al.* [5]

The general requirements to form a supramolecular gel are:

a) The gelator molecule must be moderately soluble in the solvent.
b) The gelator molecule must have the potential to form intermolecular interactions, such as, H-bond, electrostatic interactions, π-π stacking interactions, and non-specific van der Waals forces.
c) The non-covalent interactions should be directional, leading to the assembly of one-dimensional anisotropic nanoscale fibres.[20]

1.3. Gel Characterisation

In order to fully investigate these soft materials, some characterisation studies which concern rheological and thermodynamic properties must be carried out. Some of the most important methods in terms of definition, understanding of the gelation process and structural arrangements for gel characterisation are described as follows.[21-26]

1.3.1. Rheology

Rheology or viscosimetry is used when quantitative values are searched for describing the resistance to flow (the viscosity) of solutions, melts or gels. Rheology studies can also yield useful information about the structures of the assemblies (their size or cross-linking density), about their dynamics, and even about their self-assembly mechanisms. For supramolecular gels, rheology is perhaps the most important defining feature.[27-30] Steed *et al.* have detailed the application of rheology in supramolecular gels.[23] In short, rheology is the study of the deformation and flow of matter under the influence of an applied stress. When the sample is placed between two plates (or two concentric cylinders), upon applying a given oscillatory strain to one of the plates, the induced movement of the other plate is decomposed into an in- and out-of-phase component. A rheometric measurement normally consists of a strain (deformation) or a stress analysis at a constant frequency (normally 1 Hz). From the rheological point of view, a gel is an elastic solid which can fully recover the deformation when the external stresses applied on it stops. The parameters defining the rheological nature of a gel include:[31,32]

- **G'** or storage modulus, which is related to the elastic properties and the solid nature of the gel.
- **G''** or loss modulus, which is related to the viscous properties and the liquid nature of the gel.
- **Tan δ** or loss tangent which measures the viscous / elastic ratio for the material at frequency ω. Also, this parameter relates both modulus (Tan δ = G''/G'). Depending on its value, 3 different outcomes are possible:

    I.) Tan δ >1 (G'' > G'): Liquid state.

II.) Tan δ = 1 (G'' = G'): Viscoelastic or gel point.

III.) Tan δ < 1 (G'' < G'): Gel state. As a rule of thump, "the smaller the value, the stronger the gel". Both modulus should have parallel slopes in the mechanical spectra of a gel (Figure 1.4.).
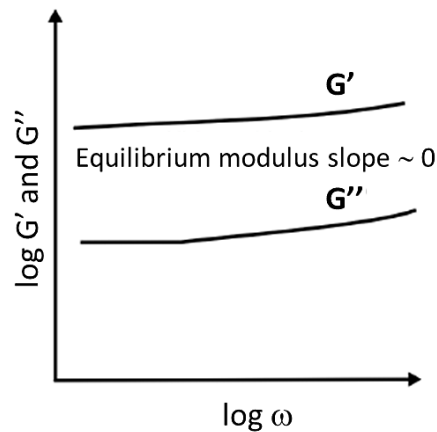
Figure 1.4. Mechanical spectra for a supramolecular gel system.[31]

1.3.2. Differential Scanning Calorimetry

Differential scanning calorimetry (DSC) is a thermoanalytic technique in which the difference in the amount of heat required to increase the temperature of a sample compared to the reference is measured as a function of temperature.[33] Supramolecular gelation is an event driven by non-covalent interactions, with initial self-assembly of the gelator molecules only occurring in one dimension. An endothermic peak can be monitored when the gel undergoes a transition from gel to solution state. Heat flowing causes the temperature of both, the reference and the sample, to increase at the same rate. On the other hand, less heat is required to raise the sample temperature as the sample undergoes exothermic processes as sol-gel transition occurred. [34] Often, the transition peaks are better defined in the cooling curves (sol-to-gel) rather than in the heating curves (gel-to-sol). This is consistent with the simultaneous occurrence of different self-assembly processes, which are characteristic of the gelation process.[35] By observing the difference in heat flow between the sample and the reference, DSCs are able to measure the amount of heat absorbed or released during such transitions. Partha Bairi *et al.* reported the DSC study of the RPAD hydrogel sample. During the heating cycle, it exhibits an

endothermic peak at 48 °C and during the cooling cycle, it exhibits an exothermic peak at 34 °C. This indicates the presence of the first order phase transition, an important criterion of thermoreversible gel formation (Figure 1.5.).[36]
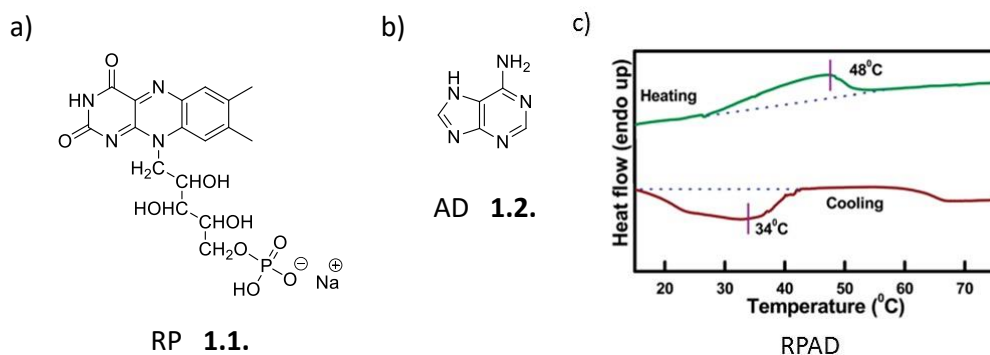
Figure 1.5. a) Riboflavin-5'-phosphate sodium salt (RP) **1.1.**; b) Adenine (AD) **1.2.**; c) DSC thermograms of the RPAD hydrogel at 3 w/v %. Heating and cooling cycles.[36]

1.3.3. X-Ray Techniques

1.3.3.1. Single-Crystal Diffraction

X-ray crystallography has provided us with a better understanding of chemical bonds and non-covalent interactions. X-ray crystallography is a method of determining the arrangement of atoms within a crystal, in which a beam of X-rays strikes a crystal and causes it to spread into many specific directions. From the angles and intensities of these diffracted beams, a crystallographer can produce a three-dimensional picture of the electron density. Therefore, the position of the atoms in the crystal can be determined, as well as their chemical bonds, their disorder and other structural information.[22]

1.3.3.2. Small-Angle X-Ray Scattering

X-ray scattering techniques are non-destructive and can reveal information about the crystalline structure, chemical composition, and physical properties of materials such as powders, xerogels, and thin films. These techniques are based on observing the scattered intensity of an X-ray beam hitting a sample as a function of incident and scattered angle, polarisation, and wavelength or energy. Small-angle X-ray scattering (SAXS), one of these techniques, probes structures in the nanometer to micrometer

range of supramolecular assemblies by measuring scattering intensity at scattering angles (2θ) close to 0°.

1.3.3.3. Wide-Angle X-Ray Scattering

Wide-angle X-ray scattering (WAXS) powder diffraction is a very similar technique to SAXS. The only difference is that the distance from the sample to the detector for WAXS is shorter than that of SAXS and thus diffraction maxima at larger angles are observed. This technique specifically refers to the analysis of Bragg peaks scattered to wide angles (2θ larger than 5°), which implies that they are caused by sub-nanometer-sized structures (by Bragg's law).[37] The diffraction pattern generated allows the determination of chemical composition, texture or phase composition of the film, crystallite size, and presence of film stress. A crystalline solid consists of regularly spaced atoms (electrons) that can be described by imaginary planes. The distance between these planes is defined as the *d*-spacing. The intensity of the *d*-spacing pattern is directly proportional to the number of electrons (atoms) that are found in the imaginary planes. Every crystalline solid will have a unique pattern of *d*-spacings (the powder pattern), which is a "finger print" for that solid. In fact, solids with the same chemical composition but different phases can be identified by their pattern of *d*-spacings. Therefore, WAXS is an effective method to confirm the packing modes of the gelators in the solid state.[38,39] It should be noted that there can be many differences between the data extracted from the xerogel samples (sometimes broad X-ray scattering features) and those obtained from the solid state (often sharper crystalline-like features). The reason is that gels have solid-like rheology and do not flow, but the solvent is still the major component.

The urea functionality has been widely incorporated into LMWOGs because it provides a convenient 1-D directionality and strong intermolecular H-bonding interactions.[40-44] Miravet and co-workers designed a super-gelator containing chiral bisurea units which can form hydrogels at very low concentrations (Figure 1.6.).[45] WAXS powder diffraction was used to investigate the structure of the dried hydrogels (xerogels) of bisurea **1.3.** (R and S). Information about the molecular packing mode of gelator molecules in neat gels can be obtained from an X-ray diffraction pattern of the xerogel. For R-bisurea **1.3.**, the xerogel showed a high degree of crystallinity. The

diffraction pattern is characterised by four sharp reflection peaks of 21.01, 10.64, 7.13, and 5.37 Å (Figure 1.6.), the relative ratios of which is almost exactly in the ratio of 1 : 1 / 2 : 1 / 3 : 1 / 4 : 1, suggesting a lamellar organisation. The low-angle peak corresponds to the extended molecular dimension and a model with the packing shown in Figure 1.6. can be proposed in which chiral columnar stacks are packed into a layered structure.
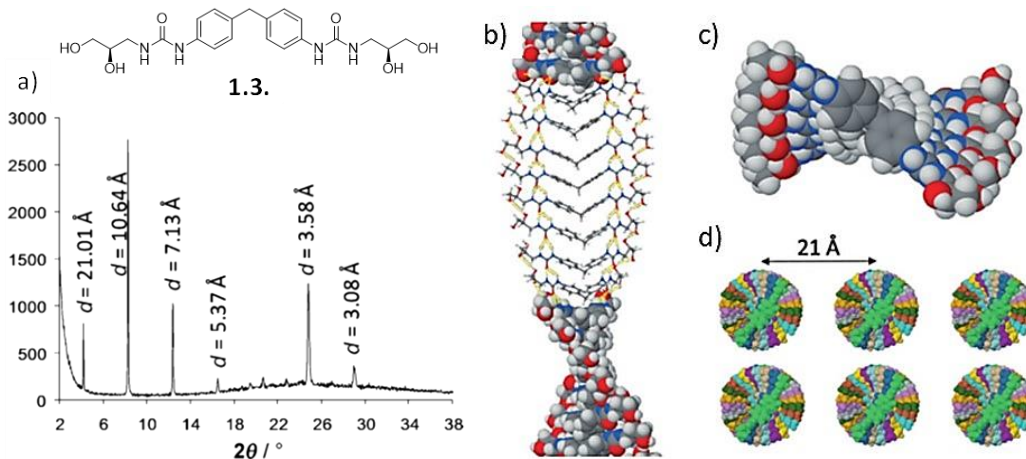
Figure 1.6. a) WAXD of the xerogel R-bisurea **1.3.**; b), c) Model of the proposed self-assembly process for hydrogelator; d) inter-columnar packing.[45]

1.3.4. Scanning Electron Microscopy

Scanning electron microscopy (SEM) is a type of electron microscopy that produces images of a sample by scanning it with a focused beam of electrons. These electrons interact with the electrons in the sample, producing various signals that can be detected, providing information about the sample's surface topography or morphology.[46] The electron beam is generally scanned in a raster scan pattern, and the beam's position is combined with the detected signal to produce an image. There are many advantages of using SEM in the imaging of supramolecular xerogels: 1) It is cheap and widely available; 2) owing to the very narrow electron beam, it has a large depth of field, which allows a large area to be in focus at one time and yields a characteristic three-dimensional appearance; 3) SEM can produce images of very high resolution (nanometer to micrometer in size). Therefore, SEM is a versatile technique for supramolecular material science to elucidate the microscopic structures of self-assembled systems (Figure 1.7.).
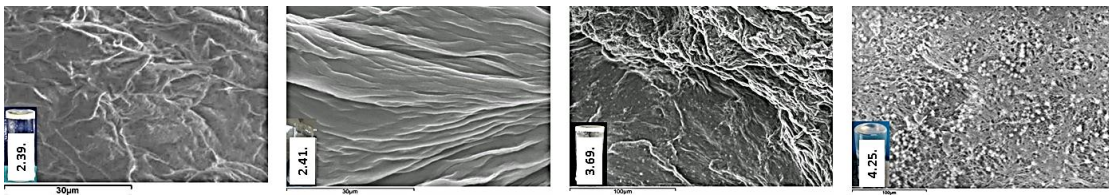
Figure 1.7. SEM images of representative xerogels. Different structures of the 3-D networks, such as, lamellar, microfibres, microbelts and porous structures can be appreciated. (Scale bar: 30, 30, 100 and 100 μm).

1.3.5. Nuclear Magnetic Resonance (NMR)

NMR spectra can provide information about the structural properties of the gelators, the resulting self-assembled structures and the functional groups participating in the interactions which play crucial roles in the stability of the dynamic networks. ^{1}H NMR probes hydrogen nuclei within the molecules of a substance in order to determine the structure and the interactions they partake in.[47,48] Chemical shift changes can be monitored when supramolecular gels form by non-covalent interactions. Concentration and temperature dependent ^{1}H NMR studies are carried out to investigate the interactions between the gelator molecules or gelator and solvent. ^{1}H NMR was used to study the gelation process of cholesterol appended ferrocene **1.4.** [Figure 1.8. a)]. It is known that the chemical shift of NH protons gradually shift downfield with increasing concentration, indicating the formation of intermolecular H-bonds [Figure 1.8. b)]. An increase in solution temperature, shift the NH protons upfield, suggesting breakage of the H-bonds [Figure 1.8. c)]. If the gel is sensitive to temperature, the reversible gel – sol transition can be achieved by heating and cooling. This reversible process can be monitored by ^{1}H NMR spectroscopy. However, this technique presents serious limitations in studying the interactions between the gelator molecules in the gel state due to the reduction of the mobility and subsequent loss of spectral resolution, while the gelator molecules within "liquid-gel" solution state have sharp NMR signals as a consequence of its molecular scale mobility.[49,50]
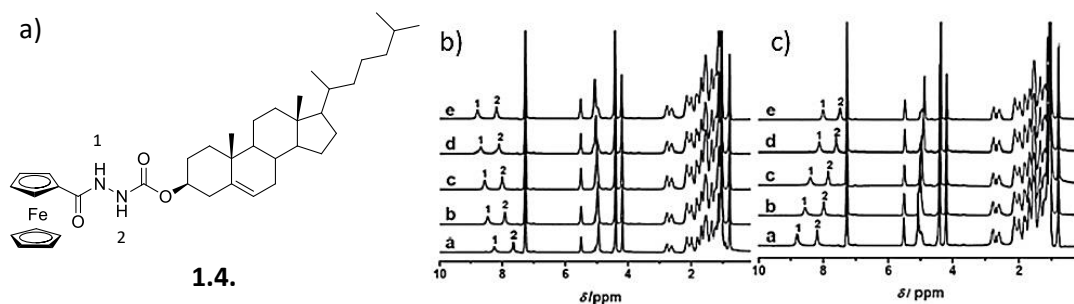
Figure 1.8. a) Chemical structure of cholesterol-appended ferrocene supramolecular gelator **1.4.**; b) ^{1}H NMR spectra of **1.4.** in C_6D_6 at different concentrations (a, 30 mg/mL; b, 35 mg/mL; c, 40 mg/mL; d, 45 mg/mL; e, 50 mg/mL); c) ^{1}HNMR spectra of **1.4.** (50 mg/mL) in C_6D_6 at different temperatures (a, 298 K; b, 303 K; c, 308 K; d, 318 K; e, 323 K).[22]

1.3.6. Infrared Spectroscopy

Infrared spectroscopy (IR) measures absorptions in the infrared region of the electromagnetic spectrum (2.5 μm to 25 μm). IR absorption occurs from the stretching and bending of the covalent bonds in molecules. Molecules absorb energy corresponding to vibration frequencies which are characteristic of their structure. The typical units in IR are wavenumbers (ν).Thus the IR spectrum runs from 4000 to 400 cm^{-1}. This technique can be used to characterise the formation process of supramolecular gels because it can provide an insight into the assembly of molecular scale building blocks and allow the determination of the non-covalent interactions responsible for gelation.[51-53] IR studies by temperature or time dependency can reveal if intermolecular H-bonding plays important roles in the aggregation process. It is known that the wavenumbers for IR bands associated with relevant functional groups in the molecule (NH and CO) shift from those recorded in solution as the gelation process takes place.

Escuder, Miravet *et al.* reported a hydrogel on the basis of a bolaform amino acid derived from L-valine.[54] Studies by temperature dependent IR spectroscopy revealed that intermolecular H-bonding played important roles in the aggregation process of the gelator in water. As shown in Figure 1.9., it was observed that the bands at 1640 cm^{-1}, corresponding to the CO stretch of the gelator in solution decreased in intensity, while new bands at 1625 cm^{-1} appeared upon cooling a solution of the gelator, indicating the formation of intermolecular H-bonds as the assembly took place.

Furthermore, the bands related to the CH stretching region shifted to lower wavenumbers as the concentration increased due to the packing of aliphatic chains.

a)
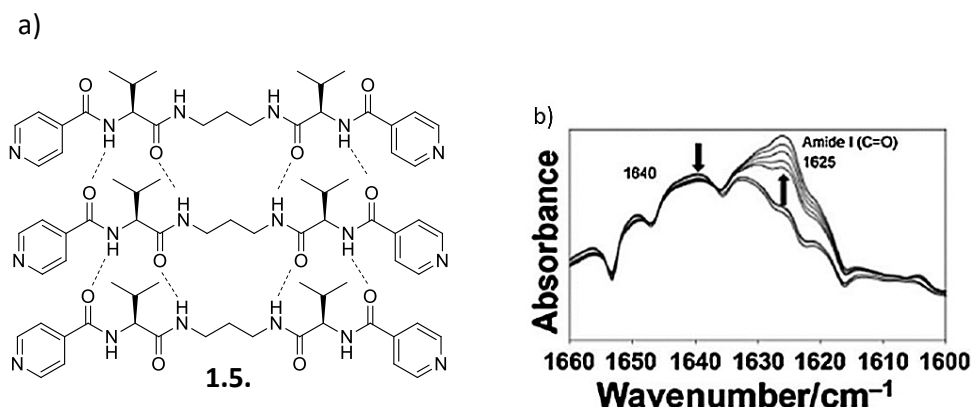
Figure 1.9. a) Schematic aggregation model of bolaform amino acid derived from L-valine **1.5.**; b) Variation of the FTIR spectrum of a hot solution (14.5 mM) in water upon cooling to rt. Arrows indicate how the signals change with time.[54]

1.3.7. Other Techniques to Study Gel Formation and Characterisation

The macroscopic properties of the supramolecular gels can be elucidated in a visual way using relatively simple methods, such as "inverted test tube method"[55] which is a visual inspection to assess gel formation by inversion of the vial containing it. Gel formation is considered to have occurred if no flow was observed upon vial inversion. "Critical Gel Concentration" (CGC), which is the minimal gelator concentration required for it to entrap the required solvent and "Transition temperature from gel to solution" (T_{gs}), which is determined by heating the gel sample and monitoring the temperature of the melting process, can also be determined by visual inspection. These methods are fully explained in Chapter 7 (Experimental Procedures). The qualitative data obtained from these methods can vary or have certain error of measurement. However, quantitative measurements can be obtained with the techniques described in previous sections.

1.4. Aims of the Thesis

Supramolecular gels based on LMWGs have attracted much attention in recent years due to the range of potential applications, aforementioned in Section 1.2. of this chapter. Even with the plethora of substances reported to date, capable of inducing the formation of supramolecular gels, it still remains a challenge to accurately anticipate the gelation ability of a given compound in specific solvents.[56] This thesis describes the synthesis of different types of gelators, focusing on lipid derivatives which are ideal candidates to form supramolecular self-assembled gels. The main aims were: I.) Characterising LMWGs using rheological properties and spectroscopic techniques and II.) Making different structural changes to understand better the requirements for the gelation process. Different types of gelators were studied: amino acid derivatives [e.g. serine (Chapter 2) and aspartic acid (Chapter 3)] and squaramide derivatives (Chapter 4). In particular, we were interested in the various applications of LMWGs such as: I.) Removal of aromatic pollutants, organic solvents or toxic dyes, from water (discussed in Chapter 2) and II.) Modification of electrospinning fibres using LMWGs for biomedical applications as tissue scaffolds and drug delivery systems (discussed in Chapter 5).

Chapter 2

Lipoamino Acid Derivatives of L-Serine as LMWGs

2.1. Introduction to Lipoamino Acids Based Gelators

Peptides and amides are considered privileged scaffolds for the design of LMWGs because they can self-assemble using various non-covalent interactions. They are easy to manufacture in large quantities, and they can also be easily modified chemically and biologically. In addition, they are among the most commonly used H-bond donors and acceptors in LMWG systems. These H-bonding units cooperate with other groups to promote gelation. In this context, LMWGs containing amino acid and amide groups as the key structural components will be discussed to demonstrate the importance of complementary H-bonding for the formation of stimuli responsive self-assembled networks.[57]

2.1.1. Structural Requirements of a LMGW

Several broad statements can be made about a typical gelator molecule: I.) the molecule must have partial solubility in the gelation solvent; II.) the molecule must have the potential to form weak non-covalent intermolecular interactions, such as H-bonds, electrostatic interactions, π-π stacking interactions, van der Waals forces, and dipole–dipole interactions; III.) the non-covalent interactions should be directional, leading to the assembly of anisotropic nanoscale fibres[20]; for this reason, often LMWGs are chiral molecules.[43,58]

2.1.2. Amphiphilic Gelators

Amphiphilic LMWGs are efficient structures capable of self-assembly owing to the appropriate hydrophobic-lipophilic balance (HLB). This leads to enough solubility of the molecule to get dissolved in the solvent of choice and allow for the non-covalent interactions to occur.

The efficiency of peptidic-amphiphiles as hydrogelators has been reported in the literature, however, fewer lipidated amphiphiles are found to form supramolecular gels only in the presence of some organic solvents or at a particular pH.[59-61]

Das and co-workers designed a library of lysine hydrogels **2.1.** – **2.5.** (Figure 2.1.). The chemical structures had features necessary for gel formation, such as, π-stacking region (aromatic groups), H-bonding sites (CO, NH), protonation site (NH_2) and hydrophobic region (van der Waals interactions). Compound **2.1.**, with a C_{16}

hydrophobic tail, was capable of forming van der Waals. It also has an aromatic π-electron system, the fluorenyl group (Fmoc). Appropriate solubility of the molecule was an essential criteria in order to self-organise. For that reason, they maintained a hydrophilic group in the form of a free amine of the lysine side chain, which allowed the solubilisation of the molecule in water and also maintained the proper HLB to self-assemble. Four structurally similar compounds (**2.2.** - **2.5.**) were also synthesised. In compounds **2.2.** and **2.3.**, the chain lengths were varied (C_{14} and C_{12} respectively). Compound **2.4.** was the ester analogue of compound **2.1.** while compound **2.5.** was synthesised using the D-lysine isomer to get the D-analogue of compound **2.1.,** which influenced the formation of helical nanofibres network.[59]
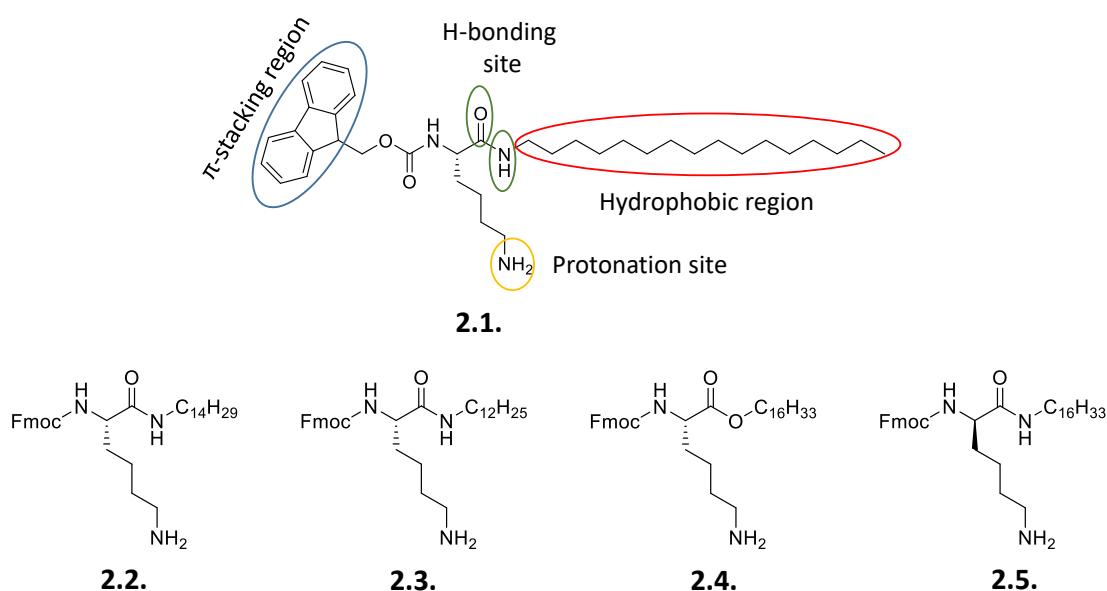
Figure 2.1. Chemical structures of **2.1.** – **2.5.**[59]

Other important studies related to the relationship between molecular structure and gelation properties have been carried out by Weiss and co-workers. They have worked with long-chain fatty acids with small structural differences to each other. They have formed LMWOGs making three structural changes: I.) Stereochemistry; II.) Presence of hydroxyl groups and III.) The length of the alkyl chains. They used 12-hydroxystearic acid (HAS) **2.6.** and stearic acid (AS) **2.7.** as the starting point of this "structure-gelation activity" study (Figure 2.2.).[62,63]
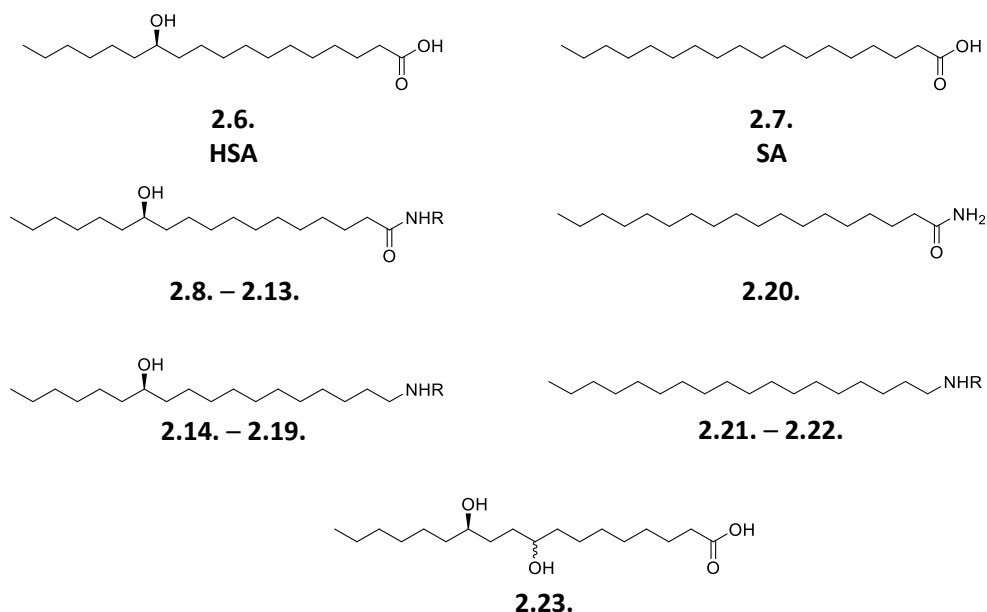
Figure 2.2. Chemical structures of LMWOGs **2.6.** – **2.23.** derived from HSA (**2.6.**) and SA (**2.7.**) upon which comparisons are made for **2.8.**, **2.14.**, and **2.21.** (R = H); for **2.9.** and **2.15.** (R = CH₃); for **2.10.** and **2.16.** (R = C₂H₅); for **2.11.** and **2.17.** (R = C₃H₇); for **2.12.** and **2.18.** (R = C₄H₉); for **2.13.**, **2.19.**, and **2.22.** (R = C₁₈H₃₇). **2.23.** diastereomeric (9,12*R*-diol).[62,63]

Compounds **2.6.** – **2.23.** (Figure 2.2.) were insoluble in water. The introduction of a hydroxyl group along the alkyl chain of SA, as in HSA (**2.6.**, **2.8.** - **2.19.**), changes the gelation ability of the LMWOGs. The efficiencies were improved when the carboxylic acid functionality was transformed into a primary amide (**2.8.**), but decreased when a primary amine was used instead (**2.14.**). Further changes of **2.8.** to a secondary amide (**2.9.** or **2.10.**) lead to decreased overall efficiencies. Increasing the alkyl chain length of the *N*-alkyl group of the secondary amide (e.g., from methyl in **2.9.** to *N*-octadecyl in **2.13.**) decreased the range of solvents used to form a gel. Removal of the hydroxyl group in **2.8.** yields stearamide (**2.20.**), a very good LMWOG capable of gelling higher-polarity solvents and precipitates from *n*-alkanes in comparison to **2.8.** or HAS (**2.6.**). The primary differences in the gelated solvents can be understood on the basis of solubility considerations. The importance of the ability of the head groups to act as both H-bonding donors and acceptors was demonstrated by the higher efficiency of the amides (**2.8.** – **2.13.**) than that of their corresponding amines (**2.14.** - **2.19.**).[62] **2.23.** was able to gelate both high- and low-polarity aprotic aromatic solvents, as well as chloroalkanes, such as CHCl₃, DCM or CCl₄. As indicated by the CGC values, **2.23.** was a more efficient gelator than HSA (**2.6.**) in the same solvents,

but it was unable to gelate alkanes (although **2.6.** could). It appeared that the increased polarity from the two hydroxyl groups of **2.23.** decreased its ability to be solvated efficiently by low polarity solvents such as alkanes and the tendency to form precipitates was enhanced.[63]

2.1.3. Fmoc-Based LMWG

Most lipoamino acid based gelators are composed of π systems such as 9-fluorenylmethoxycarbonyl (Fmoc),[64,65] benzyloxycarbonyl (Cbz)[66], phenyl, naphthyl[67] and pyrenyl[68] groups. Many authors have reported dipeptides and amino acids that are good gelators when they contain an aromatic protecting group, such as Fmoc.[1,69-72] Indeed the self-assembly of Fmoc–based LMWG is driven by H-bonding and π-π interactions between π electrons in the aromatic fluorenyl rings.

Fmoc-Phe-Phe, **2.24.** (Figure 2.3.), is an important LMWHG.[69,73] Gazit and co-workers discovered that dissolving **2.24.** at a high concentration in an aqueous solution resulted in the formation of a rigid material with macroscopic characteristics of a gel.[74] Although the hydrogel contained less than 1% peptide material, it retained its 3-D spacious volume exceptionally well. This self-assembled gel was stable across a broad range of temperatures and a wide pH range. Gelation can be induced by either lowering the pH of an aqueous solution of **2.24.** or by the addition of water to a solution of **2.24.** in a solvent such as DMSO. Despite the volume of literature on Fmoc-Phe-Phe, the mechanical properties reported for these gels vary significantly over four orders of magnitude and the origins of this variability are unclear.[71]
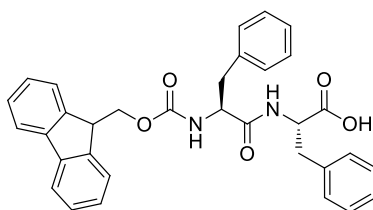
2.24.

Figure 2.3. Chemical structures of Fmoc amino acids LMWGs **2.24.**

Adams and co-workers investigated a family of commercially available Fmoc-amino acids hydrogelators. **2.25.** – **2.30.** (Figure 2.4.).[72]

2.25.   **2.26.**   **2.27.**

2.28.   **2.29.**   **2.30.**
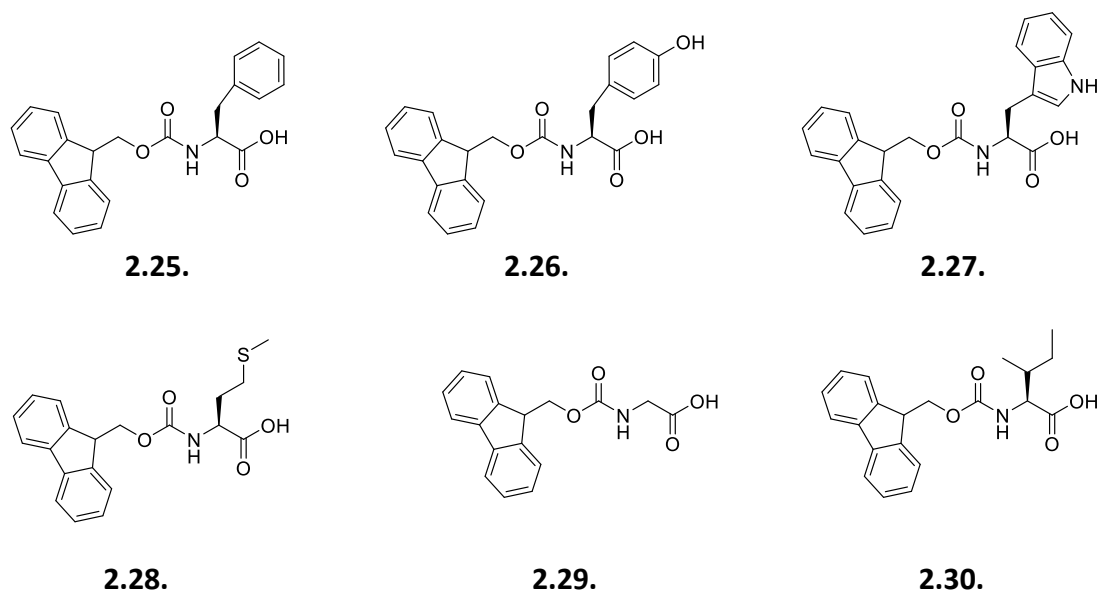
Figure 2.4. Chemical structures of Fmoc amino acids LMWGs **2.25.** – **2.30.**[72]

Compound **2.25.** formed a transparent hydrogel, **2.26.** – **2.28.** formed translucent hydrogels while **2.29.** and **2.30.** formed turbid hydrogels (Figure 2.5.).
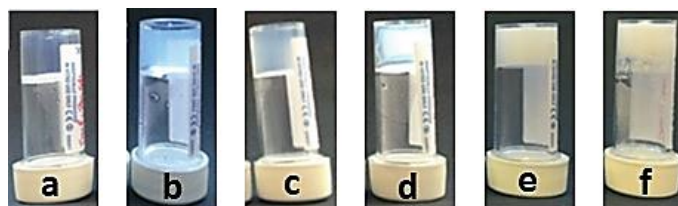
Figure 2.5. Physical appearance of the gels: a) Transparent gel **2.25.**; b) – d) Translucent gels **2.26. - 2.28.**; e) and f) Turbid gels **2.29.** and **2.30.** respectively.[72]

The different gels formed by these compounds have different rheological properties: The gels formed from **2.26.** – **2.28.**, had typical low CGC (< 1 w/v %), breaking at relatively low strain. For **2.25.**, the gel breaks at higher strain and was consistent with a better entangled network. The data for the other white turbid gels formed from **2.29.** and **2.30.**, was similar to that of the **2.25.** gel. Although all samples were self-assembled gels, there was a clear difference in the rheological behaviour for the transparent, translucent and the turbid gels. To understand these results, this group of researchers grew crystals of **2.25.** and **2.26.** X-ray diffraction data showed that for **2.25.** the fibre phase and crystal phase presented relatively similar H-bonding interaction. On the other hand, the molecules of **2.26.** were organised very differently in the hydrogel and in the crystals. The data implied that the packing of **2.26.** in the

crystal structure (Figure 2.6.) was created by interactions between the planar Fmoc groups, whereas it was clear that H-bonding drove the self-assembly into fibrillar structures in the gels.[72]
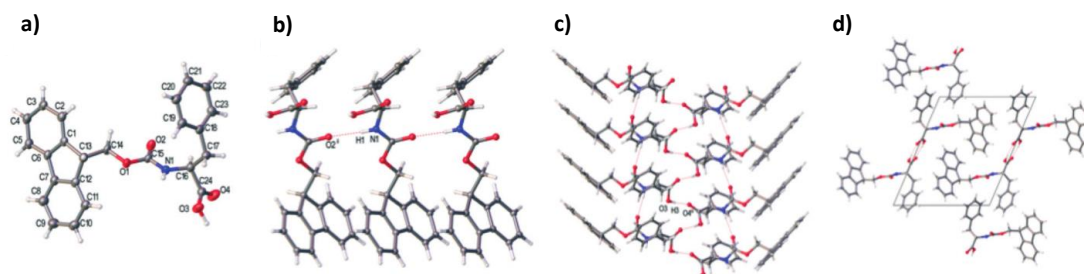
Figure 2.6. a) Labelled displacement ellipsoid plot of the asymmetric unit from the single crystal structure of **2.25.**; b) Intermolecular H-bonding of **2.25.** molecules via N1–H1···O2; c) Intermolecular H-bonding of **2.25.** molecules via carboxylic acid groups; d) Extended crystal packing of **2.25.** molecules, unit cell shown.[72]

Shanmugam and co-workers reported lysine based gelators containing Fmoc-moiety, **2.31.** – **2.34.** (Figure 2.7.).[70]

2.31.

2.32.

2.33.

2.34.
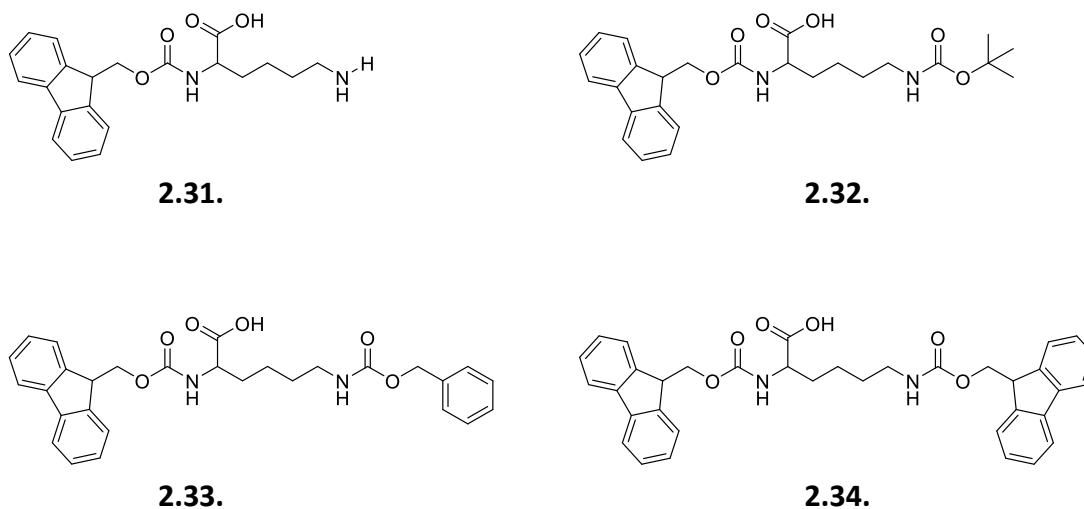
Figure 2.7. Chemical structures of Fmoc amino acids LMWGs **2.31.** – **2.34.**[70]

Lysine acts as a linker to connect both water-soluble amides and lipophilic moieties (alkyl chain). The Fmoc moiety can provide additional aromatic π–π stacking interactions during the self-assembly process. Although **2.31.** – **2.34.** are excellent hydrogels, only the double Fmoc functionalised L-lysine amino acid **2.34.**, formed organogels. Single Fmoc-functionalised L-lysine, **2.31.** – **2.33.** did not form gels in

CHCl$_3$, DCM or MeOH. The authors demonstrated the advantage of a second Fmoc-moiety in a molecule towards self-assembly and gelation.[70]

2.1.4. LMWGs as Functional Materials for Spills and Toxic Dyes Remediation

Water is an abundant natural resource. However, it is limited in some areas and it is highly contaminated in others. This is a concern to the majority of the population in the 21st century.[75] Life without industrialisation is unthinkable, but its rapid development has seriously affected global water quality. This has occurred through the release of hazardous waste such as heavy metals, dyes, pharmaceuticals, petroleum products, pesticides and fertiliser into the environment.[76] When these pollutants are released as untreated effluent into rivers, lakes, and oceans, they can affect aquatic life and the food chain. This can also predispose people to health-related problems including cancer, neurological damage, liver failure and cognitive dysfunction. As such, both biological and physicochemical methods have been devised to combat water pollution, with adsorption of dissolved organic/inorganic pollutants onto solid materials being a key current methodology. This has advantages such as simplicity, ease of operation, near-complete removal of pollutants and economic feasibility.[77,78] The use of commercial activated carbon and other non-conventional adsorbents such as chitosans, mineral clays, sawdust and waste biomatter to remove dyes and heavy metals from water is common practice. However, there are limitations such as lack of selectivity, generation of large amounts of toxic sludge, low pollutant uptake and costly regeneration processes. This means there is still significant interest in the development of innovative materials with applications in environmental remediation. As part of global efforts toward combating the increase of environmental damage, supramolecular gels based on LMWGs have begun to attract attention as emerging materials for water purification.[79-81]

2.1.4.1. LMWGs for Spill Remediation

Marine pollution predominantly through accidental or intentional discharge of crude oil and petrochemicals is a serious environmental problem. For example, the oil spill in Galicia caused by the sinking of the oil tanker "Prestige" in 2002 polluted thousands of kilometers of the coastline and more than one thousand beaches on the Spanish,

Irish, French and Portuguese coast. It also caused great harm to the local fishing industry. This is problematic from both an economic perspective through wastage of valuable non-renewable oil, as well as the potential impacts on human health through the consumption of sea foods obtained from oil-polluted oceans, impacts on climate as a result of the accumulation of volatile hydrocarbons in the stratosphere, and devastating effects on the delicate balance of the marine ecosystem.[82]

Conventional methods for remediating oil spills include absorption, dispersion, bioremediation and solidification.[83,84] However, these approaches are often either inefficient, not economically viable for large scale application, or can themselves leave behind toxic residues which bio-accumulate through food networks. LMWOGs have potential application for solidifying oil spills,[85] in particular in cases where the gelator has the following key properties: I.) Simple, cheap, scalable synthesis; II.) Rapid gelation; III.) Recyclability; IV.) Environmentally-friendly bioderived gelators; V.) Stable gels down to low temperatures; VI.) Stable gels even in the presence of shear forces.[86] Interestingly, the use of LMWGs with oil spills has actually been known since the 1970s, however, these early industrial examples are rarely cited in the more recent, academically driven literature. For example, *in situ* formation of colloidal gel forming ureas by reaction of amines and isocyanates was explored as a technology for oil-spill immobilisation in 1971, although a practical solution to the problem was not found at that point using this approach.[87] Another early example of gelling oils with small organic molecules was demonstrated in the patent of Saito *et al.* from 1976.[88] In the original patent, derivatives of *N*-acetyl amino acids were ad-mixed with non-polar organic solvents. In more recent studies, Bhattacharya and Krishnan Ghosh used a simple amino acid amphiphile, *N*-lauroyl-L- alanine **2.35.** (Figure 2.8.) to selectively gel aromatic and aliphatic hydrocarbons as well as commercial oils such as kerosene, petrol and paraffin in biphasic oil–water mixtures.[89] An amount, typically < 1 w/v %, of the gelator was added to the biphasic oil–water mixture either by dissolving the gelator in the solvent mixture by heating, or by adding it as a solution in EtOH. The oil-phase was selectively gelled leaving the aqueous phase unaffected, with the gels remaining stable for one week.
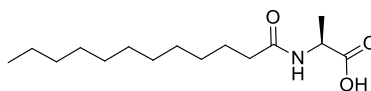
2.35.

Figure 2.8. Chemical structure of *N*-lauroyl-L- alanine **2.35.** used by Bhattacharya and Krishnan-Ghosh for the gelation of commercial oils in biphasic mixtures.[89]

2.1.4.2. Dye Adsorption into Self-Assembled LMWGs

Dyes are useful in textile, plastics, rubbers, printing, drugs, food, paper and cosmetics industries. Most dyes are non-biodegradable and sadly there are significant discharges into the aquatic environment.[90] Even at low concentrations, dyes have destructive effects on environmental quality and potential toxic effects. Eliminating dyes from the biosphere is therefore an important goal. Unlike remediation of oil spills, where the pollutant itself becomes the solvent phase of an organogel, the pollutant dyes will be typically dissolved in water, from which they need to be removed. Gels based on LMWGs can be easy to synthesise and modify, their high surface areas give potential for direct interaction with solvated dyes, while their reversibility and responsiveness gives potential for recycling and reuse. Gels are also often amphiphilic in nature which can also assist in forming interactions with dye molecules.[91]

The hydrophilic cationic dye rhodamine B (RhB), a good organic-soluble toxic dye, is often used as an example to prove the removal of toxic dyes from contaminated water. Amino acid based LMWOGs **2.36.**[92] and **2.37.**[47,93] (Figure 2.9.) have been effectively used as phase-selective gelators to entrap and immobilise into the 3-D network of the gel the toxic dye. The dye absorption was quantified using an UV-Vis spectra measurement of the water contaminated by the RhB dye. The compounds, **2.36.** and **2.37.**, were able to achieve up to 97 % removal of the dye after treatment.
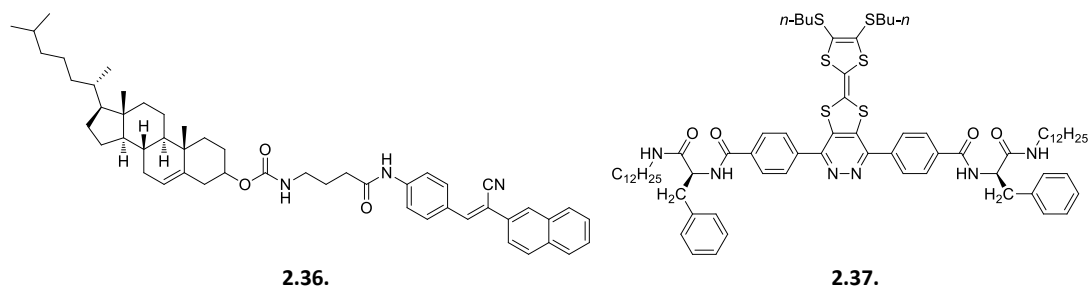
Figure 2.9. Chemical structures of amino acid LMWOGs **2.36.** and **2.37.** reported by S. Jiang, *et. al.*[92] and B. Yin, *et. al.*[47,93]

2.2. Aims and Objectives of Chapter 2

This chapter deals with the synthesis of *N*-Fmoc lipoamino acid derivatives and their evaluation as LMWGs. As discussed earlier, Fmoc-based derivatives are good candidates for LMWGs as the fluorenyl group provides the aromatic surfaces required for intermolecular π–π stacking interactions.[94-96] *N*-Fmoc peptide gelators have been extensively studied for their ability to form hydrogels[72] but there are few examples of their application as organogelators.[70] We aim to study how differences in the chemical nature of the side chains can tune the solubility and the additional interactions that drive the self-assembly process that may eventually lead to the formation of gels. The side chain of L-serine can be easily modified by protecting group chemistry to feature either an *O*-tert-butyl ether or a free hydroxyl group. These transformations can act as a "switch" to access compounds which are structurally similar, but may have very different gelling properties. We investigated how structural features such as I.) The nature of the functional group in the side chain and II.) The length of the hydrocarbon chain of *N*-Fmoc-L-serine lipoamino acids **2.38.** - **2.41.** (Figure 2.10.) affects their ability to form gels. In addition, the lipoamino acids were tested as phase selective gelators of organic solvents in biphasic aqueous mixtures and their ability to remove aromatic pollutants from water was evaluated.[86]
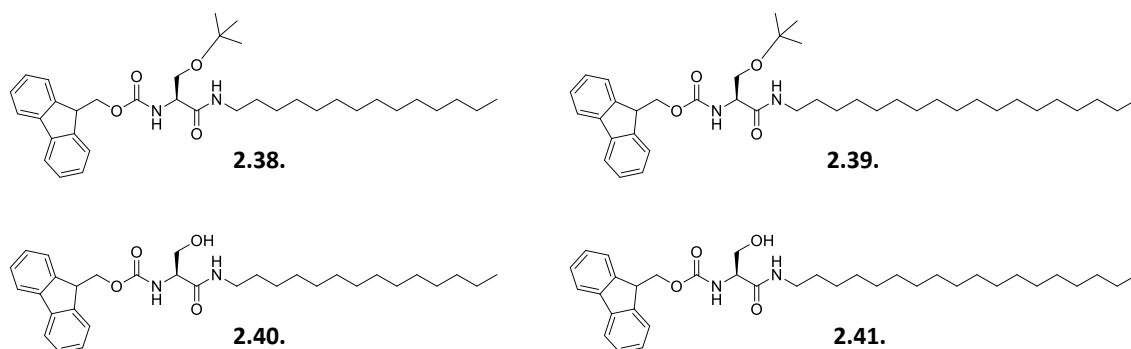
Figure 2.10. Chemical structures of *N*-Fmoc-L-serine lipoaminoacids gelators **2.38.** – **2.41.**

2.3. Results and Discussion

2.3.1. Synthesis of Lipoamino Acids

The lipoamino acids **2.38.** - **2.41.** were readily prepared as shown in Scheme 2.1. Commercially available *N*-Fmoc-*O*-*tert*-butyl-L-serine was reacted with either 1-tetradecylamine or 1-octadecylamine using *N,N'*-diisopropylcarbodiimide (DIC) as the coupling reagent to give compounds **2.38.** or **2.39.**, respectively.

2.38. n = 14
2.39. n = 18

2.40. n = 14
2.41. n = 18
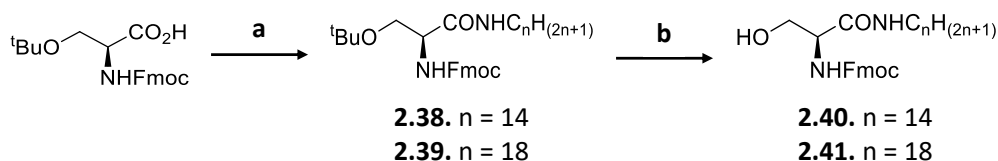
Scheme 2.1. Synthesis of lipoamino acids **2.38.** - **2.41.**; Reagents and conditions: a) DIC, DCM, $C_{14}H_{29}NH_2$ (95%) or $C_{18}H_{37}NH_2$ (88%), under N_2 at rt. 18 h; b) TFA, DCM (85%) or (51%) at rt. 15 h.

DIC is a coupling agent often used in organic chemistry for the synthesis of amides, peptides, esters and various heterocycles. Carbodiimide based reagents have been routinely used in chemistry for the formation of amide bonds since the introduction of dicyclohexylcarbodiimide (DCC). The diisopropylurea by-product formed during the coupling reaction is more soluble in DCM than that formed if DCC was used. This makes DIC a more suitable coupling agent.[97,98] The general mechanism for the formation of amides or peptides using DIC as a coupling reagent is shown in Scheme 2.2. It proceeds via the formation of an *O*-acylisourea intermediate. This species subsequently reacts with an amine nucleophile to form the amide bond and diisopropylurea.
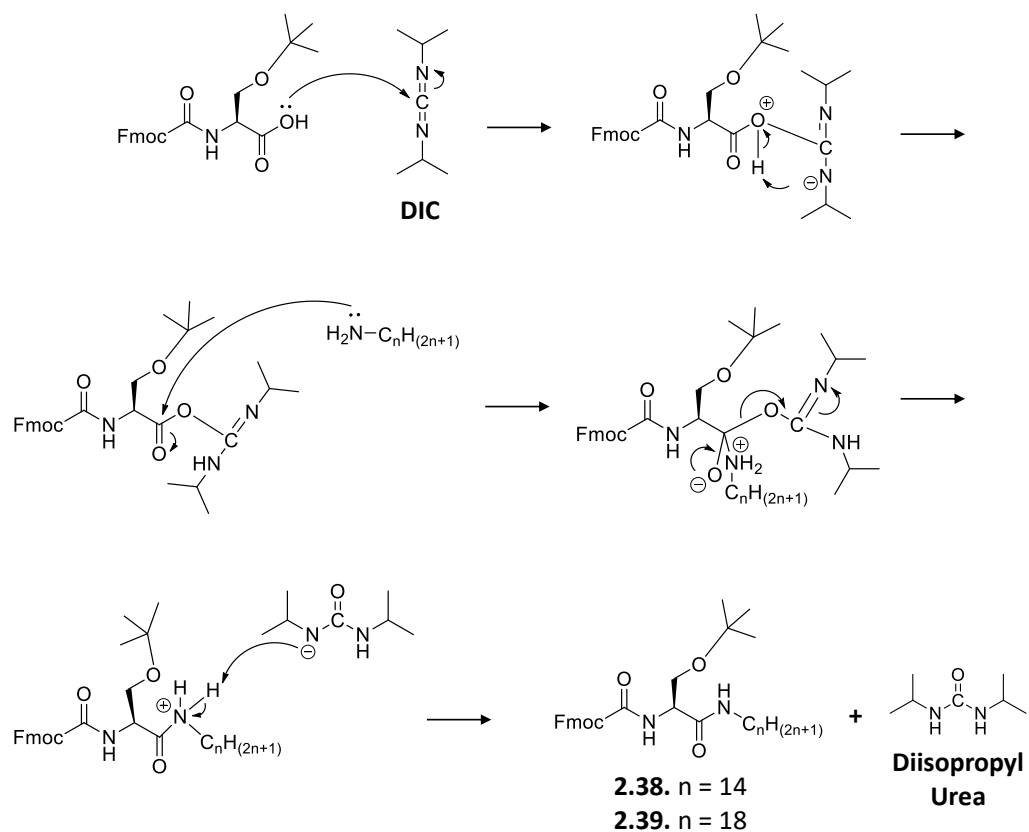
Scheme 2.2. Reaction mechanism of DIC coupling to form lipoamino acids **2.38.** and **2.39.**

Figure 2.11. shows the ^{1}H NMR spectrum of compound **2.38.** in CDCl$_3$. Characteristic peaks such as NH$_a$ and NH$_b$ of the amide groups, α-H, β-H and β'-H and ^{t}Bu group were assigned in the spectrum.
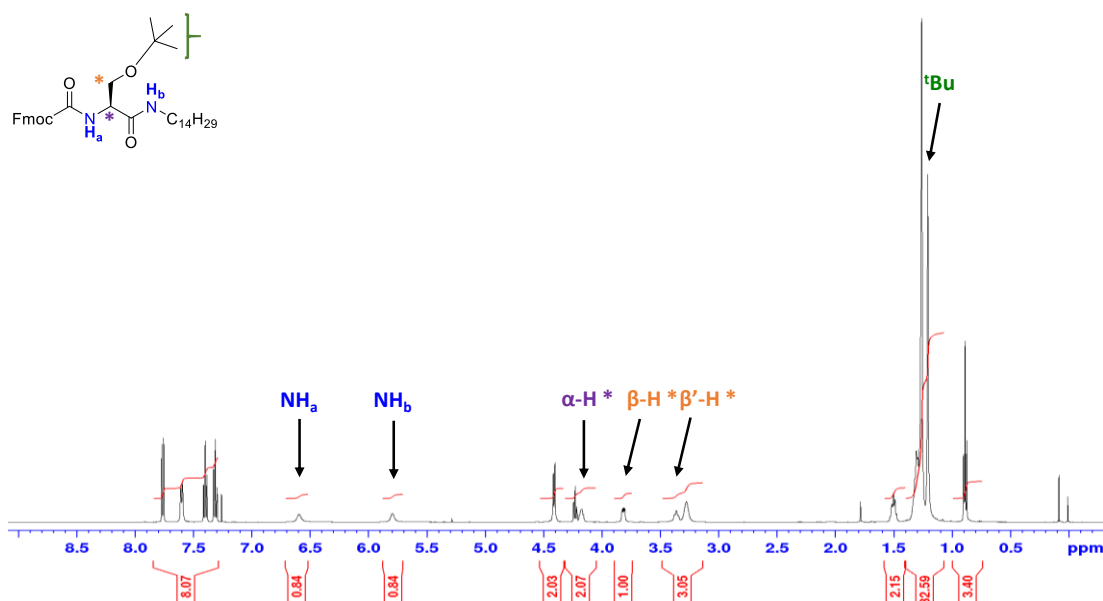
Figure 2.11. ^{1}H NMR spectrum of compound **2.38.** (CDCl$_3$, 500 MHz).

The removal of the side chain *tert*-butyl ether protecting group was accomplished by treatment with trifluoroacetic acid (TFA) in DCM, yielding the corresponding compounds **2.40.** and **2.41.** The mechanism of this reaction is shown in scheme 2.3.

2.38. n = 14
2.39. n = 18

2.40. n = 14
2.41. n = 18
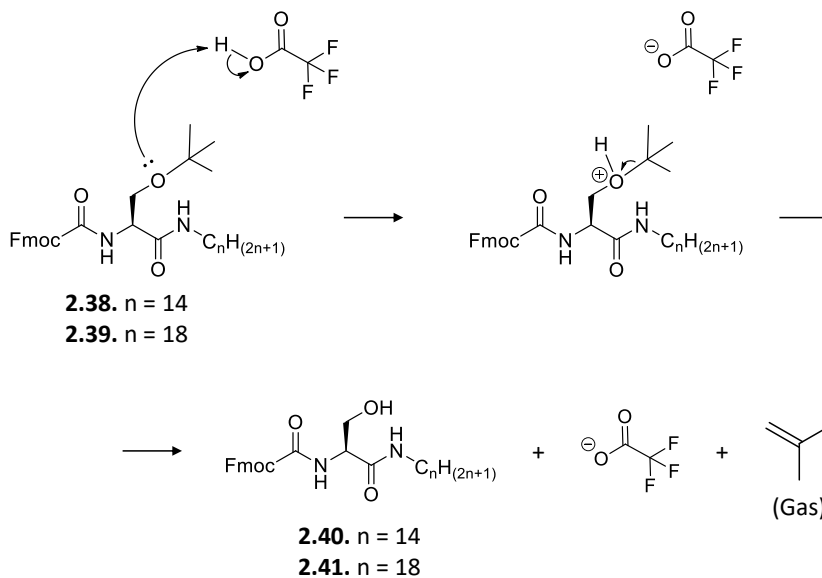
Scheme 2.3. Reaction mechanism of TFA removal of t-butyl group to give the target lipoamino acid gelators **2.40.** and **2.41.**

Figure 2.12. shows the ^{1}H NMR spectrum of compound **2.40.** in CDCl$_3$. Characteristic peaks such as NH$_a$ and NH$_b$ of the amide groups, α-H, β-H and β'-H were assigned in the spectrum. ^{t}Bu group at 1.20 ppm, which appeared as a singlet, was not present after deprotection.
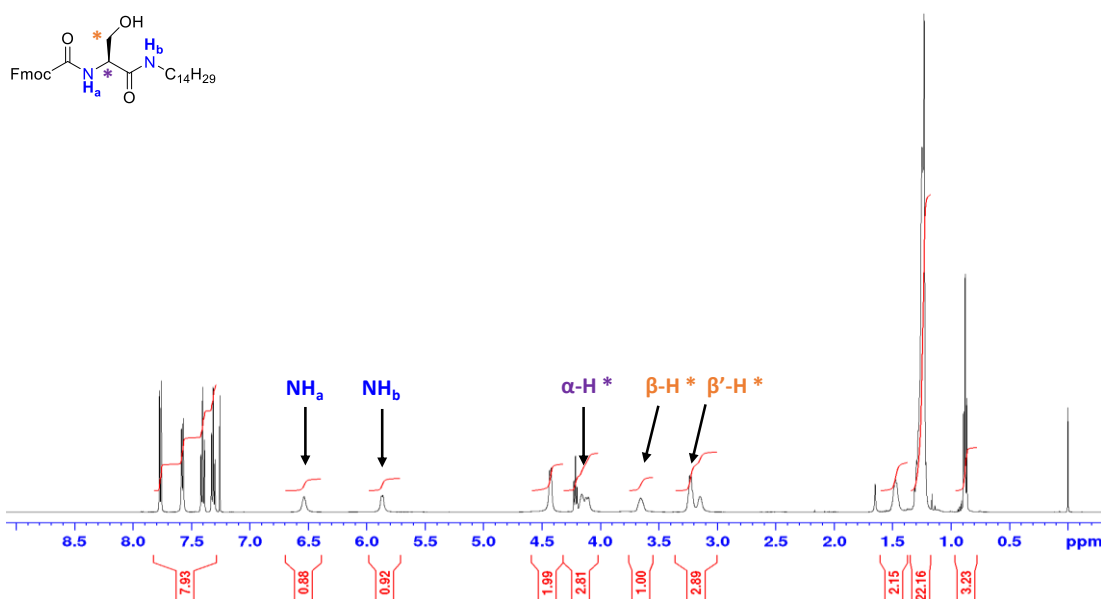
Figure 2.12. ^{1}H NMR spectrum of compound **2.40.** (CDCl$_3$, 500 MHz).

2.3.2. Gelation Ability

The ability of **2.38.** - **2.41.** to induce the formation of supramolecular gels was then screened in a range of organic solvents of different polarities and structural characteristics (Table 2.1.). Compounds **2.38.** - **2.41.** were capable of forming organogels by sonication or by heating/cooling. The gel was formed upon sonication at rt in less than 5 min. Organogels were also formed by thermal treatment. The gelator was heated in the required solvent to increase the solubility of the sample. The gel was formed after cooling down at rt in less than 2 h. For both techniques, the formation of the gel was confirmed by the "inverted test tube" method (Figure 2.13., see also experimental section, Chapter 7).

It was found that the C_{14} lipoamino acid **2.38.**, in which the serine side chain hydroxyl group is protected as a *tert*-butyl ether, showed a preference to form transparent gels with low polarity aliphatic hydrocarbon solvents such as pentane, hexane, heptane etc., with critical gel concentrations (CGC) generally in the "supergelator" range (CGC < 1 w/v %).[13] – (Table 2.1.). The increase in hydrophobicity imparted by the C_{18} hydrocarbon tail in **2.39.** resulted in a reduction in its ability to gel low polarity solvents. Compound **2.39.** was only able to form gels in hexane and heptane but with higher CGCs than its C_{14} analogue.

On the other hand, compound **2.40.**, featuring the free hydroxyl group on the side chain, behaved as a selective gelator of aromatic solvents, such as benzene, toluene and xylene. **2.40.** was also capable of gelation with commercial petrol, which contained a mixture of aromatic and saturated hydrocarbons. The chain extension in the C_{18} hydroxyl derivative **2.41.** resulted in this case in a retention of the ability to gel aromatic solvents (or even an improvement, considering the remarkable CGC of 0.2 w/v % for the formation of xylene gels). However, the ability to selectively induce aromatic over aliphatic solvent gelation was lost, as **2.41.** also gelled heptane and cyclohexane. This situation is common to the vast majority of organogelators described in the literature, which are incapable of discriminating the gelation of low polarity solvents. *N-tert*-butoxycarbonyl (*N*-Boc) protection / deprotection of amines in peptide gelators has been reported to promote the formation of organo- or hydrogels, respectively.[99] In this case, selective hydrocarbon gelation can be achieved

depending on the nature of the functional groups (hydroxyl or *tert*-butyl ether) present in the gelators' side chain. The solubility differences between the C_{14} derivatives **2.38.** and **2.40.** may account for the observed distinction in gelation abilities. The elongation of the hydrocarbon chain in the C_{18} derivative **2.39.** and **2.41.** increases their solubility and consequently overrides the side chain effect. None of the compounds **2.38.** – **2.41.** formed transparent gels in the higher polarity solvents. **2.38.** and **2.40.** remained in solution, while the increase in the chain length in the C_{18} derivatives prompted them to self-associate and form aggregates (**2.39.**) or opaque gels (**2.41.**) in EtOH and MeCN. These observations correlate well with the reported consequences of alkyl chain extension in organogelators, increasing the lipophilicity of a molecule increases its tendency to self-assemble in polar liquids, provided that sufficient solubility is maintained.[100]

Figure 2.13. Physical appearance of the organogels: (**lipoamino acid gelator**) *solvent:* a) (**2.38.**) *pet. ether*; b) (**2.38.**) *petrol*; c) (**2.38.**) *hexane*; d) (**2.38.**) *pentane*; e) (**2.38.**) *cyclohexane*; f) (**2.38.**) *heptane;* g) (**2.39.**) *hexane;* h) (**2.39.**) *heptane;* i) (**2.40.**) *toluene;* j) (**2.40.**) *xylene;* k) (**2.40.**) *benzene;* l) (**2.40.**) *petrol;* m) (**2.41.**) *toluene;* n) (**2.41.**) *MeCN;* o) (**2.41.**) *xylene;* p) (**2.41.**) *benzene;* q) (**2.41.**) *EtOH;* r) (**2.41.**) *cyclohexane;* s) (**2.41.**) *heptane.* (All gels were prepared at CGC).

Table 2.1. Gelation abilities of lipoamino acids **2.38.** - **2.41.** in different solvents: physical appearance, CGC (Critical Gelation Concentration, w/v %) at rt and gel-sol transition temperature T_{gs} (°C) at the specified CGC.

Solvent	2.38. (OᵗBu-C$_{14}$)	2.39. (OᵗBu-C$_{18}$)	2.40. (OH-C$_{14}$)	2.41. (OH-C$_{18}$)
Pentane	TG(1.3) / T$_{gs}$(25-30)	A	I	I
Hexane	TG(0.7) / T$_{gs}$(40-47)	TG(1.3) / T$_{gs}$(43-53)	I	I
Heptane	TG(0.7) / T$_{gs}$(25-30)	TG(1.7) / T$_{gs}$(26-32)	I	TG(2) / T$_{gs}$(43-50)
Pet. ether	TG(0.4) / T$_{gs}$(48-59)	A	A	I
Cyclohexane	TG(0.7) / T$_{gs}$(28-34)	S	I	TG(0.6) / T$_{gs}$(45-53)
Petrol	TG(2) / T$_{gs}$(46-52)	S	TG(1.4) / T$_{gs}$(26-40)	I
Xylene	S	S	TG(0.6) / T$_{gs}$(37-43)	TG(0.2) / T$_{gs}$(39-44)
Toluene	S	S	TG(1.3) / T$_{gs}$(35-39)	TG(1.4) / T$_{gs}$(36-49)
Benzene	S	S	TG(1.3) / T$_{gs}$(28-46)	TG(1.2) / T$_{gs}$(35-54)
Et$_2$O	S	A	S	A
CHCl$_3$	S	S	S	S
DCM	S	S	S	S
EtOAc	S	S	S	A
MeCN	A	A	A	OG(1.7)/ T$_{gs}$(49-61)
Pyridine	S	S	S	S
EtOH	S	A	S	OG(1) / T$_{gs}$(38-46)

S = Soluble, I = Insoluble, A = Aggregates, TG = Transparent gel, OG = Opaque gel.

2.3.3. Comparison of the *N*-Fmoc Gelator 2.40. with the *N*-Cbz Analogue 2.42.[101]

In order to investigate the requirement of the Fmoc group to retain gelation ability of the lipoamino acids **2.38.** - **2.41.**, the *N*-Cbz derivative **2.42.**[101] was synthesised.

The lipoamino acid **2.42.** was readily prepared as shown in Scheme 2.4. Commercially available *N*-Benzyloxycarbonyl-L-serine was reacted in dimethylformamide (DMF) under N_2 at rt, with 1-tetradecylamine using DIC as the coupling reagent to give compound **2.42.**
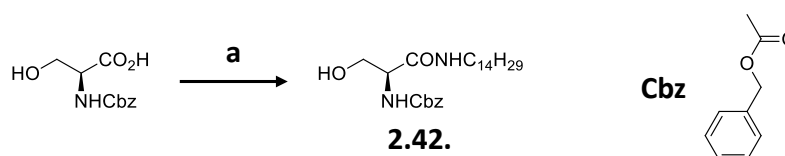
Scheme 2.4. Synthesis of lipoamino acid **2.42.**; Reagents and conditions: a) DIC, DMF, $C_{14}H_{29}NH_2$ (82%), under N_2 at rt. 18 h.

The gelation ability of **2.42.** was evaluated with a range of solvents of different polarity as for compound **2.39.** – **2.41.** It was found that at 20 mg/mL, the compound was only capable of forming aggregates in toluene, xylene and benzene. Gels in toluene were formed in concentrations as high as 100 mg/mL. These results show that the Cbz analogue **2.42.**, lacked the ability to form gels in organic solvents efficiently. These observations seem to agree with recent studies that support the evidence that van der Waals dispersion forces account for the attractive interactions between aromatic moieties in organic solvents and become more favorable as the size of the stacking surfaces increase.[102]

2.3.4. Rheological Evaluation

The rheological characterisation of the organogels of **2.38.** and **2.39.** in hexane and of **2.40.** and **2.41.** in toluene was carried out at Santiago de Compostela University (Figure 2.14.). The gel formed by **2.38.** in cyclohexane was also studied.
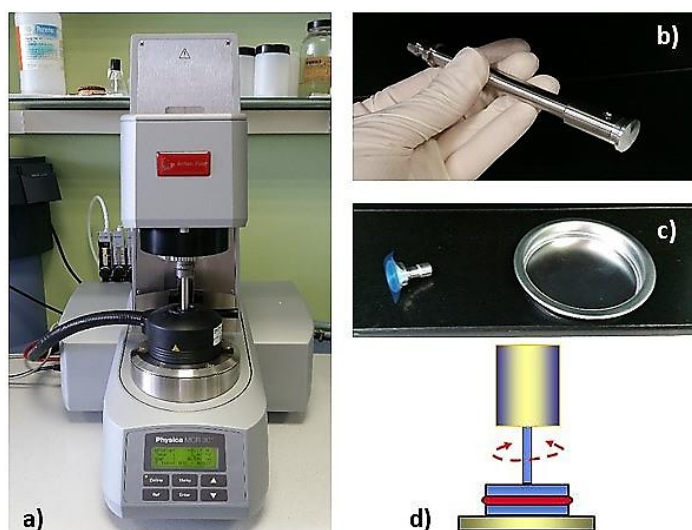
Figure 2.14. a) Rheometer MCR 301, Anton Paar; b) Rotating upper plate(15 mm diameter);
c) Parallel plates; d) Schematic representation with parallel plate geometry (0.5 mm gap).

The strain sweep tests allowed the determination of critical strain (γc) of the samples (Figure 2.15.). This technique provides easy-to-interpret information about the soft-solid rigidity and yield stress (gel strength). The Linear Viscoelastic Regime (LVER) is defined as a level of stress and/or strain above which actual behaviour varies from behaviour predicted on the basis of linearity assumption. However, stress and strain are interrelated time-dependent functions strongly influenced by test type and action of external factors.[103] To be in the Lineal Regime of a sample, G' and G'' must be constant, with parallel trends. That means the sample can recover its structure after the stresses are released. Increasing the strain, G' and G'' collapse (both modules fall). That means the structure is deformed without recovery of the system.[104] LVER test is previous to SAOS (Small Amplitude Oscillatory Shear) which helps to identify the structure of the system without modifying it. SAOS test measures the elastic properties (storage modulus = G') and the viscous properties (loss modulus = G'') of viscoelastic fluids (solutions, mels or gels), depending on the value of tan δ. See section 1.3.1. for the definition of the parameters which define the rheological nature of a gel.

Figure 2.15. shows the LVER for **2.38.** - **2.41.** in cyclohexane, hexane and toluene which was 0.1 %. In that way, the tests are done without affecting the structure of the gels.
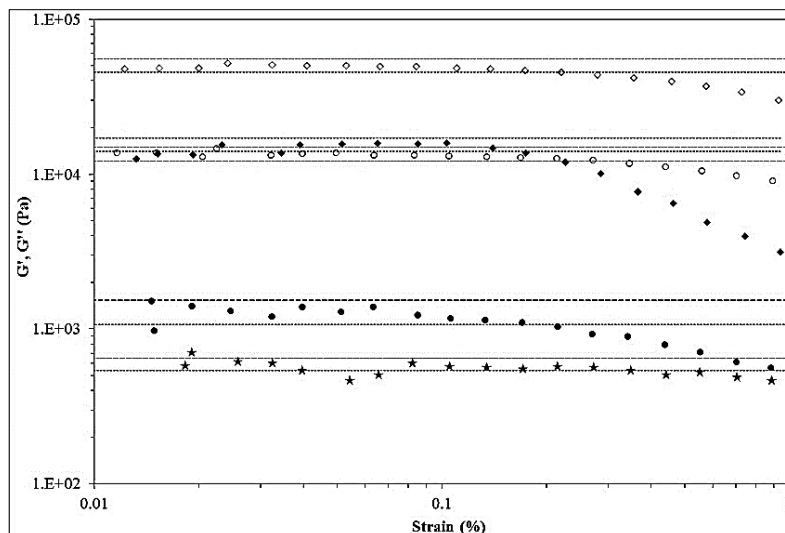
Figure 2.15. Strain sweep at 1 Hz of frequency. G′ at 25 °C for **2.40.** (♦, toluene 1.3 w/v %) and **2.41.** (◊, toluene 1.4 w/v %) at 96 h and at 5 °C for **2.38.** (●, hexane, 0.7 w/v %), **2.39.** (o, hexane, 1.3 w/v %) and **2.38.** (★, cyclohexane, 0.7 w/v %) at 24 h.

Mechanical spectra of the gels were carried out after 24, 48, 76, 96 and 120 h of gel formation in order to evaluate the rheological stability of their structure. Figure 2.16. shows the evolution over time of the mechanical spectra for the gel of compound **2.38.** in hexane (Figure 2.16. a) and compound **2.40.** in toluene (Figure 2.16. b). It can be seen that the values of the viscoelastic moduli (G' and G'') for compound **2.38.** and **2.40.** did not significantly increase with time after 24 h and 96 h respectively. At longer times (120 h), the moduli values remained constant indicating that a stable gel structure was achieved. This fact can also be clearly observed by analysing the decrease of tanδ from 0.41 at 24 h to 0.33 at 120 h for compound **2.38.** and from 0.34 at 24 h to 0.13 at 96-120 h for compound **2.40.** (at 1 rad/s of angular frequency). That confirms the increase of a dominant elastic (i.e. gel) character of the material over time. Similar behavior was observed in the gels formed in hexane, **2.39.**, and cyclohexane, **2.38.**, or the gel in toluene, **2.41.**, which reached the stable state after 24 h or 96 h of gel formulation.
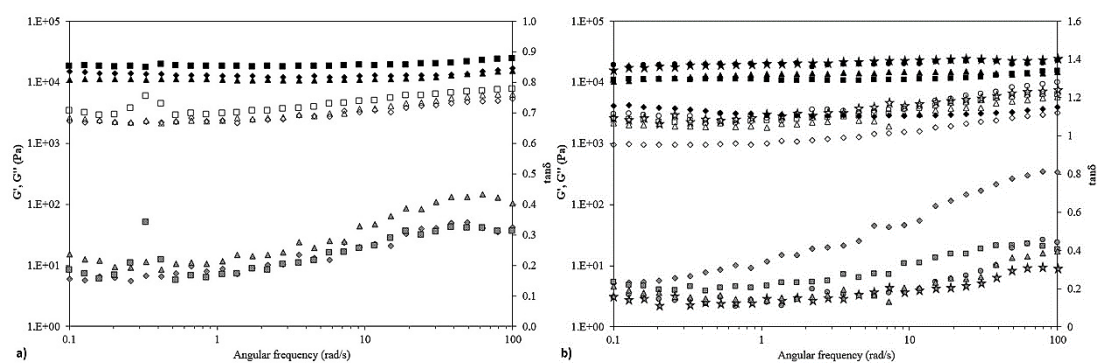
Figure 2.16. Frequency sweep of a) at 5 °C at a strain of 0.1 % of **2.38.** in hexane 0.7 w/v % at 24 (♦), 48 (▲) and 120 h (■); b) at 25 °C at a strain of 0.1 % of **2.40.** in toluene 1.3 w/v % at 24 (♦),72 (▲), 96 (●) and 120 h (★). G' (filled markers), G" (empty markers) and tanδ [dot filled markers with values, < 0.4 (**2.38.**) and < 0.8 (**2.40.**)].

Mechanical spectra of the gels of compounds **2.40.** and **2.41.** in toluene at 25 °C and at 96 h after their formation, as well as those for compounds **2.38.** and **2.39.** in hexane and cyclohexane at 5 °C and at 24 h after their formation, are shown in Figure 2.17.
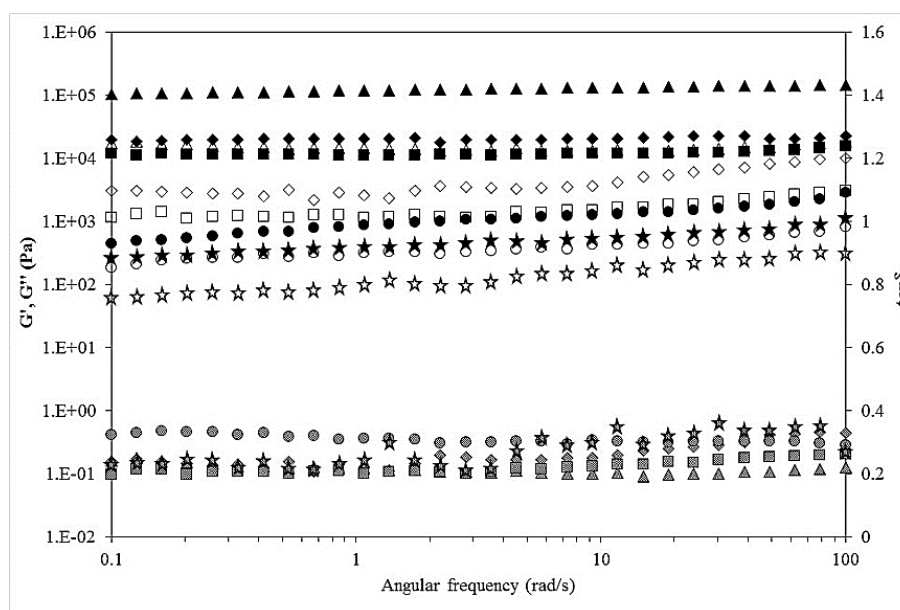
Figure 2.17. Frequency sweep at 25 °C at a strain of 0.1 % for **2.40.** (♦, toluene, 1.3 w/v %) and **2.41.** (▲, toluene, 1.4 w/v %) at 96 h and at 5 °C for **2.38.** (●, hexane, 0.7 w/v %), **2.39.** (■, hexane, 1.3 w/v %) and **2.38.** (★, cyclohexane, 0.7 w/v %) at 24 h. G' (filled markers), G" (empty markers), and tanδ (dot filled markers with values < 0.4).

All studied gels showed G´ > G´´ throughout the angular frequency range that was studied, with low values of tanδ (See Table 2.2.). This indicates that the elastic nature of the samples prevailed over the viscous one, which is the typical behavior of a gel structure. The gels in toluene of the hydroxyl derivatives **2.40.** and **2.41.**, as well as the hexane gel of the *tert*-butyl ether C_{18} compound **2.39.** showed the highest values of both rheological moduli, indicating that they are stronger gels (only at the CGC) than those formed by the shorter C_{14} compound **2.38.** in either hexane or cyclohexane. When toluene was used as a solvent, the gel formed by the C_{18} compound **2.41.** presented higher values of G´ and G´´ and higher elastic character (lower values of tanδ) than the corresponding gel formed by the C_{14} compound **2.40.** (See Table 2.2.). Thus, **2.41.** can be considered to be the strongest gel. The extension of the alkyl chain length in the gelators induce different behaviors in these systems. In the gel formed by the C_{14} compound **2.40.** in toluene, G´´$(2.6 – 7.6 \cdot 10^3)$ increased appreciably with increasing angular frequency, while in the toluene gel formed by C_{18} compound **2.41.** it is almost constant (G'' $= 1.7 – 1.8 \cdot 10^4$). This fact is easily observable through the increase of tanδ at high angular frequencies in the gel of **2.40.** in toluene (See Table 2.2.). This result could be related to the promotion of mobility of the gel structure (higher viscous component) in this organogel while for that formed by the longer chain gelator **2.41.** the response is almost stationary. When hexane is employed as the solvent, the gels **2.38.** and **2.39.** showed lower values of viscoelastic parameters than **2.40.** and **2.41.** in which toluene was used as the solvent. This indicates that the hexane gels are weaker.

Table 2.2. Summary of SAOS results for **2.38.** - **2.41.** The data are displayed from the weakest (top) to the strongest (bottom) gel.

Compound	Solvent	Temperature	Time	G' (Pa)	G'' (Pa)	Tan δ
2.38.	Cyclohexane	5 °C	24 h	$2.7 \cdot 10^2 – 1.2 \cdot 10^3$	$6.3 \cdot 10^1 – 3.2 \cdot 10^2$	0.23 - 0.30
2.38.	Hexane	5 °C	24 h	$4.4 \cdot 10^2 – 2.9 \cdot 10^3$	$1.9 – 8.1 \cdot 10^2$	0.42 - 0.29
2.39.	Hexane	5 °C	24 h	$1.5 – 1.2 \cdot 10^4$	$3.1 – 1.3 \cdot 10^3$	0.21 - 0.18
2.40.	Toluene	25 °C	96 h	$1.7 – 2.5 \cdot 10^4$	$2.6 – 7.6 \cdot 10^3$	0.16 - 0.31
2.41.	Toluene	25 °C	96 h	$1.0 – 1.4 \cdot 10^5$	$1.7 – 1.8 \cdot 10^4$	0.16 - 0.12

2.3.5. Thermal Analysis: Gel-Sol Transition Temperature (T_{gs}) and Differential Scanning Calorimetry (DSC) Measurements

The formation of the organogels was found to be thermoreversible. The heating/cooling cycle could be repeated several times without any apparent degradation of the sample or loss of integrity of the gels formed. The gel-sol transition temperatures (T_{gs}) are shown in Table 2.1. and were measured by the "melting" method, as described in Section 7.3.3. The extension in the alkyl chain length from C_{14} to C_{18} resulted in a slight increase of the corresponding T_{gs}. The thermoreversibility of the systems could also be confirmed by DSC measurements (Figure 2.15.). The DSC analysis of the gels formed by **2.38.** and **2.39.** in hexane and **2.40.** and **2.41.** in toluene were carried out at 24 h and 96 h respectively after formulation to ensure that the gel formation was completed following rheological results.
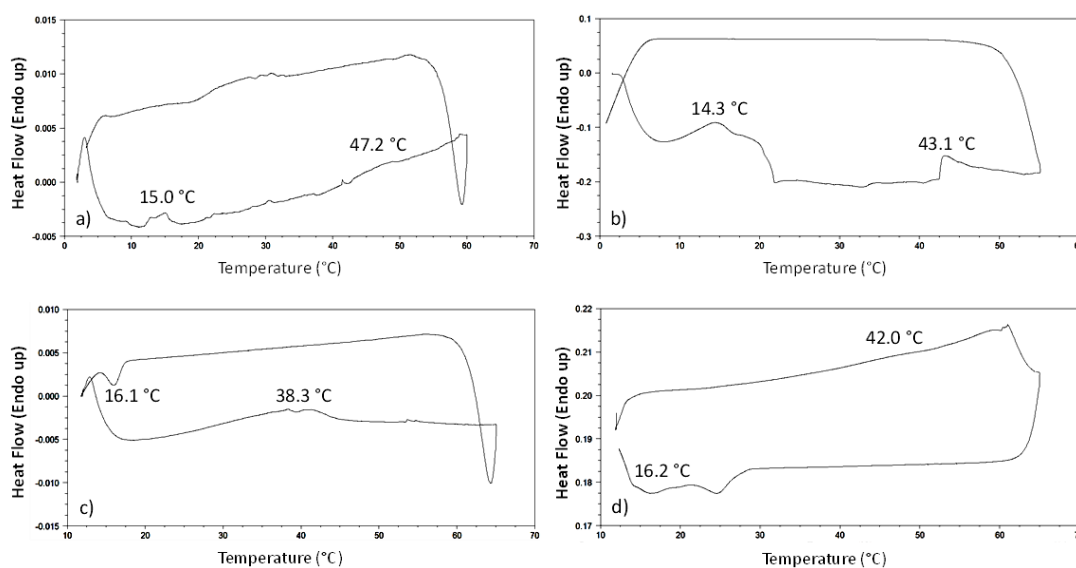
Figure 2.18. DSC of the gel formed by a) **2.38.** in hexane (0.7 w/v %) and b) **2.39.** in hexane (1.3 w/v %) during the heating/cooling cycles. The sample was heating from 2 °C to 60 °C at 2 °C/min and cooling the same range of temperature; c) **2.40.** in toluene (1.3 w/v %) and d) **2.41.** in toluene (1.4 w/v %) during the heating/cooling cycles. The sample was heating from 11 °C to 65 °C at 2 °C/min and cooling the same range of temperature. Reproducible / duplicated cycles for the four samples.

The thermograms a) - d) in Figure 2.18. show the endotherms (the system absorbs energy or heat) and exotherms (the system gives out energy or heat) for the four gelators. Thermograms a) and b) show an endotherm at 47.2 °C for **2.38.** and 43.1 °C for **2.39.** in the first heating cycle corresponding to the gel-sol transition. This correlated well with the T_{gs} (40 - 47 °C) for **2.38.** and T_{gs} (43 - 53 °C) for **2.39.** determined by the "melting" method. On the cooling cycle we cannot see the exotherm as gels **2.38.** and **2.39.** are weaker gels and they need more time than the run cool cycle to form the 2-D structure, so no significant changes can be appreciated in the thermogram.

Thermograms c) and d) show an endotherm at 38.3 °C for **2.40.** and 42.0 °C for **2.41.** in the first heating cycle corresponding to the gel-sol transition. This correlated well with the T_{gs} (35 - 39 °C) for **2.40.** and T_{gs} (36 - 49 °C) for **2.41.** determined by the "melting" method. On cooling they show a sol-gel transition exotherm ~ 16 °C for both gels (**2.40.** and **2.41.**) indicating the thermoreversible nature of the gels.[28,105] The enthalpies associated with the transitions were calculated from the DSC data (Table 2.3.). In agreement with the results found in the rheological evaluation, gels **2.40.** and **2.41.** were stronger, as the ΔHs of fusion are 1.542 J/g and 5.004 J/g respectively, comparing to **2.38.** and **2.39.** (~ 0.0800 J/g) which correspond to weaker gels. Additionally, it is important to note that the enthalpy of fusion was always higher than the enthalpy of formation. (See summary of results in Table 2.3.) This apparent disparity can be explained by the rheological analysis that showed that the gels need 96 h to complete gel formation of the network. Each DSC cycle takes ~ 30 min, thus, DSC measurements only probe the initial assembly of the gelator molecules into 2-D structures, which subsequently organise into 3-D networks that can entrap the solvent.[2,106-108] The difference in the heating and cooling peak temperatures in thermograms c) and d) indicate a hysteresis characterising a first order nature in the gelation process. This type of behavior has been reported for other organogelators.[34] In addition, the transition peaks are better defined in the cooling curve (sol-to-gel) rather than in the heating curves (gel-to-sol). This is consistent with the simultaneous occurrence of different self-assembly processes, which are characteristic of the gelation process.[35]

Table 2.3. Summary of $T_{(gel-to-sol)}$, $T_{(sol-to-gel)}$ and ΔH (J/g) for **2.38.** - **2.41.**

Compound	T_{gs}	$T_{(gel-to-sol)}$	ΔH (J/g)	$T_{(sol-to-gel)}$	ΔH (J/g)
2.38.	40 - 47 °C	15.0 °C	0.085	-	-
		47.2 °C	0.072	-	-
2.39.	43 - 53 °C	14.3 °C	0.089	-	-
		43.1 °C	0.084	-	-
2.40.	35 - 39 °C	38.3 °C	1.542	16.1 °C	0.139
2.41.	36- 49 °C	42.0 °C	5.088	16.2 °C	1.009

2.3.6. Morphological Studies

The morphology of the xerogels of compounds **2.38.** - **2.41.** was investigated using SEM imaging (see section 7.3.6.3.). The xerogels were formed from the corresponding organogels in different solvents using a spatula to transfer the gel from the closed vial to the metal stub. The presence of densely packed fibrous structures, which appear as grooves on the surface of the xerogels, can be observed for all the xerogels; the dimension and aggregation patterns of the fibres seem to vary depending on the nature of the solvent and the organogelator (Figure 2.19.).
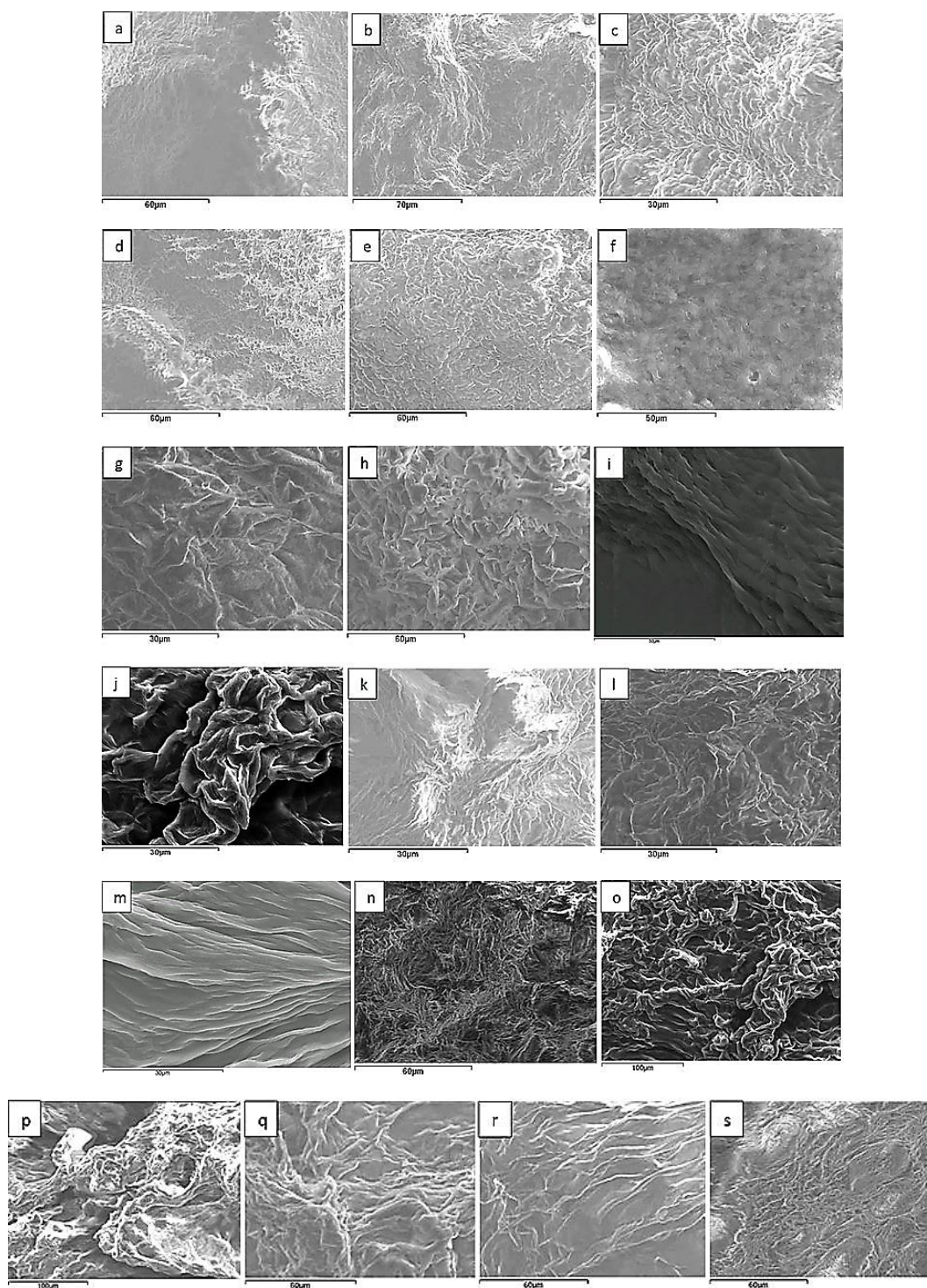
Figure 2.19. SEM images of xerogels formed by lipoamino acids **2.38.** – **2.41.** *Solvent:* a) (**2.38.**) *pet. ether*; b) (**2.38.**) *petrol*; c) (**2.38.**) *hexane*; d) (**2.38.**) *pentane*; e) (**2.38.**) *cyclohexane*; f) (**2.38.**) *heptane*; g) (**2.39.**) *hexane*; h) (**2.39.**) *heptane*; i) (**2.40.**) *toluene;* j) (**2.40.**) *xylene*; k) (**2.40.**) *benzene*; l) (**2.40.**) *petrol*; m) (**2.41.**) *toluene*; n) (**2.41.**) *MeCN*; o) (**2.41.**) *xylene*; p) (**2.41.**) *benzene*; q) (**2.41.**) *EtOH;* r) (**2.41.**) *cyclohexane*; s) (**2.41.**) *heptane*; (All gels were prepared at CGC). [Scale bar: o), p) 100 μm; b) 70 μm; a),d), e), h), n), q), r), s) 60 μm; f) 50 μm; c), g), i), j), k), l), m) 30 μm].

The images reveal striking differences in the morphologies of the SAFINs for the hexane xerogels formed from the *O-tert*-butylated compounds **2.38.** and **2.39.** and the toluene xerogels from the hydroxyl derivatives **2.40.** and **2.41.** The images for the hexane xerogels from **2.38.** and **2.39.** present ridge-like structures [Figure 2.19. c) and g)], which are likely caused by the aggregation of densely packed fine fibrils. Similar morphologies were observed for the xerogels in aliphatic solvents such as pentane, cyclohexane and heptane [Figure 2.19. d), e), f) and h)]. In contrast, the presence of well-defined fibrous structures or "microbelts",[109] can be clearly observed in the images of the toluene xerogels from **2.40.** and **2.41.** [Figure 2.19. i) and m)]. The fibres appear to twist, which could be an indication of a helical structure. The lengthening of the alkyl chain does not seem to impart significant differences in the morphology of the xerogels. This suggests that the nature of the functional group in the serine side chain is a structural feature critical to direct the assembly of gelator molecules, which in turn determines the morphology of the subsequently formed xerogels.

2.3.7. Spectroscopic Analysis

The role of H-bonding interactions in gel formation was studied by ^{1}H-NMR and FTIR analysis.

2.3.7.1. ^{1}H-NMR Spectroscopic Analysis

^{1}H-NMR spectra of *O-tert*-butylated **2.38.** in (D_{12})-cyclohexane [Figure 2.20. a)] and of the hydroxyl derivative **2.40.** in (D_8)-toluene [Figure 2.20. b)] were recorded at increasing concentrations. The solutions were prepared in the NMR tube, heated to aid the solubility of the gelator in the required solvent and it was measured at 300 K (27 °C), which is the standard operation temperature of the NMR spectrometer.
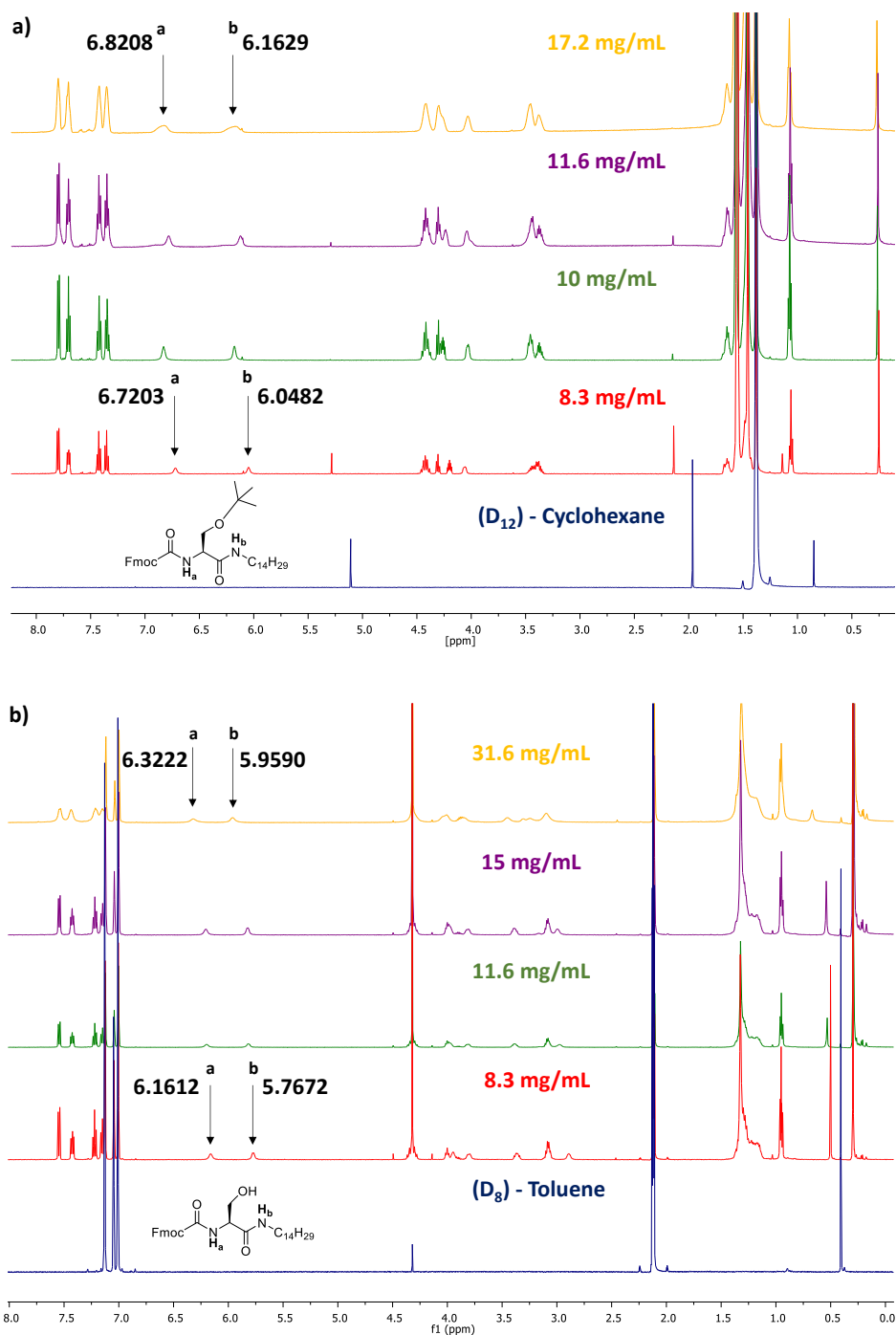
Figure 2.20. ^{1}H-NMR spectra at different concentrations: a) **2.38.** in (D$_{12}$)-cyclohexane and b) **2.40.** in (D$_8$)-toluene.

In both cases, a downfield shift for the resonances corresponding to the amide (δNH$_a$) and carbamate NH (δNH$_b$) protons were observed (Table 2.4.). These values are consistent with the formation of intermolecular H-bonding in organogels. The comparable increments in chemical shifts ($\Delta\delta$) shown in Table 2.4. upon changes in concentration observed in the NH signals suggest that both groups are similarly

involved in intermolecular H-bonding, independently of the groups present in the gelators' side chain.

Table 2.4. Chemical shifts (δ) of the NH signals (ppm) in the ^{1}H-NMR spectra at different concentrations of **2.38.** in (D_{12})-cyclohexane and **2.40.** in (D_8)-toluene.

Compound	Solvent	Concentration	Temperature	δ NH$_a$ (ppm)	δ NH$_b$ (ppm)
2.38.	Cyclohexane	8.3 mg/mL (Solution)	27 °C	6.720	6.048
		17.2 mg/mL (Gel)	27 °C	6.821	6.163
	Δδ NH (ppm)		-	**0.101**	**0.115**
2.40.	Toluene	8.3 mg/mL (Solution)	27 °C	6.161	5.767
		31.6 mg/mL (Gel)	27 °C	6.322	5.959
	Δδ NH (ppm)		-	**0.161**	**0.192**

The samples recorded at the gel state, highest concentration, for **2.38.** and **2.40.**, showed broadening of all resonances (Figure 2.20.). This is a clear indication that the cross-linking of the SAFINs, as a consequence of the gelation process, is taking place.[48] It is important to note that the signals corresponding to the aromatic protons did not experience significant upfield shifts; these shifts are usually associated with the formation of strong aromatic π-π stacking interactions.

2.3.7.2. FTIR Spectroscopic Analysis

FTIR spectroscopic data were obtained for the lipoamino acid gelators in different physical states in order to determine if H-bonding was an important factor for gel formation. Previous studies have shown that when organogel formation was promoted by H-bonding, the IR bands associated with the relevant functional groups in the molecule shift to lower wavenumbers from those recorded of the gelator free in solution.[51,52] FTIR spectra of lipoamino acids **2.38.** and **2.40.** were recorded as a bulk solid sample (NaCl disk), as gels in cyclohexane and toluene (cell), respectively, and as the solvated gelator molecules in a CHCl$_3$ solution. The positions and assignments of the noteworthy IR bands (νNH and νCO) of gelators **2.38.** and **2.40.** in the three states is given in Table 2.5. The νOH band of gelator **2.40.** in CHCl$_3$ solution could not be distinguished from the overlapping solvent bands. No νOH band could be identified for **2.40.** in the gel or bulk states and we would propose that due to H-bonding it has shifted to a sufficiently low wavenumber so that it overlaps with the νNH band. Assignments of the CO stretching bands are based on the studies by Fleming *et al.* on related systems.[53] The spectra recorded for the bulk and gel state

showed similar peak positions for the three bands, whereas all three bands were shifted to higher wavenumbers in the spectrum recorded in solution. For gelator **2.38.**, the bands for the νNH, νCO$_{carbamate}$ and νCO$_{amide}$ shifted to higher frequency by 142, 25 and 20 cm^{-1} respectively between the gel and CHCl$_3$ solution. For gelator **2.40.**, the band associated with the νNH stretch shifts 128 cm^{-1} between that of the gel and the solution state going from 3299 to 3427 cm^{-1}, while those of the νCO$_{carbamate}$ and νCO$_{amide}$ shift 22 and 15 cm^{-1} respectively. In both cases the magnitudes of the shifts are similar to those recorded for other H-bonded gels[51,52] and indicate that in the gel and bulk states the NH groups of one molecule are H-bonding with both the carbamate and amide CO acceptor groups of other gelator molecules.

Table 2.5. Position of characteristic IR bands of the lipoamino acids **2.38.** and **2.40.** in the solid state, gel state and CHCl$_3$ solution. *ν(OH) band not distinguishable from overlapping solvent peaks. **possibly also includes an overlapping ν(OH) band.

Compound	Sample state	νNH Amide and carbamate / cm^{-1}	νCO Carbamate / cm^{-1}	νCO Amide I / cm^{-1}
2.38.	Bulk (NaCl plate)	3313	1691	1659
	Solution (in cell, 0.7 w/v %, CHCl$_3$)	3432(br)	1719	1670
	Gel (in cell, 0.7 w/v %, cyclohexane)	3290	1694	1650
2.40.	Bulk (NaCl plate)	3300**	1687	1650
	Solution (in cell, 1.3 w/v %, CHCl$_3$)	3427 (br)	1709	1666
	Gel (in cell, 1.3 w/v %, toluene)	3299**	1687	1651

As there is a clear distinction between the spectra of **2.40.** recorded in both solution and the gel state, studies were carried out to directly follow the formation of the gel using IR spectroscopy. In the first study, **2.40.** was dissolved in toluene (1.3 w/v %) which was held at 50 °C, well above the gelation temperature ($\sim$ 16 °C). The solution was transferred into an IR solution transmission cell and spectra were recorded over a period of 135 min during which time the cell cooled down to rt and gelation occurred (Figure 2.18.). The initial spectrum shows bands at 3578 (νOH), 3404 (νNH) 1727, 1709 (νCO$_{carbamate}$) and 1681 (br) (νCO$_{amide}$) cm^{-1} for **2.40.** in solution in toluene. The splitting and broadening of the CO stretching bands suggests that **2.40.** exists as more than one conformer in toluene. The position and shape of the νOH band indicates that the OH group is involved in H-bond interaction intramolecularly or that

2.40. is present in the toluene solvent as small aggregates at the start of the experiment. Over 135 min as gelation occurred these peaks decrease in intensity and new peaks associated with the formation of H-bonds are observed to concurrently grow at 3299 (νNH and νOH), 1687 (νCO$_{carbamate}$) and 1651 (νCO$_{amide}$) cm^{-1}. The presence of a number of isosbestic points, assigned with blue arrows in Figure 2.21. and Figure 2.22., indicate clean conversion from solution to gel.
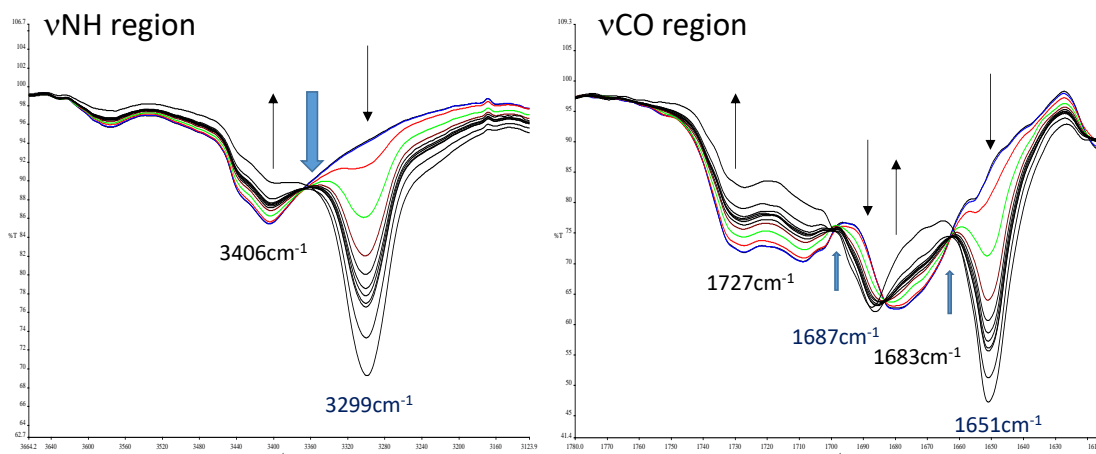
Figure 2.21. FTIR spectra of compound **2.40.** 1.3 w/v % in toluene solution from 0 – 135 min. The solution injected into the cell was held at 50 °C and was then allowed to cool to rt.

Similar results were observed, with the exception of the absence of a νOH band in the starting spectrum, when the gelation of **2.38.** in cyclohexane was followed using FTIR (Figure 2.22.).
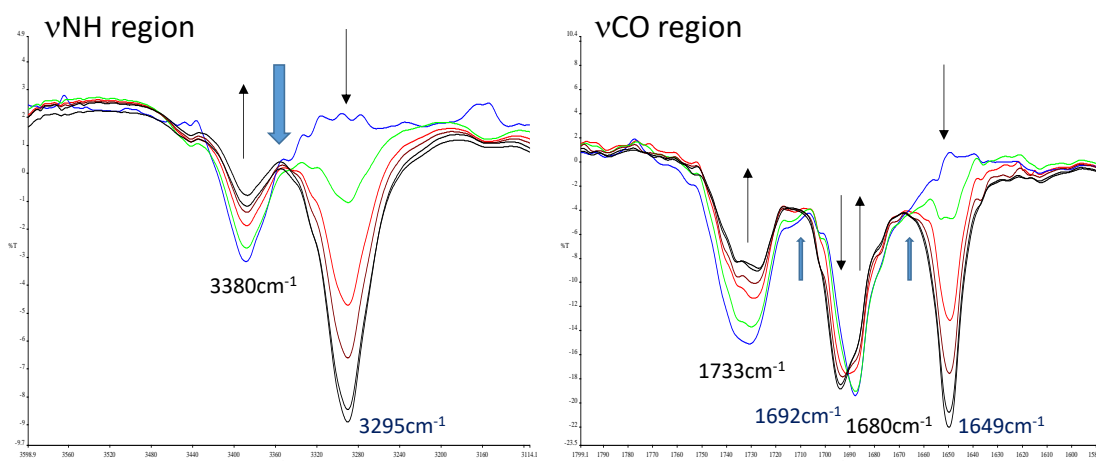
Figure 2.22. FTIR spectra of compound **2.38.** 0.7 w/v % in cyclohexane solution from 0 – 135 min. The solution injected into the cell was held at 50 °C and was then allowed to cool to rt.

A further study was carried out for **2.40.** in toluene (2.6 w/v %) at rt. The solution was placed on the crystal of the FTIR-ATR optics and spectra were recorded over a period of approximately 1 h (Figure 2.23.). Initially no compound bands were observed in the spectra of the solution but as the gel formed, bands appeared to 'grow-in' at 3290, 1692 and 1651 cm^{-1}. This difference in intensity of the FTIR bands between the solution and gel state has been observed by other authors and is proposed to be due to an increase in the concentration of **2.40.** close to the ATR crystal as the gel forms.[51,110]
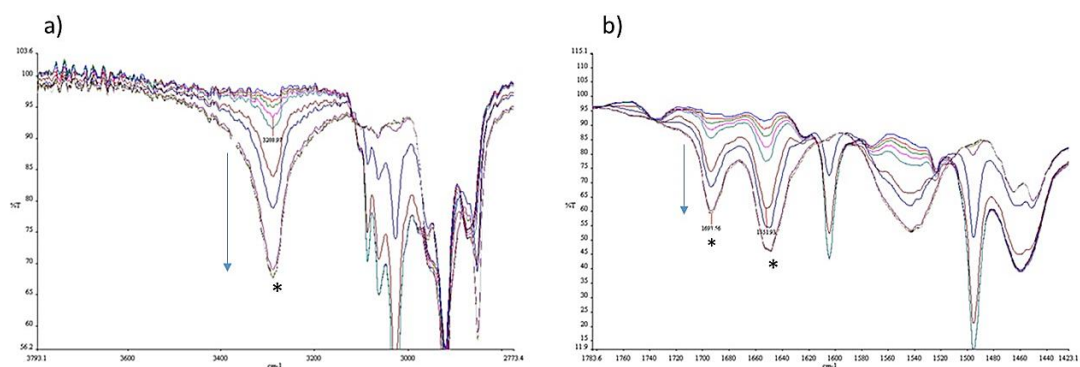
Figure 2.23. FTIR-ATR spectra of lipoamino acid **2.40.** in 2.6 w/v % in toluene solution (ATR) recorded from 0 to 52 min at rt. a) νNH region b) νCO region.

2.3.8. Powder X-Ray Diffraction Data

Powder X-ray diffraction (XRD) measurements of compounds **2.38.**, **2.39.** (xerogels from hexane gels) and **2.40.**, **2.41.** (xerogels from toluene gels) were carried out to further investigate the structure of the self-assembled gelators. The spacings d were calculated from the Bragg's equation (for full list see Table A.1. in the Appendix). In all diffractograms (Figure 2.24.), a prominent reflection in the wide angle region corresponding to d spacing values ranging from 4.0 - 4.5 Å can be clearly observed. It can be attributed to the intermolecular distances of one molecule of gelator and the next, bonded through a network of H-bonds, $\pi - \pi$ stacking of the fluorenyl moieties and van der Waals interactions between the alkyl chains. The peaks observed for all the xerogels were broad, however the diffractograms of the C_{18} derivatives (gelators **2.39.** and **2.41.**) showed more defined reflections than their C_{14} counterparts. This suggests that the extended alkyl chain establish a more ordered gel structure. The diffraction patterns observed for the hexane xerogel of gelator **2.39.** and the toluene

xerogel of gelator **2.41.** differ significantly, which indicates that the molecular organisation in the self-assembled materials is also different.
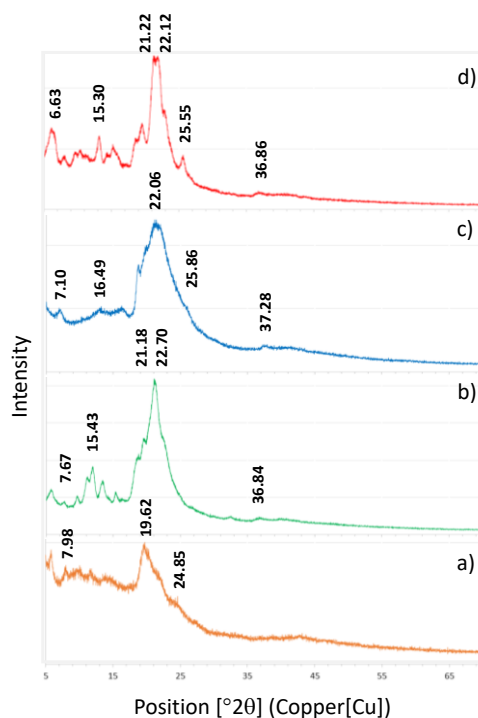
Figure 2.24. XRD diffractograms of xerogels from lipoamino acids a) **2.38.** and b) **2.39** from hexane gels; c) **2.40.** and d) **2.41.** from toluene gels. (All gels were prepared at CGC).

This is consistent with the different morphologies observed in the SEM images of the xerogels (Figure 2.19.). Although some of the observed peaks for lower 2θ values seem to follow a ratio of 1 : 1/2 : 1/3 : 1/4 (Table A.1.), which could correspond to a lamellar organisation, however it was not possible to identify this arrangement conclusively with the XRD data.[62] Parallel and antiparallel arrangements have been previously proposed for gelators containing fluorenyl groups.[59,70,109] A schematic representation of how the gelators could align to form the network, is described in Figure 2.25. a), b). From this, it is clear how the relative orientations of the lipoamino acids can lead to very different extended supramolecular structures. It is more likely that derivatives **2.38.** and **2.39.** may favour an antiparallel arrangement (lamellar structure), which would accommodate the bulky and hydrophobic *O-tert*-butyl group on the side chain, while it may be possible for gelators **2.40.** and **2.41.**, with a smaller hydroxyl group, to adopt a parallel alignment (microfibres or microbelts). These considerations could account for the observed differences in morphology and

rheological behaviour of the gels. It has previously been reported that the presence of hydroxyl groups in the structure of amphiphilic gelators affect their ability to induce the formation of a supramolecular gel.[62,63,111] Thus the hydroxyl groups can affect the H-bonding network between the gelator molecules through the formation of intra or intermolecular H-bonds or through steric factors and therefore influence their self-assembly. The presence of an intramolecular H-bond can be observed in both structures. This leads to similar patterns in the presentation of the H-bonding groups, which are not affected by the nature of the functional group in the side chain.

a)   b)
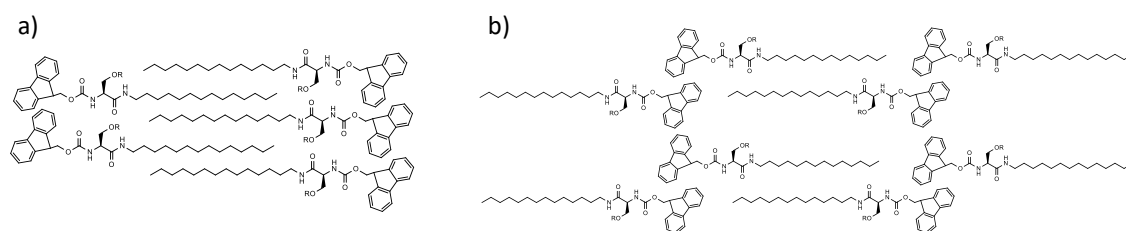
Figure 2.25. a) Schematic representation of parallel alignment proposed for the self-assembly of gelators **2.40.** and **2.41.** (not depicted). R = H; b) Schematic representation of antiparallel alignment proposed for the self-assembly of gelators **2.38.** and **2.39.** (not depicted). R = tBu.

2.3.9. Phase Selective Gelation, Malleability and Self-Healing Capability

LMWGs capable of performing organogelation in biphasic mixtures have been investigated for a range of environmental applications.[112,113] The lipoamino acids **2.38.** − **2.41.** were able to selectively gel the organic phase in biphasic aqueous mixtures. Two different tests were carried out and are explained below:

Firstly, the gelator was dissolved in a chosen organic solvent in a warm solution and poured into a vial with distilled water at rt. After several minutes, it was observed that the organogel had formed on the top, and the aqueous phase was trapped at the bottom of the vial [Figure 2.26. a) - d)].
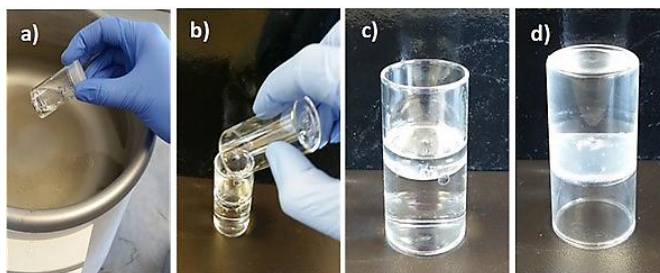
Figure 2.26. a) **2.40.** (1.3 w/v % in toluene) heated in a water bath at 45 °C; b) Introduction of the gelator solution into a vial with distilled water at rt; c) Solidified gel on the top of the distilled water in an open vial; d) Open vial was inverted, showing both layers (distilled water and gel).

Secondly, the gelation potential of these compounds were investigated using a heating-cooling cycle. A solution of the gelator in the organic solvent of choice and an aqueous phase were stirred in a water bath at 45 °C for 1 min and then allowed to cool to rt. The phases separated and an organogel formed at the top. The physical integrity of the gels permitted their easy handling and simple removal from the mixture [Figure 2.27. a) - e)].
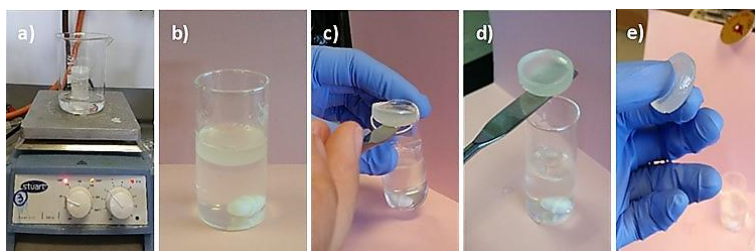
Figure 2.27. a) **2.40.** (1.3 w/v % in toluene) stirred with a magnetic bead in a vial with distilled water. The mixture was heated in a water bath at 45 °C for 1 min in a closed vial. b) The solidified gel on the top of the distilled water in an open vial after resting on the bench for 5 min. c) Removal of formed gel. d) Isolated gel on the spatula. e) Robust gel disk.

The same test was carried out with **2.38.** in petroleum ether demonstrating the ability of these gels to remove solvent spills from water. The rapid gel formation, and the ease of removal from the vial was remarkable (Figure 2.28.).
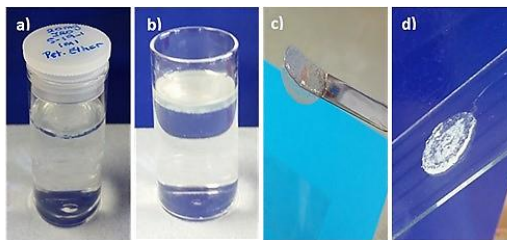
Figure 2.28. a) **2.38.** (0.4 w/v % in Pet. ether) after stirring it in a vial with distilled water. b) The solidified gel on the top of the distilled water in an open vial after resting on the bench for 5 min. c) Removal of formed gel. d) Isolated gel on a glass slide.

The SEM image of xerogel **2.40.** in toluene after biphasic gelation is shown in Figure 2.29. The microfibrous structure appeared smaller and more twisted compared to the toluene xerogel of **2.40.** shown in Figure 2.19. i). This morphology has previously been found in the self-assembled hydrogels of Fmoc supramolecular gels.[114]
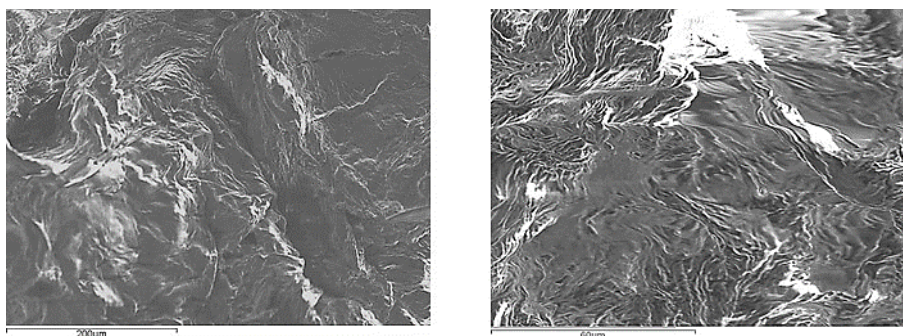
Figure 2.29. Xerogel **2.40.** in toluene after biphasic gelation at 200 and 60 μm of magnification.

The robustness of these gels allowed them to be moulded into different shapes depending on the container shape (Figure 2.30.).
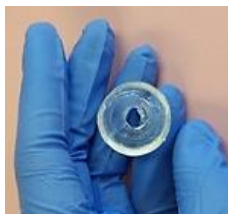
Figure 2.30. Gel malleability: gel in toluene formed by lipoamino acid **2.40.** (1.3 w/v %) moulded into a "doughnut" shape.

Interestingly, the gels also showed self-healing capabilities when severed (Figure 2.31.).
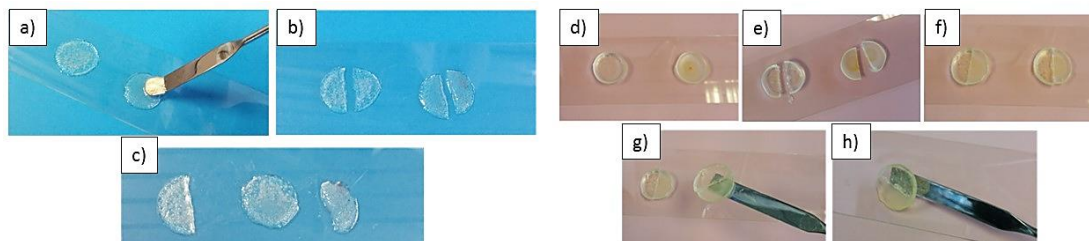
Figure 2.31. (a) Gel **2.38.** (0.4 w/v % pet. ether) moulded into two different circles; b) Gel **2.38.** cut into four semicircles c) Joined together the semicircles of gel **2.38.** and regeneration of reversible non-covalent interactions; d) Gel **2.40.** (1.3 w/v % toluene) moulded into two different circles; b) Gel **2.40.** cut into four semicircles; c) Joined together the semicircles of gel **2.40.**; d) Gel **2.40.** displayed such self-healing circles again. e) Gel **2.40.** regenerated from reversible non-covalent interactions.

2.3.10. Removal of Toxic Dyes from Water

The removal of toxic dyes from aqueous solutions using the lipoamino acid gelators was studied with the UV-Vis technique as described in section 7.3.5.4. The elimination of these and other aromatic pollutants using LMWGs has previously been reported in literature, as discussed in section 2.1.4.2.[47,92,93,115] The cationic dye rhodamine B (RhB)[92] and the anionic dye Methyl Orange (MO)[116,117] were used as a "proof of concept" for this application (Figure 2.32.).
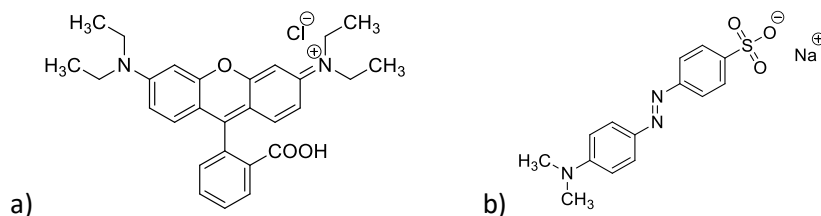
Figure 2.32. Structure of: a) Cationic dye, RhB. b) Anionic dye, MO.

Thus, an aqueous solution of RhB (0.03 mM) and MO (0.03 mM) were treated with solutions of **2.38.** (0.7 w/v % in hexane) and **2.40.** (1.3 w/v % in toluene). The mixture was allowed to settle and once the gels were formed in different vials for the four samples, they were separated from the water either manually or by gravity filtration. UV-Vis absorption spectra of the aqueous phase were recorded after treatment (Figure 2.33. for RhB and Figure 2.34. for MO). Previously, calibration curves were done for both dyes.
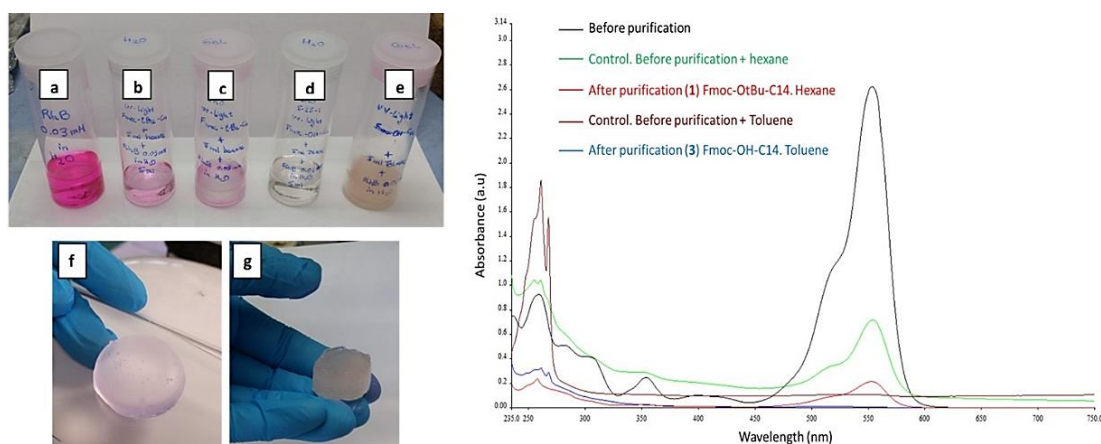
Figure 2.33. Removal of RhB from aqueous solution by phase selective gelation: *Left:* a) Aqueous solution of RhB [0.03 mM]; b) Aqueous solution of RhB before treatment with compound **2.38.** in hexane; c) Gel **2.38.** after treatment in the vial; d) Aqueous solution after treatment with compound **2.40.** in toluene; e) Gel after treatment in the vial; Isolated gels after treatment: f) **2.38** in hexane, g) **2.40.** in toluene. *Right*: UV-Vis absorption spectra of RhB aqueous solution before and after dye removal by phase selective gelation.
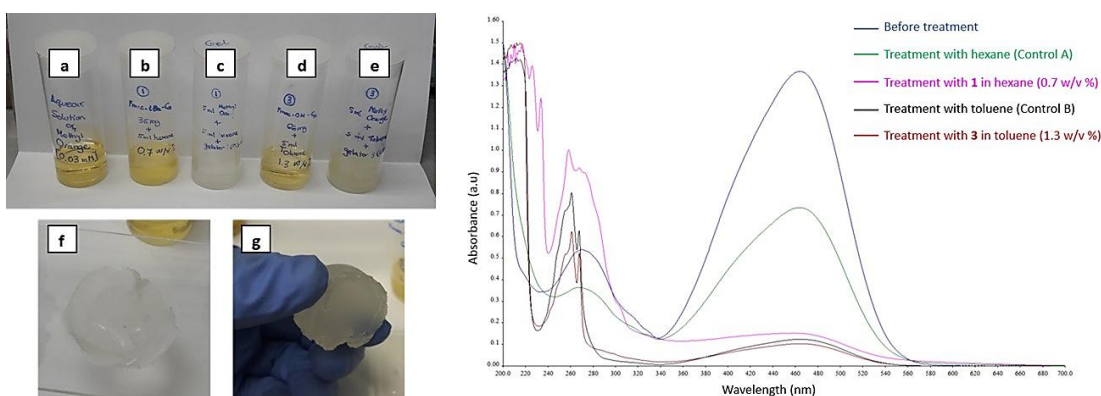
Figure 2.34. Removal of MO from aqueous solution by phase selective gelation: *Left:* a) Aqueous solution of MO [0.03 mM]; b) Aqueous solution of MO after treatment with compound **2.38.** in hexane; c) Gel **2.38.** after treatment in the vial; d) Aqueous solution after treatment with compound **2.40.** in toluene; e) Gel after treatment in the vial; Isolated gels after treatment: f) **2.38.** in hexane, g) **2.40.** in toluene. *Right*: UV-Vis absorption spectra of MO aqueous solution before and after dye removal by phase selective gelation.

The purification efficiency (E) was determined according to Equation 2.1. (A_o and A refer to absorption intensity at 553 nm for RhB and at 465 nm for MO, (Table 2.6.).

$$E = (A_o - A) \times 100 / A_o \quad \text{(Equation 2.1.)}$$

Table 2.6. Determination of purification efficiency: UV-Vis absorbance at 553 nm of aqueous phase and (RhB) before and after purification and absorbance at 465 nm of aqueous phase and (MO) before and after purification.

Aqueous Phase	Absorbance (a.u)	[RhB] (mM)	E (%)	Absorbance (a.u)	[MO] (mM)	E (%)
Before treatment	2.62	0.030	-	1.36	0.030	-
Treatment with hexane (control A)	0.71	-	-	0.73	-	-
Treatment with **2.38.** in hexane (0.7 w/v %)	0.21	0.002	**92**	0.15	0.021	**89**
Treatment with toluene (control B)	0.10	-	-	0.12	-	-
Treatment with **2.40.** in toluene (1.3 w/v %)	0.00	0.000	**100**	0.10	0.014	**93**

Controls were prepared whereby the RhB was treated with only toluene or hexane. An evident colour change in the aqueous phase after treatment indicated that the dye was extracted to the organic phase. The purification efficacy was found to be 100% when the aqueous RhB solution was treated with gelator **2.40.** in toluene, whereas it was 92% with gelator **2.38.** in hexane. While the controls also removed the dye from the aqueous phase, the purification efficiency in these cases could not be determined accurately since residual organic solvent disrupted the spectra baseline. These results indicate that the formation of the gel facilitates the removal of the dye from the aqueous phase and improves the extraction process. The entrapment of dyes in the gel network resulted in an increase in their T_{gs} (Table 2.7.).

Table 2.7. Determination of the T_{gs} with dye entrapped in the network and comparison with the T_{gs} without dye entrapped in the network.

Dye	Sample	T with dye	T without dye	**Difference**
RhB	**2.38.**	45 - 55 °C	40 - 47 °C	6.5
	2.40.	45 - 60 °C	35 - 39 °C	10
MO	**2.38.**	42 - 49 °C	40 - 47 °C	2
	2.40.	45 - 50 °C	35 - 39 °C	5

Larger differences in the T_{gs} of the gels which have RhB entrapped in the network. (45 - 55 °C for the hexane gel of **2.38.**, compared to 40 - 47 °C in absence of RhB; 45 - 60 °C for the toluene gel of **2.40.**, compared to 35 - 39 °C in absence of RhB) were

observed. In the extraction experiments with MO (42 - 49 °C for the hexane gel of **2.38.**, compared to 40 - 47 °C in absence of MO; 45 - 50 °C for the toluene gel of **2.40.** compared to 35 - 39 °C in absence of MO). This could be due to the more efficient purification of RhB or to the formation of additional interactions of this dye with the gelator molecules in the gel network (Figure 2.35.).
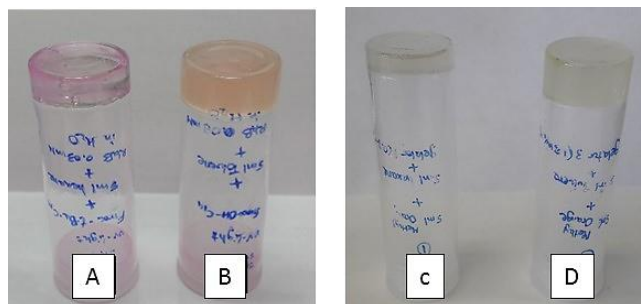
Figure 2.35. A) Gel **2.38.** and B) Gel **2.40.** after treatment with RhB in the inverted vial; C) Gel **2.38.** and B) Gel **2.40.** after treatment with MO in the inverted vial.

This remarkable increase, particularly for the toluene gel, seems to indicate that RhB was acting as a gel dopant. This observation could lead to future developments of the lipoamino acid based gels whereby doping agents structurally similar to RhB could be used to modulate the gels properties.[118] The morphology of the xerogels with the dyes entrapped in the networks was studied using SEM (Figure 2.36.).
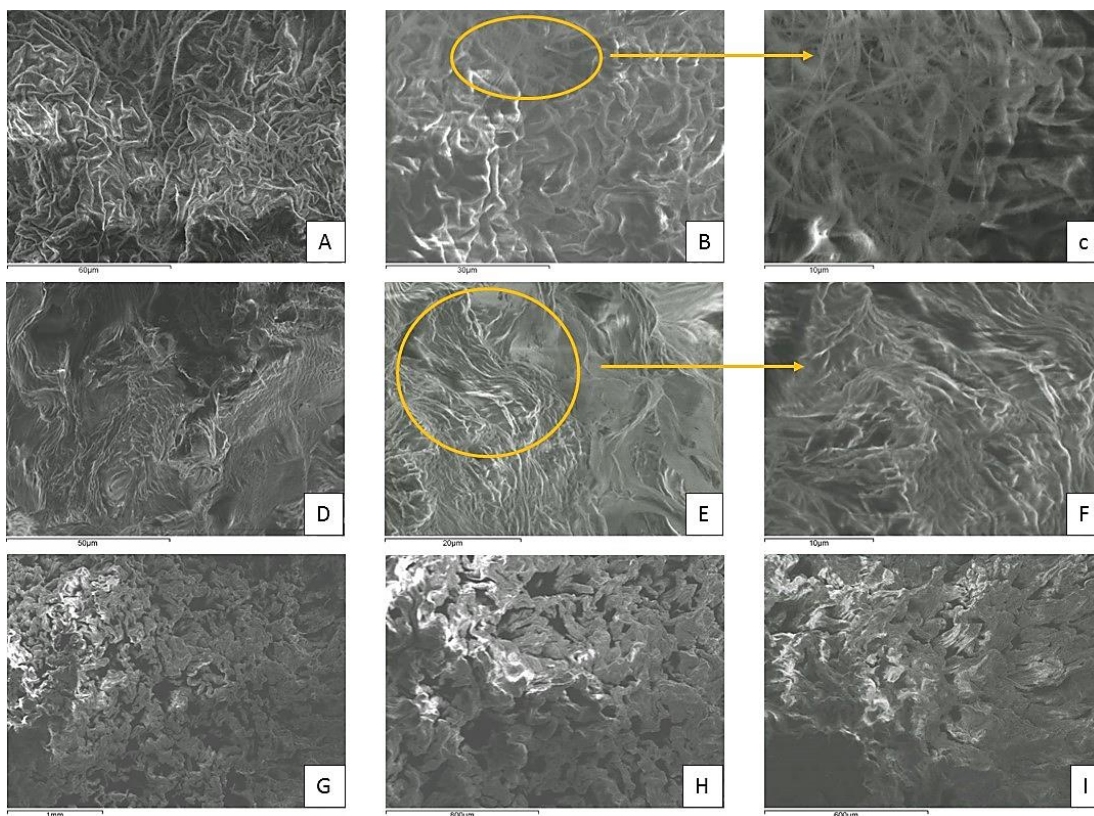
Figure 2.36. A), B), C) Hexane xerogel **2.30.** with RhB at 60 – 30 – 10 μm of magnification; D), E), F) Toluene xerogel **2.40.** with RhB at 50 – 20 – 10 μm of magnification; G), H), I) Toluene xerogel **2.40.** with MO at 1 mm – 800 – 600 μm of magnification.

The SEM images of the xerogels with (Figure 2.36.) and without [Figure 2.19. c)] **2.38.** hexane xerogel and i) **2.40.** toluene xerogel) the dye entrapped in the network show remarkable differences: an overlapping mesh of microfibres can be seen in images A - C (Figure 2.36.) from xerogel made with compound **2.38.** in hexane with RhB, however the lamellar structure of the xerogel is still visible. The images D – F (Figure 2.36.) show the xerogel made with compound **2.40.** in toluene with RhB. The microfibrous structure which was apparent in the absence of dye can still be observed, however, these fibres are smaller, and they have a twisted ribbons structure better defined than in the xerogels from biphasic gelation experiments (Figure 2.29.). The SEM images for the xerogel **2.40.** in toluene with MO have poorer definition which might be due to adsorption on the irregular, non-uniform sites of the xerogels (Images G – I, Figure 2.36.).

2.4. Conclusions

I.) The synthesis of compounds **2.38.** – **2.42.** was described and their evaluation as LMWGs in a range of organic solvents of different polarity was carried out.

II.) It was found that minor structural changes impacted the gelation abilities of LMWGs. Replacement of the side chain functional groups of *N*-Fmoc-L-serine lipoamino acids (from *O-tert*-butyl to hydroxyl) altered their solubility and self-assembly properties. For the shortest chain (C_{14}) derivatives, this structural difference achieved the selective gelation of aliphatic or aromatic solvents. The elongation of the alkyl chain length (C_{18}) improved the physical properties of the gels, however, it reduced the ability to differentiate between aliphatic and aromatic solvent gelation.

III.) Steric effects led to distinct self-assembly patterns which defined the morphology of the SAFINs and the characteristics of the gels as it was observed in the SEM images of the xerogels.

IV.) After comparing Fmoc group and Cbz analogues LMWGs, it was noticed that the presence of Fmoc group in the gelator was necessary for the gel formation.

V.) The lipoamino acids were also found to be highly effective organogelators of biphasic mixtures and enhanced the removal of organic solvents spills and toxic dyes such as RhB and MO, from aqueous solutions.

Chapter 3

Galactosylated Aspartic Acid Derivatives as LMWGs

3.1. Introduction

3.1.1. Carbohydrate-Based LMWGs

Carbohydrates have been traditionally considered as a source of energy to the organism, thus, acting as a substrate for the generation of cellular energy. However, over the last few decades, the importance of carbohydrates in the mediation of many important biological processes has been recognised. These processes include cellular communication and adhesion, fertilization and pathogen infection.[119] Supramolecular chemists aim to mimic biological architectures and functional bio-systems essential for the occurrence of life. In this regard, the self-assembly of carbohydrate-based LMWGs has received particular attention for various reasons: they may be, biocompatible, biodegradable, non-toxic and eco-friendly (Figure 3.1.). The starting materials for the synthesis of many carbohydrate-based LMWGs are commercially available and generally cheap. The gelation properties of saccharides can be easily modulated by the simple protection or deprotection of their hydroxyl groups. Thus, the structural diversity and variability of carbohydrate units, their multiple possibilities in sequence, linkage points and anomeric configuration make them uniquely suited for the creation of a wide range of organo- and hydro-gelators.[120]

Why carbohydrate?

Commercially available

Biocompatible

Carbohydrate-based LMWG

Inexpensive Precursor

Biodegradable

Non-toxic
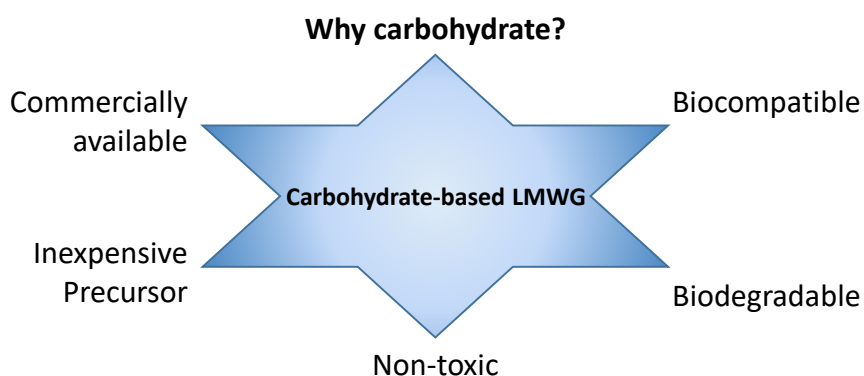
Figure 3.1. Advantages of carbohydrate-based LMWGs.[120]

Additionally, carbohydrate-based LMWGs are chiral molecules. They can exist as several stereoisomers, which usually show completely different gelation behaviour. The spatial arrangement of different diastereoisomers strongly affects their potential to form weak interactions, such as H-bonds, π - π stacking and van der Waals

interactions. Thus, changing the configuration of a single stereocentre may have a dramatic effect on the solubility, the range of solvents that can be gelled, and the physical and rheological properties of the gels formed.[43,57,58]

3.1.2. Carbohydrate-Derived Amphiphilic LMWGs

Carbohydrate-based amphiphilic LMWGs are typically composed of aliphatic hydrocarbon chains linked to hydrophilic portions which self-assemble via H-bonding and hydrophobic interactions in different solvents. As a proof of concept, some authors have focused on investigating and developing new amphiphilic-carbohydrate-based gelators which will be discussed in this section.

Shinkai and co-workers reported a new carbohydrate-based gelator, **3.1.** (Figure 3.2.) which contains a carbohydrate moiety (glucose), an aminophenyl and a long alkyl chain group. The long alkyl chain enhances its solubility in organic solvents but also promotes association between the fibres which form the network, through van der Waals forces. Compound **3.1.** can form gels in organic solvents such as butanol, hexane, DCM, $CHCl_3$, THF, DMF, EtOAc, DMSO and H_2O in the presence of a trace amount of alcohol (EtOH or MeOH $\sim$ 1 w/v %).[24]

3.1.
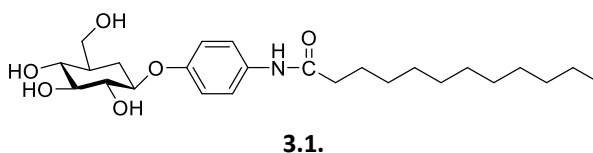
Figure 3.2. Chemical structure of glucose-based LMWG **3.1.**[24]

X-ray diffraction was used to understand the molecular packing of the gelator in the gel phase. The xerogel **3.1.** in H_2O was investigated. The molecular packing mode of gelator molecules showed periodical diffraction peaks (long spacing *d* was about 2.90, 1.46 and 0.97 nm, corresponding almost exactly to a 1:1/2:1/3 ratio) which indicated that **3.1.** self-assembles into a lamellar organisation (Figure 3.3.).
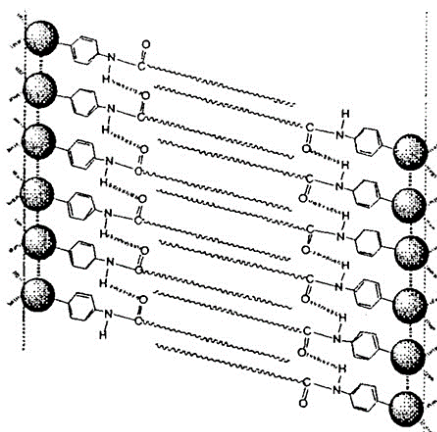
Figure 3.3. Possible lamellar self-assembled microstructure of hydrogel **3.1.**[24]

Hamachi and co-workers reported the first glycosylated amino acid LMWGs with thermal response. The authors developed a new solid phase glycolipid synthesis to obtain glycosylated amino acid derivatives **3.2.** - **3.13.** (Figure 3.4.) as supramolecular gelators that reversibly swell or shrink in response to temperature.[121] Different features were explored to improve the hydrogelation ability of this scaffold. A small library of *N*-acetyl-galactosamine-appended amino acid (GalNAc-aa) compounds **3.2.** – **3.13.** was prepared, since GalNAc derivatives showed the most effective gelation properties. Gelation ability for compound **3.2.** - **3.13.** was tested in aqueous solutions and hydrogelators were recognised by the inverted test tube method. The study indicated that structural changes such as the length of the chain or the presence of a cyclic alkane had a big effect in the gelation ability. Compounds **3.5.**, **3.6.**, **3.11.** and **3.12.** formed hydrogels (Figure 3.4).

3.2. – 3.13.

3.2. n = 1, R = (Sol.)
3.3. n = 1, R = (Sol.)
3.4. n = 0, R = (Insol.)
3.5. n = 1, R = (**Gel**)

3.6. n = 2, R = (**Gel**)
3.7. n = 1, R = (Crystl.)
3.8. n = 1, R = (Insol.)
3.9. n = 1, R = (Insol.)

3.10. n = 1, R = (Sol.)
3.11. n = 1, R = (**Gel**)
3.12. n = 1, R = (**Gel**)
3.13. n = 1, R = (Sol.)
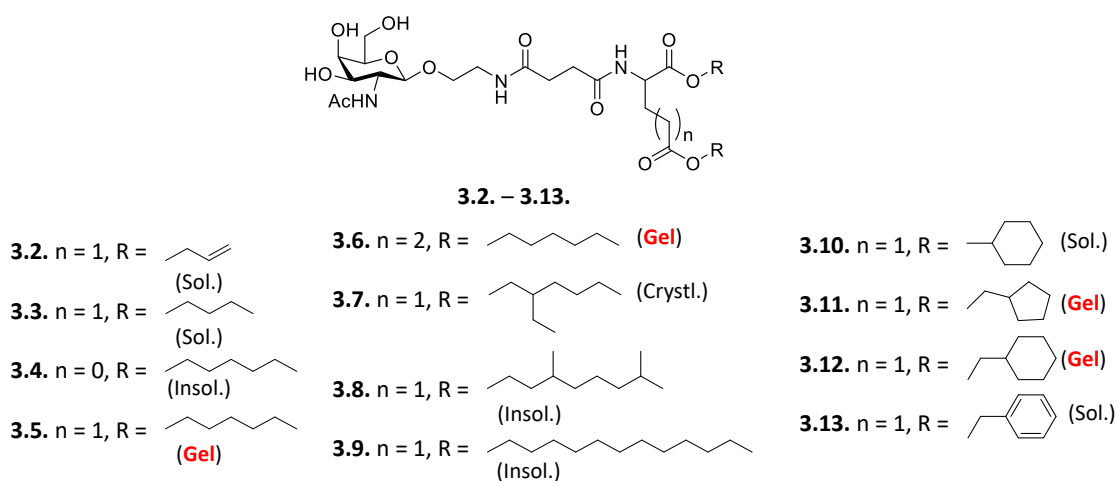
Figure 3.4. Chemical structures of Glycosylated Amino Acid LMWGs **3.2.** - **3.13.** and gelation ability.[121]

The T_{gs}, of the hydrogels formed by GalNAc-aa derivatives (ranged between 30 and 70 °C) were significantly sensitive to the molecular structure. During measurement of the T_{gs} of the hydrogel **3.12.** (containing cyclohexyl-ethyl groups), a remarkable shrinkage was noticed by heating the gelator formed in the vial due to expelling of H_2O, instead of the typical gel-sol transition. Surprisingly, the shrunken gel swelled again by cooling it so a hydrogel was formed again (Figure 3.5.).
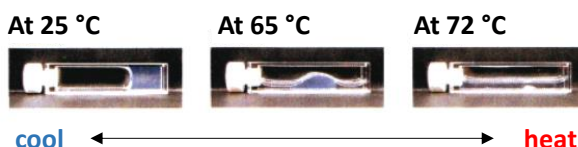
Figure 3.5. Direct observation of the T_{gs} of the thermoreversible hydrogel **3.12.**[121]

T_{gs} of **3.5.** (40 °C) having linear hydrophobic (C_7) tails was lower than that of **3.12.** (69 °C). In addition to the hydrophobic tail, the connector part also affects the phase transition behaviour as observed for gelator **3.6.** with a $T_{gs} \sim 30$ °C. On the other hand, the hydrogel **3.11.** (T_{gs} 49 °C) containing cyclopentyl-ethyl groups did not shrink by elevating the temperature, but, instead, simply displayed the conventional process. Compounds **3.2.**, **3.3.**, **3.10.** (containing cyclohexyl-methyl group) and **3.13.** (containing benzyl group) remained in solution, and did not form a gel. Slight structural modifications in the alkyl chains of compounds **3.4.**, **3.8.** and **3.9.** resulted in insoluble compounds or in crystalisation (**3.7.**). Well-defined fibrous network were observed by TEM analysis of the hydrogel formed by **3.12.**

The same authors reported some years later a simple mixture of **3.12.** with acidic molecules (**3.14.** - **3.16.**) (Figure 3.6.).[122] GalNAc-aa **3.12.**, was used as the fundamental gel matrix. Three amphiphilic carboxylic acid derivatives with different chain lengths (**3.14.** – **3.16.**) were the additional components. **3.14.** – **3.16.** were designed and synthesised with similar structural features to the hydrophobic parts of **3.12.** (Figure 3.6.). Compounds **3.14.** – **3.16**. were quite soluble in H_2O, however, they did not form a gel in H_2O. On the other hand, **3.12.** formed a stable hydrogel as discussed previously. The mixing of these components in various ratios produces solutions with distinct macroscopic phases, such as a homogeneous solution, an unstable hydrogel, and a stable hydrogel, depending on the ratio of mixing. Stable

hydrogels were formed mixing (50/50) of compound **3.12.** and compound **3.14.** or **3.15.** When mixing (75/25) of compound **3.12.** and compound **3.16.** It was observed that the gelation ability of the mixed hydrogel was influenced by the molecular structure of the acidic molecules (**3.14.** - **3.16.**). The mixture of **3.12.** and **3.15.** gelled neutral H_2O over the widest ratio range compared to the other two mixtures. The addition of excess **3.14.** - **3.16.** in different ratios with **3.12.** produced homogeneous solutions instead of a hydrogel. In the case of **3.16.**, which has the longest methylene chain (n = 10), the almost equimolar mixture ratios (~ 50/50) produced unstable hydrogels.[122]

3.12.

3.14. − 3.16.

3.14. n = 2
3.15. n = 6
3.16. n = 10
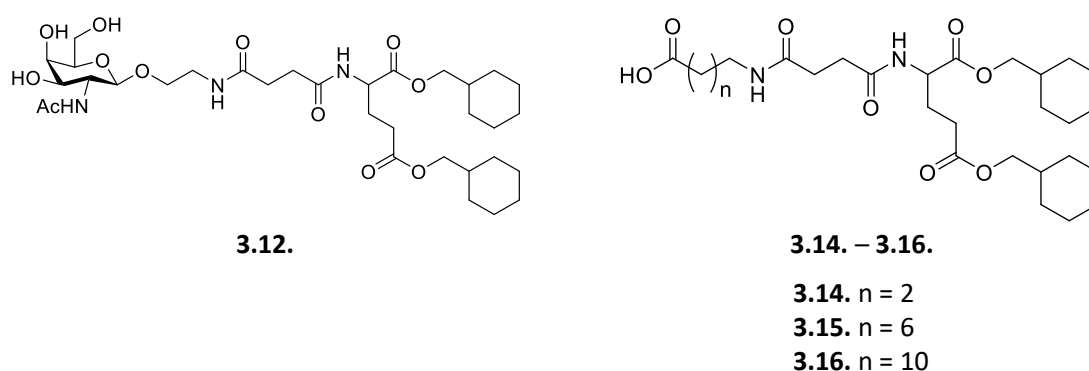
Figure 3.6. Chemical structures of **3.12.**, **3.14.** - **3.16.** which were used in different ratio mixtures for hydrogel formation.[122]

Wang and co-workers reported a large family of LMWGs (Figure 3.8.)[123-125] using simple sugar derivatives to understand their self-assembling behaviour in both organic solvents and aqueous solutions. They synthesized a series of glucose based *O*-linked carbamates (**3.17.**) and *N*-linked carbamates (**3.18.**) derivatives (Figure 3.7.). They found that several compounds were good organo-/ hydrogelators.[123-125]

3.17.   **3.18.**
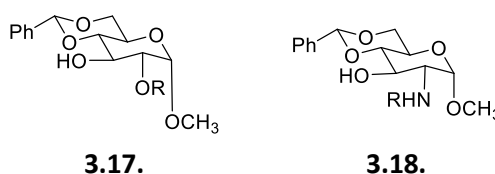
Figure 3.7. Chemical structures of glucosamine-derived headgroups **3.17.** and **3.18.**[123-125]

The structures of these good gelators (**3.19.** − **3.39.**) are shown in Figure 3.8. Compounds **3.19.** − **3.21.** are short-chain alkynyl ester derivatives that are able to

gelate both hexane and H_2O. Besides these short-chain derivatives, they also prepared a series of long-chain diacetylene-containing esters that can form polymerisable gels in EtOH:H_2O mixtures.[125] The structure-gelation ability relationship of the esters has been studied further, and it was found that the terminal alkynyl group was essential in order for the short-chain monoesters to form gels; also, functionalisation with an aryl substituent favours gel formation. Compounds **3.22.** – **3.24.** are straight-chain carbamate derivatives containing C_5, C_6 and C_7 respectively alkyl chains and they were versatile gelators in solvent mixtures such as, EtOH:H_2O (1:2) and DMSO:H_2O (1:2). Compounds **3.25.** – **3.27.**, with the 4-pentynoyl side chain, formed an opaque gel in a mixture of DMSO:H_2O (1:2) for **3.25.** and **3.27.** and a precipitate for **3.26.** However, the three compounds (**3.25.** – **3.27.**) formed transparent gels in a mixture of EtOH:H_2O (1:2). The comparable efficiency of **3.27.** with the shorter-chain derivatives was probably due to the fact that the longer alkynyl chain can increase hydrophobic interactions and compensate for the presence of the acetylene group, which may disrupt alkyl chain packing. Cyclohexyl carbamate **3.28.** formed translucent gels in EtOH:H_2O (1:2) and transparent gels in DMSO:H_2O (1:2). The other alkyl derivatives, methacrylate derivative **3.29.** and chloroethyl carbamate **3.30.**, were not able to form gels in any solvents tested. However, phenyl derivative **3.31.** and bromo-phenyl derivative **3.32.** showed excellent gelation properties in aqueous solutions [EtOH:H_2O (1:2) and DMSO:H_2O (1:2)]. Naphthyl derivative **3.33.** was able to form gels only in the a mixture of DMSO:H_2O (1:2). Compounds **3.34.** – **3.39.** also showed good gelation properties in aqueous solutions [H_2O, EtOH:H_2O (1:2) and DMSO:H_2O (1:2)] and other solvents such as EtOH, hexane, xylene, toluene and isopropyl alcohol, compared to compounds **3.19.** – **3.33.** which were less effective gelators. Comparing compounds **3.34.** – **3.39.**, the short alkyl derivatives were the most effective gelators. Ethyl derivative **3.34.** and isobutyl derivative **3.36.** were able to form gels in pure H_2O at concentrations lower than 1 w/v %. Isobutyl derivative **3.36.** was a very efficient gelator for most of the solvents tested; in contrast, analogues **3.35.** and **3.37.** did not form gels in H_2O. The isobutyl group seemed to play an important role in the molecular assembly by disturbing the ordered packing of the straight propyl chain and increasing the interactions with the solvents. However, compound **3.34.** – **3.38.** were able to form gels in both EtOH:H_2O

(1:2) and DMSO:H$_2$O (1:2)] at about 2 mg/mL or lower concentrations, whereas, compound **3.39.** formed a gel only in DMSO:H$_2$O (1:2) at a higher concentration than its analogue **3.31.** These results were interesting in terms of understanding the differences in the gelation trends between the *N*-linked and *O*-linked carbamates.

In summary, the saturated alkyl and cyclohexyl derivatives showed excellent gelation properties. Compound **3.19.** – **3.39**. were excellent gelators in aqueous mixtures of EtOH or DMSO. Switching the positions of the nitrogen and oxygen atoms of the carbamates (*N*-linked carbamates) also gave compounds (**3.34.** – **3.39.**) with better gelation ability. The ethyl (**3.34.**) and isobutyl (**3.36.**) carbamates were exceptionally good gelators and were able to form gels in pure H$_2$O, pure EtOH, aqueous solutions [EtOH:H$_2$O (1:2) and DMSO:H$_2$O (1:2)], and some organic solvents.
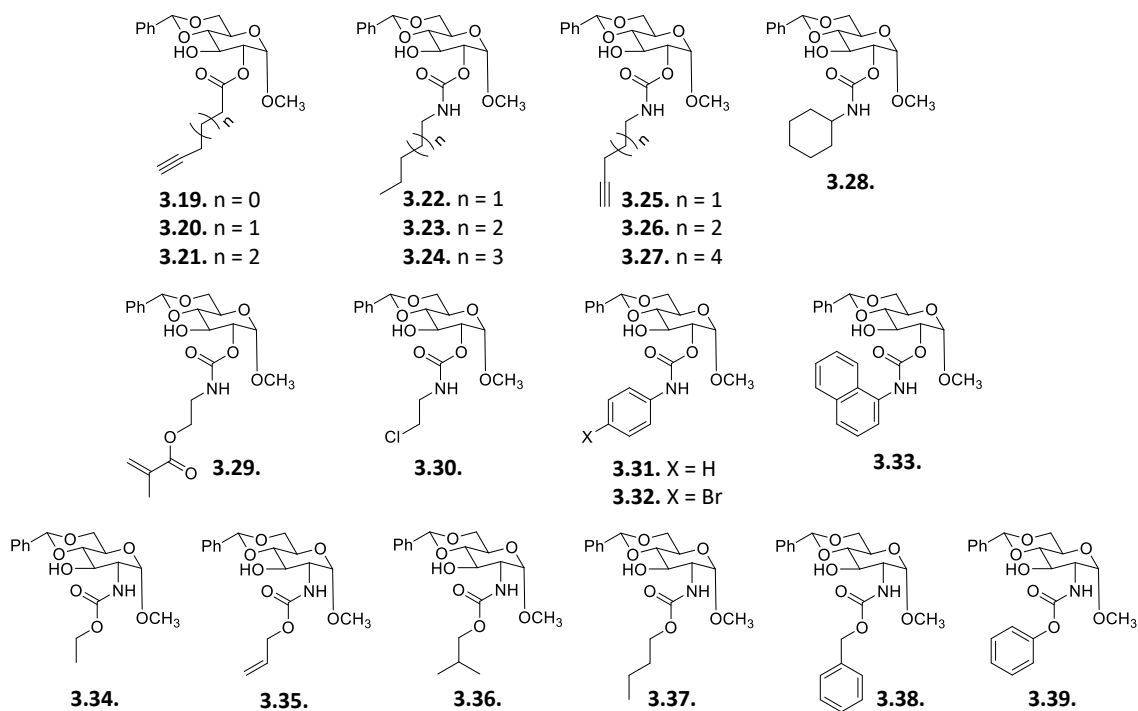
Figure 3.8. Chemical structures of **3.19.** – **3.39.** Few of them were good organo-/hydrogelators.[123-125]

Clemente and co-workers synthesised and studied the liquid crystalline and gel-forming properties of a new family of amphiphilic glycolipids containing a disaccharide polar head (Figure 3.9.). Compounds **3.40.** – **3.43.** were a combination of maltose as a hydrophilic head and a palmitic fatty chain as a hydrophobic tail

connected by a triazol linker in some cases. Phenylalanine was also incorporated in some of them in order to favour the gel formation by π-π stacking.
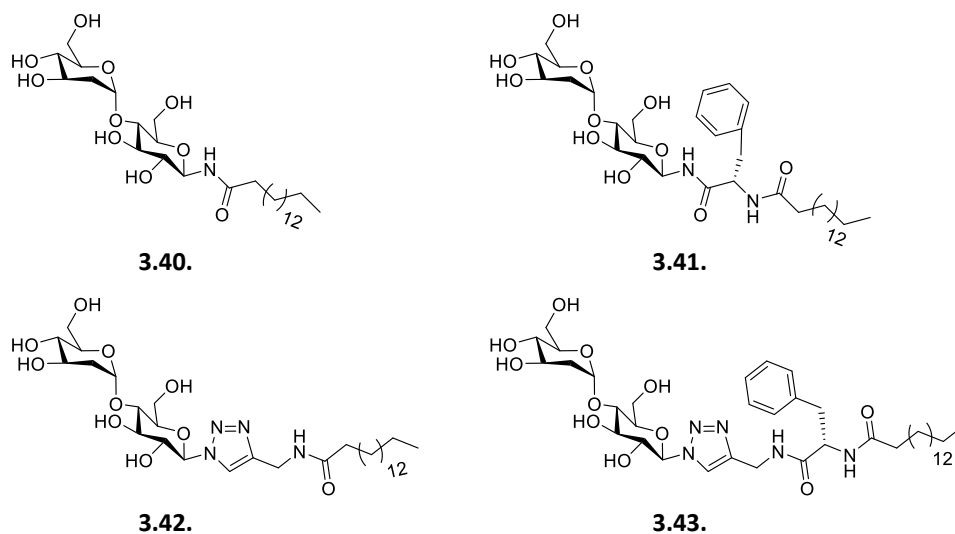
Figure 3.9. Chemical structures of glycolipids **3.40. – 3.43.**[126]

They examined the gelation ability of the amphiphilic glycolipids in different solvents. Glycoamphiphiles **3.40. – 3.43.** were insoluble in hexane, EtOAc, DCM and acetone, however, they were soluble in DMSO. **3.40.** did not form gels in any solvents. **3.42.** formed an opac gel in H_2O (Figure 3.10.) at a minimum concentration of 1 w/v % and in the absence of other organic solvents. **3.43.** also formed a stable gel in H_2O but it was found to be inhomogeneous as some precipitate was observed within the gel structure once it had cooled. The addition of MeOH as an organic solvent led to the formation of a homogeneous and stable gel in a mixture of H_2O:MeOH (3:1).In addition, **3.41.** formed a gel in a mixture of H_2O:MeOH (3:2). In all cases, the glycoamphiphiles gels (**3.40. – 3.43.**) were thermoreversible, having $T_{gs} \sim 60 - 80$ °C, and they were stable at rt. The self-assembled structure of the xerogels from compounds **3.41. - 3.43.** were studied by SEM, which revealed the typical fibrillar network that characterises the supramolecular gels. SEM imaging of the xerogel obtained from **3.42.** (gel formed in H_2O) showed a fibrillar structure with a diameter of ~ 80 nm and a length of several micrometers (Figure 3.10.).
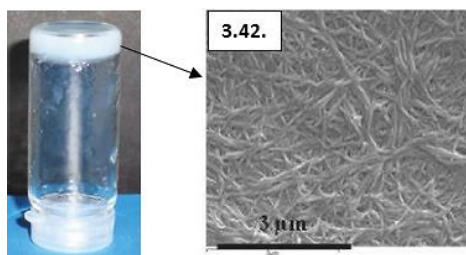
Figure 3.10. Physical appearance of the hydrogel and SEM image of xerogel formed by compound in H_2O **3.42.**[126]

3.1.3. Aspartic Acid-Based LMWGs

Amino acid-based supramolecular gelators based on aspartic acid, alanine and glutamic acid as building blocks have been reported in literature since the 1990's. [127-129] N-acyl amino acids are amphiphilic molecules that can form hydrophobic interactions between long hydrocarbon chain moieties, which are essential for the supramolecular self-assemble.

Imae and co-workers investigated the construction of N-acyl-L-aspartic acids (C_nAsp, n = 10, 12, 14, 16, 18) (Figure 3.11.), and their possible molecular arrangements to form helical self-assembled fibres in aqueous solutions at pH 5 – 6.
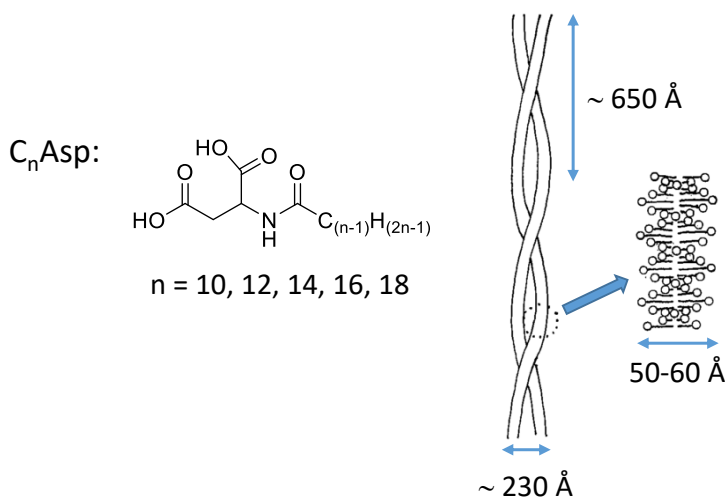
Figure 3.11. Schematic representation of a possible model for C_nAsp helical fibres.[127,128]

They reported transmission electron microscope (TEM) images to prove the formation of helical fibres in C_nAsp hydrogels at very low gelator concentrations (Figure 3.11.). They focused in the SAXS analysis for a gel-like structure in aqueous solution, (6 w/v % $C_{16}Asp$). Three Bragg peaks which corresponded to the spacings R

= 43, 112, and 233 Å, were calculated from the diffraction pattern. The minimum and maximum widths of the cross-section were ~120 and ~200 Å, respectively, and the helical pitch of the fibres was ~650 Å. Fibres were partly associated by lateral interaction. The spacing of ~230 Å obtained from a SAXS experiment was assigned to the repeating distance between the parallel orderings of fibres. Then the ~110 Å spacing corresponded to the second order of ~230 Å spacing. The 43 Å spacing may be the higher order of ~230 Å spacing or the helical pitch of the unit chain. In addition, these scaffolds provided H-bonding between amide and carboxylate groups.[127,128]

In a study comparable to those discussed in section 3.1.2. by the same group, Hamachi and co-workers reported a small library of synthetic glycolipids with different carbohydrates head structures (glucose, galactose or mannose). Aspartic acid was used as a linker to connect the carbohydrate head and the lipid part of the molecule and additionally provided a charged carboxylate group. Galactosyl derivative **3.44.**, (Figure 3.12.) did not form gels in H_2O which was the only solvent tested, however, **3.44.** formed stable aggregates with spherical vesicle morphology, consisting of bilayer membranes.

3.44.
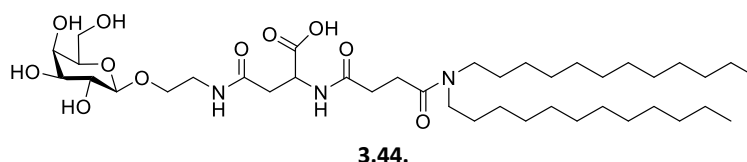
Figure 3.12. Chemical structure of aspartic acid-glycolipid **3.17.**[129]

3.2. Aims and objectives of Chapter 3

This chapter deals with the optimisation of the synthesis of a variety of amphiphilic galactosylated derivatives of L-aspartic acid previously reported by the Velasco-Torrijos research group[130] and the study of their ability to form supramolecular organo- and hydrogels. The aim of this chapter is to correlate structural features of these derivatives to their gelation ability. The structural features (Figure 3.13.) to be investigated were:

I.) The length of the alkyl chain (C_3 vs C_{14} in the amide chain and C_2 vs C_{10} in the acid chain).

II.) The α-C chirality (single diastereoisomer vs mixture of diastereoisomers).

III.) The connection of the carbohydrate moiety to the aspartic acid core (*O*-linked glycolipid vs *N*-liked glycolipid).

Aspartic acid was chosen as it provides a convenient core which allows for the introduction of multiple functionality. As a result, a range of structurally diverse LMWGs were synthesised and fully characterised to investigate how variations in structure affect the gelation process and their properties (Figure 3.13.).

Analogous synthetic routes were followed to provide access to aspartic acid derivatives, (either L-enantiomer or L/R racemic building blocks), which lead to the final glycolipids as single compounds or mixtures of diastereoisomers, respectively. Different coupling agents were explored to optimise the synthesis.
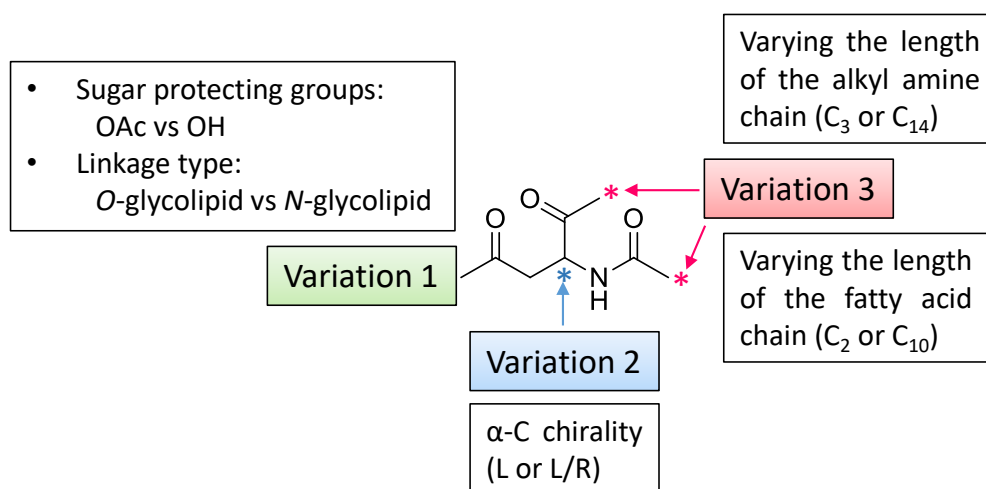
Figure 3.13. The structural features to be investigated from an aspartic acid core.

The structure of the different derivatives synthesised and evaluated as LMWGs is shown in Figure 3.14.
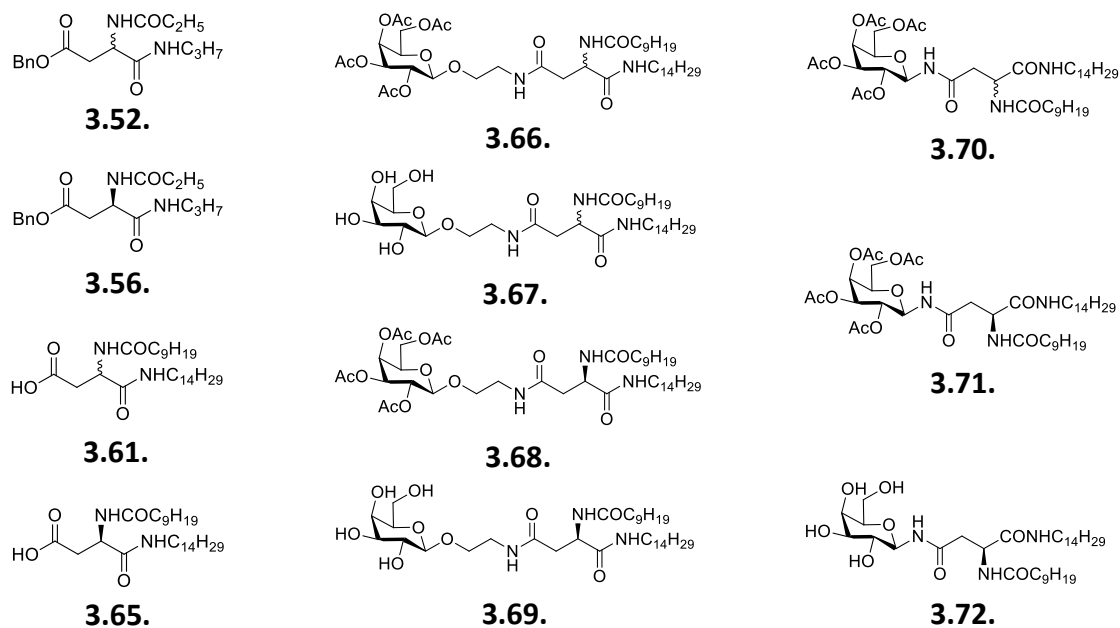
Figure 3.14. Chemical structures of crystals **3.52.** and **3.56.** and LMWGs **3.61.**, **3.66.** - **3.72.** generated from an aspartic acid core.

3.3. Results and Discussion

3.3.1. Synthesis of Aspartic Acid Amphiphilic Core

As mentioned earlier, previous work carried out in the Velasco-Torrijos research group described the synthesis of a series of galactosylated amphiphiles based on an aspartic acid core.[130] In this preliminary work, it was observed that, if TBTU was used to activate the α-carboxylic acid, the presence of a base such as NEt₃ lead to the racemisation of the product. In the absence of base, the racemisation did not occur, albeit the reaction yield was poor. One aim of the current study was to investigate if alternative coupling reagents produced the same effect in the chirality of the aspartic acid core. For this reason, reaction conditions that may improve the yield of this first step were explored (Table 3.1.).

Table 3.1. Optimisation of the reaction conditions for the coupling of *N*-(tert-Butoxycarbonyl)-*L*-aspartic acid-4-Benzyl ester and tetradecylamine.

3.58. (D,L)
3.62. (L)
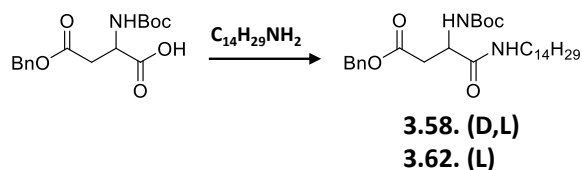
Entry	Solvent	Coupling reagent	HOBt	NEt₃	Time	Yield	[α]_D	Temperature (°C)
1	DMF	TBTU	1.1 eq	Yes	18 h	62 %	0	rt
2	DMF	TBTU	1.1 eq	No	19 h	18 %	20	rt
3	DMF	TBTU	1.1 eq	Yes	21 h	48 %	26	- 20 °C (1 h), rt
4	DMF	DIC	1.2 eq	Yes	19 h	47 %	10	rt
5	DMF	DIC	1.2 eq	No	18 h	98 %	40	rt
6	DCM	DIC	1.2 eq	Yes	17 h	9 %	17	rt
7	DCM	DIC	1.2 eq	No	17 h	75 %	19	rt
8	THF	DMTMM	-	No	19 h	10 %	35	rt

Commercially available *N*-(tert-Butoxycarbonyl)-*L*-aspartic acid-4-Benzyl ester was reacted with tetradecylamine using TBTU, DIC or DMTMM as coupling reagents, in the presence/absence of NEt₃ as a base. Different reaction solvents (DMF, DCM or THF) and temperatures were used as indicated in Table 3.1. The results from the different reactions seem to indicate that when using TBTU as a coupling reagent, not only the base but also the reaction temperature influence the racemisation of the product (Entries 1 - 3). It was found that the presence of NEt₃ also resulted in partial racemisation when DIC was used as the coupling reagent (Entries 4 and 6). Racemisation took place if the DIC coupling was carried out in DMF or DCM as a solvent and in the presence/absence of NEt₃ as a base (Entries 4 - 7). The best results in terms of yield and optical purity were obtained for: **3.62.** (L), if the coupling reaction was carried out using DIC in DMF and at rt (Entry 5) and for **3.58.** (D,L), if the coupling reaction was carried out using TBTU in the presence of NEt₃ in DMF and at rt (Entry 1). Thus, both the racemic **3.58.** (D,L) and enantiomerically pure **3.62.** (L) could be accessed upon selection of the appropriate reaction conditions.
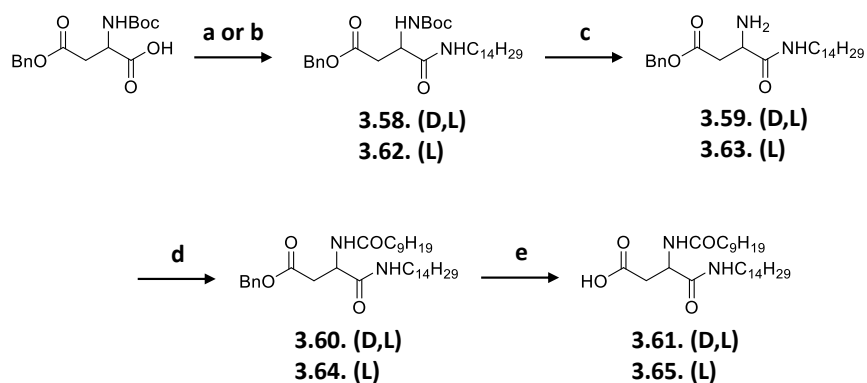
Scheme 3.1. Synthesis of aspartic acid amphiphilic core; Reagents and conditions: a) HOBt, TBTU, NEt$_3$, DMF, C$_{14}$H$_{29}$NH$_2$, under N$_2$, rt, 18 h (**3.58.**, 62 %); b) HOBt, DIC, DMF, C$_{14}$H$_{29}$NH$_2$, under N$_2$, rt, 18 h (**3.62.**, 98 %); c) DCM, 50 % TFA in DCM, 0 °C (30 min) to rt, 4 h (**3.59.**, 95 %; **3.63.**, 92 %); d) HOBt, TBTU, DMF, decanoic acid, NEt$_3$, under N$_2$, rt, 18 h (**3.60.**, 97 %; **3.64.**, 99 %); e) EtOAc, Pd/C, under H$_2$, 50 °C (4 h) to rt, overnight (**3.61.**, 99 %; **3.65.**, 99 %).

The synthesis of the aspartic acid amphiphilic core is shown in Scheme 3.1. After reaction of *N*-Boc-*L*-aspartic acid-4-Benzyl ester with tetradecylamine, *N*-Boc protecting group in **3.58.** (D,L) and **3.62.** (L) was removed with TFA to afford the amine **3.59.** (D,L) or **3.63.** (L). This was acylated with decanoic acid using TBTU / HOBt methodology to give compounds **3.60.** (D,L) or **3.64.** (L). Hydrogenolysis of the side chain benzyl ester of compound **3.60.** (D,L) or **3.64.** (L), (carried out at 50 °C and H$_2$ bubbled through for 4 h) afforded the desired L-aspartic acid **3.61.** (D,L) or **3.65.** (L), in quantitative yield.

The mechanisms of the coupling reactions are similar (mechanism for TBTU is shown in Scheme 3.2. and for DIC is shown in Scheme 3.3.). TBTU and HOBt are commonly used as coupling reagents in amide bond formation. The activation of the carboxylic acid by TBTU allows for it to be attacked by the coupling additive HOBt and form an active ester intermediate. Thus, HOBt suppresses racemization of the alpha carbon. The active ester subsequently reacts with the amine to give the corresponding amide bond.

The mechanism of the coupling mediated by DIC is similar; in this case, the carboxylic acid attacks the electrophilic carbodiimide carbon, which allows for the attack of the HOBt and formation of the active ester and diisopropyl urea as the leaving group.
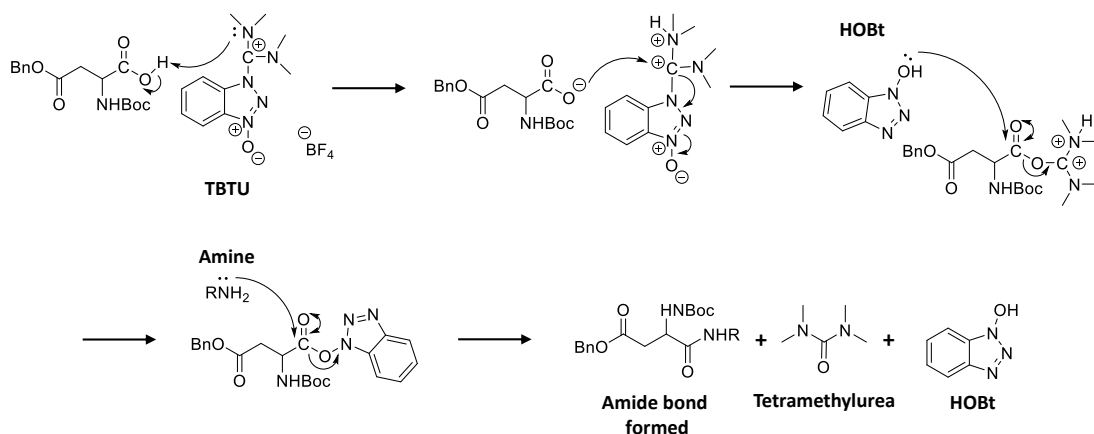
Scheme 3.2. Mechanism of TBTU and HOBt coupling reagent to form a new amide bond.
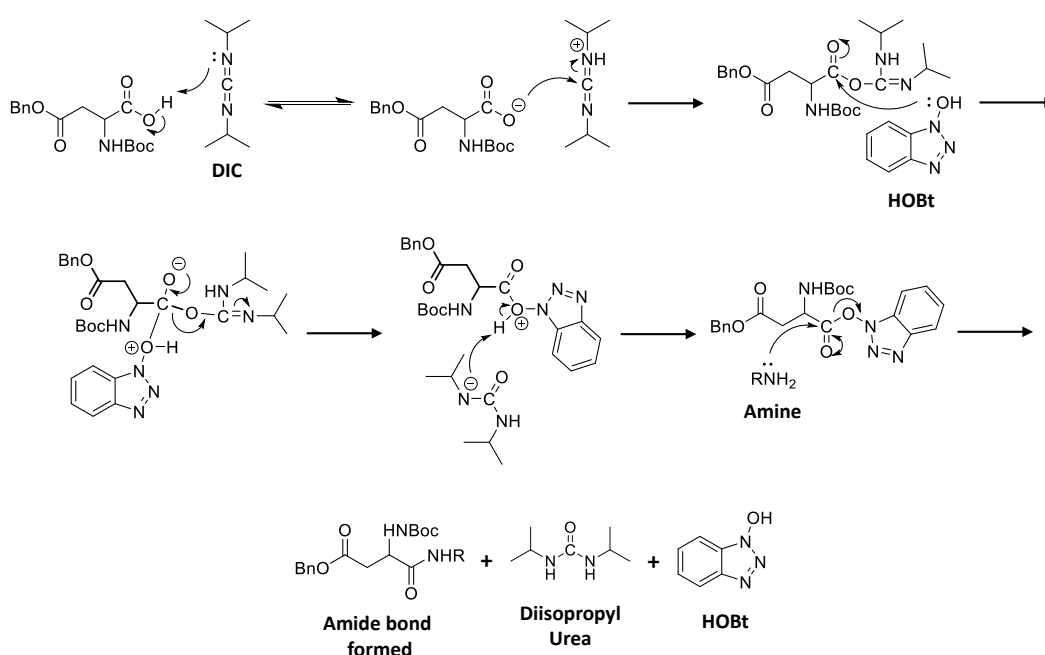
Scheme 3.3. Mechanism of DIC and HOBt coupling reagent to form a new amide bond.

3.3.2. Synthesis of Galactosyl Amino Derivatives 3.47. and 3.49.

The synthesis of β-galactosyl amino derivatives **3.47.**[131] and **3.49.**[132] was readily achieved as shown in Scheme 3.4. and Scheme 3.6., respectively. The first step in the synthesis of 2-amino-ethyl-β-galactoside **3.47.** was the reaction of commercially available β-D-galactose pentaacetate with 2-chloroethanol under Lewis acid activation (BF_3-Et_2O) (Scheme 3.4.).
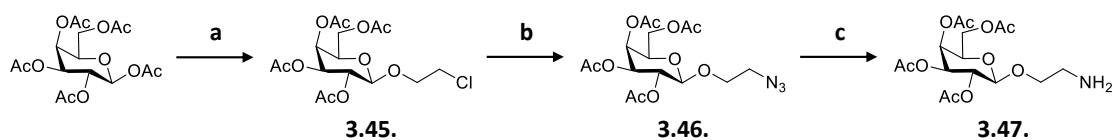
Scheme 3.4. Synthesis of *O*-glycolipid; Reagents and conditions: a) BF_3-Et_2O, $ClCH_2CH_2OH$, DCM, 3 Å MS, under N_2, 0 °C to rt, overnight (45 %); b) NaN_3, DMF, 80 °C, 16 h (53 %); c) EtOAc, Pd/C, under H_2, rt, 4 h (97 %).[133]

The mechanism for this glycosylation reaction is shown in Scheme 3.5. BF_3 promotes the formation of the oxycarbenium ion by coordination to the anomeric acetyl group. The acetyl group at the 2 position contributes to the stabilisation of the oxycarbenium ion, at the same time, this prevents attack of the nucleophile from the axial position, favouring the formation of the *β*-glycoside exclusively.
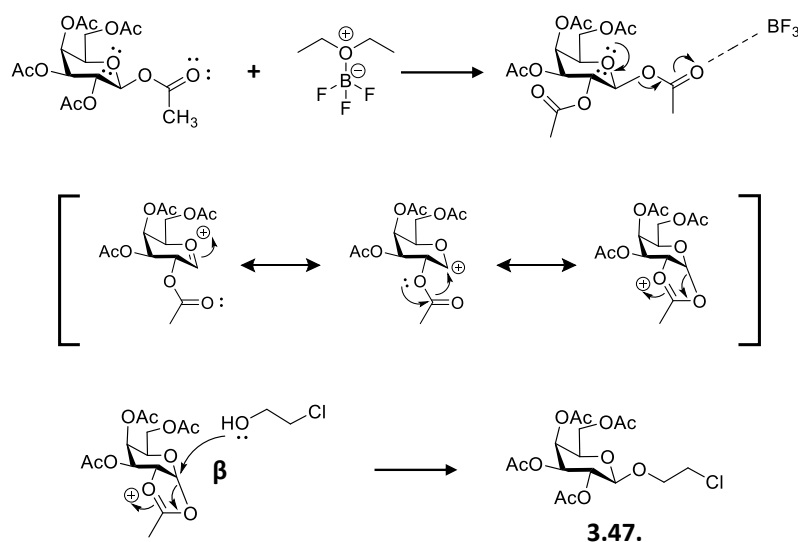
Scheme 3.5. Glycosylation reaction mechanism.

The glycosylation reaction conditions were optimsed to carry out the reaction in gram scale and galactoside **3.45.** could be obtained without the need for chromatography column purification.[133] Crude product **3.45.** was recrystallised in EtOH which obtained the compound in moderate yield (45 %). The chloride of glycoside **3.45.**[134] was then substituted with an azido moiety by reaction of NaN_3 in DMF at 80 °C, to yield the galactosyl azide intermediate **3.46.**[135] in 53 % yield and again without a need for a chromatography column purification. The final step involved the reduction of the azide to the amine using Pd catalysed hydrogenolysis in EtOAc to yield the free amine **3.47.**[131] in 97 % yield.

The glycosylation reaction for the synthesis of 1-amino-galactoside **3.49.**[132] (Scheme 3.6.) was carried out from commercially available β-D-galactose pentaacetate under Lewis acid activation (SnCl$_4$) and trimethylsilyl azide (TMSN$_3$) as the glycosyl acceptor.
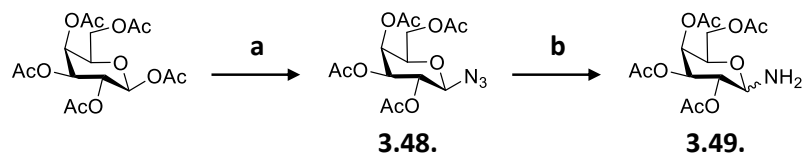
Scheme 3.6. Synthesis of N-glycolipid; Reagents and conditions: a) TMSN$_3$, DCM, SnCl$_4$ 1 M in DCM, rt, 18 h (97 %); b) EtOAc, Pd/C, under H$_2$, rt, 18 h (97 %).

The desired galactoside **3.48.**[136] was obtained in 97 % yield as the β product exclusively. The reduction of the azido to the amine was done by Pd catalysed hydrogenolysis in EtOAc to yield the free amine **3.49.** in 97 % yield.

3.3.3. Synthesis of Aspartic Acid based O-Glycolipids

The synthesis of the L-aspartic acid based O-glycolipids **3.66.** and **3.68.**[130] (Scheme 3.7.) commenced with the coupling of the aspartic acid building block **3.61.** (D,L) or **3.65.** (L) with the primary amine of the galactoside **3.47.** using TBTU as coupling reagent. The coupling yielded the acetylated glycolipids **3.66.** (D,L) in 73 % yield or **3.68.** (L) in 75 % yield. The hydrolysis of the galactose acetyl protecting groups in **3.66.** and **3.68.** gave the corresponding glycolipids (**3.67.** (D,L) in 79 % yield or **3.69.** (L) in 76 % yield).
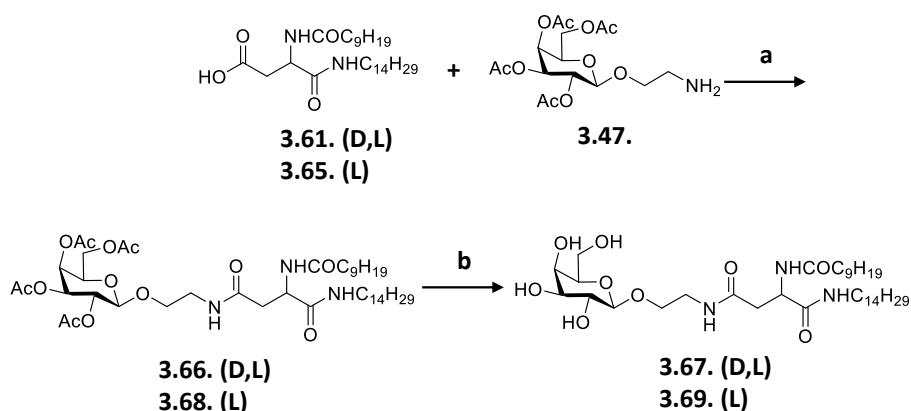
Scheme 3.7. Synthesis of Aspartic acid based O-glycolipids; Reagents and conditions: a) HOBt, TBTU, DMF, under N$_2$, 30 °C (10 min) to rt, overnight (**3.66.**, 73 %; **3.68.**, 75 %); b) NEt$_3$, DCM/MeOH/H$_2$O (1:2:1), 40 °C, 18 h (**3.67.**, 79 %; **3.69.**, 76 %).

Figure 3.15. shows the ^{1}H NMR spectrum of compound **3.66.** (D,L) in CDCl$_3$. Characteristic peaks such as NH of the amide groups, anomeric H$_1$ from galactose, α-H, β-H and β'-H and methyl from the acetyl groups were assigned in the spectrum. The duplication in the signals clearly indicates the presence of a mixture of diastereoisomers (1:1), as a result of the racemisation of the aspartic acid core. The spectroscopic data correlates well with the original one reported for this compound. The synthetic route used in this thesis is more convergent than the original on previous work carried out in the Velasco-Torrijos research group.[130] In addition, the overall yield of **3.66.** was improved.
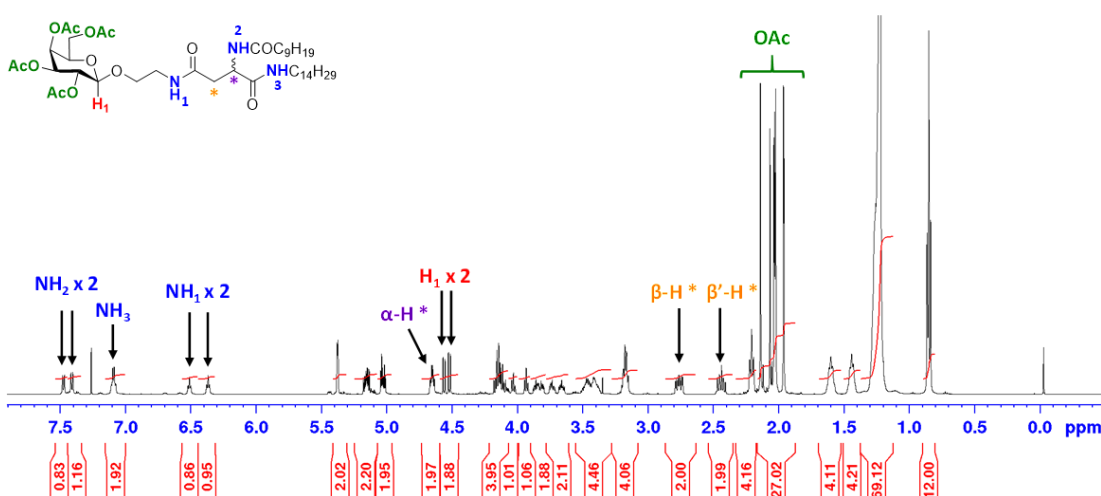
Figure 3.15. ^{1}H NMR spectrum of compound **3.66.** (CDCl$_3$, 500 MHz).

Figure 3.16. shows the ^{1}H NMR spectrum of compound **3.68.** (L) in CDCl$_3$. Characteristic peaks such as NH of the amide groups, anomeric H$_1$ from galactose, α-H, β-H and β'-H and methyl from the acetyl groups were assigned in the spectrum. In this case duplication in the signals was not observed confirming the presence of a single diastereoisomer.
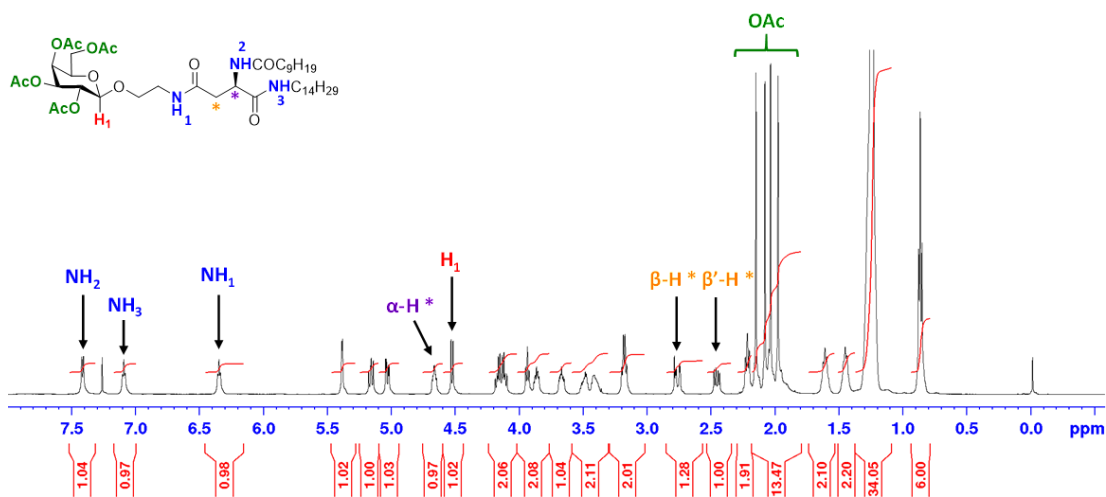
Figure 3.16. ^{1}H NMR spectrum of compound **3.68.** (CDCl$_3$, 500 MHz).

Figure 3.17. shows the ^{1}H NMR spectrum of deprotected glycolipid **3.67.** (D,L) in d_5-Pyr. Characteristic peaks such as NH of the amide groups, anomeric H$_1$ from galactose, α-H, β-H and β'-H were assigned in the spectrum. Interestingly, when the acetyl protecting groups were deprotected to free hydroxyl groups, to give compound **3.67.** (D,L), the duplication of the signals in the ^{1}H NMR spectrum could not be observed anymore. This could be due to the fact that the deprotected glycolipid has a tendency to aggregate as it eliminates the subtle differences in the chemical environment of the two diastereoisomers that lead to signal splitting in the acetylated glycolipid.
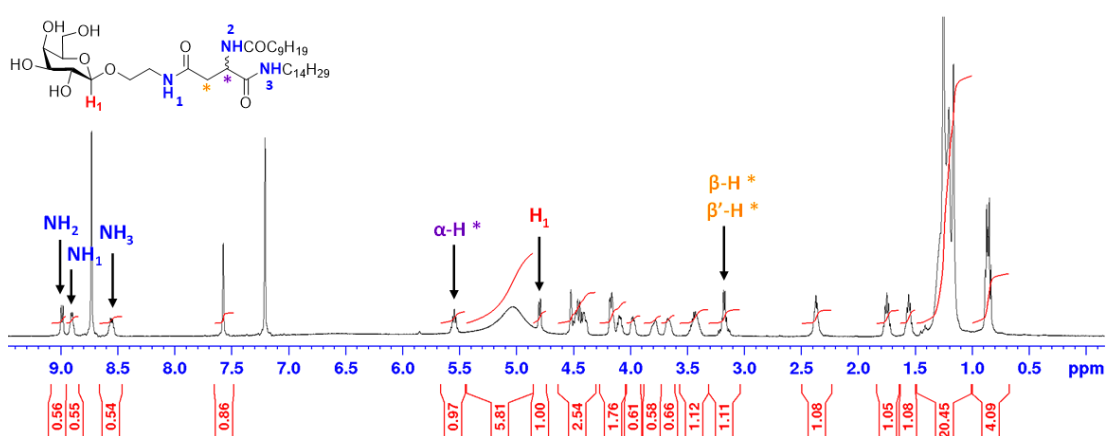
Figure 3.17. ^{1}H NMR spectrum of compound **3.67.** (D_5-Pyr, 500 MHz).

Figure 3.18. shows the ^{1}H NMR spectrum of deprotected glycolipid **3.69.** (L) in D_5-Pyr. Characteristic peaks such as NH of the amide groups, anomeric H_1 from galactose, α-H, β-H and β'-H were assigned in the spectrum.
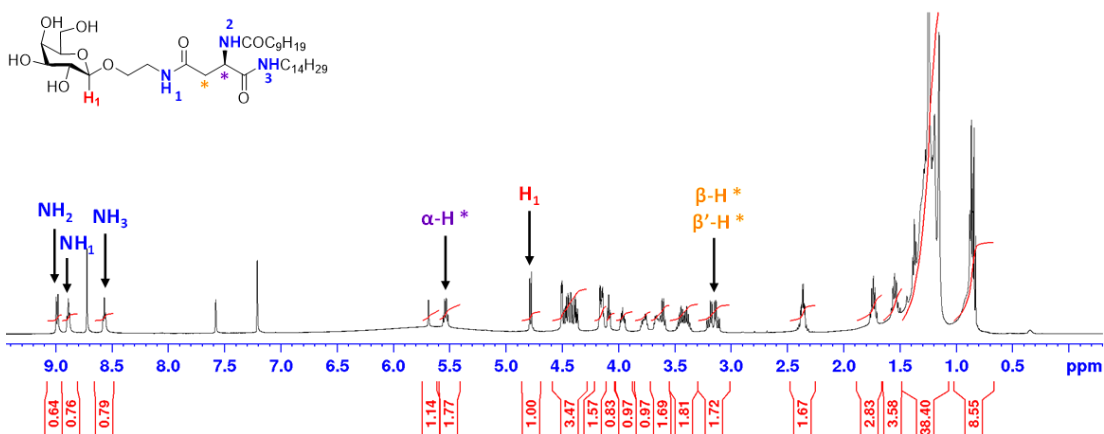
Figure 3.18. ^{1}H NMR spectrum of compound **3.69.** (D_5-Pyr, 500 MHz).

3.3.4. Synthesis of Aspartic Acid based *N*-Glycolipids

The synthesis of the L-aspartic acid based *N*-glycolipids **3.70.** and **3.71.** (Scheme 3.8.) commenced with the coupling of the aspartic acid building block **3.61.** (D/L) or **3.65.** (L). When enantiomerically pure aspartic acid, **3.65.** (L), was reacted with amino galactose **3.49.**, using TBTU / HOBt as coupling reagent, the single diastereoisomer glycolipid **3.71.** (L) was isolated as the *β*-anomer after column chromatography in 44 % yield. Figure 3.19. shows the ^{1}H NMR spectrum of compound **3.71.** (L) in CDCl$_3$. Characteristic peaks such as NH of the amide groups, anomeric H_1 from galactose, α-H, β-H and β'-H and methyl from the acetyl groups were assigned in the spectrum.
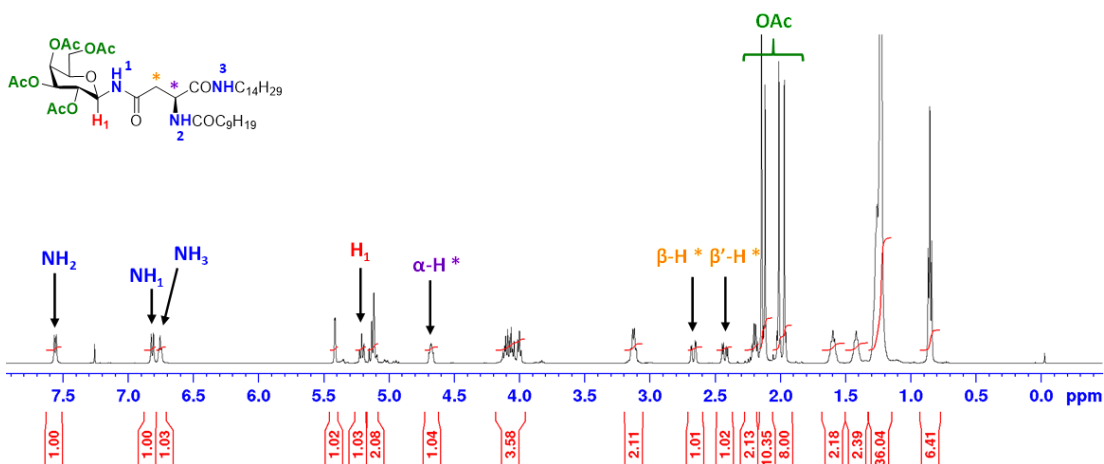
Figure 3.19. ^{1}H NMR spectrum of compound **3.71.** (CDCl$_3$, 500 MHz).

Figure 3.20. shows the ^{1}H NMR spectrum of the subsequent deacetylation of glycolipid to give the free hydroxyl groups-*N*-glycolipid compound **3.72.** (L) (Scheme 3.8.) in D_5-Pyr. Characteristic peaks such as NH of the amide groups, anomeric H_1 from galactose, α-H, β-H and β'-H were assigned in the spectrum.
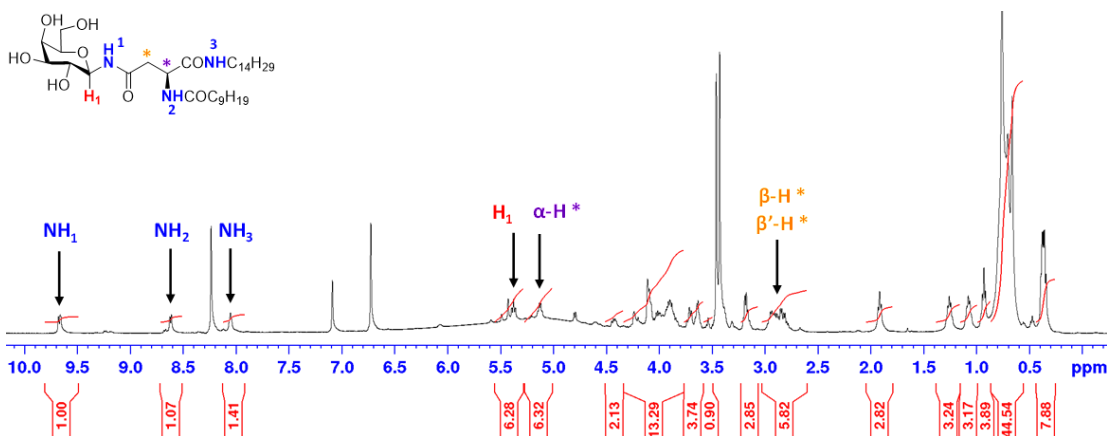
Figure 3.20. ^{1}H NMR spectrum of compound **3.72.** (D_5-Pyr, 500 MHz).

However, when the racemic aspartic acid building block, **3.61.** (D,L), was reacted with amino galactose **3.49.**, using the conditions described earlier (TBTU), an inseparable mixture of compounds was obtained. A similar situation happened when DIC was used as coupling reagent. Only when the coupling was carried out with DMTMM, the reaction proceeded in 73 % yield to give a mixture of four isomeric products **3.70.** (Scheme 3.8.), which were inseparable even after several attempts of purification by column chromatography. Careful analysis of the spectra, with the help of 2-D NMR experiments, allowed for the assignation of some of the peaks and could confirm a ratio of 0.4 α-L, 0.9 α-R, 0.9 β-L, 0.4 β-R (Experimental Chapter 7). Figure 3.21. shows the ^{1}H NMR spectrum of the mixture of products **3.70.** in CDCl₃. Characteristic peaks such as NH of the amide groups, anomeric H_1 from galactose, α-H, β-H and β'-H and methyl from the acetyl groups were assigned in the spectrum. Interestingly, some of the signals corresponding to the four isomeric products were distinctly observed.
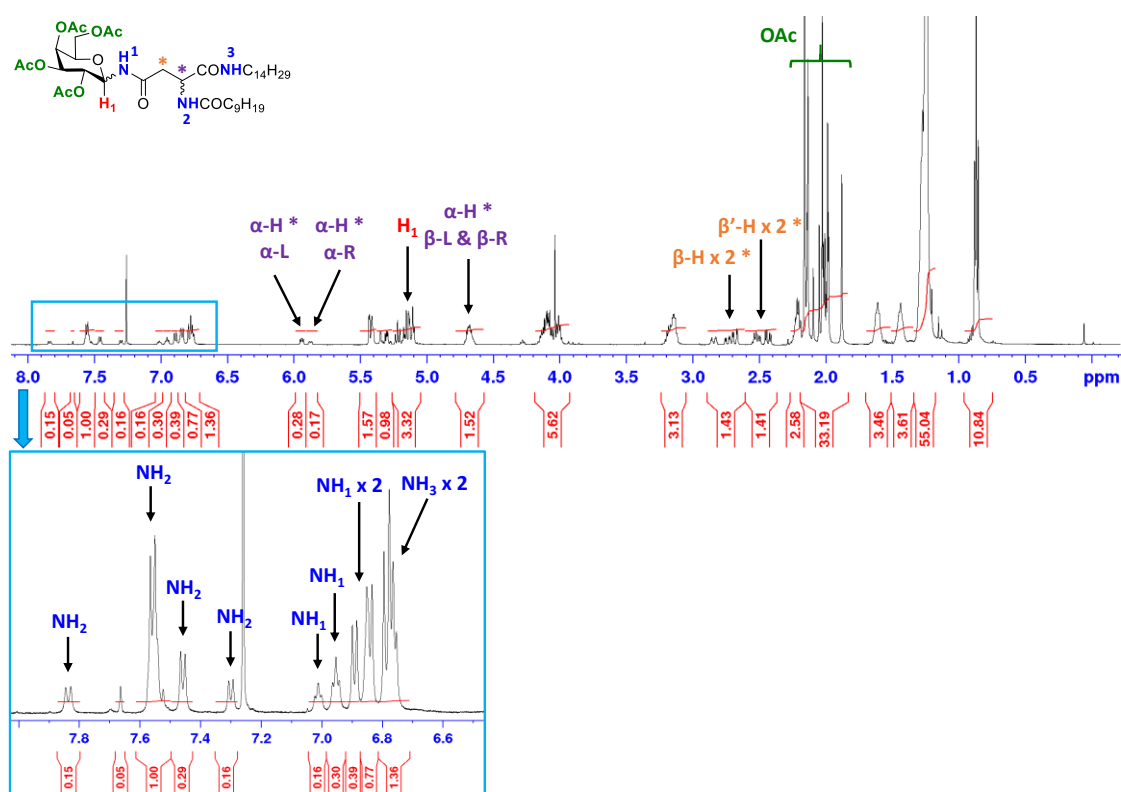
Figure 3.21. ^{1}H NMR spectrum of compound **3.70.** (CDCl$_3$, 500 MHz).
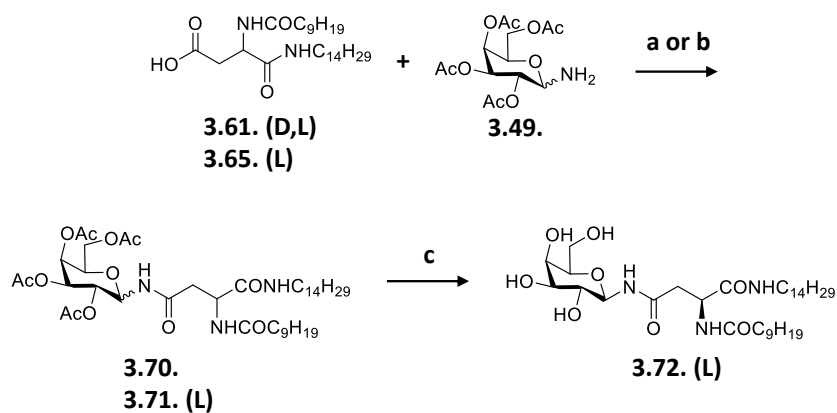
Scheme 3.8. Synthesis of Aspartic acid based *N*-glycolipids; Reagents and conditions: a) DMTMM, DMF, under N$_2$, rt, overnight (**3.70.**, 73 %); b) HOBt, TBTU, DMF, under N$_2$, 30 °C (10 min) to rt, overnight (**3.71.**, 44 %); c) NEt$_3$, DCM/MeOH/H$_2$O (1:2:1), 40 °C, 18 h (**3.72.**, 69 %).

Kunishima and co-workers optimised the use of DMTMM in 1999 for the formation of amide bonds.[137] DMTMM was freshly prepared by the reaction of 2-chloro-4,6-dimethoxy- 1,3,5-triazine (CDMT) with *N*-methylmorpholine (NMM) in anhydrous THF at rt (Scheme 3.9.). It is extremely easy to purify as the white solid product precipitates readily. However, it can be unstable and can only be stored at 0 °C for several months after synthesis.
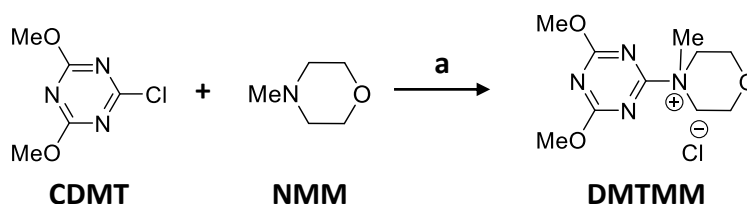
Scheme 3.9. Synthesis of DMTMM coupling agent; Reagents and conditions: a) THF, rt, 30 min (100 %).[137]

The reaction mechanism is similar to other activating reagents (Scheme 3.10.). The DMTMM reacts with the carboxylic acid to form the activated ester and regenerated NMM. The amine then attacks and displaces the activated ester to form the amide (**3.70.**) and the triazinone by-product.
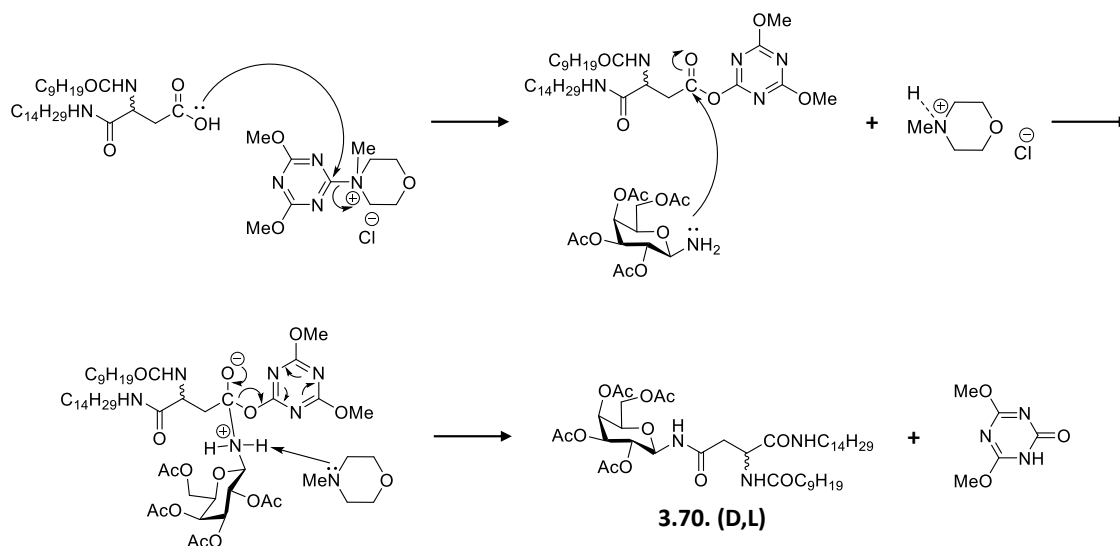
Scheme 3.10. Mechanism of DMTMM coupling reagent to form a new amide bond.

3.3.5. Gelation Ability

The ability of **3.61.**, **3.65.** − **3.69.**, **3.71.** and **3.72.** to induce the formation of supramolecular gels was then screened in a range of solvents of different polarities and structural characteristics (Tables 3.2. − 3.4.). The gels were formed upon sonication at rt in less than 5 min. Gels were also formed by thermal treatment. The gelator was heated in the required solvent to increase the solubility of the sample. The gel was formed after cooling down to rt in less than 2 h. For both techniques, the formation of the gel was confirmed by the "inverted test tube" method (Figure 3.22. - See also experimental Chapter 7).

It was found that the aspartic acid derivatives **3.61.** (D,L) and **3.65.** (L), showed distinct gelation behaviour (Table 3.2.). Changing the configuration of a single stereocentre (having a racemic mixture or a pure enantiomer compound), can change drastically the solubility properties and therefore the range of solvents in which they can form gels, the CGC and the T_{gs}.[138] Compound **3.61.** (D,L) formed gels in toluene, chloroform and DCM. However, compound **3.65.** (L) formed gels in a large range of non-protic solvents with diverse polarities such as petroleum ether, toluene, Et_2O, DCM, EtOAc and MeCN. Interestingly **3.65.** (L) formed a gel in low polarity solvents, such as petroleum ether and Et_2O, while its racemic counterpart **3.61.** (D,L) was insoluble in both solvents. On the other hand, compound **3.61.** (D,L) formed a gel in chloroform, however, compound **3.65.** (L) was soluble in this solvent.

The aspartic acid based *O*-glycolipids, **3.66.** − **3.69.**, exhibited also a distinct gelling behaviour influenced by the chirality of the α-C (Table 3.3.). The mixture of diastereoisomers, **3.66.** and **3.67.** were insoluble in aliphatic solvents, however, the pure diastereoisomers, **3.68.** and **3.69.** partially gelled these solvents at 20 mg/mL and could form gels at higher gelator concentrations. The four compounds formed gels in different solvents (images of the physical appearance of the different gels are shown in Figure 3.22.). Compound **3.66.** (D,L) formed gels in Et_2O and a mixture of EtOH:H_2O (1:1) even if the hydroxyl groups in this molecule are protected as acetyl esters. Remarkably, deacetylated compound **3.67.** (D,L) selectively gelled chloroform to form a translucent gel. Compound **3.68.** (L) formed gels in MeCN and EtOH:H_2O (1:1). The deprotected compound **3.69.** (L) formed a gel in toluene, however, it was

necessary to increase the gelator concentration to 55 mg/mL for gelation to take place.
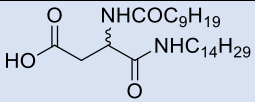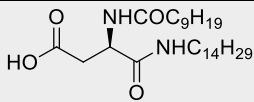
The presence of acetylated or free hydroxyl groups in the galactosyl moiety of the *O*-glycolipids strongly influenced the gelation properties. The acetylated-*O*-glycolipids **3.66.** (D,L) and **3.68.** (L), were both capable of forming opaque gels in a mixture of EtOH:H_2O (1:1) with 0.8 and 0.4 w/v % CGC respectively. However, *O*-glycolipids **3.67.** (D,L) and **3.69.** (L) with the free hydroxyl groups, were insoluble or formed aggregates in polar solvents. Compounds **3.67.** (D,L) and **3.69.** (L) were selective gelators of chloroform and toluene, respectively, albeit at higher CGC. The aspartic acid based *N*-glycolipid derivatives, **3.71.** and **3.72.** (Table 3.4.), exhibited a weaker ability to form gels than their *O*-glycolipids counterparts, **3.68.** and **3.69.** (Table 3.3.). Both acetylated compound, **3.71.**, and free hydroxyl derivative, **3.72.**, were only capable of partially gelling cyclohexane and commercial petrol at 20 mg/mL. Opaque gels by gelator **3.71.** were formed at higher CGC (CGC of 2.5 w/v % in petrol and 3 w/v % in cyclohexane).

It is interesting to note how the linkage between the galactosyl moiety and the aspartic acid core affects dramatically the gelation properties of glycolipids. The shorter, more rigid connection featured by the *N*-glycolipid derivatives clearly had a negative impact on the performance of these compounds. For this reason, it was decided to carry out characterisation tests on the other two families of gelators discussed previously. (Aspartic acid derivatives **3.61.** (D,L) and **3.65.** (L) and aspartic acid based *O*-glycolipids, **3.66.** – **3.69.**).
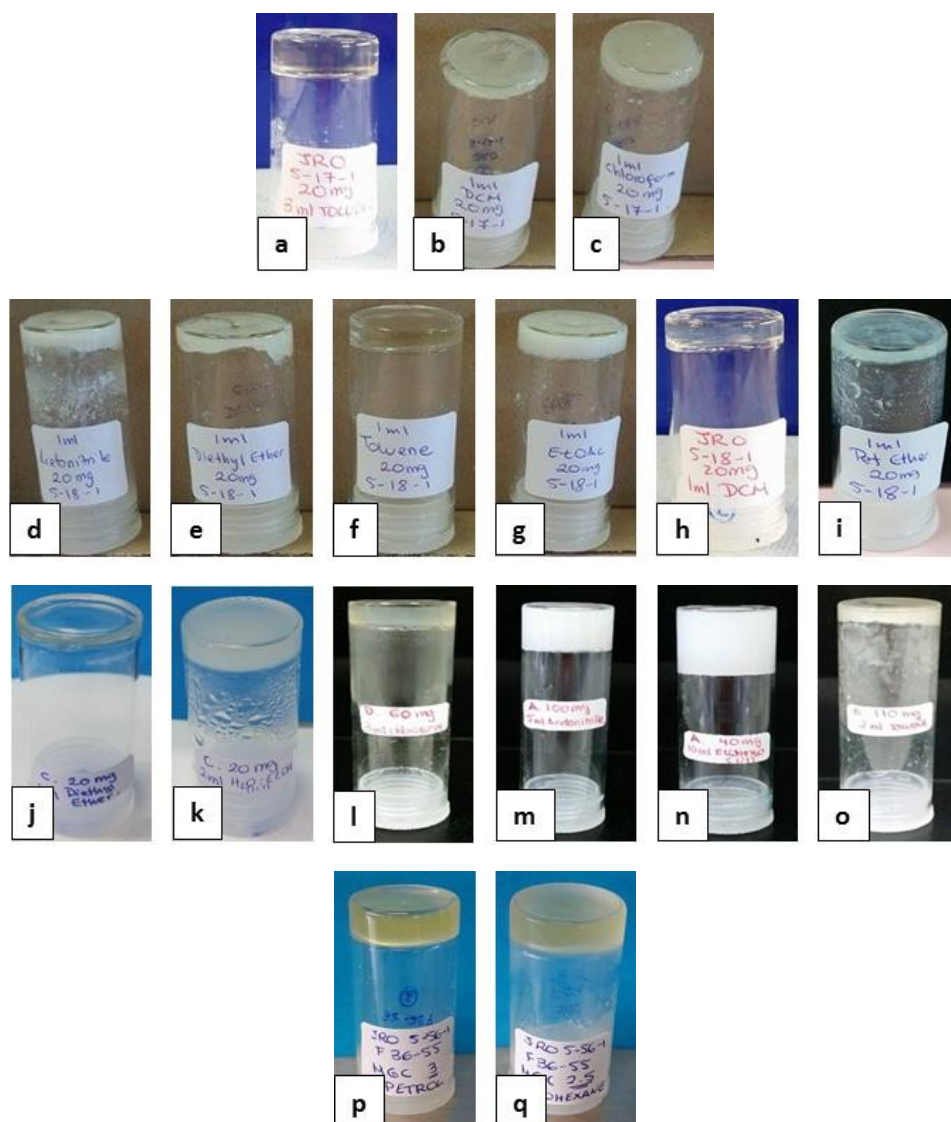
Figure 3.22. Physical appearance of the gels formed by aspartic acid derivatives. *Solvent:* a) (**3.61.**) *toluene*; b) (**3.61.**) *DCM*; c) (**3.61.**) *chloroform*; d) (**3.65.**) *MeCN*; e) (**3.65.**) *Et$_2$O*; f) (**3.65.**) *toluene;* g) (**3.65.**) *EtOAc;* h) (**3.65.**) *DCM*; i) (**3.65.**) *Pet. ether*; j) (**3.66.**) *Et$_2$O*; k) (**3.66.**) *EtOH:H$_2$O (1:1)*; l) (**3.67.**) *chloroform*; m) (**3.68.**) *MeCN*; n) (**3.25.**) *EtOH:H$_2$O (1:1)*; o) (**3.69.**) *toluene;* p) (**3.71.**) *petrol*; q) (**3.71.**) *cyclohexane*. (All gels were prepared at CGC).

Table 3.2. Gelation abilities of aspartic acid derivatives **3.61.** and **3.65.** in different solvents: physical appearance, CGC (Critical Gelation Concentration, w/v %) at rt and gel-sol transition temperature T_{gs} (°C) at the specified CGC. PG* at 20 mg/mL.

Compound / Solvent	3.61.	3.65.
Pentane	I	PG*
Hexane	PS	PS
Heptane	PS	PS
Pet. ether	I	OG(1.4) / T_{gs}(40-55)
Cyclohexane	PS	PS
Petrol	PG*	PG*
Toluene	TG(0.6) / T_{gs}(57-63)	TG(0.4) / T_{gs}(54-60)
Et$_2$O	I	OG(2.0) / T_{gs}(28-32)
Chloroform	OG(2.0) / T_{gs}(24-34)	S
DCM	OG(1.1) / T_{gs}(28-34)	TG(0.5) / T_{gs}(28-36)
EtOAc	PG*	OG(2.0) / T_{gs}(50-59)
DMSO:H$_2$O (1:1)	A	A
DMSO	PG*	S
MeCN	PG*	OG(2.0) / T_{gs}(40-50)
EtOH:H$_2$O (1:1)	I	I
EtOH	A	A
MeOH	A	A
H$_2$O	I	I
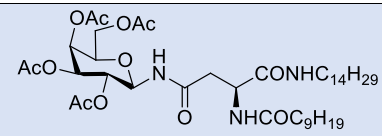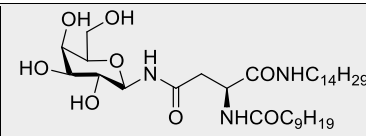
S = Soluble, PS = Partial soluble, I = Insoluble, A = Aggregates, PG = Partial gelation,

TG = Transparent / Translucent gel, OG = Opaque gel.

Table 3.3. Gelation abilities of *O*-glycolipid derivatives **3.66. – 3.69.** in different solvents: physical appearance, CGC (Critical Gelation Concentration, w/v %) at rt and gel-sol transition temperature T$_{gs}$ (°C) at the specified CGC. PG* at 20 mg/mL.

Solvent \ Compound	3.66. (D/L)	3.67. (D/L)	3.68. (L)	3.69. (L)
Pentane	–	–	PG*	PG*
Hexane	–	–	PG*	PS
Heptane	–	–	PG*	PG*
Pet. ether	–	–	PG*	PG*
Cyclohexane	PG*	PG*	PG*	PG*
Petrol	PG*	PG*	PS	PG*
Toluene	S	PG*	S	OG(5.5) / T$_{gs}$(30-46)
Et$_2$O	TG(1.7)/ T$_{gs}$(26-32)	PS	PS	–
Chloroform	S	TG(2.0)/ T$_{gs}$(31-43)	S	–
DCM	S	–	S	–
EtOAc	S	–	S	S
DMSO:H$_2$O	A	A	A	A
DMSO	S	S	S	S
MeCN	PG*	PG*	OG(1.4)/ T$_{gs}$(15-46)	–
EtOH:H$_2$O	TG(0.8)/ T$_{gs}$(36-45)	–	OG(0.4)/ T$_{gs}$(17-54)	–
EtOH	S	A	A	A
MeOH	S	A	A	A
H$_2$O	–	–	–	–

S = Soluble, PS = Partial soluble, I = Insoluble, A = Aggregates, PG = Partial gelation,

TG = Transparent / Translucent gel, OG = Opaque gel.

Table 3.4. Gelation abilities of *N*-glycolipid derivatives **3.71.** and **3.72.** in different solvents: physical appearance, CGC (Critical Gelation Concentration, w/v %) at rt and gel-sol transition temperature T_{gs} (°C) at the specified CGC. PG* at 20 mg/mL.

Compound / Solvent	**3.71.**	**3.72.**
Pentane	A	I
Hexane	I	I
Heptane	A	I
Pet. ether	A	A
Cyclohexane	TG(3.0) / T_{gs}(48-65)	PG*
Petrol	TG(2.5) / T_{gs}(17-34)	PG*
Toluene	S	PS
Et$_2$O	PS	I
Chloroform	S	PS
DCM	S	I
EtOAc	S	I
DMSO:H$_2$O (1:1)	A	A
DMSO	S	S
MeCN	PS	PS
EtOH:H$_2$O (1:1)	I	I
EtOH	S	I
MeOH	S	I
H$_2$O	I	I

S = Soluble, PS = Partial soluble, I = Insoluble, A = Aggregates, PG = Partial gelation,

TG = Transparent / Translucent gel.

3.3.6. Aspartic Acid Derivatives with Shorter Chain Lengths, 3.52. and 3.56.

Analysis of the gelation screening of aspartic acid derivatives **3.61.** and **3.65.** and *O*-glycolipids **3.66.** – **3.69.**, clearly shows that the chiral nature of these compounds is a critical structural feature that determines the gelation ability and specificity of these compounds. The importance of chirality in gelation properties has been reported previously by other authors in literature.[44,138-141] To gain an insight of how optically pure derivatives of aspartic acid self-assemble in a different manner to their racemic counterparts, the synthesis of aspartic acid derivatives with shorter side chains were synthesised. These compounds may crystallise instead of forming gels, therefore allowing for structural examination of assembling patterns.

The aspartic acid short chain derivatives, **3.53.** (D,L) or **3.57.** (L), were readily prepared as shown in Scheme 3.11. **3.53.** (D,L) or **3.57.** (L) were analogues of the aspartic acid long chain compounds discussed previously, **3.61.** (D,L) and **3.65.** (L) (Scheme 3.1.). Commercially available *N*-(tert-butoxycarbonyl)-*L*-aspartic acid-4-benzyl ester was reacted with propylamine using TBTU in the presence of NEt$_3$ (step a, for racemate, **3.50.**) or DIC in the absence of a base (step b, for pure enantiomer, **3.54.**). Subsequently, *N*-Boc protecting group was removed with TFA to afford the amine **3.51.** (D,L) or **3.55.** (L) which was acylated with propionyl chloride to give compounds **3.52.** (D,L) or **3.56.** (L). Hydrogenolysis of the side chain benzyl ester of compound **3.52.** (D,L) or **3.56.** (L), (carried out at 50 °C and H$_2$ bubbled through for 4 h) afforded the desired L-aspartic acid **3.53.** (D,L) or **3.57.** (L), in excellent yields.

3.50. (D,L)
3.54. (L)

3.51. (D,L)
3.55. (L)

3.52. (D,L)
3.56. (L)

3.53. (D,L)
3.57. (L)
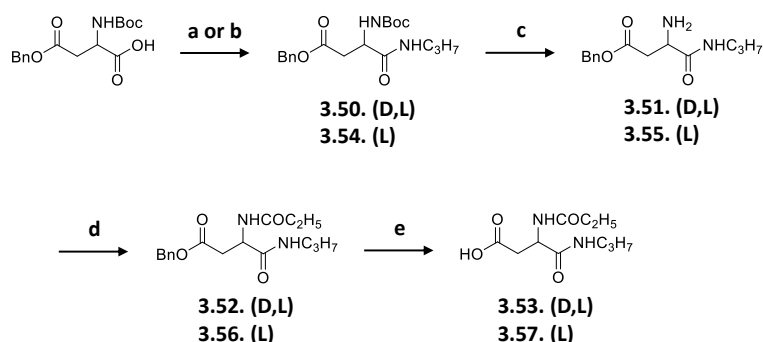
Scheme 3.11. Synthesis of Aspartic acid short side chains; Reagents and conditions: a) HOBt, TBTU, NEt$_3$, DMF, C$_3$H$_7$NH$_2$, under N$_2$, rt, 18 h (**3.50.**, 89 %); b) HOBt, DIC, DMF, C$_3$H$_7$NH$_2$, under N$_2$, rt, 18 h (**3.54.**, 98 %); c) DCM, 50 % TFA in DCM, 0 °C (30 min) to rt, 4 h (**3.51.**, 69 %; **3.55.**, 69 %); d) DMF, propionyl chloride, NEt$_3$, under N$_2$, rt, 18 h (**3.52.**, 67 %; **3.56.**, 82 %); e) EtOAc, Pd/C, under H$_2$, 50 °C (4 h) to rt, overnight (**3.53.**, 96 %; **3.57.**, 94 %).

Compounds **3.52.** (D,L) and **3.56.** (L), grew crystals in EtOAc / Et$_2$O using the vapor diffusion technique (See Chapter 7, Section 7.3.8.). The crystal structures are shown in Figures 3.23. and 3.25., respectively. (Crystallographic data is shown in the Appendix).

Mladen Zinic and co-workers studied gelation properties and supramolecular organisation of amino acid units of racemates vs pure enantiomers compound.[139,140] Their major challenge was preparing novel design strategies of versatile gelator molecules with predictable properties. For that reason, they were using an amidic core which induce self-assembly through unidirectional cooperative H-bonding, the presence of the chiral centre and a long aliphatic chain which should decrease the crystallisation tendency as it will promote van der Waals interactions. In addition, they were using spectroscopic analysis (^{1}H NMR and FTIR) combined with X-ray crystallography and molecular modelling to find the relationship between their structural characteristics (configuration, conformation), gelation properties and organisation in gel fibres.[139,140] These studies influenced the decision for conducting analysis of the crystal structures of samples **3.52.** (D,L) and **3.56.** (L) which showed differences in the packing modes between the racemate [**3.52.** (D,L)] and the enantiomerically pure compound [**3.56.** (L)].

The two enantiomers in the racemic mixture [**3.52.** (D,L)], align themselves in an anti-parallel head to tail relative orientation, directed mainly by aromatic π-π stacking interactions between the benzyl group and van der Waals interactions between the alkyl chains (Figure 3.23.). This leads to a rather extended packing, with a relatively large unit cell in the crystal structure (Figure 3.24.).
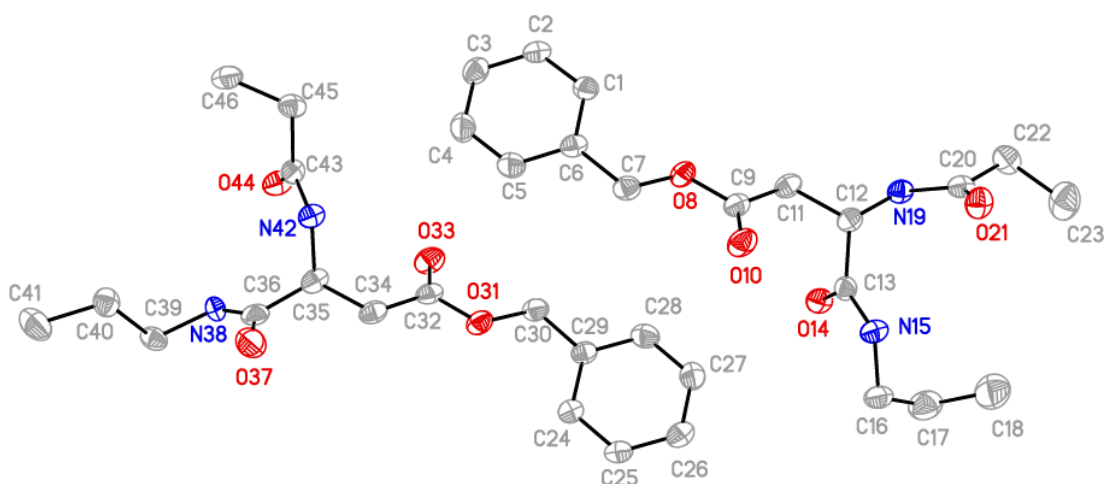
Figure 3.23. Crystal structure of **3.52.** (D,L).
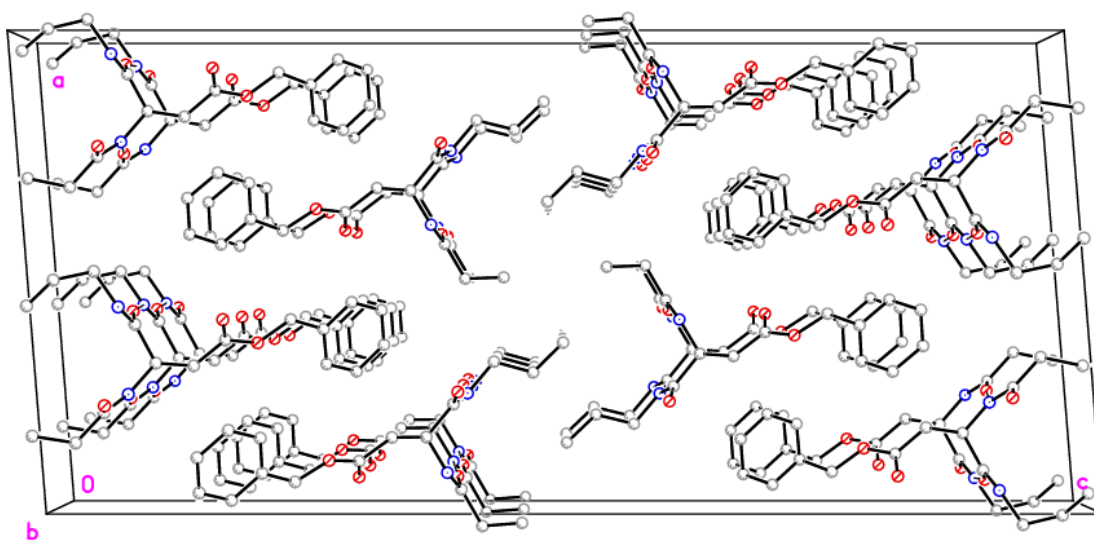
Figure 3.24. Unit cell (monoclinic) of **3.52.** (D,L). Hydrogen atoms omitted for clarity. (Unit cell constants: a = 17.627 Å, b = 5.040 Å, c = 38.375 Å).

On the other hand, a network of H-bonds between the amide groups donors and acceptors, leads to a tighter packing. The interdigitated alignment of the molecules of **3.56.** (L) (Figure 3.25.) can still be appreciated, however, in the pure enantiomer the benzyl esters are placed at the centre of the unit cell (Figure 3.26.).

Thus crystallographic analysis reveals a very distinct packing in the racemate samples **3.52.** (D,L) and enantiomerically pure **3.56.** (L). It can be suggested that in the longer alkyl chain analogues, the chirality of the aspartic acid core influences in an analogous manner the self-assembly of the gelator molecules.
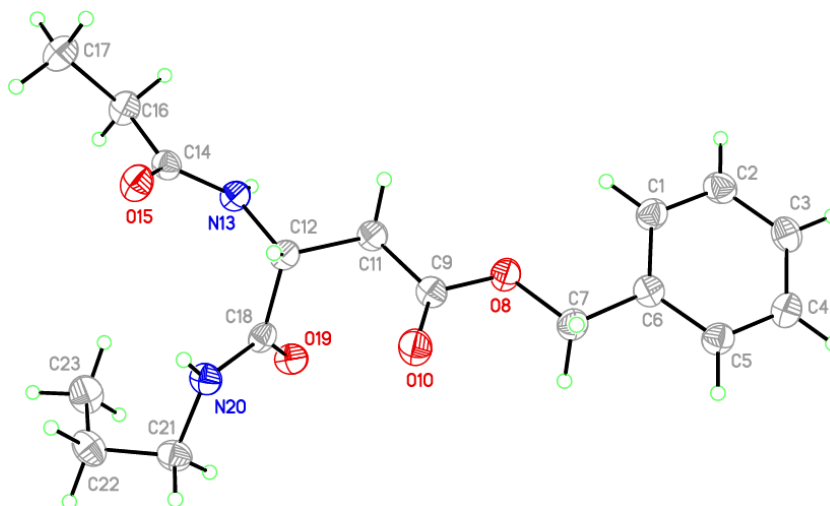
Figure 3.25. Crystal structure of **3.56.** (L).
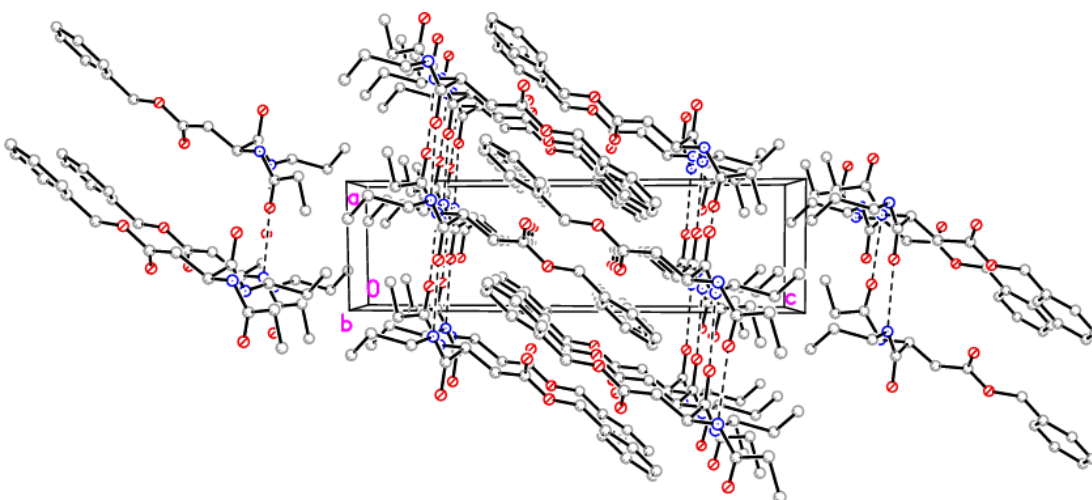
Figure 3.26. Unit cell (triclinic) of **3.56.** Dashed lines indicate strong H-bonding. (Unit cell constants: a = 5.062 Å, b = 9.776 Å, c = 17.788 Å).

Our results correlate with other literature reports which were mentioned previously, in which different gelator behaviour between racemic and enantiomer pure gelators were observed.[139,140]

3.3.7. Rheological Evaluation

3.3.7.1. Rheological Evaluation of Gels Formed by Aspartic Acid Derivatives 3.61. (D,L) and 3.65. (L)

As detailed previously in Chapter 2 (Section 2.3.4.), rheology involves the study of liquids and solids under applied stress conditions. The viscoelastic properties of the

gel formed by aspartic acid derivatives **3.61.** (D,L) and **3.65.** (L), and of the gels formed by aspartic acid based *O*-glycolipid **3.66.** – **3.69.** were investigated.

These studies were carried out in the laboratory of Professor Ramon Moreira (University of Santiago de Compostela).

A strain of 0.1 % (LVER) was used to determine the mechanical spectra of all gels (SAOS). These values were chosen after considering the results obtained for LVER tests in which G' and G'' were constant for a 0.1 % strain (Figures 3.27. - 3.32. a).

Mechanical spectra of the gels of compounds **3.61.**, **3.65.** – **3.69.** in the required solvents at 25 °C (toluene) or 10 °C [chloroform, DCM, MeCN and EtOH:H_2O (1:1)] were studied 120 h after their formation. This was decided after recording mechanical spectra of the gels after 24, 96, 120 and 144 h of gel formation in order to evaluate the rheological stability of their structure. After 120 h, it was observed that the values of the modules, G' and G'', did not significantly increase with time.

Firstly, gels formed by aspartic acid derivatives **3.61.** (D,L) and **3.65.** (L), were analysed. **3.61.** (D,L) and **3.65.** (L) showed G' > G'' throughout the angular frequency range that was studied, with low values of tanδ (Table 3.5.). This indicates that the elastic nature of the samples prevailed over the viscous one, which is the typical behavior of a gel structure. The gels in toluene formed by both gelators [**3.61.** (D,L) and **3.65.** (L)] showed the lowest values of tanδ, indicating that they are stronger gels than those formed by compounds in either DCM, chloroform and MeCN [Figure 3.27. and 3.28. 1-3 b)].

In addition, when toluene was used as a solvent, the gel formed by compound **3.61.** (D,L) presented higher values of G' and G'' than compound **3.65.** (L) (Table 3.5.). This indicated a better elastic character for **3.61.** (D,L) than the corresponding gel formed by **3.65.** (L). Also, the values of tanδ for **3.61.** (D,L) were more stable (0.16 – 0.10) compared to the values of tanδ for **3.65.** (L) which varied increasingly at high frequency (0.11 – 0.45). Thus, **3.61.** (D,L) and **3.65.** (L) in different solvents, can be considered to be real gels with values of tanδ < 0.6. The MeCN gel formed by **3.65.** (L) was found to be the weakest gel of this family (Table 3.5.).
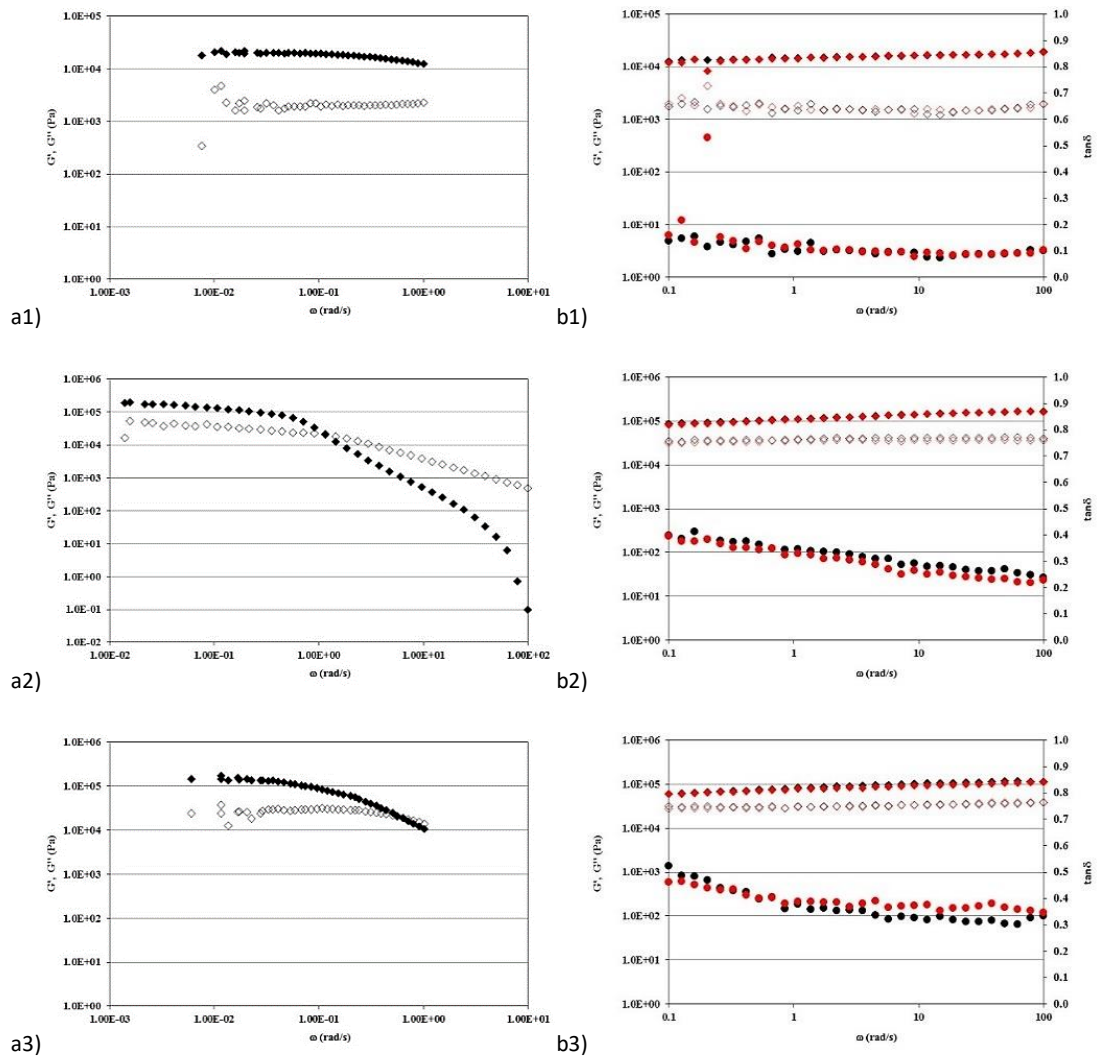
Figure 3.27. Rheological evaluation of gels formed by **3.61.** (D,L) at 25 °C (toluene) or 10 °C (Chloroform and DCM) at a strain of 0.1 % in **1)** toluene with 0.6 w/v %, tanδ < 0.2.; **2)** Chloroform with 2.0 w/v %, tanδ < 0.5; **3)** DCM with 1.1 w/v %, tanδ < 0.6. **a)** (LVER) Strain sweep at 1 Hz of frequency. G'($\blacklozenge$) and G'' ($\lozenge$); **b)** (SAOS) Frequency sweep at a strain of 0.1 %. G' ($\blacklozenge$, $\color{red}\blacklozenge$; filled markers), G'' ($\lozenge$, $\color{red}\lozenge$; empty markers) and tanδ ($\bullet$, $\color{red}\bullet$; dot filled markers).
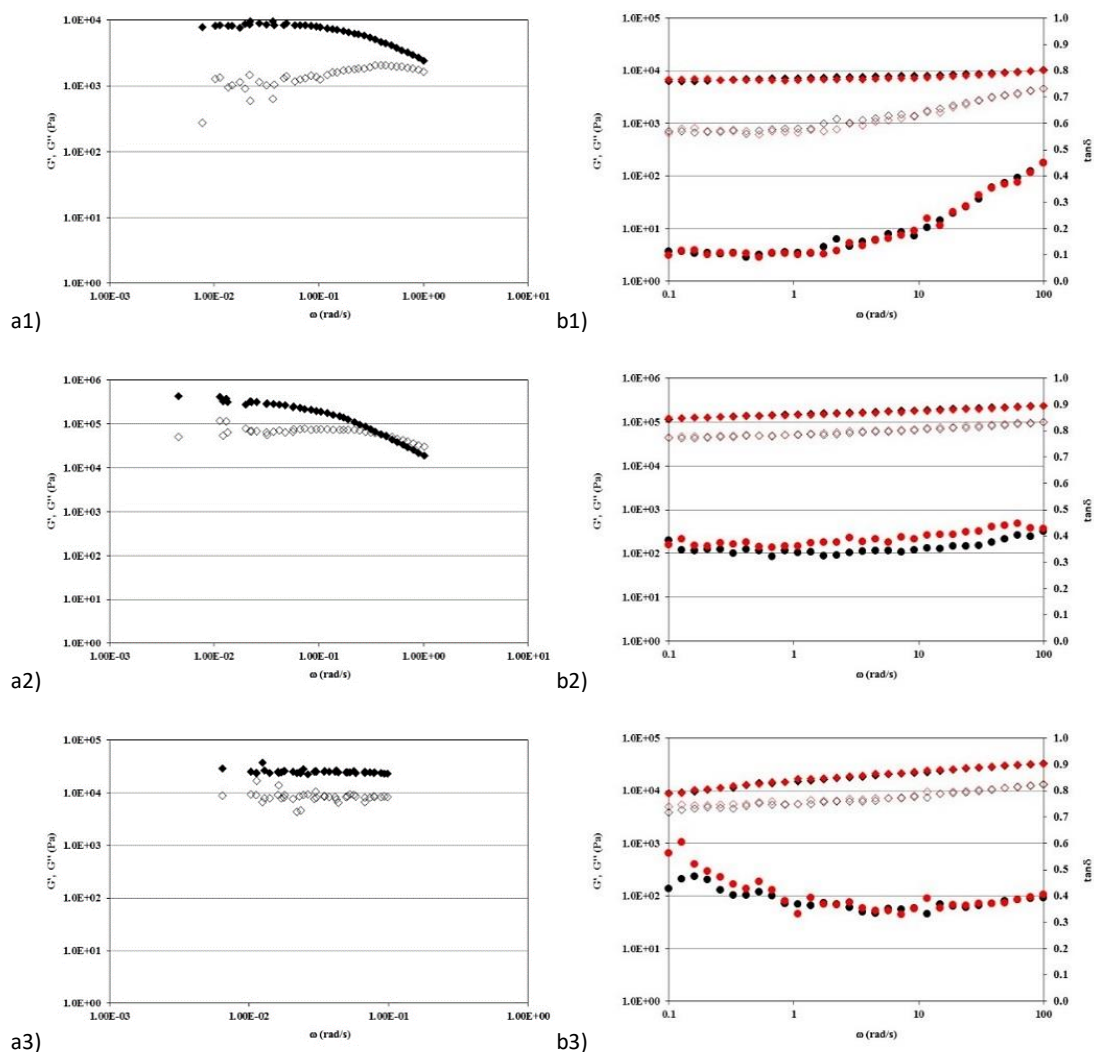
Figure 3.28. Rheological evaluation of gels formed by **3.65.** (L) at 25 °C (toluene) or 10 °C (DCM and MeCN) at a strain of 0.1 % in **1)** toluene with 0.4 w/v %, tanδ < 0.5.; **2)** DCM with 0.5 w/v %, tanδ < 0.5; **3)** MeCN with 2.0 w/v %, tanδ < 0.5. **a)** (LVER) Strain sweep at 1 Hz of frequency. G'(♦) and G'' (◊); **b)** (SAOS) Frequency sweep at a strain of 0.1 %. G' (♦, ♦; filled markers), G'' (◊, ◊; empty markers) and tanδ (●, ●; dot filled markers).

Table 3.5. Summary of SAOS results for **3.61.** (D/L) and **3.65.** (L). The data are displayed from the weakest (top) to the strongest (bottom) gel.

Compound	Solvent	Temperature	Time	G' (Pa)	G'' (Pa)	Tanδ
3.65. (L)	MeCN	10 °C	120 h	$8.8 \cdot 10^3 - 3.3 \cdot 10^4$	$4.9 \cdot 10^3 - 1.3 \cdot 10^4$	0.56 - 0.41
3.61. (D/L)	DCM	10 °C	120 h	$6.0 \cdot 10^4 - 1.1 \cdot 10^5$	$3.2 - 3.8 \cdot 10^4$	0.52 - 0.34
3.65. (L)	DCM	10 °C	120 h	$1.2 - 2.4 \cdot 10^5$	$4.4 - 9.8 \cdot 10^4$	0.38 - 0.42
3.61. (D/L)	Chloroform	10 °C	120 h	$8.0 \cdot 10^4 - 1.6 \cdot 10^5$	$3.2 - 3.7 \cdot 10^4$	0.39 - 0.23
3.65. (L)	Toluene	25 °C	120 h	$6.4 \cdot 10^3 - 1.0 \cdot 10^4$	$7.2 \cdot 10^2 - 4.6 \cdot 10^3$	0.11 - 0.45
3.61. (D/L)	Toluene	25 °C	120 h	$1.2 - 1.9 \cdot 10^4$	$1.9 - 2.0 \cdot 10^3$	0.16 - 0.10

3.3.7.2. Rheological Evaluation of Gels Formed by Aspartic Acid Based *O*-glycolipid 3.66. - 3.69.

The gels formed by the aspartic acid based *O*-glycolipids **3.66.** – **3.69.**, were analysed. All gels showed G´ > G´´ throughout the angular frequency range that was studied, with low values of tanδ (Table 3.6.). This indicates that the elastic nature of the samples prevailed over the viscous one, which is the typical behavior of a gel structure. The gel in chloroform formed by glycolipid **3.67.** (D,L) showed the lowest values of tanδ (0.15 – 0.20) indicating that it is the strongest gel in this family of compounds, followed by the gel in toluene formed by glycolipid **3.69.** (L) with 0.19 – 0.24 values of tanδ (Figure 3.30. and 3.32, respectively). These gelators [compound **3.67.** (D,L) and **3.69.** (L)] feature the free hydroxyl groups in the galactosyl moiety. The presence of the hydroxyl groups improved the rheological properties of the gels, making them stronger gels in non-protic organic solvents, like toluene or chloroform. The deprotected *O*-glycolipids can form strong H-bonding that may account for the stability and strength observed for these gels.

On the other hand, the gels formed by the acetylated glycolipids, **3.66.** (D,L) and **3.68.** (L) in EtOH:H_2O (1:1), showed the same values of tanδ (Table 3.6.), indicating that in this case, the chirality of the compound did not affect their rheological properties [Figure 3.29. and 3.31. 2 b)]. This could be accounted for as only hydrophobic interactions were leading the assembly processes. The MeCN gel formed by **3.68.** (L) was again the weakest gel of this family of compounds with 0.53 – 0.26 tanδ values (Table 3.6.).
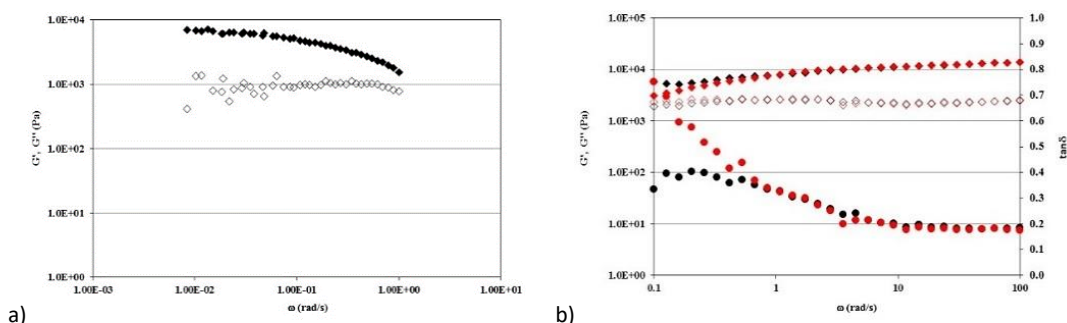
Figure 3.29. Rheological evaluation of gels formed by **3.66.** (D/L) at 10 °C at a strain of 0.1 % in EtOH:H_2O (1:1) with 0.8 w/v %. a) (LVER) Strain sweep at 1 Hz of frequency. G'(♦) and G'' (◊); b) (SAOS) Frequency sweep at a strain of 0.1 %. G' (♦, ♦; filled markers), G'' (◊, ◊; empty markers) and tanδ (●, ●; dot filled markers with values, < 0.8.

a)   b)
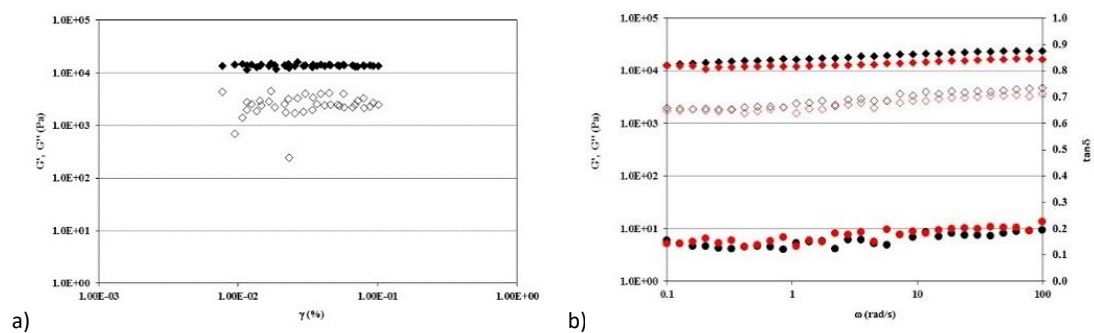
Figure 3.30. Rheological evaluation of gels formed by **3.67.** (D/L) at 10 °C at a strain of 0.1 % in chloroform with 2.0 w/v %. a) (LVER) Strain sweep at 1 Hz of frequency. G'($\blacklozenge$) and G'' ($\lozenge$); b) (SAOS) Frequency sweep at a strain of 0.1 %. G' ($\blacklozenge$, $\color{red}\blacklozenge$; filled markers), G" ($\lozenge$, $\color{red}\lozenge$; empty markers) and tanδ ($\bullet$, $\color{red}\bullet$; dot filled markers with values, < 0.3.

a1)   b1)

a2)   b2)
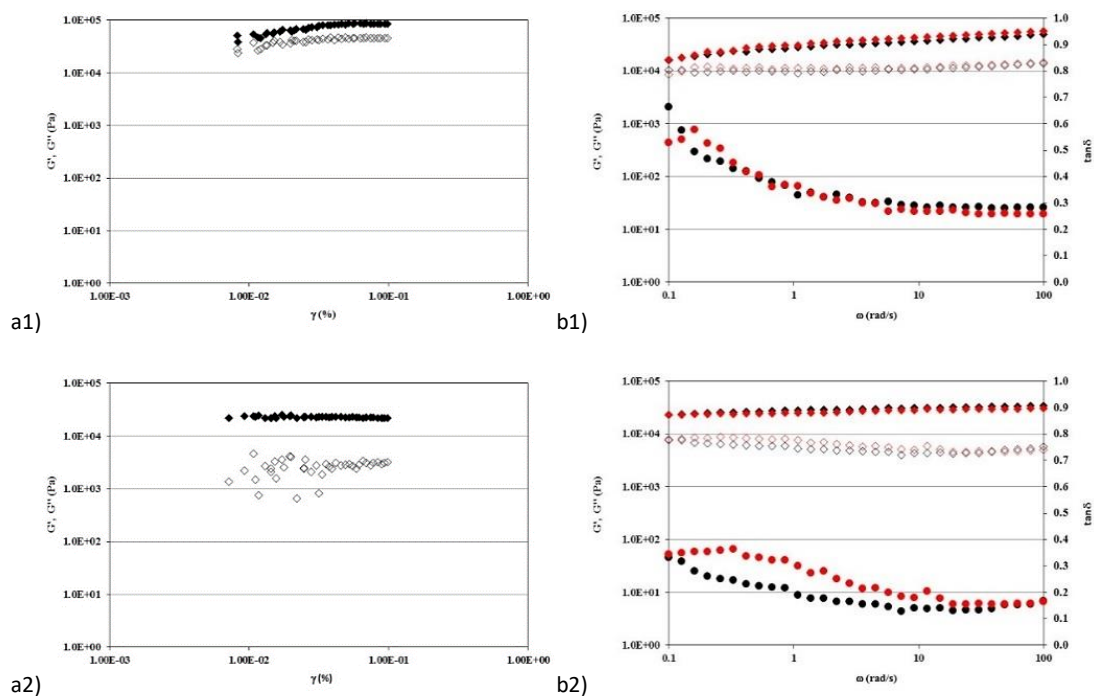
Figure 3.31. Rheological evaluation of gels formed by **3.68.** (L) at 10 °C at a strain of 0.1 % in **1)** MeCN with 1.4 w/v %, tanδ < 0.7.; **2)** EtOH:H$_2$O (1:1) with 0.4 w/v %, tanδ < 0.4. **a)** (LVER) Strain sweep at 1 Hz of frequency. G'($\blacklozenge$) and G'' ($\lozenge$); **b)** (SAOS) Frequency sweep at a strain of 0.1 %. G' ($\blacklozenge$, $\color{red}\blacklozenge$; filled markers), G" ($\lozenge$, $\color{red}\lozenge$; empty markers) and tanδ ($\bullet$, $\color{red}\bullet$; dot filled markers).
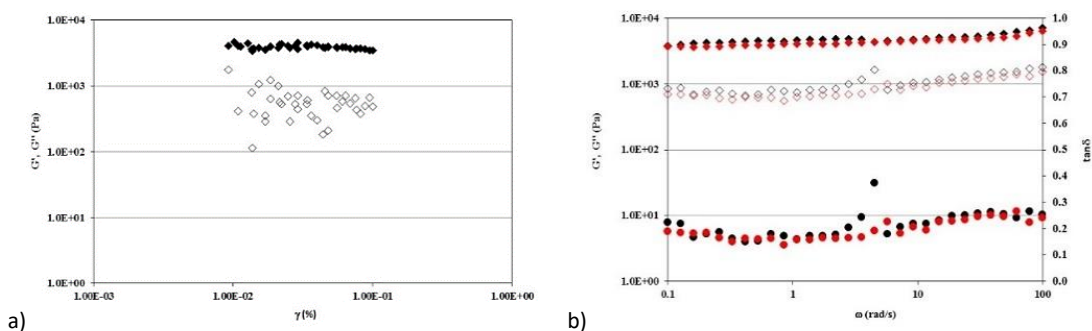
Figure 3.32. Rheological evaluation of gels formed by **3.69.** (L) at 25 °C at a strain of 0.1 % in toluene with 5.5 w/v %. a) (LVER) Strain sweep at 1 Hz of frequency. G'($\blacklozenge$) and G'' ($\lozenge$); b) (SAOS) Frequency sweep at a strain of 0.1 %. G' ($\blacklozenge$, $\blacklozenge$; filled markers), G'' ($\lozenge$, $\lozenge$; empty markers) and tanδ ($\bullet$, $\bullet$; dot filled markers with values, < 0.3.

Table 3.6. Summary of SAOS results for **3.66.** - **3.69.** The data are displayed from the weakest (top) to the strongest (bottom) gel.

Compound	Solvent	Temperature	Time	G' (Pa)	G'' (Pa)	Tanδ
3.68. (L)	MeCN	10 °C	120 h	$1.6 - 5.8 \cdot 10^4$	$8.6 \cdot 10^3 - 1.5 \cdot 10^4$	0.53 - 0.26
3.66. (D/L)	EtOH:H_2O (1:1)	10 °C	120 h	$5.8 \cdot 10^3 - 1.4 \cdot 10^4$	$1.9 - 2.6 \cdot 10^3$	0.34 - 0.19
3.68. (L)	EtOH:H_2O (1:1)	10 °C	120 h	$2.3 - 3.0 \cdot 10^4$	$7.9 - 4.9 \cdot 10^3$	0.34 - 0.16
3.69. (L)	Toluene	25 °C	120 h	$3.7 - 6.3 \cdot 10^3$	$6.9 \cdot 10^2 - 1.5 \cdot 10^3$	0.19 - 0.24
3.67. (D/L)	Chloroform	10 °C	120 h	$1.3 - 2.4 \cdot 10^4$	$1.9 - 4.6 \cdot 10^3$	0.15 - 0.20

3.3.8. Thermal Analysis: T_{gs} and DSC Measurements

3.3.8.1. Thermal Analysis of Gels Formed by Aspartic Acid Derivatives 3.61. (D,L) and 3.65. (L)

The thermoreversible behaviour of the gels formed in different solvents by aspartic acid derivatives **3.61.** (D,L) and **3.65.** (L) was analysed by DSC.

The DSC analysis of the gels was carried out 120 h after formulation to ensure that the gel formation was completed, following rheological results. DSC analysis (Table 3.7. and 3.8.) showed thermoreversibility of the gels giving reproducible cycles after performing duplicates of each experiment.

Firstly, the results for gels formed by aspartic acid derivatives **3.61.** (D,L) and **3.65.** (L) were compared (Table 3.7.). T_{gs} measurements followed the procedure described in Section 7.3.3. and DSC analysis was carried out as described in Section 7.3.5.1.

Table 3.7. T_{gs} (°C) by heating / monitoring the meting temperature and DSC transition temperatures (gel-to-sol. and sol.-to-gel) of thermoreversible gels formed by **3.61.** and **3.65.** for two heating (1st and 3rd cycles) and two cooling (2nd and 4th cycles) cycles at the specified CGC.

Gelator	Solvent	T_{gs} (°C)	1st cycle	2nd cycle	3rd cycle	4th cycle
3.61. (D/L)	Toluene	**57 – 63**	45.3 °C	1.5 °C	41.0 °C	1.2 °C
	Chloroform	**24 – 34**	29.2 °C	11.9 °C	25.8 °C	-
	DCM	**28 – 34**	24.9 °C	4.7 °C	18.1 °C	4.6 °C
3.65. (L)	Toluene	**54 – 60**	50.1 °C	36.3 °C	50.0 °C	33.6 °C
	DCM	**28 - 36**	24.4 °C	3.5 °C	22.1 °C	3.2 °C

The thermograms a) - c) in Figure 3.33. show the endotherms and exotherms for the gels formed by gelators **3.61.** The thermograms d) and e) in Figure 3.33. show the endotherms and exotherms for the gels formed by gelators **3.65.** Thermograms a) - c) show an endotherm at 45.3 (toluene), 29.2 (chloroform), 24.9 (DCM) °C for **3.61.**; 50.1 (toluene) and 24.4 (DCM) °C for **3.65.** in the first heating cycle corresponding to the gel-sol transition. This correlated well with the T_{gs} determined by the "melting" method. The third cycle, which was another heating cycle, showed lower T_{gs} values, which is consistent with rheological results, as the gel's 3-D network needs 120 h for complete formation. The exotherms in the cooling cycles (second and fourth cycles) are shown at 1.5 (toluene), 11.9 (chloroform), 4.7 (DCM) °C for **3.61.**; 36.1 (toluene) and 3.5 (DCM) °C for **3.65.** which can be assigned to the formation of the initial 2-D assembles in the gel network, as discussed previously in Chapter 2. It can also be seen that T_{gs} correlate well with the gels strenghts stablised by the rheological analysis.
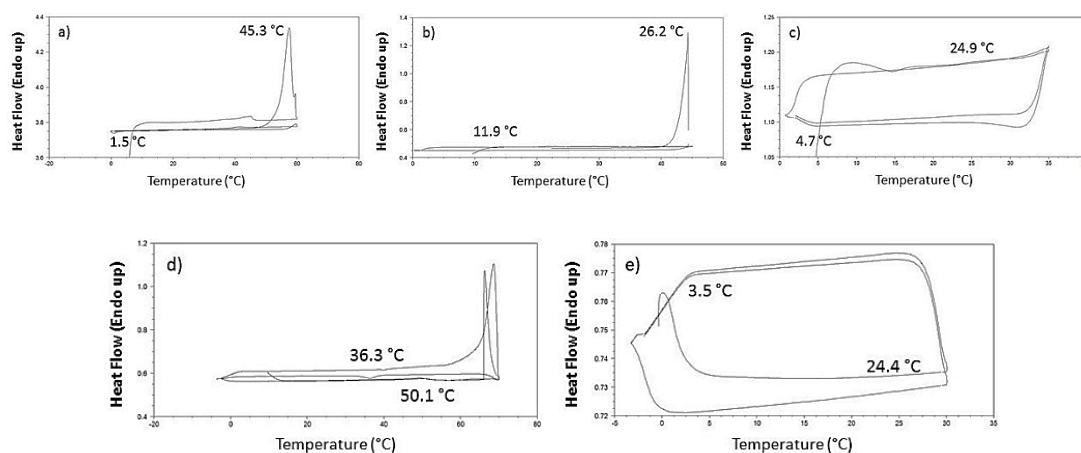
Figure 3.33. DSC of the gel **3.61.** and **3.65.**: a) **3.61.** in toluene (0.6 w/v %); b) **3.61.** in chloroform (2.0 w/v %); c) **3.61.** in DCM (1.1 w/v %); d) **3.65.** in toluene (0.4 w/v %); e) **3.65.** in DCM (0.5 w/v %), during the two heating / two cooling cycles. The sample was heating from 0 °C to temperature lower than boiling point of the solvent used, at 2 °C/min and cooling the same range of temperature. Reproducible / duplicated cycles for each sample.

3.3.8.2. Thermal Analysis of Gels Formed by Aspartic Acid Based *O*-glycolipid 3.66. - 3.69.

The results for the thermal analysis of gels formed by aspartic acid based *O*-glycolipids **3.66.** – **3.69.** using DSC are presented in Table 3.8. T_{gs} measurements followed the procedure described in Section 7.3.3. and DSC analysis was carried out as described in Section 7.3.5.1.

Table 3.8. T_{gs} (°C) by heating / monitoring the meting temperature and DSC transition temperatures (gel-to-sol. and sol.-to-gel) of thermoreversible gels formed by **3.66.** – **3.69.** for two heating (1st and 3rd cycles) and two cooling (2nd and 4th cycles) cycles at the specified CGC.

Gelator	Solvent	T_{gs} (°C)	1st cycle	2nd cycle	3rd cycle	4th cycle
3.66. (D/L)	EtOH:H_2O (1:1)	**36 - 45**	54.4 °C	3.1 °C	51.4 °C	2.9 °C
3.67. (D/L)	Chloroform	**31 - 43**	30.3 °C	2.9 °C	24.9 °C	2.8 °C
3.68. (L)	MeCN	**15 - 46**	30.8 °C	10.5 / 15.8 °C	27.7 °C	10.4 / 15.4 °C
	EtOH:H_2O (1:1)	**17 - 54**	40.9 °C	34.8 °C	37.8 °C	34.6 °C
3.69. (L)	Toluene	**30 - 46**	30.8 °C	3.4 °C	27.3 °C	2.9 °C

The thermogram a) in Figure 3.34. show the endotherms (54.4 °C) and exotherms (3.1 °C) for the gels formed by gelator **3.66.** in EtOH:H_2O (1:1). The thermogram b) in Figure 3.34. show the endotherms (30.3 °C) and exotherms (2.9 °C) for the gels formed by gelators **3.67.** in chloroform. The thermograms c) and d) in Figure 3.34. show the endotherms and exotherms for the gels formed by gelators **3.68.** in MeCN and EtOH:H_2O (1:1), respectively. Thermograms c) and d) show an endotherm at 30.8 (MeCN) and 40.9 [EtOH:H_2O (1:1)] °C; in the first heating cycle corresponding to the gel-sol transition. The exotherms in the cooling cycles (second and fourth cycles) are shown at 10.5 and 15.8 (MeCN) and 34.8 [EtOH:H_2O (1:1)] °C for **3.68.** The thermogram e) in Figure 3.34. show the endotherms (30.8 °C) and exotherms (3.4 °C) for the gels formed by gelators **3.69.** in toluene.

This correlated well with the T_{gs} determined by the "melting" method. The third cycle, which was another heating cycle, showed lower T_{gs} values, which is consistent with rheological results, as the gel's 3-D network needs 120 h for complete formation. The exotherms in the cooling cycles (second and fourth cycles) shown before can be assigned to the formation of the initial 2-D assembles in the gel network. As discussed in previous chapters, the transition peaks are better defined in the cooling curves (sol-to-gel) rather than in the heating curves (gel-to-sol).[35]

However, in these systems, a less conventional behaviour was observed by the exotherms in the cooling cycles (second and fourth cycles) which appears as two peaks at 10.5 and 15.8 (MeCN) °C for **3.68.** This could be due to the fact that **3.68.** in MeCN was a weak gel from a rheological point of view. As the weak gel is forming, a colloidal suspension is appearing amongst the network (the gel appeared as a white opaque gel – vial m. Figure 3.22.). However, stronger gels displayed a single exothermic peak which may correspond to the formation of the SAFINs being the results of a single assembly phenomenon.
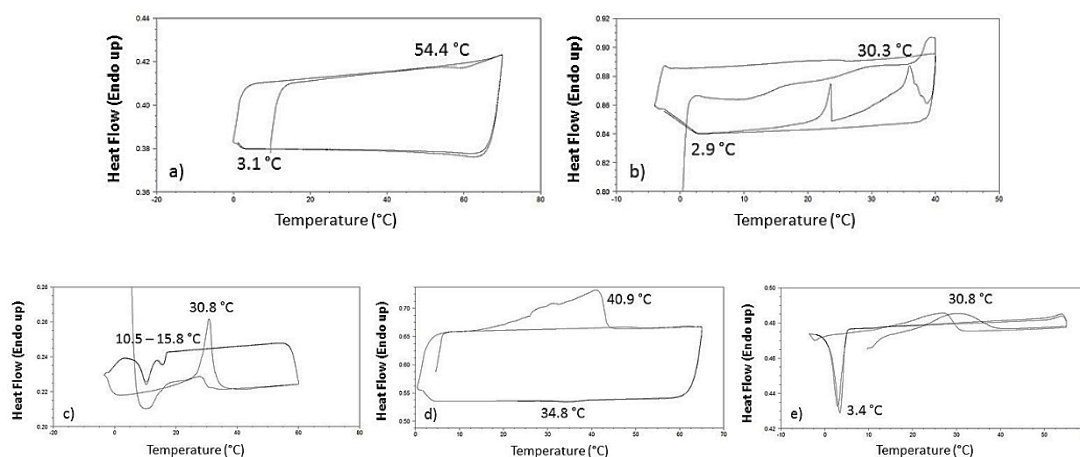
Figure 3.34. DSC of the gel **3.66.** - **3.69.**: a) **3.66.** in EtOH:H$_2$O (1:1) (0.8 w/v %); b) **3.67.** in chloroform (2.0 w/v %); c) **3.68.** in MeCN (1.4 w/v %); d) **3.68.** in EtOH:H$_2$O (1:1) (0.4 w/v %); e) **3.69.** in toluene (5.5 w/v %), during the two heating / two cooling cycles. The sample was heating from 0 °C to temperature lower than boiling point of the solvent used, at 2 °C/min and cooling the same range of temperature. Reproducible / duplicated cycles for each sample.

3.3.9. Morphological Studies

The morphology of the xerogels of the gels formed by the aspartic acid derivatives **3.61.** (D/L) and **3.65.** (L), aspartic acid based *O*-glycolipids **3.66.** - **3.69.** and aspartic acid based *N*-glycolipid **3.71.** was investigated using SEM imaging (Section 7.3.6.3.). The xerogels were formed from the corresponding gel in different solvents using a spatula to transfer the gel from the closed vial to the metal stub. The gels formed in EtOH:H$_2$O (1:1) were dried, in the freeze dryer prior to imaging.

The self-assembled structures, dimension and aggregation patterns of the fibres seem to vary significantly depending on the chemical structure of the gelator and on the nature of the solvent (Figure 3.35.).

The presence of thickly packed fibrous structures can be observed in xerogels of the aspartic acid derivatives **3.61.** (D/L) and **3.65.** (L) formed in toluene. These gels were both found to be strong gels from rheological evaluation [images a) and f)]. Short bundles of fibres such as spikes and needles, were observed in xerogels formed by compound **3.61.** (D/L) in DCM and chloroform [images b) and c)].

Long bundles of rod-like fibres were observed in xerogel formed by compound **3.65.** (L) in EtOAc [image g)]. Less defined structures such as lamellar display were observed in xerogels formed by compound **3.65.** (L) in Et$_2$O, DCM and petroleum ether [images e), h) and i)]. The presence of compact aggregates, in which non defined fibres could be observed, was found in xerogel formed by compound **3.65.** (L) in MeCN [image d)].

The morphology of the xerogels formed by the aspartic acid based *O*-glycolipids **3.66.** - **3.69.** was completely different from each other (Figure 3.35.). The strongest gel as determined from rheological evaluation, showed the presence of a porous structure, as can be observed in xerogel of the chloroform gel formed by compounds **3.67.** [image l)].

On the other hand, long packed fibres resembling a laminated topographic map were observed in xerogels formed by compound **3.68.** in EtOH:H$_2$O (1:1) and compound **3.69.** in toluene [images n) and o), respectively]. However, compact aggregates like blisters were observed in xerogel formed by compound **3.66.** in EtOH:H$_2$O (1:1) [image k)]. The presence of lamellar structure following defined patterns was observed in xerogels formed by compound **3.66.** in Et$_2$O [image j)] and formed by compound **3.68.** in MeCN [image m)].

Finally, the xerogel morphology of the aspartic acid based *N*-glycolipids from **3.71.** in petrol and cyclohexane were relatively similar (Figure 3.35.). The self-assembled structure was better defined for cyclohexane xerogel, however, thick fibre structures were detected in both xerogels [images p) and q)].
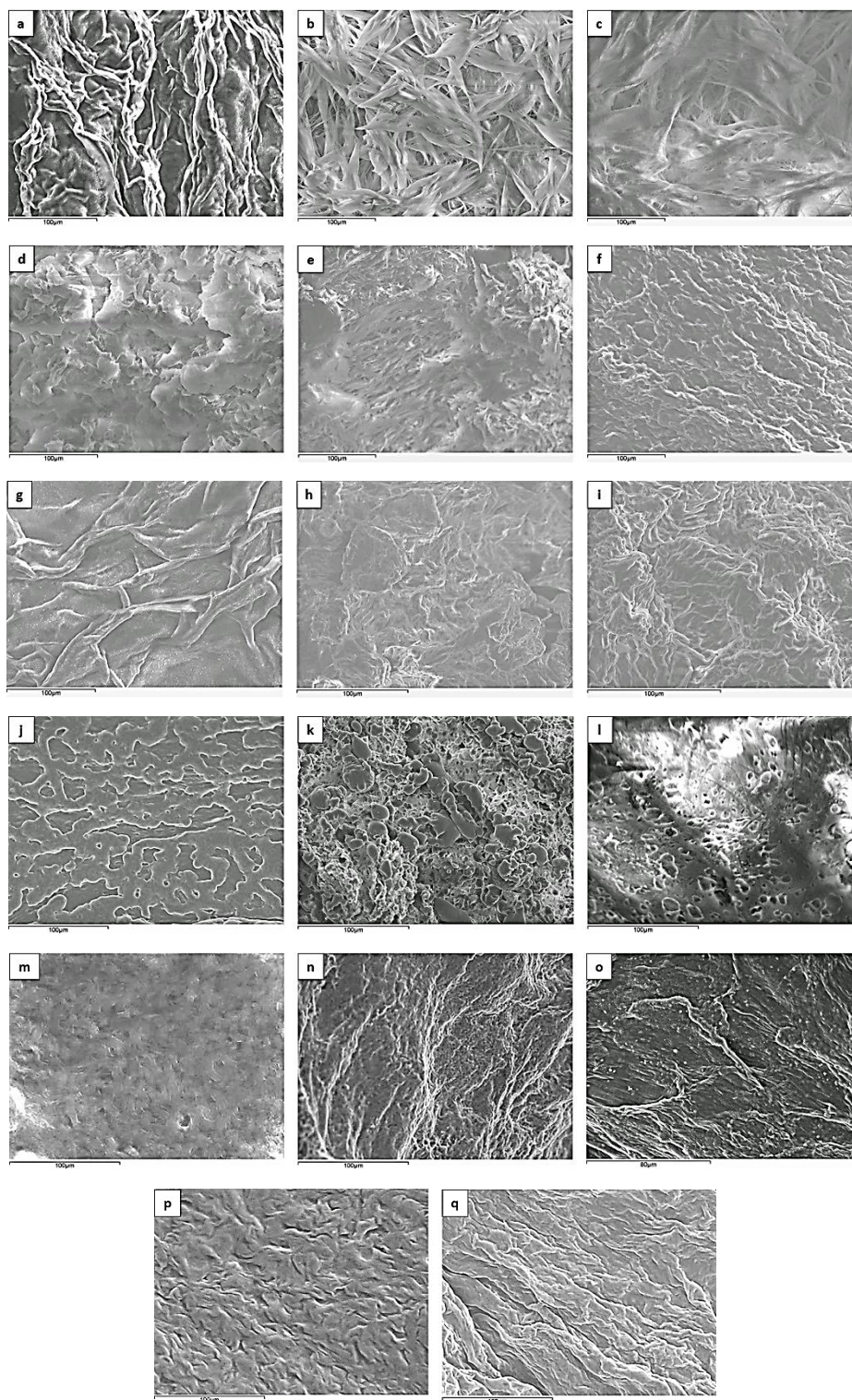
Figure 3.35. SEM images of Aspartic acid-xerogels **3.61.**, **3.65.** – **3.69.**, **3.71.** *Solvent:* a) (**3.61.**) *toluene*; b) (**3.61.**) *DCM*; c) (**3.61.**) *chloroform*; d) (**3.65.**) *MeCN*; e) (**3.65.**) *Et$_2$O*; f) (**3.65.**) *toluene;* g) (**3.65.**) *EtOAc*; h) (**3.65.**) *DCM*; i) (**3.65.**) *Pet. ether*; j) (**3.66.**) *Et$_2$O*; k) (**3.66.**) *EtOH:H$_2$O (1:1)*; l) (**3.67.**) *chloroform*; m) (**3.68.**) *MeCN*; n) (**3.68.**) *EtOH:H$_2$O (1:1)*; o) (**3.69.**) *toluene;* p) (**3.71.**) *petrol*; q) (**3.71.**) *cyclohexane*. (All gels were prepared at CGC). [Scale bar: a) – n), p), q) 100 μm; o) 80 μm].

3.3.10. Spectroscopic Analysis

^{1}H-NMR and FTIR analysis was carried out in order to investigate the role of H-bonding interactions in the gelation process induced by the aspartic acid based gelators discussed in the previous sections.

3.3.10.1. ^{1}H-NMR Spectroscopy Analysis

^{1}H-NMR spectra of the aspartic acid derivatives **3.61.** and **3.65.** and aspartic acid based *O*-glycolipids **3.67.** - **3.69.** were recorded in different deuterated solvents in which these compounds were found to form gels. Spectra were measured at increasing concentrations and/or different temperatures, as appropriate. The solutions were prepared below CGC in a NMR tube and heated if required to increase the solubility of the gelator in the solvent.

^{1}H-NMR expanded region of interest spectra for all the gelators studied in different deuterated solvents are shown in Appendix.

*3.3.10.1.1. ^{1}H-NMR Studies of Aspartic Acid Derivatives **3.61.** and **3.65.***

^{1}H-NMR spectra of the aspartic acid gelator **3.61.** was studied in (D$_8$)-toluene, (D$_2$)-DCM and CDCl$_3$ at different concentrations and different temperatures (Table 3.9). Figure 3.36. shows the full ^{1}H-NMR spectra of **3.61.** in (D$_8$)-toluene. Initial measurements carried out at low concentration of **3.61.** (1.6 mg/mL) and at 27 °C showed an overlapping of the NH signals with residual solvent peaks. When the gelator concentration was increased (3 mg/mL), the NH signals shifted downfield slightly ($\Delta\delta$ = 0.09 for NH$_a$ and 0.02 for NH$_b$). When the experiments were carried out at increasing temperatures, NH signals moved upfield ($\Delta\delta$ = - 0.37 for NH$_a$ and - 0.25 for NH$_b$). These shifts correlate well with reports in literature that suggest the involvement of amide groups in intermolecular H-bolding.[47] (Table 3.9).
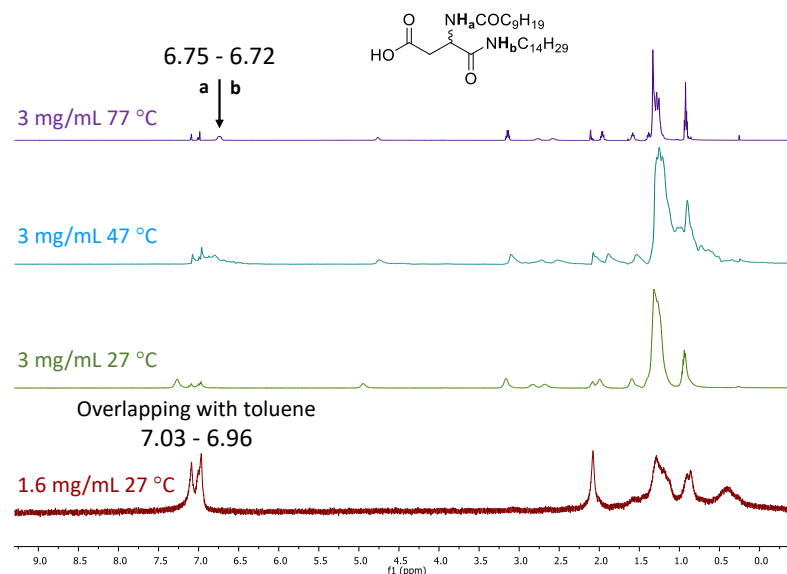
Figure 3.36. Full ^{1}H-NMR spectra of **3.61.** in (D$_8$)-toluene at concentrations 1.6 and 3 mg/mL at different temperature.

Figure 3.37. shows the full ^{1}H-NMR spectra of **3.61.** in (D$_2$)-DCM at increasing concentrations and temperatures. At low concentration (1.6 mg/mL), the NH signals overlapped. Upon increasing the concentration of **3.61.** (up to 6 mg/mL), the NH signals started splitting and small downfield shifts could be appreciated ($\Delta\delta$ = 0.16 for NH$_a$ and 0.09 for NH$_b$).The spectrum was recorded at higher temperature to prove intermolecular H-bonding. Thus, NH signals moved upfield when the temperature was 32 °C, ($\Delta\delta$ = - 0.12 for NH$_a$ and – 0.08 for NH$_b$). (Table 3.9).
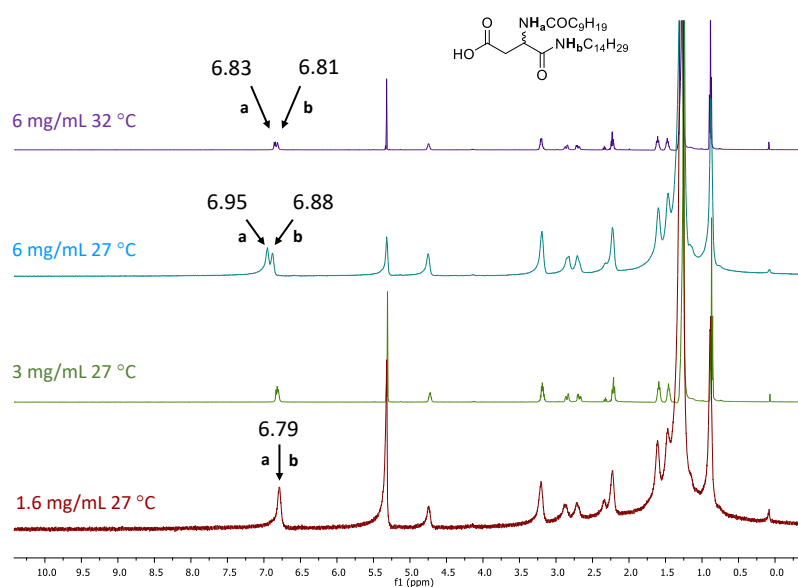
Figure 3.37. Full ^{1}H-NMR spectra of **3.61.** in (D$_2$)-DCM at concentrations 1.6, 3 and 6 mg/mL at different temperature.

Figure 3.38. shows the full ^{1}H-NMR spectra of **3.61.** in (D)-Chloroform at increasing concentrations and at the same temperature (27 °C). As previously discussed solvents, the NH signals shifted downfield upon increasing the concentration ($\Delta\delta$ = 0.16 for NH_a and 0.09 for NH_b). These values are consistent with the formation of weak intermolecular H-bonding in gels.[47] (Table 3.9).
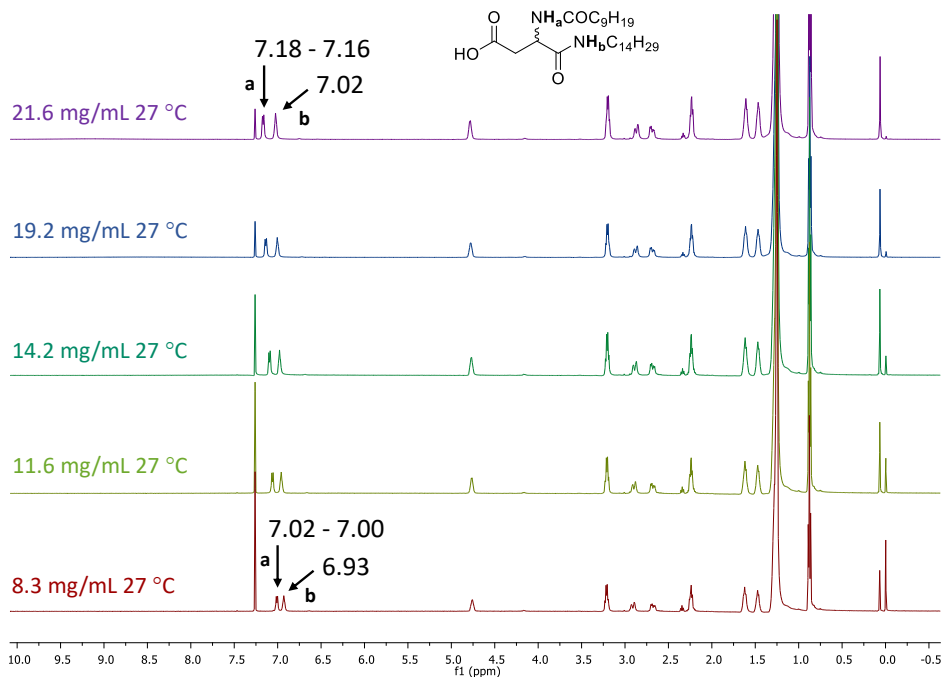
Figure 3.38. Full ^{1}H-NMR spectra of **3.61.** in (D)-chloroform at different concentrations.

Similar behaviour was observed for the enantiomerically pure compound **3.65.** Figure 3.39. shows the full ^{1}H-NMR spectra of **3.65.** in (D_8)-toluene at increasing concentrations and temperatures. Once again, a small downfield shift could be observed for NH resonances upon increasing concentration ($\Delta\delta$ = 0.02 for NH_a and 0.05 for NH_b). At higher temperatures (77 °C), the NH signals shifted upfield as expected ($\Delta\delta$ = - 0.19 for NH_a and – 0.19 for NH_b), an indication that intermolecular H-bonding was being disrupted. Also, the resolution of the spectrum improved considerably. (Table 3.9).
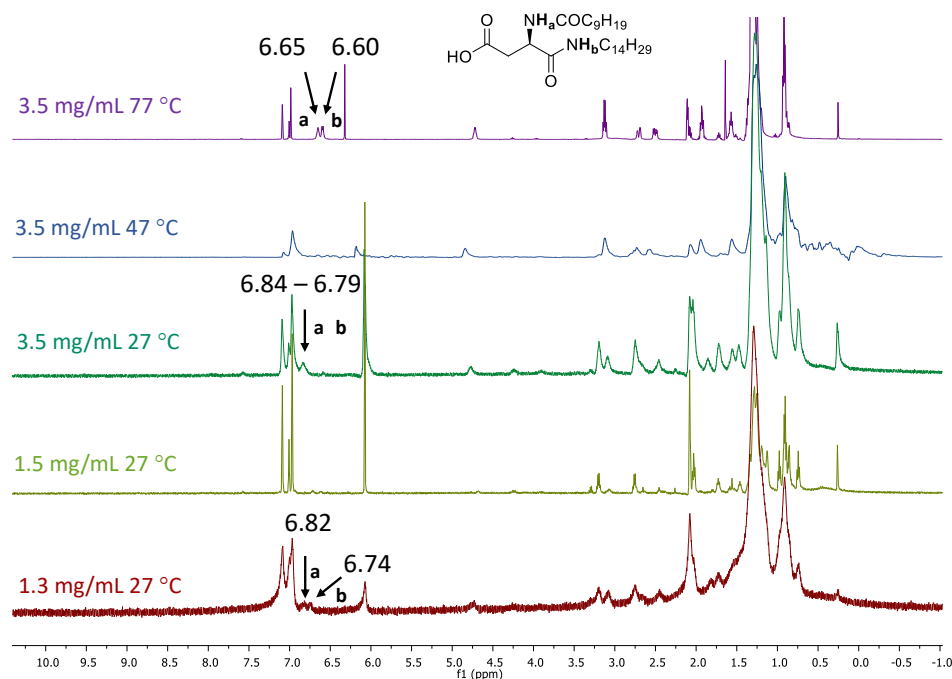
Figure 3.39. Full ^{1}H-NMR spectra of **3.65.** in (D$_8$)-toluene at concentrations 1.3, 1.5 and 3.5 mg/mL at different temperature.

Figure 3.40. shows the full ^{1}H-NMR spectra of **3.65.** in (D$_2$)-DCM at increasing concentrations and temperatures. At 27 °C, the NH signals showed downfield shifts ($\Delta\delta$ = 0.23 for NH$_a$ and 0.14 for NH$_b$). Again, the NH signals which were overlapping at 1.5 mg/mL, started splitting upon increasing the concentration. The spectrum was measured at a higher temperature and as expected, NH signals shifted upfield at 32 °C, ($\Delta\delta$ = - 0.17 for NH$_a$ and - 0.09 for NH$_b$). (Table 3.9). Interestingly, the $\Delta\delta$ values of the NH signals, upon increasing concentrations were slightly larger for the pure enantiomer **3.65.** (L) ($\Delta\delta$ = 0.23 for NH$_a$ and 0.14 for NH$_b$) compared to those for the racemic sample **3.61.** (D/L) ($\Delta\delta$ = 0.16 for NH$_a$ and 0.09 for NH$_b$). This may suggest a different nature of the interactions between the molecules of gelator in the racemic and the optically pure compound.
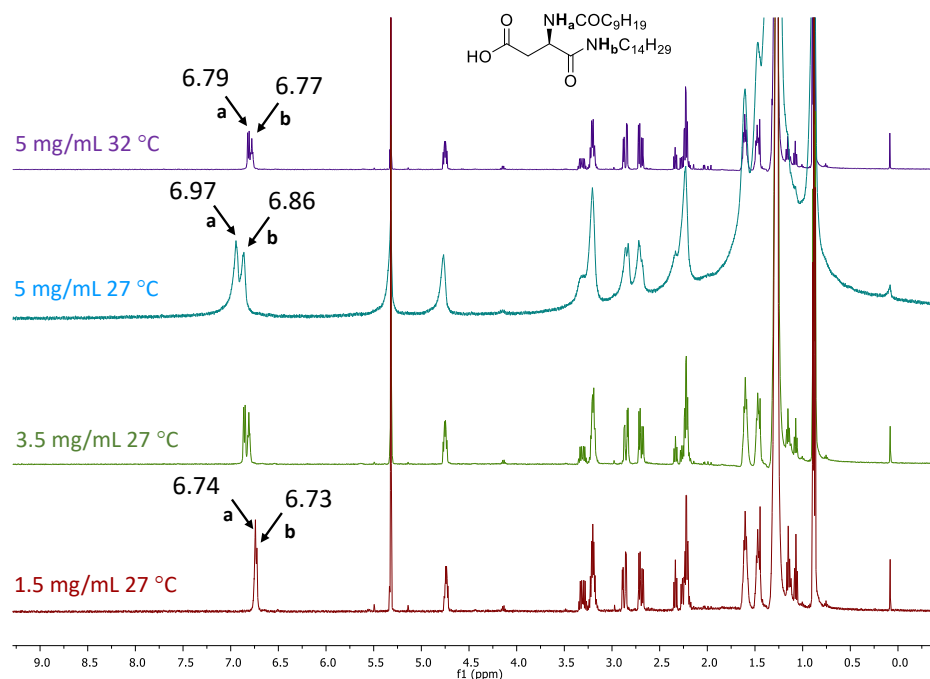
Figure 3.40. Full ^{1}H-NMR spectra of **3.65.** in (D$_2$)-DCM at concentrations 1.5, 3.5 and 5 mg/mL at different temperature.

Table 3.9. Chemical shifts (δ) of the NH signals in the ^{1}H-NMR spectra in solution and in gel phase of **3.61.** and **3.65.** in (D$_8$)-toluene, (D$_2$)-DCM, (D)-chloroform.

Compound	Solvent	Concentration	Temperature	δ NH$_a$ (ppm)	δ NH$_b$ (ppm)
3.61. (D/L)	Toluene	1.6 mg/mL	27 °C	7.03	6.96
		3 mg/mL	27 °C	7.12	6.96
		3 mg/mL	77 °C	6.75	6.72
	DCM	1.6 mg/mL	27 °C	6.79	6.79
		6 mg/mL	27 °C	6.95	6.88
		6 mg/mL	32 °C	6.83	6.81
	Chloroform	8.3 mg/mL	27 °C	7.01	6.93
		21.6 mg/mL	27 °C	7.17	7.02
3.65. (L)	Toluene	1.3 mg/mL	27 °C	6.82	6.74
		3.5 mg/mL	27 °C	6.84	6.79
		3.5 mg/mL	77 °C	6.65	6.60
	DCM	1.5 mg/mL	27 °C	6.74	6.73
		5 mg/mL	27 °C	6.97	6.86
		5 mg/mL	32 °C	6.79	6.77

*3.3.10.1.2. ^{1}H-NMR Studies of Aspartic Acid Based O-glycolipids **3.67. - 3.69.***

Figure 3.41. shows the full ^{1}H-NMR spectra of the deprotected glycolipid **3.67.** (D/L) in (D)-Chloroform at increasing concentrations at the same temperature (27 °C). The NH signals of the amide linker shifted downfield as expected upon increasing the concentration ($\Delta\delta$ = 0.15 and 0.21 for NH$_a$). (Table 3.10). However, the NH signals for the amides on the α-C (NH$_b$ and NH$_c$) did not show significant shifts. This could indicate that these groups are not significantly involved in intermolecular H-bonding with other gelator molecules. The resonance at 4.13 ppm (8.3 mg/mL) corresponding to the free hydroxyl (OH), also shifted at increasing concentration ($\Delta\delta$ = 0.44).
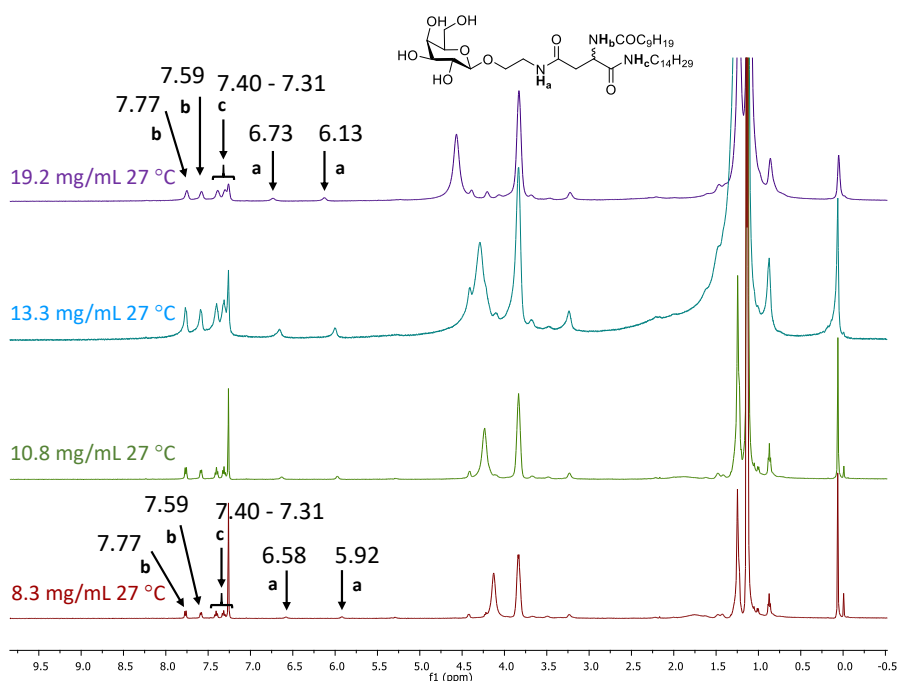
Figure 3.41. Full ^{1}H-NMR spectra of **3.67.** in (D)-chloroform at different concentrations.

Figure 3.42. shows the full ^{1}H-NMR spectra of the acetylated glycolipid **3.68.** (L) in (D$_3$)-MeCN at increasing concentrations and at the same temperature (27 °C). The NH signals of the amide linker shifted downfield very slightly as expected upon increasing the concentration ($\Delta\delta$ = 0.09 for NH$_a$, 0.06 for NH$_b$ and 0.07 for NH$_c$). (Table 3.10). These small values could account for the formation of weak intermolecular H-bonding in gels.[47] (Table 3.10).
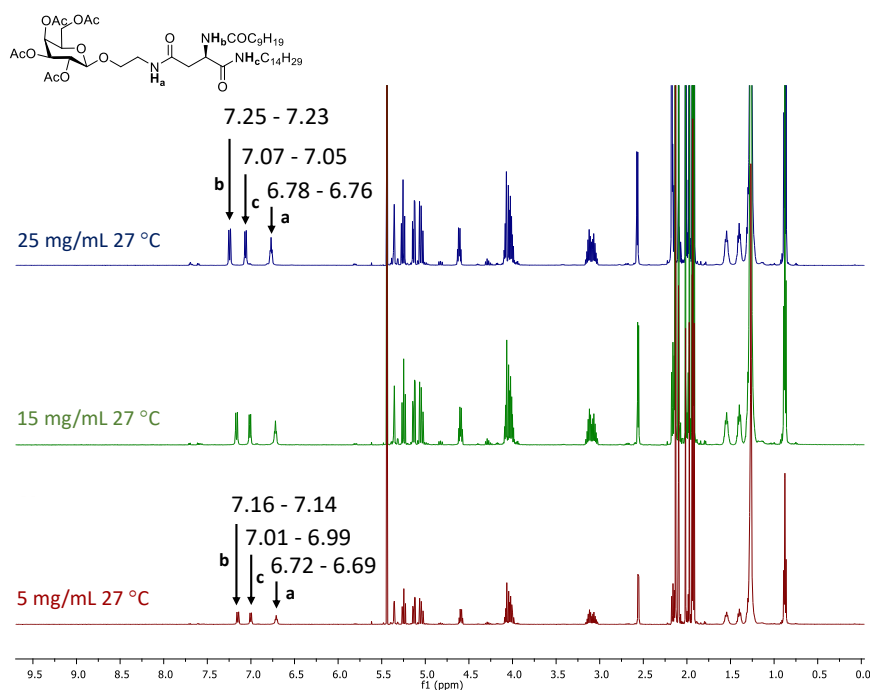
Figure 3.42. Full ¹H-NMR spectra of **3.68.** in (D₃)-MeCN at different concentrations.

Figure 3.43. shows the full ¹H-NMR spectra of the deprotected glycolipid **3.69.** (L) in (D₈)-toluene at increasing concentrations and at the same temperature (27 °C). As it is shown in the ¹H-NMR spectra, the signals for the protons in the compound (other than the alkyl tails) could not be appreciated. This could be due to the fast gel formation that would lead to a decrease in the mobility of the gelator molecules due to entrapment in the gel matrix. This resulted in a strong gel forming immediately in the NMR tube even at the lower concentration.
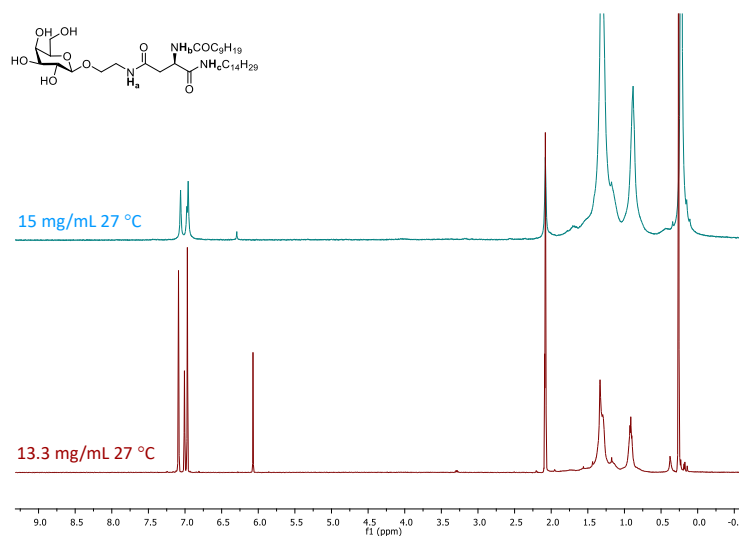
Figure 3.43. Full ¹H-NMR spectra of **3.69.** in (D₈)-toluene at different concentrations.

Table 3.10. Chemical shifts (δ) of the NH signals in the ^{1}H-NMR spectra in solution and in gel phase of **3.67.** - **3.69.** in (D)-chloroform, (D$_3$)-MeCN, (D$_8$)-toluene.

Compound	Solvent	Concentration	Temperature	δ NH$_a$ (ppm)	δ NH$_b$ (ppm)	δ NH$_c$ (ppm)
3.67. (D/L)	Chloroform	8.3 mg/mL	27 °C	6.58-5.92	7.77-7.59	7.40-7.31
		19.2 mg/mL	27 °C	6.73-6.13	7.77-7.59	7.40-7.31
3.68. (L)	MeCN	5 mg/mL	27 °C	7.16-7.14	7.01-6.99	6.72-6.69
		25 mg/mL	27 °C	7.25-7.23	7.07-7.05	6.78-6.76

3.3.10.2. FTIR Spectroscopy Analysis

Previous studies have shown that when organogel formation is promoted by H-bonding, the IR bands associated with the relevant functional groups in the molecule shift to lower wavenumbers from those recorded of the gelator free in solution, as discussed in earlier chapters.[51,52] FTIR spectroscopic data were obtained for gelators **3.61.**, **3.65.**, **3.67.** - **3.69.** in different solvents and different physical states in order to ascertain if H-bonding was involved in gel formation. FTIR spectra were recorded: I.) as a bulk solid sample in NaCl plate; II.) in solution and III.) as gels in the required solvent in a closed cell or with an ATR accessory (diamond crystal). The positions and assignments of the noteworthy IR bands (νNH and νCO) in the three states, are given in Table 3.11. for gelators **3.61.** and **3.65.**, and in Table 3.12. for gelators **3.67.** - **3.69.** In all cases studied, the spectra recorded for the bulk and gel state showed similar peak positions, however the bands were shifted to higher wavenumbers in the spectra recorded in solution.

*3.3.10.2.1. FTIR Analysis of Gels Formed by Aspartic Acid Derivatives **3.61.** and **3.65.***

The bands corresponding to the NH and CO stretches in compound **3.61.** appeared at 3386 cm^{-1} (only one band could be appreciate for the NH bands), 1736 cm^{-1} and 1699 cm^{-1} (for the CO groups) when in solution in toluene. The bands for the NH and CO shifted to higher frequencies by 95, 33 and 32 cm^{-1} respectively when gelation takes place (Figure 3.44.). A similar observation could be recorded for the FTIR spectra of pure enantiomer compound **3.65.** in toluene (Figure 3.45.). The shifts observed for the bands of interest in this case were 93, 15 and 32 cm^{-1} between the solution and gel state for the NH and CO stretch values (Table 3.11.).
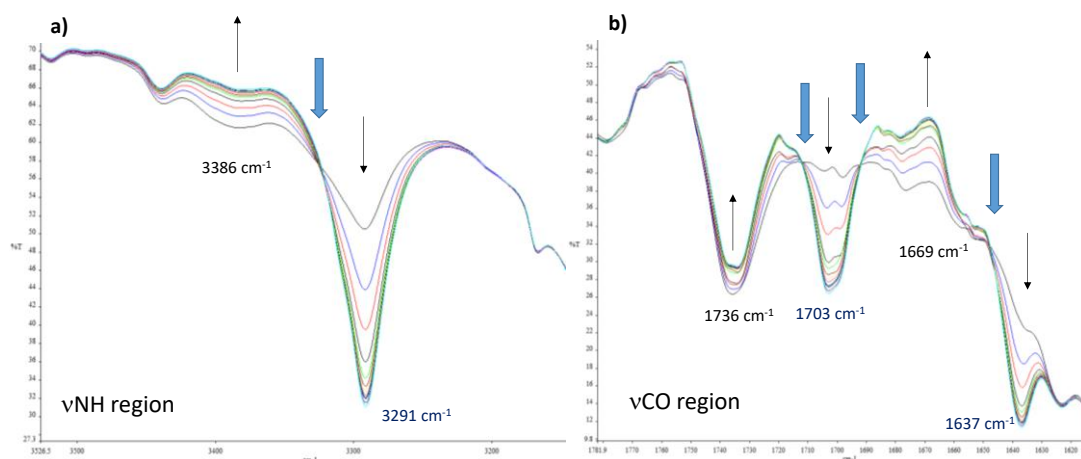
Figure 3.44. FTIR spectra of compound **3.61.** (D/L) 0.6 w/v % in toluene solution from 0 – 30 min. The solution injected into the cell was warm and was allowed to cool to rt. a) νNH region; b) νCO region.
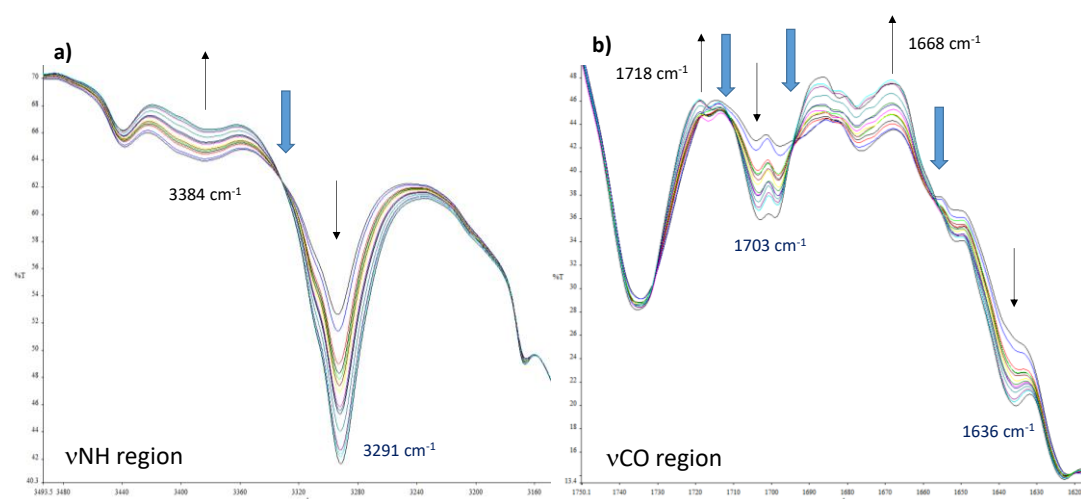
Figure 3.45. FTIR spectra of compound **3.65.** (L) 0.4 w/v % in toluene solution from 0 – 60 min. The solution injected into the cell was warm and was allowed to cool to rt. a) νNH region; b) νCO region.

The bands for the NH and CO stretches in gelator **3.61.** (D/L) appeared at 3417 cm^{-1}, 1738 cm^{-1} and 1670 cm^{-1}, respectively. in DCM solution. Upon gelation, the bands for the NH and CO shifted to higher frequencies by 126, 36 and 34 cm^{-1} respectively (Figure 3.46.). In all the cases the magnitudes of the shifts are comparable to those reported for other supramolecular gels and indicate H-bonding formation.[52,142] A similar observation could be recorded for the FTIR spectra of pure enantiomer compound **3.65.** (L) in DCM (Figure 3.47.). The shifts observed for the bands of interest in this case were 119, 24 and 35 cm^{-1} between the solution and gel state for the NH and CO stretch values (Table 3.11.).

- 110 -
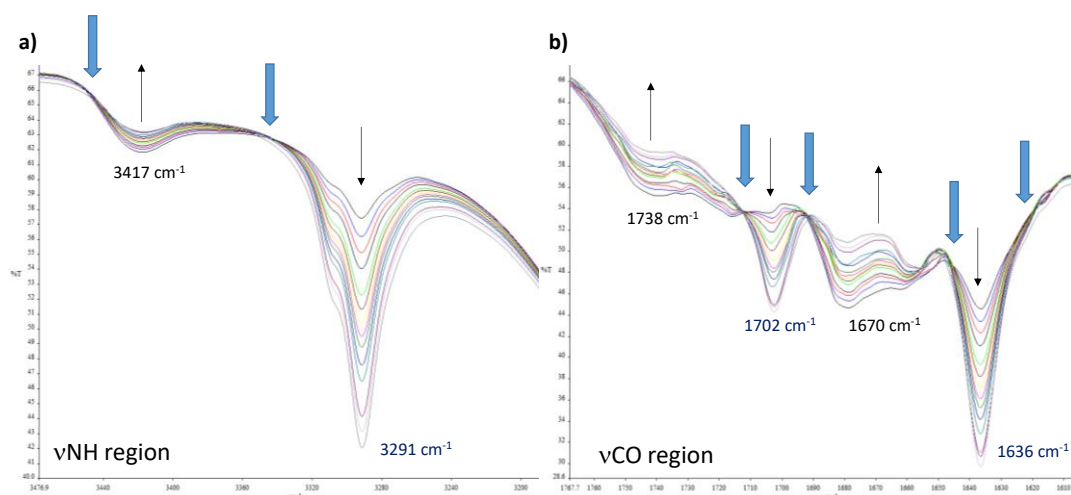
Figure 3.46. FTRI spectra of compound **3.61.** (D/L) 1.1 w/v % in DCM solution from 0 – 60 min. The solution injected into the cell was warm and was allowed to cool to rt. a) νNH region; b) νCO region.
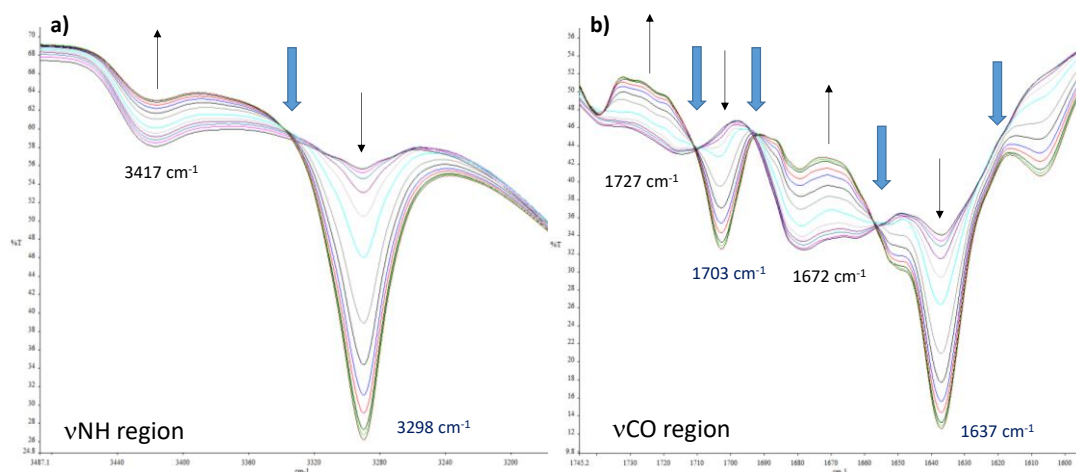
Figure 3.47. FTIR spectra of compound **3.65.** (L) 0.5 w/v % in DCM solution from 0 – 90 min. The solution injected into the cell was warm and was allowed to cool to rt. a) νNH region; b) νCO region.

The formation of a chloroform gel induced by aspartic acid derivative **3.61.** was also studied (Figure 3.48.). In this case, the bands of interest (νNH and νCO) could not be distinguished clearly in the chloroform solution. Nevertheless, changes in the intensities of the spectra as the gelation process was taking place (0 – 60 min) were comparable with those observed in the gelation processes of toluene and DCM induced by **3.61.** which were discussed earlier (Table 3.11.). However, the bands were significantly broader as shown in Figure 3.48.
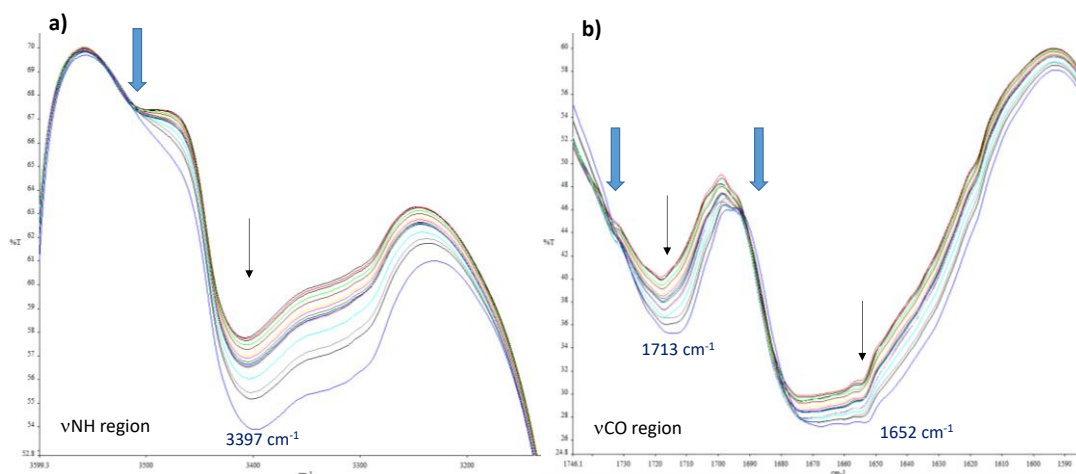
Figure 3.48. FTRI spectra of compound **3.61.** (D/L) 2.0 w/v % in chloroform solution from 0 – 60 min. The solution injected into the cell was warm and was allowed to cool to rt. a) νNH region; b) νCO region.

Table 3.11. Position of characteristic IR bands of **3.61.** (D/L) and **3.65.** (L) in the solid state (Bulk. NaCl disk), solution and gel state in a cell.

Compound	Solvent	State	νNH (cm^{-1})	νCO (cm^{-1})	
3.61. (D/L)	-	Bulk (NaCl disk)	3299	1749	1636
	Toluene (cell)	Solution	3386	1736	1669
		Gel	3291	1703	1637
	DCM (cell)	Solution	3417	1738	1670
		Gel	3291	1702	1636
	Chloroform (cell)	Solution	-	-	-
		Gel	3397	1713	1652
3.65. (L)	-	Bulk (NaCl disk)	3291	1702	1638
	Toluene (cell)	Solution	3384	1718	1668
		Gel	3291	1703	1636
	DCM (cell)	Solution	3417	1727	1672
		Gel	3298	1703	1637

*3.3.10.2.2. FTIR Analysis of Gels Formed by Aspartic Acid Based O-glycolipids **3.67.** - **3.69.***

The gelation of a chloroform solution of the deprotected *O*-glycolipid **3.67.** appeared to be very quick. It was not possible to unambiguously assign a NH stretch frequency in solution. The CO stretch of *O*-glycolipid **3.67.** in chloroform solution was assigned at 1670 cm^{-1}. Upon gelation, this band shifted to higher frequencies by 30 cm^{-1} (Figure 3.49. Table 3.12.).
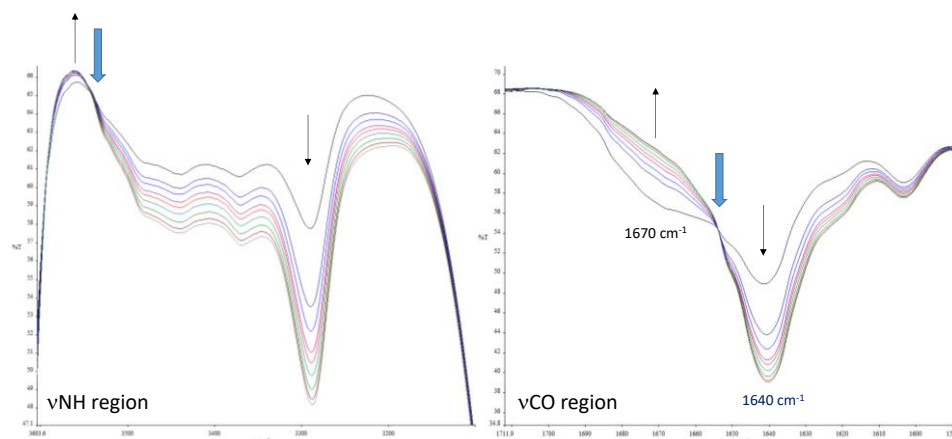
Figure 3.49. FTIR spectra of compound **3.67.** 2.0 w/v % in chloroform solution from 0 – 40 min. The solution injected into the cell was warm and was allowed to cool to rt. a) νNH region; b) νCO region.

The bands for NH and CO stretches in MeCN solution of the acetylated *O*-glycolipid **3.68.** shifted to higher frequencies by 104 and 38 cm^{-1} respectively between the solution and gel state (Figure 3.50. Table 3.12.).
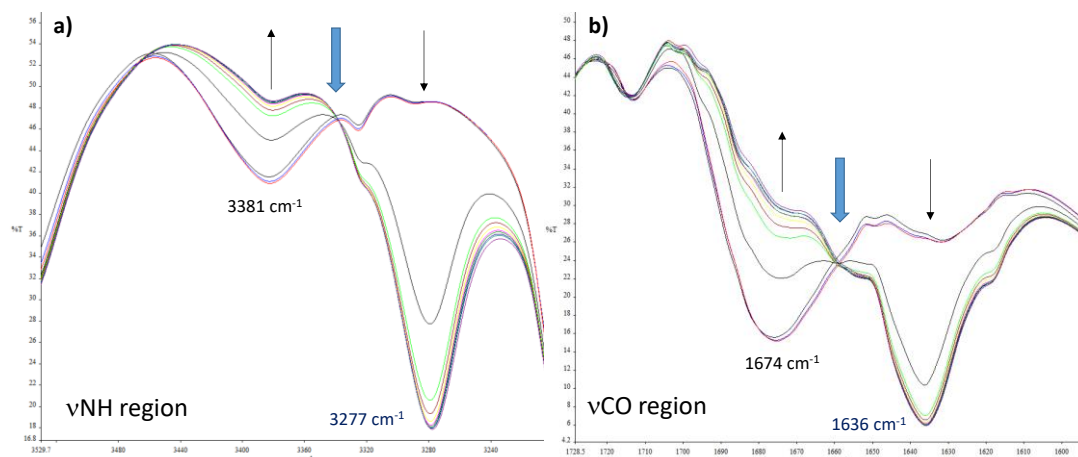
Figure 3.50. FTIR spectra of compound **3.68.** 1.4 w/v % in MeCN solution from 0 – 60 min. The solution injected into the cell was warm and was allowed to cool to rt. a) νNH region; b) νCO region.

The gelation in toluene induced by deprotected *O*-glycolipid **3.69.** had to be studied using FTIR-ATR optics, as this process was very quick with very minor changes being observed, even when using the solution cell set-up, as for previous experiments. The gelation of toluene occurred almost immediately and it is shown in Figure 3.51.

As observed for the deprotected *O*-glycolipid **3.67.**, again it was not possible to assign a frequency for the NH stretch in solution for the deprotected *O*-glycolipid **3.69.** The CO stretches in toluene solution for **3.69.** were assigned at 1639 and 1543 cm^{-1}. Upon gelation, these bands shifted to higher frequencies by 35 and 48 cm^{-1}, respectively (Table 3.12.). These values are consistent with those observed for other gelators described earlier and are indicative of the formation of intermolecular H-bonds.
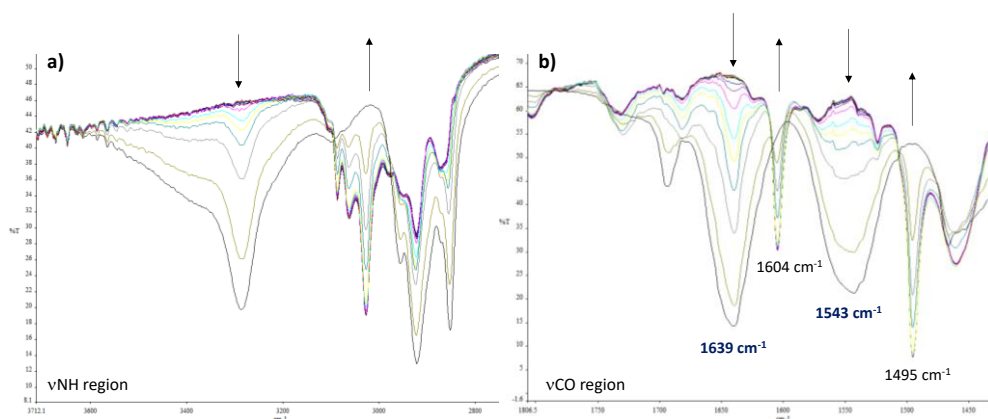
Figure 3.51. ATR spectra of compound **3.69.** 5.5 w/v % in toluene solution from 0 – 60 min. The solution was placed on the ATR optics when it was warm and was allowed to cool to rt. a) νNH region; b) νCO region.

Table 3.12. Position of characteristic IR bands of **3.67.** - **3.69.** in the solid state (Bulk. NaCl disk), solution and gel state in a cell or ATR optics.

Compound	Solvent	State	νNH (cm^{-1})	νCO (cm^{-1})	
3.67. (D/L)	-	Bulk (NaCl disk)	3283	1687	1626
	Chloroform (cell)	Solution	3561	1670	-
		Gel	3281	1640	-
3.68. (L)	-	Bulk (NaCl disk)	3289	1751	1646
	MeCN (cell)	Solution	3381	1674	-
		Gel	3277	1636	-
3.69. (L)	-	Bulk (NaCl disk)	3066	1654	1540
	Toluene (ATR)	Solution	-	1639	1543
		Gel	-	1604	1495

3.4. Conclusion

I.) The syntheses of aspartic acid derivatives **3.61.** (D,L) and **3.65.** (L) was accomplished using amide coupling methodologies and were optimised as described. In addition, galactosyl compound **3.66.** – **3.69.** (*O*-glycolipids) and **3.70.** - **3.72.** (*N*-glycolipids) were also synthesised and characterised.

II.) The ability of the above derivatives to act as LMWGs was screened in a range of solvents with different polarities. It was found that **3.65.** (L) formed gels in a larger range of solvents than the racemic **3.61.** (D,L). The introduction of the galactosyl moiety resulted in a more selective gelation profile for *O*-glycolipid **3.66.** - **3.69.** It was found that the chirality of the α-C strongly influenced the assembly mode of these derivatives and therefore, their gelation properties. It was also observed that the deprotected *O*-glycolipid **3.67.** and **3.69.** formed strong gels in organic non-protic solvents, while the corresponding acetylated derivatives were able to form gels in a mixture of EtOH:H_2O (1:1). The aspartic acid based *N*-glycolipids **3.71.** and **3.72.** exhibited a weaker ability to form gels than the other derivatives studied.

III.) Crystal structures of shorter alkyl chain aspartic acid benzyl ester derivatives of both the pure enantiomer **3.52.** (L) and the racemate **3.56.** (D,L). were obtained. Clear differences in the packing of both structures could be observed.

IV.) The gels formed were characterised by study of their rheological and thermal properties. Rheological analysis proved they were gels with different strength and rheological parameters. DSC analysis showed that the gels were thermoreversible. The morphological studies of the xerogels using SEM revealed very different xerogel structures depending on the solvent and gelator. Better defined fibrous structures were observed in the strong gels, while the weak gels revealed compact aggregates and/or multi-lamellar structures.

V.) Spectroscopic analysis using NMR and FTIR were carried out to better understand the intermolecular interactions involved in the gelation process. These studies indicated that H-bond formation was involved in the gelation process of the organic non-protic solvents studied.

VI.) The free hydroxyl groups-*O*-glycolipid compound **3.69.** formed a gel in toluene at 5.5 w/v %. It is a strong gel from the point of view of rheological properties ($\tan\delta$ = 0.19 - 0.24). This opens new possibilities for the application of **3.69.** in materials and biomedical science such as, scaffolds for tissue engineering which will be discussed in Chapter 5.

Chapter 4

Galactosylated

Squaramides as LMWGs

4.1. Introduction to Squaramides

Derivatives of squaric acid (diketocyclobutene) were first synthesised in the 1960s by Cohen and co-workers.[143] Squaramides (Figure 4.1.) are four-membered vinylogously conjugated diamides derived from squaric acid.[144] One of the most important features of these scaffolds is their capability for selectively binding to different H-bond acceptors through their acidic NH groups. Remarkably, squaramides play a double role as they are also able to act as good H-bond acceptors, making them suitable as receptors for anion/cation recognition. This property has been explored to find promising candidates for the development of novel drugs[145-147] and in the field of organocatalysis[148-151] as chiral H-bond donor catalysts. Additionally, squaramides have been recognised as bioisosteres of ureas exhibiting interesting properties for diverse research areas such as biomedicine,[145,152] synthesis,[153] crystal engineering[154-156] and the most relevant for this thesis, LMWGs.[157]

The physical properties of squaramides and their complexes with anions and cations have been discussed by Quinonero, Ballester and co-workers among others.[158-160] It was recognised that secondary squaramides offer the potential to H-bond to acceptors, donors and to mixed acceptor–donor groups (Figure 4.1.).[160]

H-bond acceptor

H-bond donor
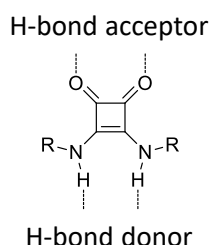
Figure 4.1. H-bonding donor-acceptor ability of squaramide.[145]

Although there are evident similarities between amides and squaramides, one distinguishing feature of squaramides is the rigid and planar structure of the cyclobutadienedione ring containing two coplanar carbonyl groups and two amide protons that are almost coplanar. This arrangement is stabilised by the nitrogen orbitals that are essentially sp_2-hybridised, making the lone pairs available for conjugation from N(p-orbital) into the π-system orthogonal to the plane (Figure 4.2.).[145]
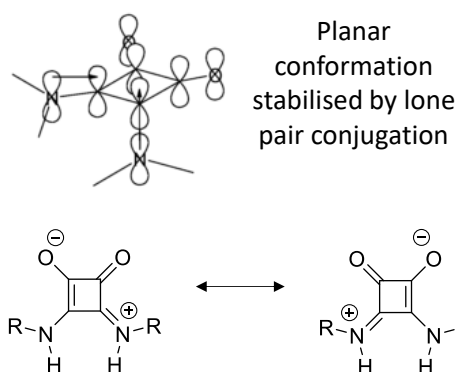
Figure 4.2. Planar conformation and resonance forms of squaramides.[145]

4.1.1. Squaramides as LMWGs

As explained previously, the squaramide frame possesses remarkable H-bonding capacity containing two H-bond donors (NH) and two carbonyl acceptors (CO), due to its tendency to increase the aromaticity of the four-membered ring at the time of binding. This feature has been used in the preparation of diverse compounds for the field of supramolecular chemistry.[159,161,162] However, few examples exist in the literature that incorporate squaramides in LMWGs.

Ohsedo and co-workers were the first group to publish research based on squaramides in LMWGs. In this research, they developed a new family of organogelators based on squarylium monoalkylamides and dialkylamides using a simple, one step synthesis (Scheme 4.1.).[162]

4.2. n = 12
4.3. n = 16
4.4. n = 18

4.5. n = 12
4.6. n = 16
4.7. n = 18
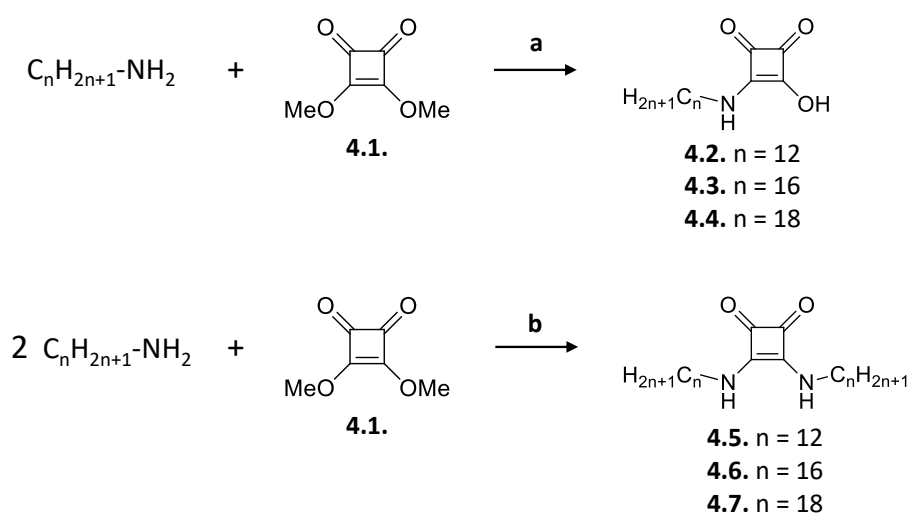
Scheme 4.1. One-pot synthesis of monosubstituted squaramides **4.2.** – **4.4.** and disubstituted squaramides **4.5.** – **4.7.**; Reagents and conditions: a) MeOH, reflux, 2 h; 2) THF, HCl, reflux, 1 h; b) MeOH, reflux, 2 h.[162]

The gelation ability of those two families of squaramides with different chain lengths (C_{12}, C_{16} and C_{18}), was studied in a range of solvents (e.g. DMF, DMSO, H_2O, MeOH, DCM, n-hexane and toluene). **4.3.** − **4.7.** formed opaque gels only in DMF. The monosubstituted family (**4.3.** and **4.4.**), were poor gelators of DMF and required 1.5 w/v %, cooling to -15 °C and a longer alkyl chain length (C_{16} and C_{18}) for the formation of organogels to occur. The disubstituted family (**4.5.** − **4.7.**), were more efficient gelators of DMF, requiring 0.5 w/v % for gel formation. In these compounds, the alkyl chain length proved insignificant role in the ability of the compound to form organogels. When DMSO was used as a solvent, precipitation was observed in **4.2.** - **4.4**. (1.5 w/v %) after cooling the gelator solutions. When 1.0 w/v % solutions of **4.5.** - **4.7.** were used, they became viscous after cooling.

The work reported by Alegre and co-workers describes the synthesis of new squaramide derivatives and the development of their supramolecular applications.[149,157,163] During the synthesis of squaramide **4.10.** (Scheme 4.2.) a clear tendency to increase the viscosity of the solvent used (e.g., MeOH) was observed. For that reason, the formation of supramolecular aggregates in solution was studied in detail.
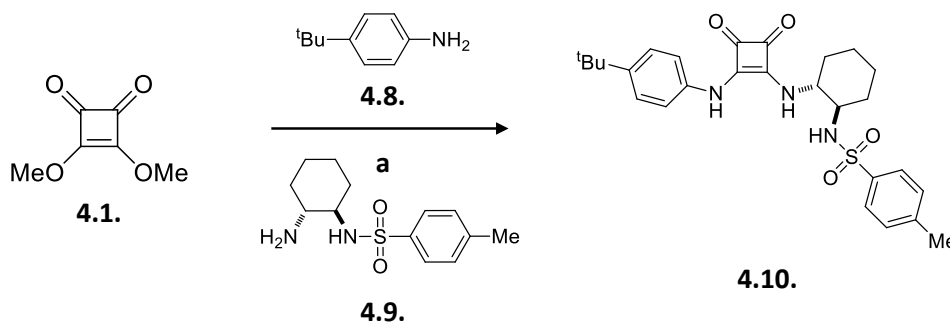
Scheme 4.2. One-pot synthesis of squaramide **4.10.** Reagents and conditions: a) MeOH, rt, 2 h.[157]

To correlate the structural functionalities of **4.10.** with its gelation properties, the authors designed and synthesised different analogous squaramides (Figure 4.3.). Specifically, they incorporated substituents with different steric and electronic properties, following the same synthetic procedure. Squaramides **4.11.** and **4.12.** were also included for comparison with **4.10.** Additionally, the synthesis of compounds **4.13.**, **4.14.** (no substituents in the aromatic ring) and **4.15.**, were also

carried out to compare with squaramide **4.10.** Squaramides **4.16.** and **4.18.**, with electron-withdrawing groups, squaramide **4.17.** with an electron-donating substituent, and compound **4.19.**, which lacks the aromatic ring, were also synthesised. In these cases (**4.16.** - **4.19.**), the stereochemical configuration and the structural core were maintained as in **4.10.** The gelation ability of compound **4.10.** was screened for 34 different solvents using the heating-cooling procedure at concentrations ranging from 3 to 21 g/L. Surprisingly, **4.10.** showed an unusual selectivity to form stable gels in a number of alcoholic solvents (alcogels), and acetone. In contrast, no gelation tendency was detected for squaramides **4.11.** – **4.19.** These results suggested the existence of unique molecular interactions and appropriate HLB that favour the self-assembly of **4.10.** in alcohols. These conclusions were confirmed after computational studies. The results indicated that **4.10.** had a larger and more complex network of inter- and intramolecular interactions (H-bonds, NH…π and C-H…π interactions and intramolecular π-π stacking) that provides an additional stabilising property to the compound. A weaker network of interactions was formed for the compounds **4.11.** – **4.19.**

4.11. **4.12.** **4.13.** (R$_1$ = H; R$_2$ = CF$_3$)
4.14. (R$_1$ = H; R$_2$ = H)
4.15. (R$_1$ = OMe; R$_2$ = H)

4.16. (R$_1$ = H; R$_2$ = F) **4.19.**
4.17. (R$_1$ = OMe; R$_2$ = H)
4.18. (R$_1$ = H; R$_2$ = CF$_3$)
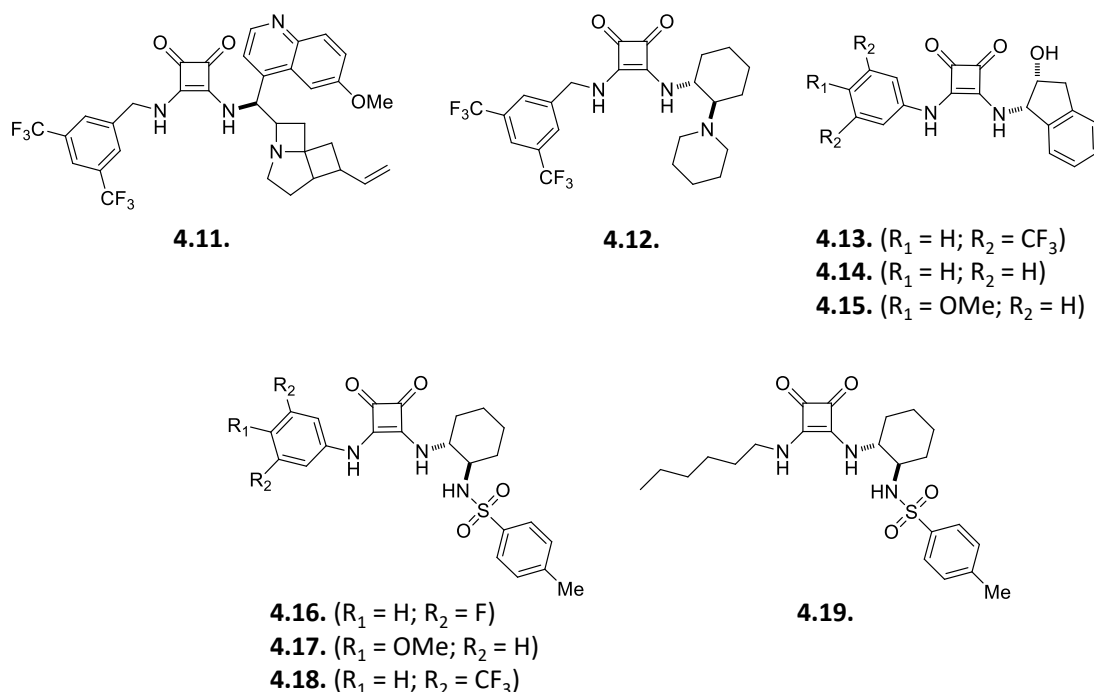
Figure 4.3. Library of additional squaramides **4.11.** – **4.19.** synthesized for LMWGs.[157]

In a recent report (2017), Lopez and co-workers have established the formation of hydrogels based on squaramide-squaramate analogues in different solvent mixtures of DMSO/H_2O (Figure 4.4.).[164] This work describes the use of squaramic acids, for the first time, as the hydrophilic component of LMWHGs, joined to an arylsquaramide unit as the hydrophobic moiety. The aryl substituents, NO_2 and CF_3, were used to modulate the molecular aggregation of the hydrogels and improve their macroscopic properties. Also, the hydrogel from **4.20.** was found to be thermoreversible, thixotropic, injectable and could be loaded with biomolecules.[164]

4.20. ($R_1 = NO_2$; $R_2 = H$)
4.21. ($R_1 = H$; $R_2 = CF_3$)
4.22. ($R_1 = R_2 = H$)
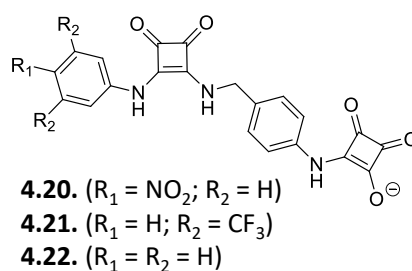
Figure 4.4. Chemical structures of amphiphilic squaramide-squaramic LMWHGs **4.20.** – **4.22.**[164]

4.2. Aims and objective of Chapter 4

This chapter deals with the synthesis of squaramide-carbohydrate conjugates. As discussed earlier, squaramides are good scaffolds for supramolecular assemblies and they have great potential as LMWGs.[165,166] However, there are very few examples mentioned in literature.[157,162,164]

To the best of our knowledge, there are no examples reported in literature of squaramide-carbohydrate conjugates as LMWGs. For this reason, compounds **4.24.** and **4.25.**, featuring galactose (Figure 4.5.) were synthesised. Their ability to behave as LMWGs was evaluated in a range of solvents of different polarities. Finally, the gels formed by the squaramide-carbohydrate conjugates were characterised with rheological evaluation, thermal analysis, morphological studies and spectroscopic analysis.

4.24.   **4.25.**
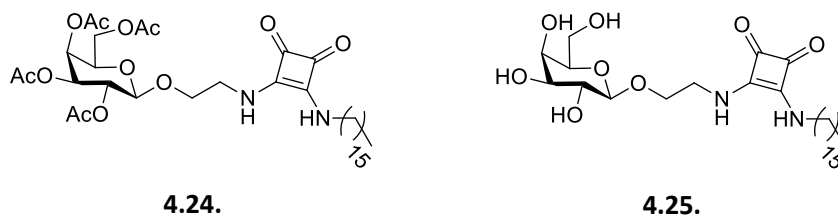
Figure 4.5. Chemical structures of *O*-glycolipid squaramide gelators **4.24.** and **4.25.**

4.3. Results and Discussion

4.3.1. Synthesis of Squaramides

Squaramide-galactosyl derivatives **4.24.** and **4.25.** were prepared as shown in Scheme 4.3. Commercially available diethyl squarate was reacted with hexadecylamine (Scheme 4.3.) according to literature procedures.[152,162] 2-Aminoethyl 2,3,4,6-tetra-*O*-acetyl-*β*-*D*-galactopyranoside **3.47.** was then added to give compound **4.24.** (Scheme 4.3.) Compound **4.25.** was obtained from the hydrolysis of the galactose acetyl protecting groups in **4.24.**
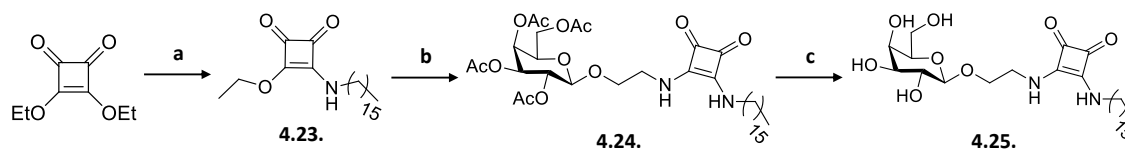
Scheme 4.3. Synthesis of squaramides **4.23. – 4.25.**; Reagents and conditions: a) EtOH, $C_{16}H_{33}NH_2$, rt, overnight (49 %); b) EtOH, **3.47.**, NEt$_3$, rt, overnight (92 %); c) DCM/MeOH/H$_2$O (1:2:1), NEt$_3$, 40 °C, 18 h (98 %).

The mechanism for the formation of **4.23.** is shown in Scheme 4.4. A similar mechanism takes places in the reaction of **4.23.** with the galactosyl amine **3.47.** to give compound **4.24.**
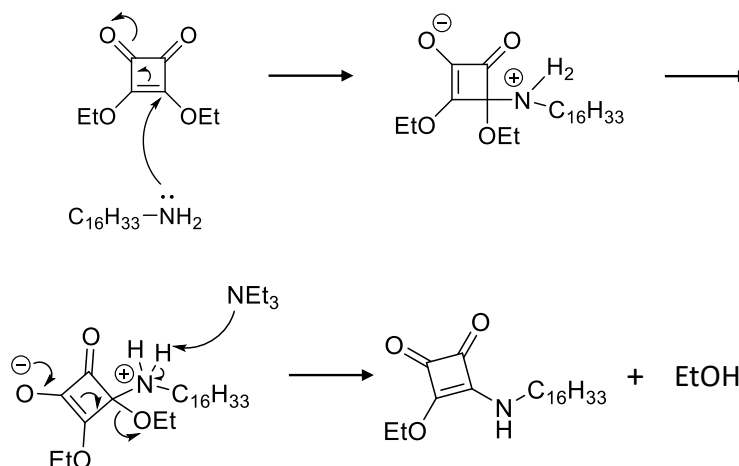
Scheme 4.4. Reaction mechanism of commercial available diethyl squarate and hexadecylamine to give product **4.23.**

Figure 4.6. shows the ^{1}H NMR of compound **4.24.** in CDCl$_3$. Characteristic peaks such as NH broad peak at 7.29 ppm, anomeric H$_1$ from the galactose at 4.56 ppm and methyl from the acetyl groups (2.13, 2.03, 2.00 and 1.95 ppm) were assigned in the spectrum.
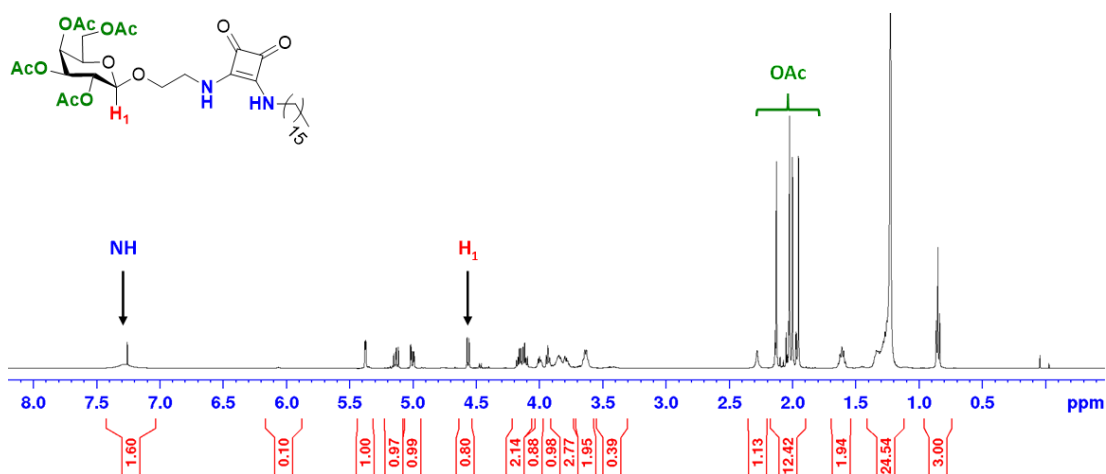
Figure 4.6. ^{1}H NMR spectrum of galactose acetyl-squaramide **4.24.** (CDCl$_3$, 500 MHz).

Figure 4.7. shows the ^{1}H NMR of compound **4.25.** in d_6-DMSO. Characteristic peaks such as NH broad peak at 7.50 ppm, OH showing at 4.82, 4.74 and 4.68-4.64 ppm and anomeric H$_1$ from the galactose at 4.13 ppm were assigned in the spectrum.
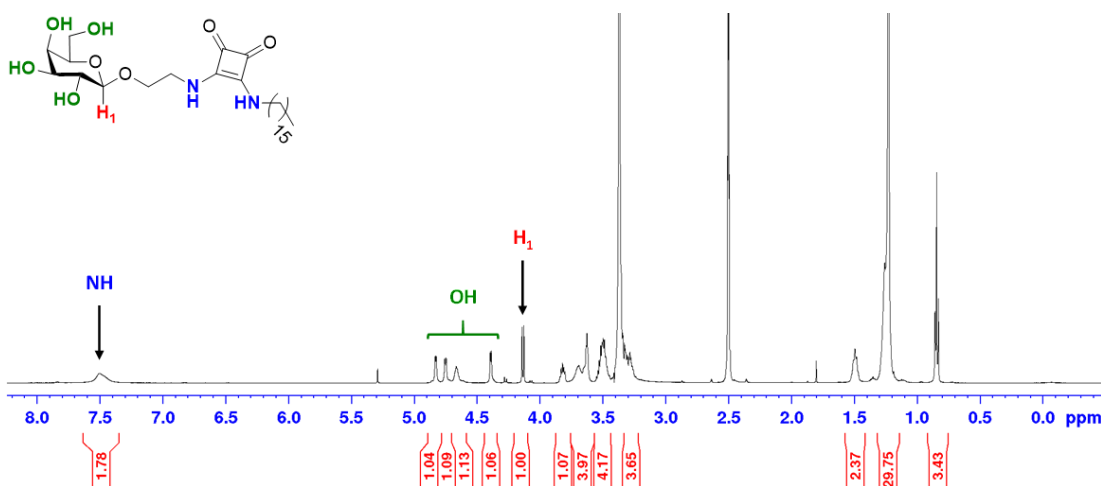
Figure 4.7. ^{1}H NMR spectrum of galactose hydroxyl-squaramide **4.25.** (d_6-DMSO, 500 MHz).

4.3.2. Gelation Ability

The ability of **4.24.** and **4.25.** to induce the formation of supramolecular gels was then screened in a range of solvents of different polarities and structural characteristics (Table 4.1.). The gels were formed upon sonication at rt in less than 5 min. Gels were also formed by thermal treatment. The gelator was heated in the required solvent to increase the solubility of the sample. The gel was formed after cooling down at/to rt in less than 2 h. For both techniques, the formation of the gel was confirmed by the "inverted test tube" method (Figure 4.8.). - See experimental Chapter 7. It was found that the acetylated derivative **4.24.**, showed a preference to form opaque gels with relatively high polarity solvents such as EtOAc, MeCN, EtOH and a solvent mixture of EtOH:H_2O (1:1), with CGCs ranging from 0.7 [EtOH:H_2O (1:1)]) to 1.7 (EtOH) w/v %.

On the other hand, compound **4.25.**, which features the free hydroxyl groups, was able to form a transparent gel in EtOH:H_2O (1:1) with 0.1 w/v % CGC. This classified this gelator as a "supergelator" (CGC < 1 %).[13] As mentioned in Section 4.1.1., squaramides are very efficient gelators of alcoholic solvents.[157] This is possibly due to the presence of the squaramide group, which contributes both as H-bond donor and acceptor to aid solubility of the gelator in the alcohol solvent. Interestingly, the squaramide-carbohydrate conjugates **4.24.** and **4.25.** were efficient gelators of a mixture of EtOH:H_2O (1:1), which could be due to the H-bonding network formed between gelator and solvent.[89] In particular, the CGC for the gel formed by **4.25.** was remarkably low (0.1 w/v %). This means **4.25.** can self-assemble to form a 3-D
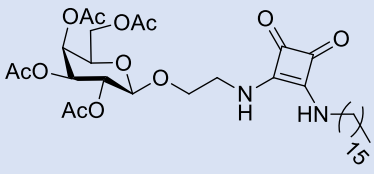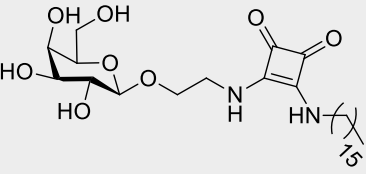
network capable of entrapping large volumes of the solvent mixture. However, **4.25.** was not capable of gelling either EtOH or H_2O alone, resulting in aggregation or partial solubility respectively. The EtOH:H_2O (1:1) system allowed for an optimal balance of solubility to allow self-assembly, which was critical for the formation of supramolecular gels.
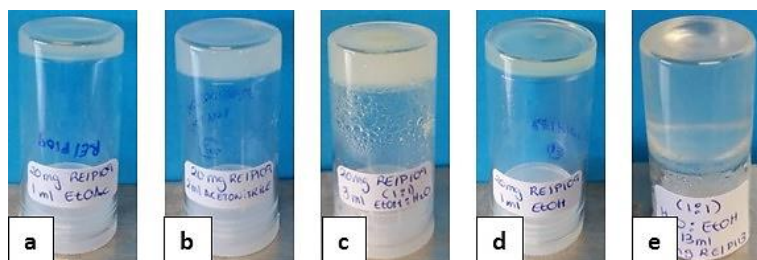
Figure 4.8. Physical appearance of the squaramide-gels: *solvent:* a) (**4.24.**) *EtOAc*; b) (**4.24.**) *MeCN*; c) (**4.24.**) *EtOH:H_2O (1:1)*; d) (**4.24.**) *EtOH*; e) (**4.25.**) *EtOH:H_2O (1:1)*.

Table 4.1. Gelation abilities of squaramides **4.24.** – **4.25.** in different solvents: physical appearance, CGC (Critical Gelation Concentration, w/v %) at rt and gel-sol transition temperature T_{gs} (°C) at the specified CGC. PG* at 20 mg/mL.

Compound / Solvent	4.24.	4.25.
Pentane	I	I
Hexane	I	I
Heptane	PS	PS
Pet. ether	I	I
Cyclohexane	PG*	PG*
Petrol	PG*	PS
Toluene	S	PS
Et$_2$O	I	PS
Chloroform	S	PS
DCM	S	I
EtOAc	OG(1.4) / T$_{gs}$(26-32)	PS
DMSO:H$_2$O (1:1)	A	A
DMSO	S	S
MeCN	OG(0.9) / T$_{gs}$(24-30)	PS
EtOH:H$_2$O (1:1)	OG(0.7) / T$_{gs}$(50-57)	TG(0.1) / T$_{gs}$(48-60)
EtOH	OG(1.7) / T$_{gs}$(26-29)	A
MeOH	PG*	PG*
H$_2$O	I	PS

S = Soluble, PS = Partial soluble, I = Insoluble, A = Aggregates, PG = Partial gelation, TG = Transparent gel, OG = Opaque gel.

4.3.3. Rheological Evaluation

As detailed previously in Chapter 2, Section 2.3.4., rheology involves the study of liquids and solids under applied stress conditions. The viscoelastic properties of the gel formed by squaramide-carbohydrate **4.24.** and **4.25.** were investigated.

A strain of 0.1 % (LVER) was used to determine the mechanical spectra of all gels (SAOS). These values were chosen after considering the results obtained for LVER tests in which G' and G'' were constant for a 0.1 % strain [Figures 4.9. 1-4 a) and 4.10. a)].

Mechanical spectra of the gels of compounds **4.24.** and **4.25.** in the required solvents at 10 °C were studied 120 h after their formation. This was decided after recording mechanical spectra of the gels after 24, 96, 120 and 144 h of gel formation in order to evaluate the rheological stability of their structure. After 120 h, it was observed that the values of the modules, G' and G'', did not significantly increase with time. All gels formed by **4.24.** and **4.25.**, showed G´ > G´´ throughout the angular frequency range that was studied, with low values of tanδ (Table 4.2.). This indicates that the elastic nature of the samples prevailed over the viscous one, which is the typical behavior of a gel structure. The gels in EtOAc and EtOH:H_2O (1:1) formed by **4.24.** showed the lowest values of tanδ indicating that they are stronger gels than those formed by compound **4.24.** in either MeCN or EtOH [Figure 4.9. 1-4 b)]. In addition, when EtOH was used as a solvent, the gel formed by compound **4.24.** presented the highest values of G´ and G´´ (Table 4.2.). This indicated a better elastic character than the corresponding gels formed by **4.24.** in other solvents, followed by MeCN, EtOAc and EtOH:H_2O (1:1). Thus, they can be considered to be strong gels. All the gels were found to have thixotropic behaviour.[167] Thixotropic gels are dynamic self-assembled systems which are thick (viscous) under static conditions which flow (become thin or less viscous) when stresses are involved. When the stresses are released, the gels return to a more viscous state. Shinkai *et. al.* demonstrated the requirements for thixotropic gelator,[168] which are:

a) Gelation should be efficient. Close to a supergelator (< 1 w/v %).

b) Gel should present thixotropic behaviour even at a very low concentration. This means the gel gets deformations when pressure or stresses are applied and remains intact when the forces are removed.

c) Gel should not lose thixotropic character after the cycles of breaking (stresses apply) and after the regeneration process (stresses release).

1a)   1b)

2a)   2b)

3a)   3b)

4a)   4b)
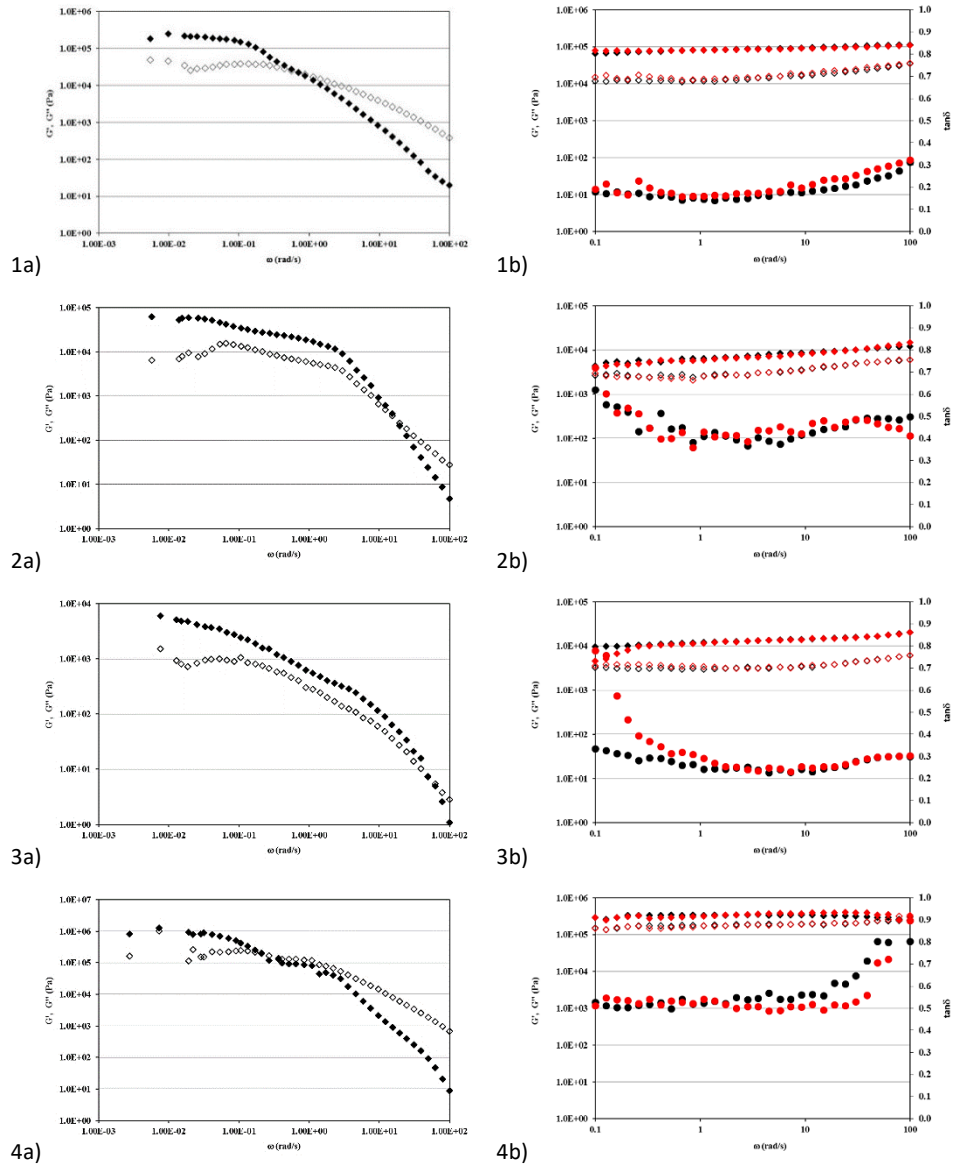
Figure 4.9. 4.24. at 10 °C at a strain of 0.1 % in **1)** EtOAc with 1.4 w/v %, $\tan\delta < 0.5$.; **2)** MeCN with 0.9 w/v %, $\tan\delta < 1$; **3)** EtOH:H$_2$O (1:1) with 0.7 w/v %, $\tan\delta < 0.5$; **4)** EtOH with 1.7 w/v %, $\tan\delta < 1$. **a)** (LVER) Strain sweep at 1 Hz of frequency. G'(♦) and G'' (◊); **b)** (SAOS) Frequency sweep at a strain of 0.1 %. G' (♦, ♦; filled markers), G'' (◊, ◊; empty markers) and $\tan\delta$ (●, ●; dot filled markers).

The same thixotropic-gel behaviour was observed by the gel formed by **4.25.** in EtOH:H_2O (1:1), in which G' > G'' (gel-like behaviour) in the plateau region switched to closer modules, G' = G'' (solid-like behaviour) with increased strain, as shown in Figure 4.10. b). The gel in EtOH:H_2O (1:1) with 0.1 w/v %, of **4.25.** showed the lowest values of tanδ (< 0.15) indicating that it is the strongest gel formed by the squaramide gelators studied in this chapter. This can be explained as the hydroxyl groups in the galactose part of **4.25.** were efficiently H-bonding with the solvent. These results mean that the gel formed by **4.25.** in EtOH:H_2O (1:1) has appropriate rheological characteristics for real-life applications in gel-based materials.[5,169]
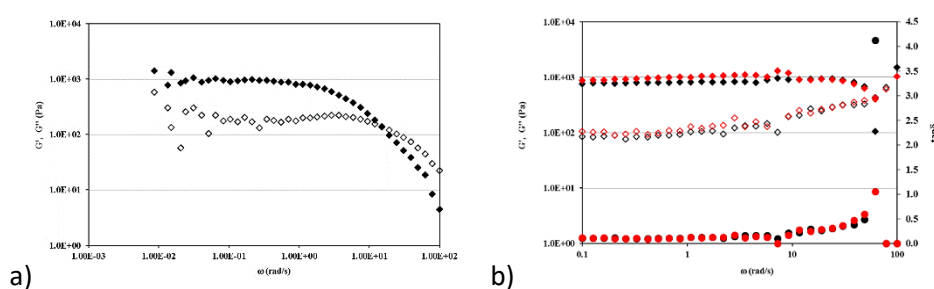
Figure 4.10. 4.25. at 10 °C at a strain of 0.1 % in EtOH:H_2O (1:1) with 0.1 w/v %. a) (LVER) Strain sweep at 1 Hz of frequency. G'(♦) and G'' (◊); b) (SAOS) Frequency sweep at a strain of 0.1 %. G' (♦, ♦; filled markers), G'' (◊, ◊; empty markers) and tanδ (●, ●; dot filled markers with values, < 0.15.

Table 4.2. Summary of SAOS results for **4.24.** − **4.25.** The data are displayed from the weakest (top) to the strongest (bottom) gel.

Compound	Solvent	Temperature	Time	G' (Pa)	G'' (Pa)	Tanδ
4.24.	EtOH	10 °C	120 h	$2.9\cdot10^5 - 3.3\cdot10^5$	$1.5\cdot10^5 - 2.9\cdot10^5$	0.51 - 0.89
	MeCN	10 °C	120 h	$4.1\cdot10^3 - 1.5\cdot10^4$	$2.9 - 6.1\cdot10^3$	0.72 - 0.41
	EtOH:H_2O	10 °C	120 h	$9.7\cdot10^3 - 2.1\cdot10^4$	$3.3 - 6.1\cdot10^3$	0.34 - 0.30
	EtOAc	10 °C	120 h	$6.6\cdot10^4 - 1.1\cdot10^5$	$1.2 - 3.5\cdot10^4$	0.19 - 0.32
4.25.	EtOH:H_2O	10 °C	120 h	$8.8\cdot10^2 - 1.0\cdot10^3$	$1.1 - 4.3\cdot10^2$	0.12 - 0.13

4.3.4. Thermal Analysis: T_{gs} and DSC Measurements

We analysed the thermoreversible behaviour of the gels formed in different solvents by compound **4.24.** and **4.25.** by T_{gs}. These results are shown in Table 4.1. T_{gs}

measurements followed the procedure described in Section 7.3.3. and DSC analysis was carried out as described in Section 7.3.5.1.

The DSC analysis of the gels was carried out 120 h after formulation to ensure that the gel formation was completed, following rheological results. DSC analysis (Table 4.3.) showed thermoreversibility of the gels formed by squaramide-carbohydrate conjugates **4.24.** and **4.25.** giving reproducible cycles after performing duplicates of each experiment.

Table 4.3. T_{gs} (°C) by heating / monitoring the meting temperature and DSC transition temperatures (gel-to-sol. and sol.-to-gel) of thermoreversible squaramide-gels **4.24.** and **4.25.** for two heating (1st and 3rd cycles) and two cooling (2nd and 4th cycles) cycles at the specified CGC.

Gelator	Solvent	T_{gs} (°C)	1st cycle (heating)	2nd cycle (cooling)	3rd cycle (heating)	4th cycle (cooling)
4.24.	EtOAc	**26 - 32**	37.3 °C	13.9 °C	36.7 °C	13.8 °C
4.24.	MeCN	**24 - 30**	25.7 °C	11.5 °C	24.2 °C	11.1 °C
4.24.	EtOH:H_2O (1:1)	**50 - 57**	46.1 °C	32.9 °C	43.6 °C	32.3 °C
4.24.	EtOH	**26 - 29**	31.5 °C	5.4 °C	23.3 °C	5.0 °C
4.25.	EtOH:H_2O (1:1)	**48 - 60**	61.6 °C	58.6 °C	53.4 °C	57.9 °C

The thermograms a) - d) in Figure 4.11. and thermogram in Figure 4.12. show the endotherms and exotherms for the gels formed by gelators **4.24.** and **4.25.** Thermograms a) - d) show an endotherm at 37.3 (EtOAc), 25.7 (MeCN), 46.1 [EtOH:H_2O (1:1)] and 31.5 (EtOH) °C for **4.24.** in the first heating cycle corresponding to the gel-sol transition. This correlated well with the T_{gs} determined by the "melting" method. The third cycle, which was another heating cycle, showed lower T_{gs} values, which is consistent with rheological results, as the gel's 3-D network needs 120 h for complete formation. The exotherms in the cooling cycles (second and fourth cycles) are shown at 13.8 (EtOAc), 11.1 (MeCN), 32.3 [EtOH:H_2O (1:1)] and 5.0 (EtOH) °C for **4.24.**, which can be assigned to the formation of the initial 2-D assembles in the gel network. As commented in previous chapters, the transition peaks are better defined in the cooling curves (sol-to-gel) rather than in the heating curves (gel-to-sol).[35]
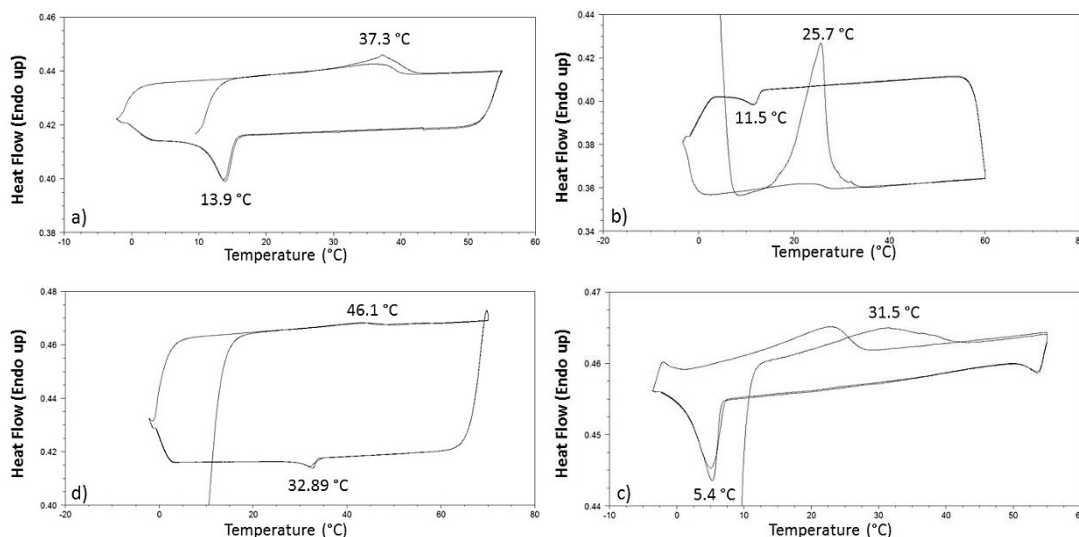
Figure 4.11. DSC of the gel **4.24.**: a) in EtOAc (1.4 w/v %); b) in MeCN (0.9 w/v %); c) in EtOH:H$_2$O (1:1) (0.7 w/v %) and d) in EtOH (1.7 w/v %), during the two heating / two cooling cycles. The sample was heated from 0 °C to a temperature lower than the boiling point of the solvent used, at 2 °C/min and cooling the same range of temperature. Reproducible / duplicated cycles for each sample.

A DSC thermogram of the gel formed by **4.25.** in EtOH:H$_2$O (1:1) (0.1 w/v %) from 0 – 75 °C (Figure 4.12) exhibits an endothermic peak at 61.6 °C (1st cycle) and an insignificant peak at 53.4 °C (3rd cycle). This thermoreversible gel required a high temperature for formation, presenting a non-well-defined exothermic peak at 58.6 °C (2nd cycle) and a reproducicle peak at 57.9 °C in the 4th cycle. This almost flat line display can indicate that gel **4.25.** formed in EtOH:H$_2$O (1:1) was thermally stable as a super gelator. In addition, this gel requires longer analysis time to show breaking / forming of intermolecular interactions.
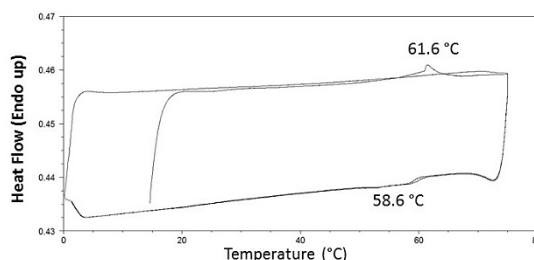
Figure 4.12. DSC of the gel **4.25.** in EtOH:H$_2$O (1:1) (0.1 w/v %) during the two heating / two cooling cycles. The sample was heated from 0 °C to 75 °C, at 2 °C/min and cooling the same range of temperature. Reproducible / duplicated cycles for each sample.

4.3.5. Morphological Studies

The morphology of the xerogels of the squaramide-carbohydrate gels from **4.24.** and **4.25.** (Figure 4.13., 4.14.) was investigated using SEM imaging (see section 7.3.6.3.). The gels formed in EtOH:H$_2$O (1:1) were dried, in the freeze dryer prior to imaging. The xerogels were formed from the corresponding squaramide-carbohydrate gel in different solvents using a spatula to transfer the gel from the closed vial to the metal stub. The presence of thickly packed fibrous structures can be observed in xerogels of the acetylated compound **4.24.** formed in EtOAc and MeCN [Figure 4.13. a) and b)]. The dimension and aggregation patterns of the fibres seem to vary slightly depending on the nature of the solvent. Long bundles of woven fibres were observed for EtOAc xerogel [image a)] and MeCN xerogel [image b)]. Less but thicker fibres were detected in EtOH xerogel [image c)]. Those were much more spread without forming a pattern as observed in images a) or b). Xerogel **4.24.** in image d) in EtOH:H$_2$O (1:1) solvent mixture (Figure 4.14.) had a honeycomb morphology which was totally different to that of the xerogels formed with the same gelator in single solvents. This results indicated: I.) The strong solvent influence in xerogel structure and therefore, in the self-assembly mode of the gelation molecules and II.) Even the small amount of gelator used (0.7 w/v %) can give rise to a thick porous morphology.
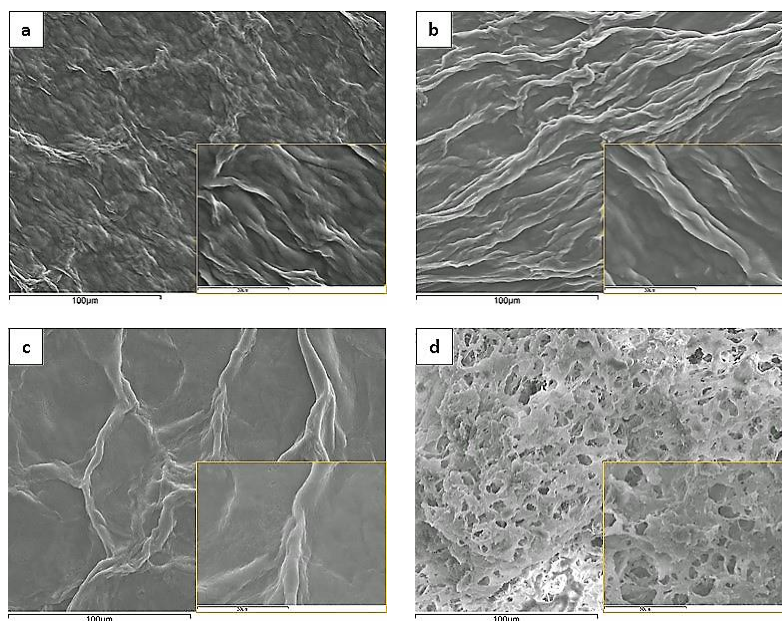
Figure 4.13. SEM images of xerogels formed by **4.24.** *Solvent:* a) *EtOAc*; b) *MeCN*; c) *EtOH* and d) *EtOH:H$_2$O (1:1)*. (All gels were prepared at CGC). [Scale bar: a) – d) 100 μm].

Figure 4.14. shows the xerogel of the gel formed by deprotected galactosyl squaramide **4.25.** in EtOH:H$_2$O (1:1), which has similar morphology to that of xerogel of the acetylated compound **4.24.** in the same solvent system. In this case, a "bead-needle" formation amply distributed in the porous network can be well distinguished. These results are consistent with literature, in which squaramide hydrogels formed disordered bundled fibrous assemblies.[164]
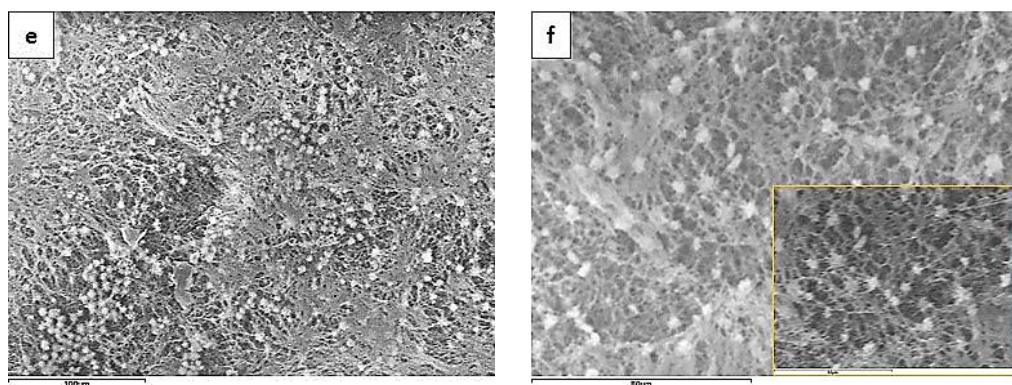
Figure 4.14. SEM image of xerogel formed by **4.25.** *Solvent: EtOH:H$_2$O (1:1)*. e) 100 μm; f) 80 – 50 μm of magnification (Gel was prepared at CGC).

A comparison of SEM images of the xerogels from the partial gelation observed in cyclohexane of acetylated gelator **4.24.** [Figure 4.15. a)] and of aggregates in DMSO:H$_2$O (1:1) [**4.24.** Figure 4.15. b)] and EtOH [**4.25.** Figure 4.15. c)] revealed interesting differences which helped to explain the morphologies found in previous xerogels. The cyclohexane xerogel [image a)] shows amorphous aggregates. In comparison with the well-defined fibres found in xerogel formed from gels of **4.24.** in EtOAc or MeCN [Figure 4.13. a), b)]. Figure 4.15. image b) shows fibril structures similar to a bundle of hair. The micrometer-fibres were disordered short filaments made by **4.24.** in DMSO:H$_2$O (1:1). Figure 4.15. image c) shows the aggregates formed by **4.25.** in EtOH. The spherical aggregates are similar in morphology to the beads observed in the xerogel from **4.25.** in EtOH:H$_2$O (1:1) (Figure 4.14.). However, the structures are too dense to entrap solvent efficiently.
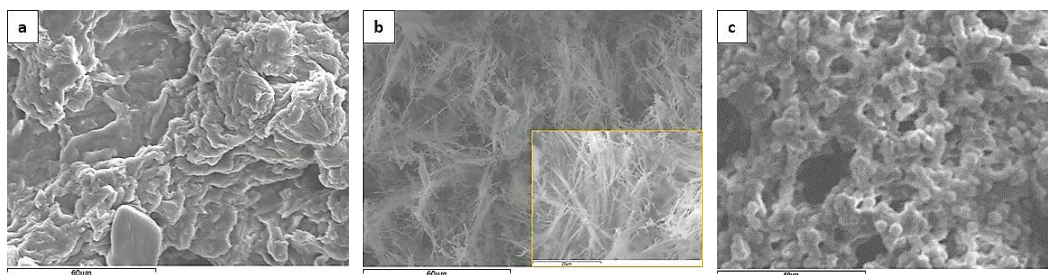
Figure 4.15. SEM image of: a) Partial gelation formed by **4.24.** in cyclohexane; b) Aggregates formed by **4.24.** in DMSO:H_2O (1:1); c) Aggregates formed by **4.25.** in EtOH. (All gels were prepared at CGC). [Scale bar: a) – c) 60 μm].

4.3.6. Spectroscopic Analysis

The role of H-bonding interactions in the gelation process could be followed using ^{1}H-NMR and FTIR analysis which will be explained in sections 7.3.5.2. and 7.3.5.3.

4.3.6.1. ^{1}H-NMR Spectroscopic Analysis

^{1}H-NMR spectra of acetylated galactosyl squaramide **4.24.** in (D_3)-acetonitrile (Figure 4.16.) were recorded at increasing concentrations. The solutions were prepared in a NMR tube and heated to aid the solubility of the gelator in the solvent. Spectra were measured at 300 K (27 °C), which is the standard operation temperature of the NMR spectrometer.
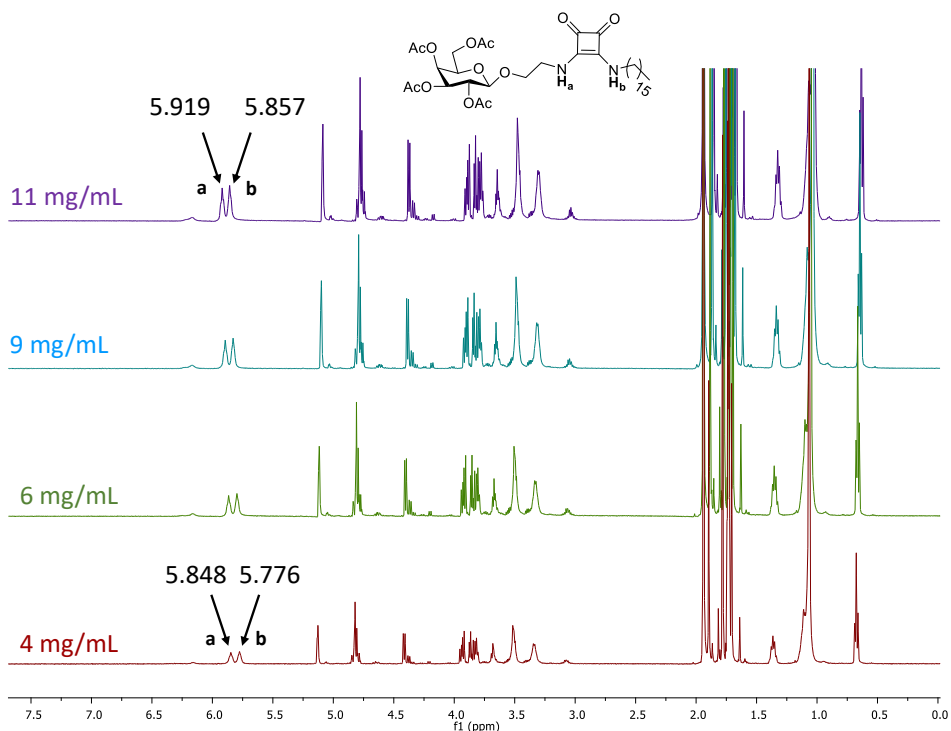
Figure 4.16. Full ^{1}H-NMR spectra of **4.24.** in (D_3)-acetonitrile at different concentrations.

Analysis of the data (Table 4.4.) showed small downfield shifts of the NH protons upon increasing concentrations ($\Delta\delta$ = 0.071 for NH_a and 0.081 for NH_b). These values are consistent with the formation of weak intermolecular H-bonding in gels. The comparable increments in chemical shifts ($\Delta\delta$) upon changes in concentration observed in the NH signals suggest that both NH protons are similarly involved in intermolecular H-bonding, which is consistent with literature reports.[145]

Table 4.4. Chemical shifts (δ) of the NH signals in the ^{1}H-NMR spectra in solution and in gel phase of **4.24.** in (D_3)-acetonitrile.

Compound **4.24.** in (D_3)-acetonitrile			
Concentration	Temperature	δ NH$_a$ (ppm)	δ NH$_b$ (ppm)
4 mg/mL (Solution)	27 °C	5.848	5.776
11 mg/mL (gel)	27 °C	5.919	5.857
$\Delta\delta$ NH (ppm)	-	**0.071**	**0.081**

4.3.6.2. FTIR Spectroscopic Analysis

Previous studies have shown that when organogel formation is promoted by H-bonding, the IR bands associated with the relevant functional groups in the molecule shift to lower wavenumbers from those recorded of the gelator free in solution, as discussed in previous chapters.[51,52] FTIR spectroscopic data were obtained for gelators **4.24.** and **4.25.** in different physical states in order to ascertain if H-bonding was involved in gel formation. FTIR spectra: I.) As a bulk solid sample in NaCl plate or KBr disk; II.) In solution and III.) As gels in the required solvent in a close cell or with an ATR accessory (diamond crystal). The positions and assignments of the noteworthy IR bands (νNH and νCO) of gelators **4.24.** and **4.25.** in the three states are given in Table 4.5. The νNH band of gelator **4.25.** in EtOH:H_2O (1:1) solution and gel could not be distinguished from the overlapping solvent bands. The spectra recorded for the bulk and gel state showed similar peak positions for the bands, however the bands were shifted to higher wavenumbers in the spectra recorded in solution. For gelator **4.24.** in EtOAc, the bands for the νNH, νCO shifted to higher frequencies by 105 and 28 cm^{-1} respectively between the solution and gel state (Figure 4.17.). For gelator **4.24.** in MeCN, the bands for the νNH, νCO shifted to higher

frequencies by 143, 37 and 28 cm^{-1} respectively between the solution and gel state. In this case two distinct νCO bands can be appreciated for the carbonyl groups present in the molecule. (Figure 4.18.). In both cases the magnitudes of the shifts are similar to those recorded for other H-bonded gels and indicate H-bonding formation.

Table 4.5. Position of characteristic IR bands of **4.24.** and **4.25.** in the solid state (NaCl plate or KBr disk), solution and gel state.

Compound	Solvent	State	νNH (cm^{-1})	νCO (cm^{-1})	
4.24.	-	Bulk (NaCl plate)	3174	1570	
	EtOAc	Solution	3274	1597	
		Gel	3169	1569	
	MeCN	Solution	3344	1684	1607
		Gel	3201	1647	1578
4.25.	-	Bulk (KBr disk)	3233	1570	
	EtOH:H$_2$O (1:1)	Solution	Overlapping with solvent peaks	1569	
		Gel		1568	
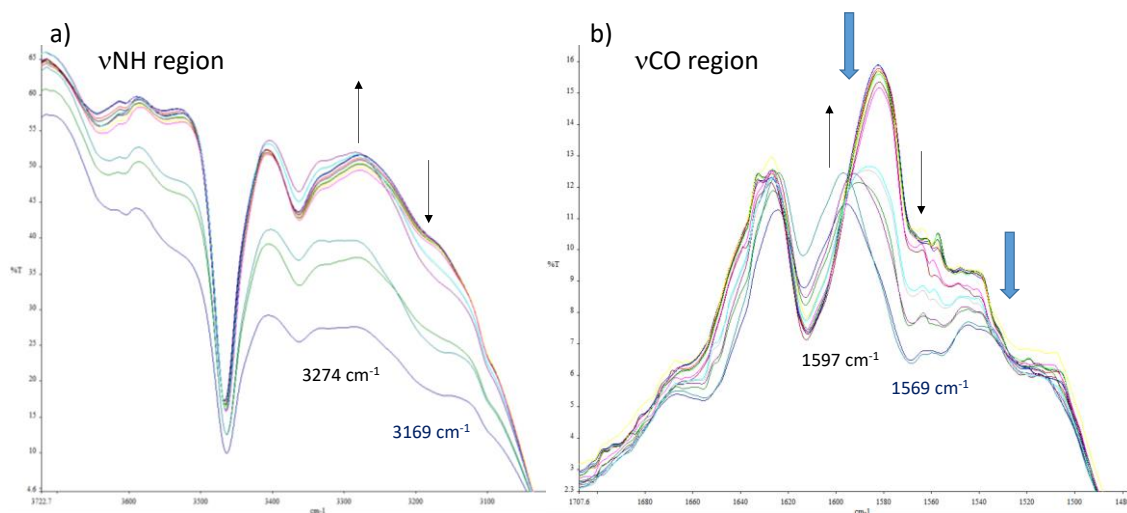
Figure 4.17. FTIR spectra of compound **4.24.** 1.4 w/v % in EtOAc solution from 0 – 90 min. The solution injected into the cell was warm and was allowed to cool to rt. a) νNH region; b) νCO region.
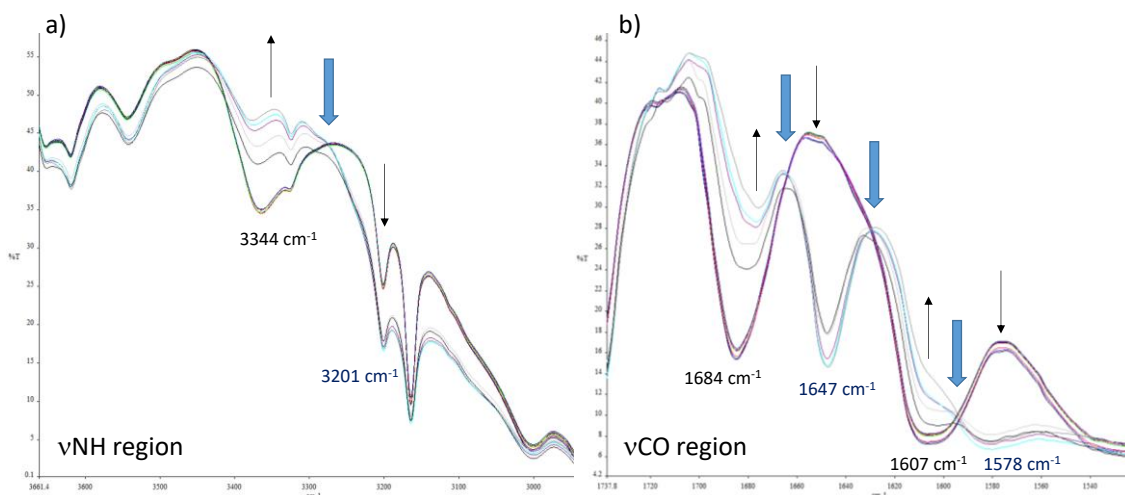
Figure 4.18. FTIR spectra of compound **4.24.** 0.9 w/v % in MeCN solution from 0 – 75 min. The solution injected into the cell was warm and was allowed to cool to rt. a) νNH region; b) νCO region.

Figure 4.19. shows a) FTIR-ATR spectra of the compound **4.25.** [0.1 w/v % in EtOH:H$_2$O (1:1)] from 0 – 60 min; b) **4.25.** Bulk state (KBr disk) and c) FTIR-ATR spectra of EtOH:H$_2$O (1:1). No νNH band could be identified in the solution or gel states as the band was overlapping with solvent peaks. At the same time, it was very difficult to follow the gelation process as it occurred very quickly. However, after subtracting the solvent from the background, it could be observed that the peak ~ 1569 cm^{-1} characteristic as CO, was growing in intensity with time, which could indicate a gel-formation-process was taking place.
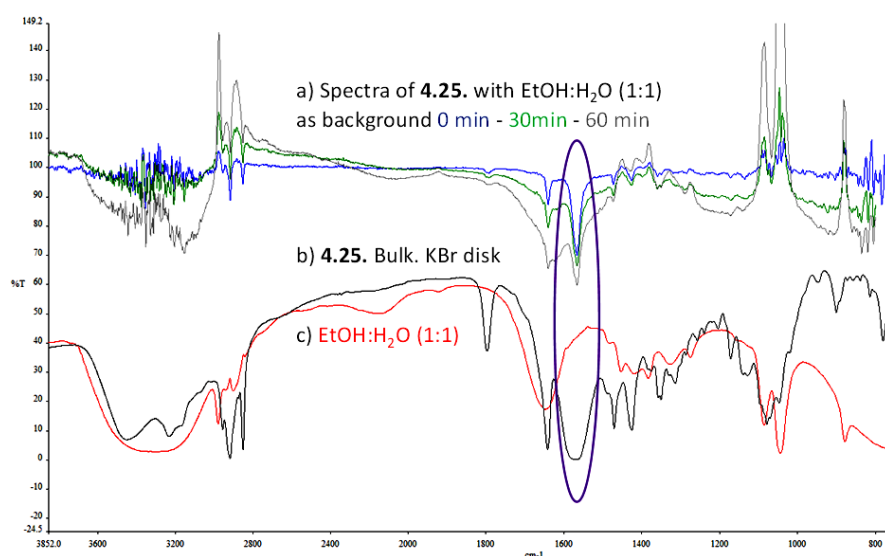
Figure 4.19. a) FTIR-ATR spectra of **4.25.** 0.1 w/v % with EtOH:H$_2$O (1:1) as background from 0 – 60 min; b) **4.25.** Bulk state (KBr disk) and c) FTIR-ATR spectra of EtOH:H$_2$O (1:1).

4.4. Conclusion

I.) A novel type of squaramide based LMWGs was created combining diethyl squarate and 2-aminoethyl galactoside as building blocks. These squaramide-carbohydrate conjugates could be obtained in good yield.

II.) The gelation ability of the protected compound **4.24.** and the free-hydroxyl compound **4.25.** were tested in a range of solvents with different polarities.

III.) The gels formed were fully characterised to better understand their gel-formation-process. Rheological properties showed the gels were very strong and had a thixotropic behaviour. DSC analysis showed that the gels were thermoreversible. The morphological studies using SEM revealed very different xerogel structures depending on the solvent.

IV.) Spectroscopic analysis using NMR and FTIR, indicated that H-bond formation was involved in the gelation process.

V.) Remarkably, the gel **4.25.** formed in a mixture of EtOH:H_2O (1:1) had a distinct morphology and excellent rheological properties. This opens new possibilities for the use of squaramide-carbohydrate conjugates in materials and biomedical science, other than their classical application in catalysis. The application of **4.25.** in scaffolds for tissue engineering will be discussed in Chapter 5.

Chapter 5

Supramolecular Gelators in the Formation of PCL Electrospun Fibres

5.1. Introduction to Electrospinning

Micro- and nano-fibres or structures can be produced using an accessible technique called electrospinning. The use of electrostatic forces to form ultrafine fibres (UFs) has been reported over 100 years ago, however, the first patented report was by Formhals in 1934.[170] Almost 60 years later, Reneker and Chun restored interest in the technique by demonstrating the possibility of electrospinning a wide range of organic polymers.[171] Since then, the technique of electrospinning has become extremely useful in a variety of applications such as: water purification,[172,173] protective clothing as barriers to liquid penetration,[174,175] wound dressing nanofibres (wound healing or as composites which have antimicrobial and antifungal purposes),[176,177] micro-sensor for toxic gases,[178-180] or even energy related applications. An excellent example of this is the absorption of solar radiation in electrospun photovoltaic cells.[181-183] Some of the applications of this technique and the most relevant for the work described in this thesis, involve the fabrication of drug delivery systems and tissue engineering scaffolds.[184-189]

Electrospinning involves exposing a solution of polymer to high electric field (See Chapter 7. Section 7.6. Preparation of electrospun materials). When a sufficiently high voltage is applied to a viscous liquid droplet, the body of the liquid becomes charged, and electrostatic repulsion (interaction between two particles of the same charge that drive away each other) overcomes the surface tension and the droplet is extended; at a critical point a stream of liquid erupts from the surface. At this point, the liquid droplet forms a conical shape, known as, "Taylor cone".[190-192] If the molecular interactions within the liquid are sufficiently high, stream breakup does not occur (if it does, droplets are electrosprayed) and a charged liquid jet is formed. The jet is then elongated by a process caused by electrostatic repulsion initiated at small bends or curves in the fibre, until finally deposited on the grounded collector. The technique has a relatively straight forward set-up and is commonly used to produce a range of micro- and/or nano-fibres with promising potential in numerous fields, as mentioned above.

There are many different set-ups for electrospinning (core shell, rotating drum, ring collector or multiplying the needles, to name a few)[193]. The basic electrospinning set-up, which has been used for the work discussed in this thesis, consists of three main components (Figure 5.1.):

1) - Spinneret which is connected to a high-voltage supply (1-20 kV).

2) - Syringe pump. A digital syringe pump controls the flow rate of the solution of polymer.

3) - Collector. Solid fibres (non-woven) are gradually deposited as layers on the flat conductive plate collector.
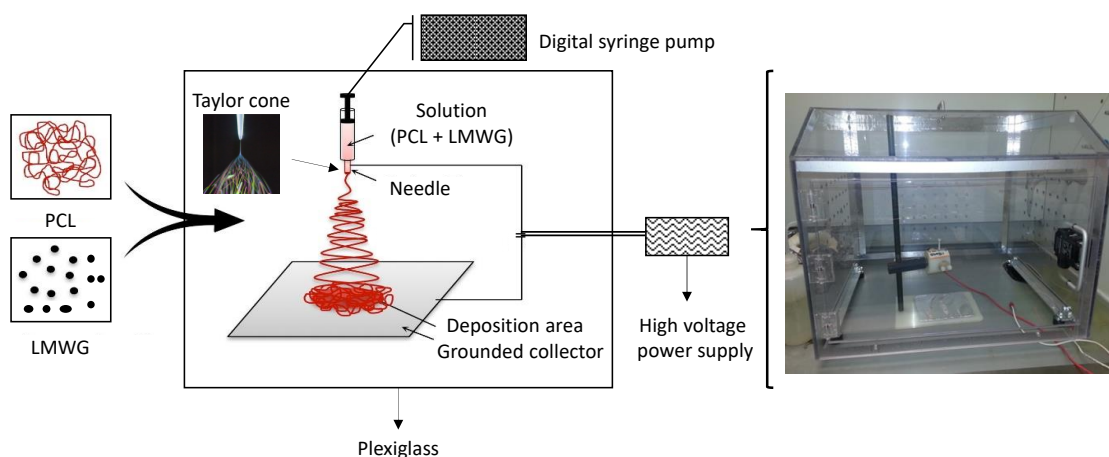
Figure 5.1. Left: Schematic diagram of an electrospinning set-up. Right: Image of the electrospinning set-up at MU. (See Section 7.6. Preparation of electrospun materials).

There are many parameters which affect the electrospinning process[185,194,195] such as solution concentration, viscosity, conductivity, solvent volatility, applied voltage, flow rate, environmental factors, collector shape and distance between needle tip and collector (Figure 5.2.). These parameters have a significant effect on the fibre properties such as diameter, morphology, porosity, mechanical strength, and surface area.
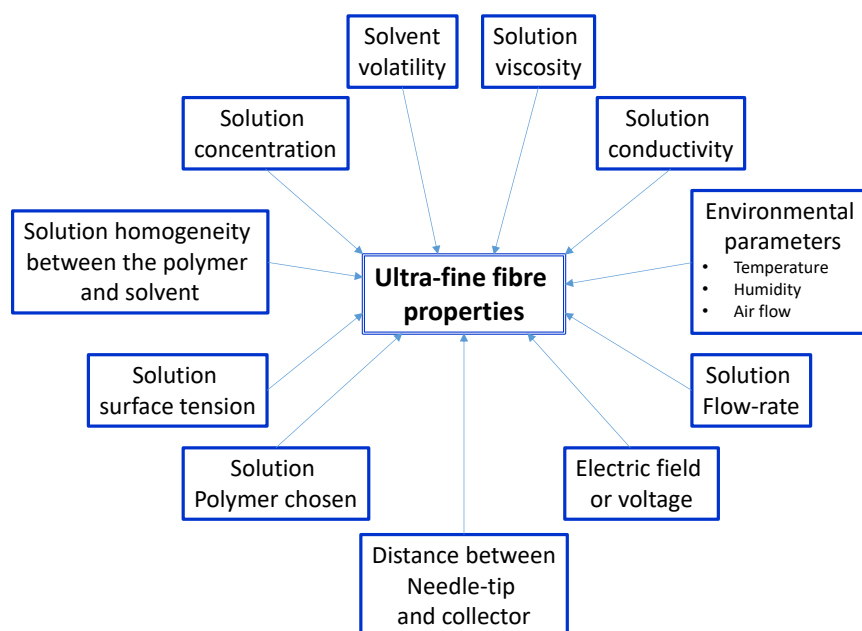
Figure 5.2. Parameters which affect UFs morphology in the electrospinning process.

Solutions of polymers are often used in electrospinning applications as they fulfil the requirements defined to produce UFs.

i) - The *concentration* and *viscosity* of the polymer solution determines the spinnability and the potential to make fibres. In order to obtain low bead-formation, smooth fibres with a minimum diameter and excellent mechanical strength, the concentration of the polymer solution to be electrospun has to be low. However, if the concentration and viscosity is too low, it will form broken fibres with poor structure and beads. On the other hand, a super-high concentration makes fibre formation and control of process parameters more difficult.

ii) - *Solvent volatility* is another critical factor, especially when the fibres are proposed for drug delivery and biomedical applications. In order to prepare a solution for electrospinning, a broad variety of solvents like $CHCl_3$, MeOH, EtOH, DCM, DMF, toluene, water, etc. are used. However, the used solvent is expected to disappear during the transit of the solid fibres to the collector. This will ensure the biocompatibility of the fibres. Also, the highly volatile nature of the solvent used to dissolve the polymer, is particularly significant for the production of a porous mesh of solid fibres with increased surface area. On the other hand, solvents with poor volatility are reported to form fibres with increased pore size.[196]

iii) - *Humidity* is also known to play a significant role in determining the fibre diameter and pore size. It was reported that a low humidity (less than 50%) is ideal for spinning; humidity higher than 50% can make it difficult for the jet to spin continuously, which will affect the number of pores on the surface, the pore diameter and the pore size distribution.[197]

iv) - *Temperature* also influences fibre morphology, as beadless fibres with decreased diameter are reported to be produced at high temperatures. This is mainly due to the lower viscosity of the polymer solution at higher temperatures. However, elevated temperatures could result in an increase of the solution concentration and lead to difficulties to produce fibres, as the polymer could become solidified.

v) - *Voltage*. The strength of the electric field will chiefly determine the diameter of the fibres. At optimal voltage, non-beaded smooth fibres with minimum size are usually formed, meanwhile if the field strength is very high or too low, fibres with poor morphology and beads can be observed.

vi) - *Flow rate* serves as an essential factor to prevent any fibre breakage. However, at high flow rates undesired effects like beads, poor fibrous morphology, and increased pore size can be noted, mainly due to partial drying.

vii) - *Distance*. The drying of fibres and solvent vaporisation depend on the space between the spinneret or needle tip and the collector. If they are separated by a proper distance, beadless, porous microfibres with the required diameter range can be obtained. This also ensures complete drying of the solvent before the solid fibres reach the collector.[198]

5.2. Applications of Electrospinning

As it was mentioned previously, a wide range of biodegradable polymers can be electrospun into mats with a randomly (non-woven) or a specific (woven) fibre arrangement. The surface of the mats can be functionalised to display specific biochemical characteristics. Electrospinning method is very suitable to process natural polymers and synthetic biocompatible or bioabsorbable polymers for biomedical applications.[192,199-201] Almost all of the tissues and organs are deposited

in micro- and nano-fibrous forms or structures. Therefore, electrospun micro and nano-fibres find promising applications in this area.

5.2.1. Drug Delivery Systems

Drug delivery systems can be defined as: "engineered technologies which refer to approaches, formulations, route of administration, systems for transporting and releasing a pharmacological compound in the body as needed to safely achieve its desired therapeutic effect".[198] The concept of a drug delivery system based on electrospun materials was formulated in the early 1970s and the first reliable system demonstrated was polymer (lactic acid) based.[198] Even though it was introduced decades ago, extensive research has been reported in the last five to ten years especially after the popularisation of "micro-nano-technology". Modern drug delivery systems are exploited to carry drugs, growth factors, genes, and biomolecules for treating cancer, promoting tissue regeneration, and curing different illnesses.[198] Micro-nano-scale delivery vehicles can:

1) - Enhance the therapeutic efficacy and minimise adverse side effects associated with some currently available drugs.

2) - Enable new classes of therapeutics.

3) - Encourage the re-investigation of pharmaceutically suboptimal but biologically active molecules that were previously considered undevelopable.

Various kinds of UFs based drug delivery systems have been investigated for the delivery of a broad spectrum of bioactive compounds, including therapeutic drugs,[202] proteins,[203] genes[204] and even living cells.[205,206] Electrospun micro- and nano-fibres have been regarded as the most suitable candidates for this purpose, mainly due to the unique functionality and broad selection of building materials. Depending on the polymer carrier and fabrication method used, different bioactive compounds can be formulated in rapid, immediate and delayed delivery systems.[207,208] Different techniques have been reported for the incorporation of active substances into electrospun material as shown in Figure 5.3.

- Co-electrospinning or blended electrospinning: The drug is dispersed in the polymer matrix before electrospinning.

- Side-by-side electrospinning: This technique ensures that both components (drug and polymer solution), have equal exposure on the surface. This is mainly used when the drug is not soluble in a common solvent.

- Multi-layer electrospinning: This is a triaxial electrospinning which results in different drugs being "sandwiched" in between the polymer.

- Co-axial electrospinning: Drug particles, which are completely isolated from the electric field, will be sealed in the centre core surrounded by the polymer.

- Emulsion electrospinning: This technique is similar to co-axial. The main difference is the emulsion composition which normally involves the polymer, drug and emulsifier. This leads to the formation of droplets of one liquid in another immiscible liquid.

- Surface immobilisation electrospinning: The drug is incorporated into the surface of the polymeric mat after electrospinning.
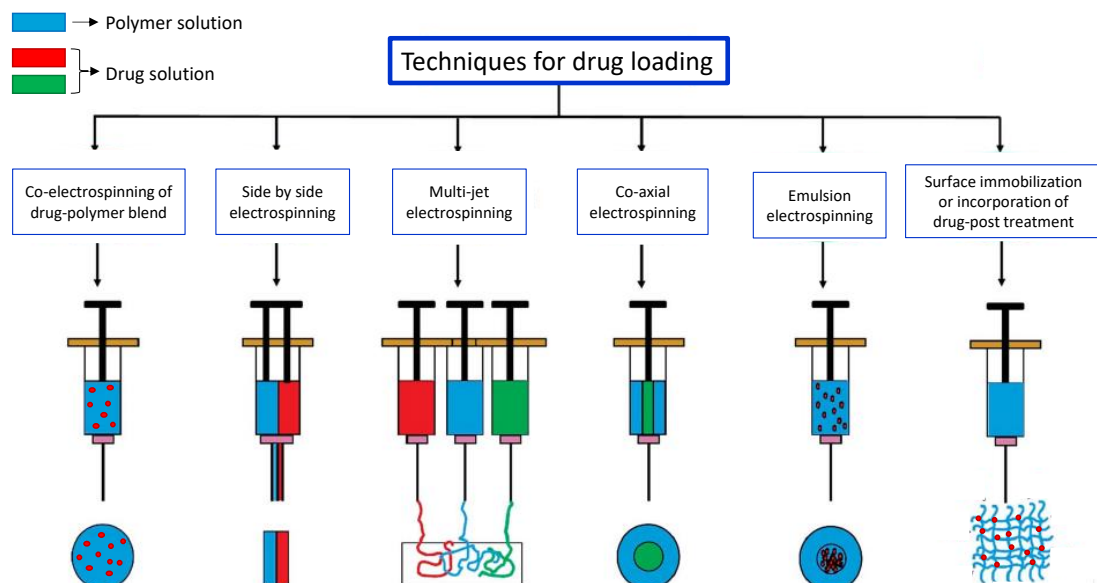
Figure 5.3. Techniques for loading drug molecules into electrospun fibres. Figure adapted from Bajali, A. *et al.*[198]

Some of the advantages of electrospun micro- and nano-fibres as drug carriers are the high surface-to-volume ratio, which can accelerate the solubility of the drug in the aqueous solution and improve the efficiency of the drug. The surface morphology and the structure of the fibres are important factors for controlling the releasing rate and amount of the drug. In order to control those two factors, the fibres must be homogenous in terms of shape and diameter. Furthermore, biodegradable polymers would protect drug from gastric acid and enzyme degradation, maintaining the bioactivity of the drug.[209]

Interest in the development of drug-eluting sutures for a variety of clinical applications has grown over the past decade.[210-212] Drug-eluting sutures may prevent complications and/or serve in a therapeutic role while simultaneously closing wounds and holding tissue together. This next generation of sutures could provide for additional functionality through local and sustained drug release.[213] Sutures are, in general made up of fibres from natural or synthetic polymers. Polymeric fibres could be absorbable or non-absorbable. The most important advantage of synthetic absorbable sutures such as those made of aliphatic polyesters, is their reproducible degradability inside a biological environment. Poly (ε-caprolactone) (PCL) based sutures have been regarded as tissue compatible and used as a biodegradable suture in Europe. The polymer undergoes hydrolytic degradation due to the presence of hydrolytically labile aliphatic ester linkages in physiological conditions.

5.2.2. Tissue Engineering

Tissue engineering can be defined as: "an interdisciplinary field that applies the principles of engineering and life sciences toward the development of biological substitutes that restore, maintain, or improve tissue function or a whole organ".[214] It involves the use of a combination of cell culture, engineering and material methods, taking into account suitable biochemical and physico-chemical factors to improve or replace biological functions. Powerful developments in the multidisciplinary field of tissue engineering have yielded a novel set of tissue replacement parts.[192,214,215] Scientific advances in research, related to biomaterials and biomimetic environments, have developed tissues in the laboratory from combinations of engineered extracellular matrices scaffolds, cells, and biologically active molecules.

Various materials have been exploited as scaffolds for tissue regeneration. The following characteristics are desirable as scaffolds:[216]

I.) 3-D and highly porous structures with an interconnected pore network for cell growth and flow transport of nutrients and metabolic waste.

II.) Biocompatible and bioresorbable with a controllable degradation and resorption rate to match cell/tissue growth *in vitro* and/or *in vivo*.

III.) Suitable surface chemistry for cell attachment, proliferation and differentiation.

IV.) Mechanical properties to match those of the tissues at the site of implantation.

Polymeric biodegradable scaffolds combine the advantages of synthetic and natural materials. The physical properties of synthetic polymers, such as mechanical strength and degradation rate, can be manipulated according to requirements. Biocompatible materials can be used as medical implants (e.g. dental restoratives and bone substitutes).[217] Micro-nano-coatings or micro-nano-structured surfaces can also improve the biocompatibility and adhesion of biomaterials. Nanotechnology can design and build the biocompatible scaffolds at the nanoscale and control the release of biological factors to direct cell behaviours and eventually lead to the creation of implantable tissues.[218]

In order to be successful in tissue regeneration, the living cells should be effectively reorganised into a 3-D scaffold with morphological and physiological features similar to those *in vivo*. In this context, the scaffold should be properly designed to provide more than temporary physical support for cells but also the correct mechanical, topographical and biological factors to regulate cellular responses and direct tissue growth. The role of the scaffold is to mimic the behaviour of the extracellular matrix (ECM) and provide the appropriate environment for the cellular growth. Cells are supported *in vivo* by a 3-D network of ECM, which contains various proteins, growth factors and polysaccharides that contributes physical structure and a biochemical context to the extracellular microenvironment (Figure 5.4.).[186,219,220]

—	Elastic fiber	🔴	Proteoglycan complex	✕	Collagen
🟦	Phospholipids	🟧	Adhesion and receptor proteins	🟩	Channel protein
🔵	Soluble signal	🟣	Cytoskeleton filament	⬤	Cell nucleus
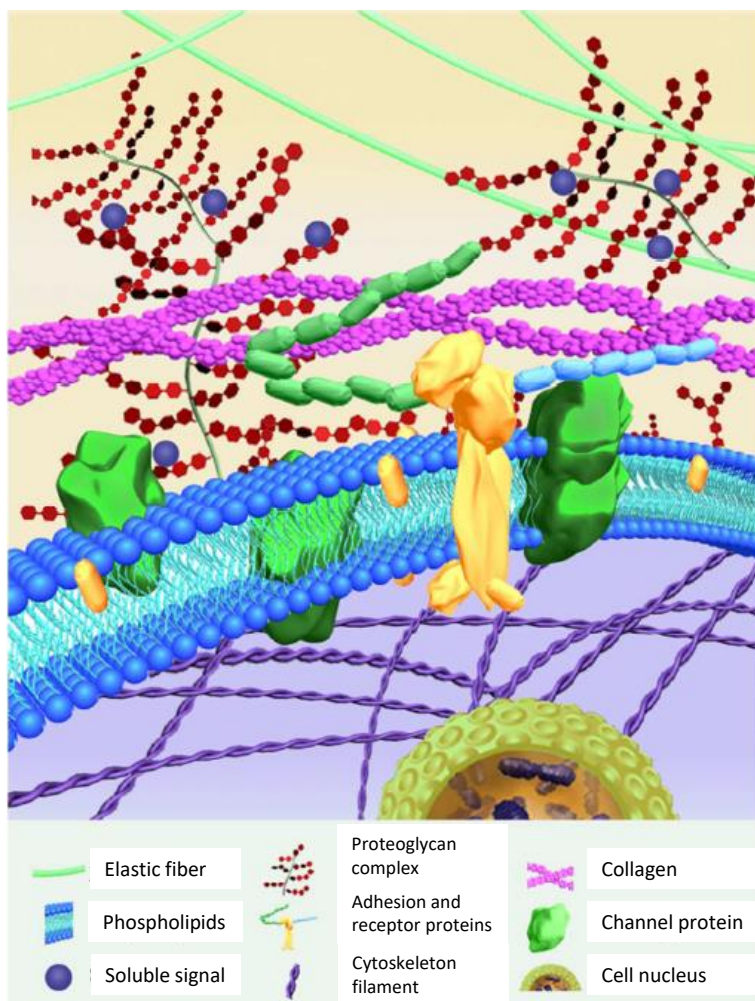
Figure 5.4. Schematic of the ECM. The major ECM components such as collagen and elastin exist in the form of interwoven nanofibres, which provides a fibrillar matrix network to support cells and direct their behaviour.[186]

5.3. Ultrafine Fibres (UFs) from PCL

Aliphatic polyesters, due to their favourable features of biodegradability and biocompatibility, comprise one of the most important classes of synthetic polymers used in biomedical applications. The advantages of these polyesters are their biocompatibility, ability to undergo hydrolysis in the human body,[221] low melting points and exceptional blend-compatibility with other polymers. These properties stimulated extensive research into their potential application in the biomedical field.[215,222]

Poly-ε-caprolactone,(PCL), (Figure 5.5.), is a synthetic biodegradable aliphatic polyester which has attracted considerable attention in recent years, in the

biomedical areas of controlled-release drug delivery systems, absorbable surgical sutures and 3-D scaffolds for use in tissue engineering.[223] Amongst the different classes of biodegradable polymers, PCL is an incredibly versatile polymer and due to its excellent rheological properties it can be used in many polymer processing technologies to produce an enormous variety of scaffolds.

$$\left[O - (CH_2)_5 - \overset{\overset{\displaystyle O}{\|}}{C} \right]_n$$
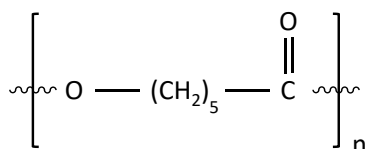
Figure 5.5. Structure of PCL.

The main advantages of the use of PCL are: 1) its approval by the Food and Drug Administration (FDA) for use in humans; 2) its biodegradability; 3) its compatibility with a wide range of other polymers; 4) its good processibility which enables fabrication of a variety of structures and forms; 5) its suitability for melting; 6) its high thermal stability; 7) its low melting point ($\sim$ 60 °C); 8) its relatively low cost.[224,225]

There are many polymers that have been used for electrospinning applications (e.g. PGA, PLA, PLGA, etc).

5.4. Surface Modification

Surface modification provides the means to improve the physicochemical and biological properties of UFs. Several techniques have been reported for surface modification of UFs to increase the hydrophilicity and to introduce active sites for further biomolecule immobilisation. Various biomolecules with specific bioactive moieties can be physically absorbed or chemically bonded to the surface of polymer UFs without affecting the bulk properties. Such biologically functionalised fibres possess optimised surface hydrophilicity and chemical compositions, thus providing a more favourable environment for cell growth and tissue regeneration.[187]

5.4.1. Physical Absorption

Physical absorption is the simplest technique to immobilise biomolecules onto the micro- and nano-fibre surfaces, which is driven by non-covalent interactions such as

van der Waals forces, electrostatic forces, hydrophobic interactions and H-bonding.[226] However, the immobilisation strength and efficiency of biomolecules is relatively weak by direct physical coating.[227] In order to avoid this limitation, plasma modification which generates a more hydrophilic surface, is often applied to increase the efficiency of physical absorption onto hydrophobic micro- and nano-fibre scaffolds.[228] Plasma is considered to be the fourth distinct state of matter. It can broadly be defined as a gas containing charged and neutral species, including electrons, ions, radicals, atoms and molecules. The presence of charge carriers makes the plasma electrically conductive.[229] Plasma-treated polymer micro- and nano-fibres can enhance cell attachment and migration because of the increased quantities of hydrophilic amine and carboxyl surface groups.[230] Furthermore, several types of ECM protein components such as collagen,[231] gelatin,[232,233] laminin[234] and fibronectin[235] can be subsequently immobilised onto the plasma treated UFs surface for enhanced cell function.

5.4.2. Chemical Bonding

Chemical bonding provides a more efficient method for long term attachment of biomolecules. Reactive functional groups need to be introduced in the polymer prior to biomolecule immobilisation. Carboxyl and amine groups are the most widely used functional groups for surface modification of polymer micro- and nano-fibre. These groups can be introduced to the surface of UFs by hydrolysis reactions under mild conditions. For example, carboxyl groups can be exposed on the surface of several polyester nanofibres after treating with an alkaline aqueous solution.[236] In addition, amine groups can also be implanted onto the surface of polyester micro- and nano-fibres by treating the scaffold after producing the fibres. Amino molecules are then covalently attached to the carboxylic groups on the polyester micro- and nano-fibres [199] or be incorporated into the bulk material of nanofibres during the fabrication, commonly by using free amines and polymer blend [237,238] A variety of biomolecules such as ECM proteins, ECM-derived peptides, antibodies and heparin have been covalently bonded to the surface of polymer nanofibrous scaffolds for various applications in tissue engineering.[239,240]

5.4.3. Click Chemistry

''Click'' chemistry is another approach for surface modification of polymeric fibres with biomolecules via the formation of heterocyclic linkages between two specific functional groups. For a ''click'' chemistry reaction the following characteristics are desirable: 1) the reaction must be modular, 2) stereospecific, 3) high yielding, 4) starting materials must be readily available, and 4) product isolation must be simple.[241] A number of ''click'' methodologies have been demonstrated in recent years (Table 5.1.); specifically, copper(I)-catalysed azide–alkyne cycloaddition (CuAAC) chemistry has been used to attach biofunctional ligands to the surface of PCL fibres to inhibit degradation during cell seeding, while presenting a hydrophilic surface for cellular attachment.[242]

Table 5.1. Examples of click chemistry methodologies used in the surface modification of UFs.[242]

Reaction type	Reactants		Products
Copper catalysed azide-alkyne cycloaddition (CuAAc)	R_1—N_3	+ ≡—R_2 CuI →	R_1 triazole R_2
Michael addition	R_1—SH	+ maleimide N—R_2 →	R_1—S succinimide N—R_2
Thiol-ene chemistry	R_1—SH	+ ═—R_2 hν →	R_1—S—R_2
Thiol-yne chemistry	R_1—SH	+ ≡—R_2 hν →	R_1—S / R_1—S R_2
Diels-Alder chemistry	R_1 diene	+ maleimide N—R_2 →	bicyclic N—R_2 R_1
Oxime chemistry	R(C=O)R_1	+ H_2N—O—R_2 H_2O →	R(C=N—O—R_2)R_1

5.5. Electrospun Peptide-Based Scaffolds

Peptides are a class of self-assembling and co-assembling biomolecules that have been widely investigated for different uses, including biomedical applications for regenerative medicine, as was discussed in Chapter 2. Peptides have received large attention in the area of supramolecular chemistry in recent years due to the potential

to self-assemble and form micro- and nanostructures. In addition, their easy biocompatibility and capability of creating microenvironments suited for growing cells makes them attractive to develop materials for tissue regeneration.[243,244]

Maleki and co-workers have investigated a library of diverse self-assembling and co-assembling peptides (Table 5.2.) in order to understand better the electrospinnability of these systems. In addition, they studied the optimal conditions to produce peptide-based electrospun nanofibrous scaffolds.[244] They were able to successfully achieve this by choosing of right electrospinning solvent to obtain spinnable peptide solutions. The mixture of solvents selected [1,1,1,3,3,3-hexafluoro-2-propanol (HFIP), 2,2,2-trifluoroethanol (TFE) and TFA] had the following characteristics: a) dissolved the peptide completely, b) avoided formation of aggregates prior to electrospinning, c) ensured rapid solidification of the collected fibres and d) had lower dielectric constant to induce less net charge density in the electrospinning solution to avoid self-aggregation when no high-voltage was applied. In addition, the authors used concentrated solutions to provide sufficient physical entanglements and optimise electrospinning parameters.[244]

Table 5.2. Synthetic peptides tested for electrospinning.[244]

Peptide Sequence	Peptide Chemical Formula	Molecular Weight [g/mol]
Ac-(LDLK)$_3$-CONH$_2$	C$_{68}$H$_{122}$N$_{16}$O$_{19}$	1467.82
Biotin-KKGGG(LDLK)$_3$-CONH$_2$	C$_{94}$H$_{167}$N$_{25}$O$_{25}$S	2079.55
Ac-KKGGG(LDLK)$_3$-CONH$_2$	C$_{86}$H$_{155}$N$_{23}$O$_{24}$	1895.29
Ac-CGG(LKLK)$_3$GGC-CONH$_2$	C$_{88}$H$_{165}$N$_{25}$O$_{19}$S$_2$	1941.54
Ac-(CDLK)$_4$-CONH$_2$	C$_{78}$H$_{137}$N$_{21}$O$_{25}$S$_4$	1897.34
Ac-(RADA)$_4$GGGGGGPFSSTKT-CONH	C$_{112}$H$_{183}$N$_{43}$O$_{42}$	2803.92
Biotin-GGGPFSCTKT-CONH$_2$	C$_{50}$H$_{78}$N$_{14}$O$_{15}$S$_2$	1179.37
Ac-DDGGG(LDLK)$_3$-CONH$_2$	C$_{82}$H$_{141}$N$_{21}$O$_{28}$	1869.12
Ac-FAQRVPPGGG(LDLK)$_3$-CONH$_2$	C$_{112}$H$_{188}$N$_{30}$O$_{30}$	2434.91
Ac-(LDLD)$_5$-CONH$_2$	C$_{102}$H$_{165}$N$_{21}$O$_{41}$	2341.56
Biotin-GGGAASSTKT-CONH$_2$	C$_{42}$H$_{72}$N$_{14}$O$_{16}$S	1061.17
Ac-(LKLK)$_3$-CONH$_2$	C$_{72}$H$_{140}$N$_{18}$O$_{13}$	1507.07
Ac-(LKLK)$_5$-CONH$_2$	C$_{122}$H$_{235}$N$_{31}$O$_{21}$	2472.41
Ac-YIIPMHDGGG(LDLK)$_3$-CONH$_2$	C$_{115}$H$_{190}$N$_{28}$O$_{32}$S	2508.97

5.6. Aims and Objectives of Chapter 5

As discussed earlier, many different methods have been investigated to modify the physicochemical and surface characteristics of electrospun UFs and improve their biocompatibility. To date, the use of supramolecular gelators in the generation of electrospun materials has not yet been extensively studied. The work described in this chapter aims to investigate the use of supramolecular gelators to:

> I.) Achieve modification of PCL electrospun fibre morphologies.

> II.) Improve solvent tolerance.

> III.) Generate functional electrospun fibres with applications as drug delivery systems and tissue scaffolds.

For this "proof of concept" investigation, the supramolecular gelators studied in previous chapters were employed. The application of the *N*-Fmoc lipoamino acid gelators (described in Chapter 2) to optimise solvent tolerance parameters was investigated. Moreover, these gelators were used in the electrospinning of fibres loaded with the drugs Fusidic acid (an antibiotic) and Betamethasone valerate (an anti-inflammatory), to mimic the drug release from a bactericidal cream formulation. In addition, the application of galactose-based aspartic acid (Chapter 3) and squaramide (Chapter 4) gelators for the generation of scaffolds suitable for tissue engineering was explored in a preliminary study.

5.7. Results and Discussion

5.7.1. Investigation of PCL Blended with Fmoc Lipoamino Acid Supramolecular Gelators for the Generation of Electrospun Fibres

5.7.1.1. Preparation of PCL Stock Solution

Commercially available PCL was dissolved in $CHCl_3$:EtOH (75:25) to prepare a 10 w/v % stock solution (Chapter 7. Section 7.6.). Once the PCL solution was prepared, some of the parameters that influence the electrospinning process were optimised for the formation of electrospun fibres. The PCL solution was placed in a 10 mL syringe and delivered by the syringe pump at predetermined flow rates for each experiment (in the range of 1 - 6 mL/h). The distance from the needle to the collector plate (ground

electrode) was set for each experiment (in the range of 3 – 15 cm). The positive voltage applied to the polymer solution was also set for each experiment (in the range of 5 – 20 kV). The amount of time collecting electrospun fibres varied, depending on the experiment, from 1 to 10 min. All experiments were carried out in the plexiglass cabinet located in a fumehood with flow air, at rt.

5.7.2. PCL Electrospun Fibres. Influence of Needle Gauge and Voltages

To investigate the effect of the needle gauge and voltages, a 10 w/v % PCL polymer stock solution in $CHCl_3$:EtOH (75:25) was prepared and placed in the syringe at a distance from the syringe tip to the collector plate of $\sim$ 8 cm with a flow rate of 1 mL/h. In each case, the sample was electrospun for 1 min. on a collector plate (normally it was a copper collector plate covered with tinfoil), a glass slide or a SEM stub (see section 7.3.6.3. Chapter 7), in the presence of air. The samples prepared were analysed under an optical microscope and/or SEM.

A preliminary experiment was performed in order to compare the diameter and length of the fibres when two different gauge needles (18 and 21 G) were used. Two different voltages were chosen for these experiments (15 and 20 kV), in which the formation of fibres with very distinctive characteristics could be observed in Figure 5.6.
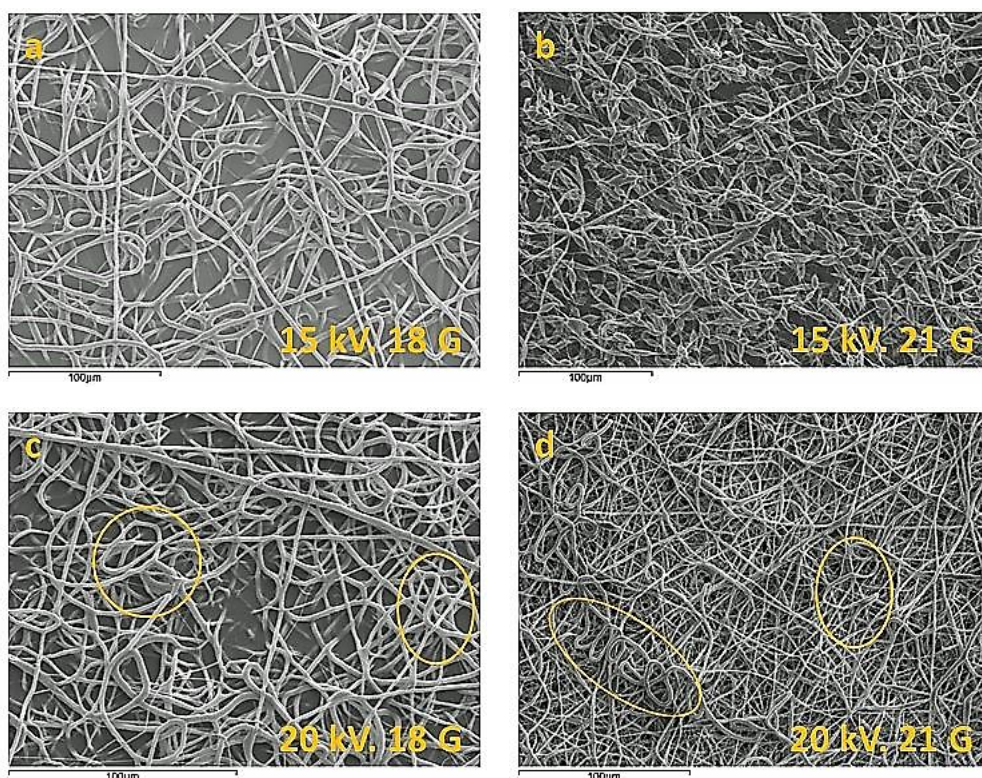
Figure 5.6. SEM images of 1 min. electrospun PCL stock soln. on a SEM stub at 1 mL/h, and a distance of ~ 8 cm. a) 15 kV, 18 G; b) 15 kV, 21 G; c) 20 kV, 18 G; d) 20 kV, 21 G. [Scale bar: a) – d) 100 μm].

In Figure 5.6. it can be observed that the 18 G needle delivered fibres with a more regular shape at either 15 or 20 kV [images a) and c)]. These fibres were more uniform with similar average diameters. Comparing images a) and b), both at 15 kV, it can clearly be seen that the increase of the needle gauge, from 18 G to 21G, changed drastically the morphology of the fibre, resulting in bead formation. The images of samples prepared at higher voltage [20 kV, images c) and d)], show the formation of wavy fibres (highlighted areas) from both needle gauges.

When a high voltage (e.g. 10 kV) is applied to the polymer solution, repulsion charges opposite to the surface tension of the solution give rise to what is known as the Taylor cone.[191,245-247] After a critical point, where the surface tension is overcome, a charged jet of the polymer solution is ejected from the needle tip of the cone. Generally, it has been established that increasing the applied voltage increases the deposition rate, due to the higher mass flow from the needle tip.[248] In Figure 5.7. the images show the samples prepared in which the applied voltage was varied from 9 - 20 kV.
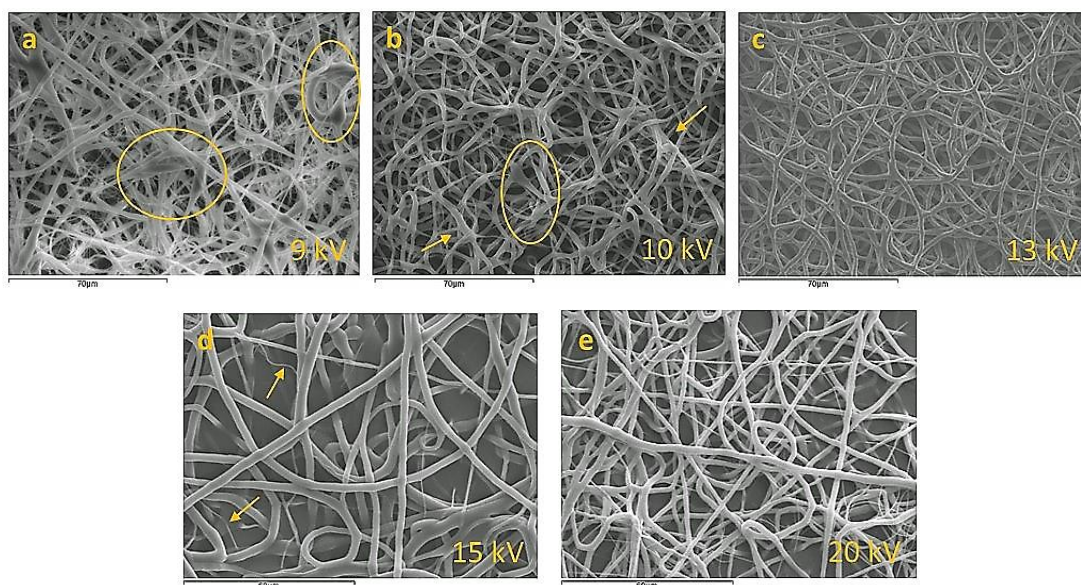
Figure 5.7. SEM images of 1 min. electrospun PCL stock soln. on a SEM stub at 1 mL/h, 18 G, and a distance of ~ 8 cm at an applied voltage of a) 9 kV; b) 10 kV; c) 13 kV; d) 15 kV; and e) 20 kV. [Scale bar: a) – c) 70 μm; d), e) 60 μm].

In agreement with literature reports, it was observed that as the voltage was increased there was a significant increase in the amount of fibres collected without apparent deformations. The formation of lumps or irregularities, as beads, also changed at higher voltages as the surface tension is no longer dominant in the fibre formation shape. It is evident from Figure 5.7. that as the voltage was increased, the fibres become smoother and longer and slightly thinner fibres were formed, which is consistent with literature. Zong and co-workers confirmed that an increase in the applied electrospinning voltage altered the shape of the initial droplet and, in consequence, the diameter / length of the fibre.[249] As a result of these observations, 13 kV was chosen as the optimal voltage to apply for future experiments, since the resulting fibres have a more regular morphology and diameter.

5.7.3. Effects of Solvents: Controls

The solvent used for electrospinning must be a volatile liquid, as when the process is taking place, the solvent must evaporate in order to form the solid fibre on the chosen collector.[190] As the charged jet leaves the needle tip the increase in surface area enhances the rate of evaporation of the volatile solvent which results in a charged, solid polymer fibre. However, if the rate of evaporation is too high, e.g., if

the solvent is very volatile, the evaporation process occurs too fast on the outer surface of the polymer jet, so the solution could solidify at the tip of the needle. This could block the needle without producing any fibres and raise the pressure in the pump causing it to malfunction.[250] For this reason, it is important to find the optimal solvent that produces smooth and regular fibres.

One of the aims of this work is to study the effect of supramolecular gelators in electrospun PCL fibres. The first gelators evaluated (Fmoc lipoamino acids described in Chapter 2) were capable of forming gels in aromatic solvents such as toluene and xylene, both VOC (Volatile Organic Compounds). For this reason, the PCL solution was electrospun in the presence of various different solvents as controls. For the preparation of "PCL solution-controls", the aromatic solvents replaced $CHCl_3$ or EtOH in the preparation of the PCL stock solution. 1 g of PCL was dissolved in a) toluene (7.5 mL) and EtOH (2.5 mL); b) xylene (7.5 mL) and EtOH (2.5 mL); c) chloroform (7.5 mL) and toluene (2.5 mL); d) chloroform (7.5 mL) and xylene (2.5 mL). (Table 5.3.).

Table 5.3. Composition of "PCL solution-controls"

Solvent Control	Chloroform	EtOH	Toluene	Xylene
a)	-	2.5 mL	7.5 mL	-
b)	-	2.5 mL	-	7.5 mL
c)	7.5 mL	-	2.5 mL	-
d)	7.5 mL	-	-	2.5 mL

(1 g PCL)

Once the first solvent was added, the solution was stirred overnight at rt in a closed vial. After addition of the second solvent, the mixture was stirred for further 1 - 2 h until a viscous clear polymer solution was formed (Figure 5.8.). The control solutions were electrospun as described previously.

The SEM images for the electrospun "PCL solution-controls" are shown in Figure 5.8. It can be clearly seen that these samples do not show the typical fibre morphology observed for those formed from the PCL stock solution in $CHCl_3$:EtOH (75:25) (Figure 5.8.). On the other hand, it can be easily appreciated that the presence of aromatic solvents prevents fibre formation: images a) and b) show electrosprayed polymer and images c) and d) show globules and truncated fibre morphologies.
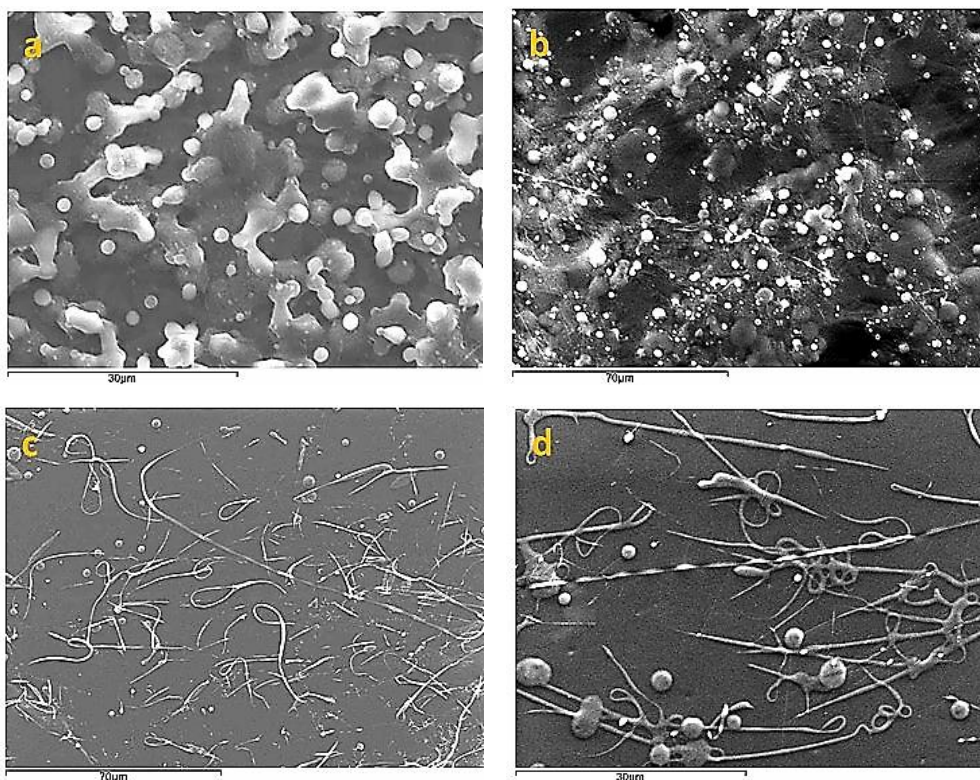
Figure 5.8. SEM images of 1 min. electrospun "PCL solution-controls" on a SEM stub at 1 mL/h, 18 G, 13 kV, and a distance of ∼ 8 cm. a) tol. (7.5 mL) and EtOH (2.5 mL); b) xylene (7.5 mL) and EtOH (2.5 mL); c) chloroform (7.5 mL) and tol. (2.5 mL); d) chloroform (7.5 mL) and xylene (2.5 mL). [Scale bar: a), d) 30 μm; b), c) 70 μm].

A second set of controls was prepared in which toluene and xylene were used as ternary solvents. The PCL stock solution [1 g PCL in $CHCl_3$ (7.5 mL) and EtOH (2.5 mL)] was prepared. Toluene or xylene were added as tertiary solvents in different ratios to evaluate the impact of the aromatic solvent in the fibre morphology (Table 5.4.).

Table 5.4. Composition of "PCL solution-controls". Ratios of tertiary solvent used for preparation of the control solutions.

Control	Ratio	PCL stock solution (1 g PCL. + 7.5 mL chloroform + 2.5 mL EtOH)	Ternary solvent
a)	1 : 1	1.5 mL	1.5 mL toluene
b)	5 : 1	5 mL	1 mL toluene
c)	5 : 1	5 mL	1 mL xylene

Figure 5.9. shows the SEM images of the electrospun second set of control solutions. As observed in the first set of experiments, it can be clearly seen that the presence of toluene or xylene impaired the formation of smooth fibres, independently of the ratio

used. Presence of electrosprayed material, rounded and globular morphologies can be observed, similar to those found for the first set of "PCL solution-controls" (Figure 5.9.).
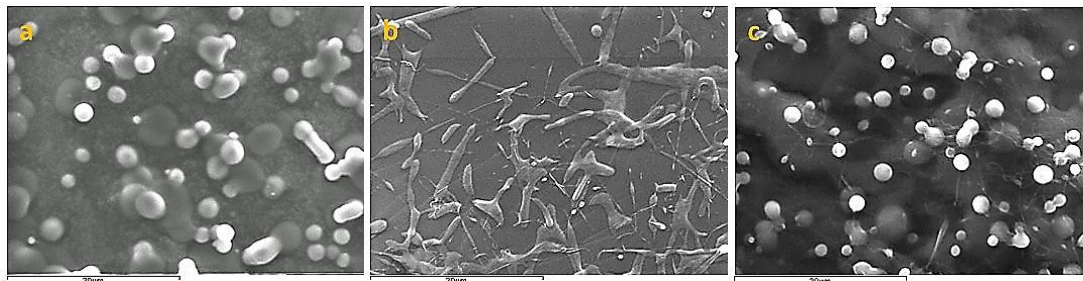
Figure 5.9. SEM images of 1 min. electrospun of the second set of "PCL solution-controls" on a SEM stub at 1 mL/h, 18 G, 13 kV, and a distance of ~ 8 cm. a) **(1:1)** 1.5 mL PCL stock soln. + 1.5 mL tol.; b) **(5:1)** 5 mL PCL stock soln. + 1 mL tol.; c) **(5:1)** 5 mL PCL stock soln. + 1 mL xylene. [Scale bar: a) - c) 30 μm].

5.7.4. Effect of C$_{14}$ Fmoc Lipoamino Acid Gelator 2.40. in PCL Electrospinning

For the purpose of this thesis, the main focus will be the method of co-electrospinning of substance-polymer blend. This method is the simplest and most cost-effective technique, as mentioned in section 5.2.1. In this process, the polymer solution, an additional substance (gelator) and the required solvent were mixed 24 h prior to electrospinning, to ensure homogenous mixing of the gelator and polymer.

Electrospinning of the mixed PCL stock solution and a solution of different concentrations of C$_{14}$ Fmoc lipoamino acid gelator **2.40.** (Figure 5.10.) (which was an efficient toluene gelator, as discussed in Section 2.3.2.) at different voltages (11, 13 and 20 kV) was performed (Table 5.5.).

Figure 5.10. Structure of C$_{14}$ Fmoc lipoamino acid gelator **2.40.**

Table 5.5. Composition of mixtures of PCL stock solution with solutions of gelator **2.40.** in toluene at different ratios (1:5 or 5:1) at different voltage (11, 13 and 20 kV).

Sample	Voltage	Ratio	PCL stock solution (1 g PCL. + 7.5 mL chloroform + 2.5 mL EtOH)	**2.40.** (100 mg)
a)	11 kV	1 : 5	1 mL	5 mL toluene
b)	13 kV	1 : 5	1 mL	5 mL toluene
c)	20 kV	1 : 5	1 mL	5 mL toluene
d)	11 kV	5 : 1	5 mL	1 mL toluene
e)	13 kV	5 : 1	5 mL	1 mL toluene
f)	20 kV	5 : 1	5 mL	1 mL toluene

Firstly, taking into account the ratios of PCL stock solution and gelator solution, (Figure 5.11.), it was observed that, at higher toluene solution ratio (1:5), images a) – c), only an electrosprayed polymer was formed; whereas at lower toluene solution ratio (5:1), images d) – f), fibres with beads were produced. In samples a) – c), the concentration of gelator was not sufficient to form a toluene gel (2 w/v %) under the studied conditions. However, in samples d) – e), the concentration of **2.40.** was higher (10 w/v %), thus it was possible for this compound to gel toluene and promote fibre formation, as toluene did not interact with the PCL as in previous studies.

Regarding the voltage used for these tests, sample a) at 11 kV produced a "honeycomb" like formation [image a), Figure 5.11.], which could be due to a more uniform distribution of the spray which is lost once the voltage was increased [images b) and c), Figure 5.11.]. Considering the morphologies observed for increasing voltages at ratios 5:1 [Samples d) – f)], it can be observed that at a lower voltage [images d) and e), 11 and 13 kV, respectively], the formation of beaded fibres appears very similar.

It can be speculated that the beads are originated due to formation of toluene gel droplets in which the polymer is entrapped, resulting in a very thin, low density fibre mat being formed. As the voltage is increased, it is capable of overcoming the surface tension in the gel droplets and pull the polymer to form a fibre mat with smaller beads embedded on it.[251]
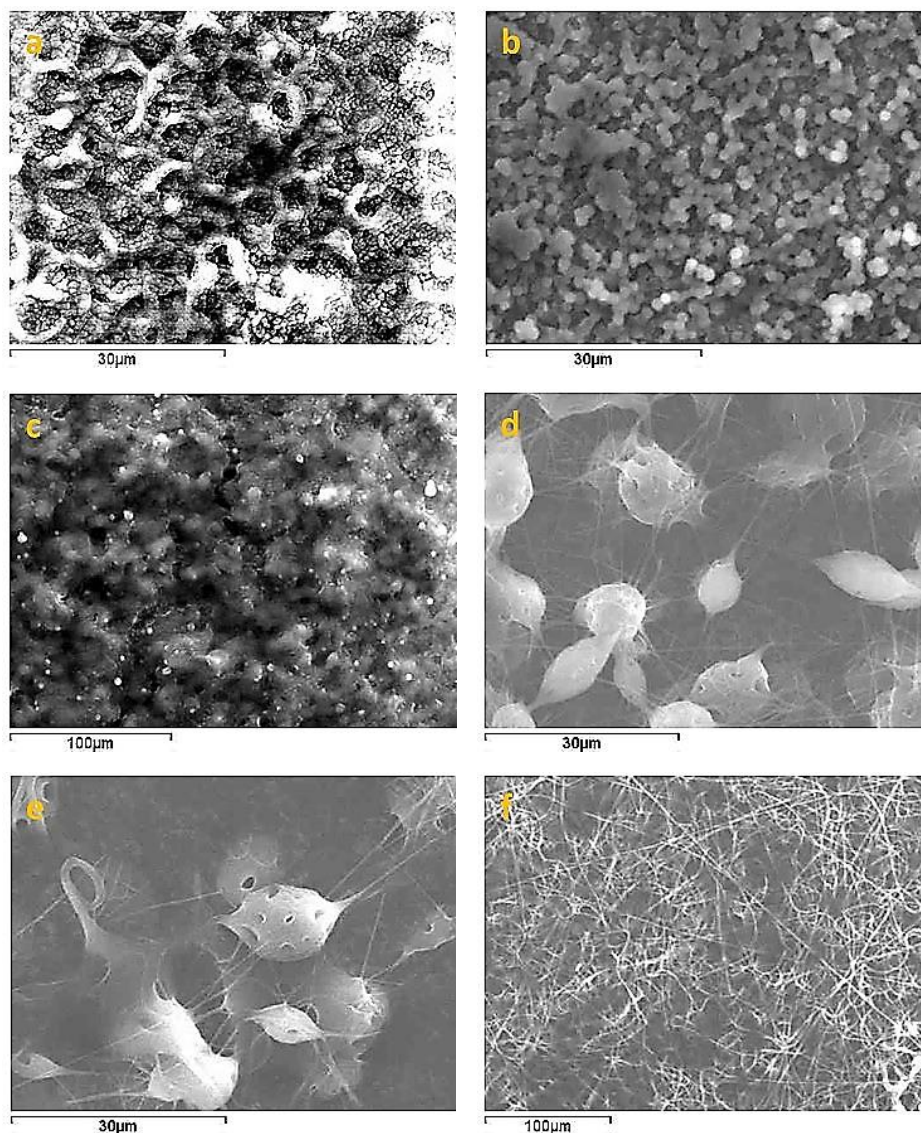
Figure 5.11. SEM images of 1 min. electrospun of PCL soln. on a SEM stub at 1 mL/h, 18 G, and a distance of ~ 8 cm. a) 11 kV; b) 13 kV; c) 20 kV of **(1:5)** 1 mL PCL stock soln. + **2.40.** (100 mg in 5 mL tol., 2 w/v %); d) 11 kV; e) 13 kV; f) 20 kV of **(5:1)** 5 mL PCL stock soln. + **2.40.** (100 mg in 1 mL tol., 10 w/v %). [Scale bar: a), b), d), e) 30 μm; c), f) 100 μm].

As the optimal voltage for the formation of smooth and regular PCL fibres was found to be 13 kV (discussed in Section 5.7.2. Figure 5.7.), the ratio of the PCL stock solution and solutions of gelator **2.40.** in toluene were optimised. Different ratios (1:1, 2:1, 3:1, 5:1 and 10:1) of these solutions (see Table 5.6.) produced successfully electrospun fibres. The morphology of the fibres were imaged by SEM after electrospinning (Figure 5.12.).

Table 5.6. Composition of mixtures of PCL stock solution with solutions of gelator **2.40.** in toluene at different ratios (1:1, 2:1, 3:1, 5:1 and 10:1) at the same voltage (13 kV).

Sample	Ratio	PCL stock solution (1 g PCL. + 7.5 mL chloroform + 2.5 mL EtOH)	**2.40.** in toluene
a)	1 : 1	1.5 mL	30 mg in 1.5 mL (2 w/v %)
b)	2 : 1	2 mL	20 mg in 1 mL (2 w/v %)
c)	3 : 1	3 mL	20 mg in 1 mL (2 w/v %)
d)	5 : 1	5 mL	20 mg in 1 mL (2 w/v %)
e)	10 : 1	10 mL	20 mg in 1 mL (2 w/v %)

The examination of images a) to e) show that as the percentage of the PCL stock solution increases, so does the amount and thickness of the fibres (Figure 5.12.). At the highest PCL concentration (ratio 10:1), the diameter of the fibres was larger, leaving more gaps between fibres. In addition, problems such as high pressure at the pump and blockage of the needle tip started to occur at this ratio. In order to obtain fibres with a more uniform distribution, regular fibre diameter, less spray and less beads, the ratio 5:1 was chosen for optimisation of the system [image d). Figure 5.12.].

Figure 5.12. SEM images of 1 min. electrospun of PCL stock soln. on a SEM stub at 1 mL/h, 18 G, 13 kV, and a distance of ~ 8 cm. a) **(1:1)** 1.5 mL PCL stock soln. + **2.40.** (30 mg) in 1.5 mL tol.; b) **(2:1)** 2 mL PCL stock soln. + **2.40.** (20 mg) in 1 mL tol.; c) **(3:1)** 3 mL PCL stock soln. + **2.40.** (20 mg) in 1 mL tol.; d) **(5:1)** 5 mL PCL stock soln. + **2.40.** (20 mg) in 1 mL tol.; e) **(10:1)** 10 mL PCL stock soln. + **2.40.** (20 mg) in 1 mL tol. [Scale bar: a) 20 μm; b), c) 30 μm; d), e) 40 μm].

5.7.5. Effect of Other Fmoc Lipoamino Acid Gelators in PCL Electrospinning

The other Fmoc lipoamino acid gelators discussed previously in Chapter 2 were blended with the PCL stock solution in order to carry out electrospinning experiments. The fibres were studied and compared with those produced by blending with gelator C_{14}, **2.40.**

Solution of gelators **2.38.**, **2.39.** and **2.42.** in toluene (20 mg/mL, 2 w/v %) were prepared. 1 mL of each solution was mixed with 5 mL of the PCL stock solution (ratio 5:1). After electrospinning, SEM images were taken and they are shown in Figure 5.13.

Figure 5.13. SEM images of 1 min. electrospun of PCL soln. on a SEM stub at 1 mL/h, 18 G, 13 kV, and a distance of ∼ 8 cm. a) **2.38.** 20 mg in 1 mL tol. + 5 mL PCL stock soln.; b) **2.39.** 20 mg in 1 mL tol. + 5 mL PCL stock soln.; c) **2.40.** 20 mg in 1 mL tol. + 5 mL PCL stock soln.; d) **2.41.** 20 mg in 1 mL tol. + 5 mL PCL stock soln. [CA included on images c) and d)]. [Scale bar: a) – d) 100 μm].

Figure 5.13. shows how the gelators **2.38.** - **2.41.** (20 mg) in toluene affected the fibre formation / morphology of the electrospun PCL. According to the gelation tests discussed in Chapter 2 (Section 2.3.2.), gelators **2.38.** and **2.39.** did not form gels in toluene. Thus, the formation of a mat of regular PCL fibres was not successful, as can

be observed in images a) and b). However, in the mixture with gelator C$_{18}$, **2.39.** [image b)] some irregular fibres can be observed. On the other hand, the mixtures of PCL with toluene gelators **2.40.** and **2.41.** [images c) and d), respectively], clearly show formations of PCL fibre mats. It was observed that the fibres for gelator **2.40.** [image c)] had more beads or string-of-pearls structure, whereas, the fibres for the longer chain gelator C$_{18}$, **2.41.** [image d)], had the typical cylindrical-long morphology observed for PCL fibres in the absence of gelator. It can be argued that, when gelators **2.38.** and **2.39.**, which cannot form gels in toluene, are used, the solvent is not entrapped in the gel network, thus affecting the fibre formation as shown in previous examples with PCL solution and toluene (Figures 5.8. and 5.9.). When using gelators **2.40.** and **2.41.**, both capable of forming a gel in toluene, the solvent is entrapped in the network of the gelators, thus the fibre can be formed [images c) and d)]. The longer chain gelator C$_{18}$, **2.41.**, was the most effective toluene gelator and also the one that formed the most regular PCL fibres without beads. In addition, **2.41.** was also capable of gelling EtOH, which could have contributed to the observed regularly morphology of the fibre mat.

Some additional control experiments were carried out to confirm the observed effects of supramolecular gelators in the electrospun PCL fibres. The next control involved the use of *N*-Cbz lipoamino acid compound **2.42.** As discussed previously in Chapter 2, Section 2.3.3., this compound was not capable of forming gels in toluene, however it formed aggregates. Therefore, it was anticipated that the addition of a solution of non-gelator, **2.42.** (20 mg) in toluene (1 mL) to 5 mL of PCL stock solution would prevent fibre formation. Figure 5.14. image a) shows that, as expected, only some short fibres with irregular, curly morphology were formed.

A final control was carried out where by compound **2.40.** (20 mg), was dissolved in 1 mL of EtOH. This solution was then mixed with another solution of PCL (1 g) in 7.5 mL of chloroform. Figure 5.14. image b) shows that **2.40.** does not hamper the formation of PCL fibres, although some beads are observed.
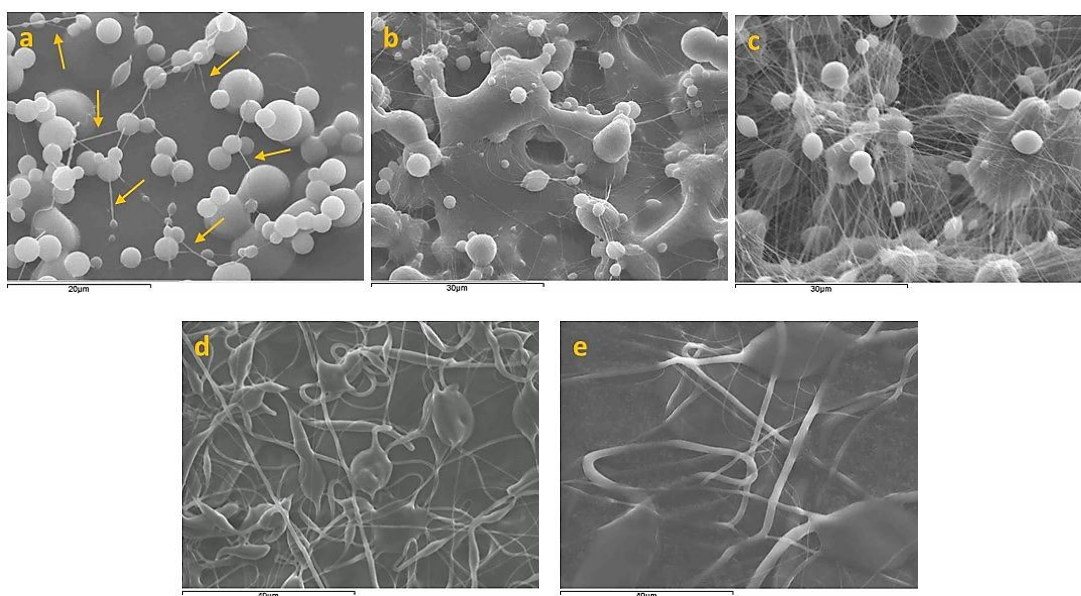
Figure 5.14. SEM images of 1 min. electrospun of PCL soln. on a SEM stub at 1 mL/h, 18 G, 13 kV, and a distance of ∼ 8 cm. a) **Control *N*-Cbz**, **2.42.** 20 mg in 1 mL tol. + 5 mL PCL soln. and b) **Control b) (2.40.** 20 mg in 1 mL EtOH + 1 g PCL. + 7.5mL chloroform). [CA included on image a)]. [Scale bar: a) 100 μm; b) 20 μm].

5.7.6. Contact Angle Measurements of PCL Fibres Modified with Lipoamino Acid Gelators

High surface area is one of the main features of electrospun tissue scaffolds, as discussed in Section 5.4. For that reason, understanding, characterising and controlling their surface properties is very important. Water wetting or wettability properties, for example, will help define the performance of tissue scaffolds for several possible applications where there is interaction with aqueous solutions, such as separation and filtration membranes or for tissue engineering.[173,232,248,252] Electrospun tissue scaffolds are generally classified as hydrophobic or hydrophilic. In the case of many polymers,[198,208,253] the tissue scaffolds produced by electrospinning are hydrophobic and need to be modified by post-treatment in order to present hydrophilicity. This can be achieved by hydrolysis,[254,255] plasma,[256,257] immersion precipitation,[258,259] or click chemistry,[242] as discussed previously in Section 5.4., but this adds time and cost. Another approach is to use polymer blending to incorporate hydrophilic[260] or amphiphilic compounds[261,262] to the polymers to alter the surface properties of the fibres and have the desired hydrophilicity. Wettability studies usually involve the measurement of contact angles (CA) as the primary data, which indicates the degree of wetting when a solid and liquid interact. Small CA (< 90°) correspond to high wettability (hydrophilic character); wetting of the surface is favourable and the fluid will spread over a large area of surface; while large CA (> 90°) correspond to low wettability (hydrophobic character); wetting of the surface is

unfavourable and the fluid will minimise its contact.[263] Wettability has received huge interest from both fundamental and applied points of view. It plays an important role in many industrial processes, such as oil recovery, lubrication, liquid coating, printing, and spray quenching.[264-267] In recent years, there has been an increasing interest in the study of superhydrophobic surfaces, due to their potential applications in, for example, self-cleaning, nanofluidics, and electrowetting.[268-272]

In this section different electrospun fibres were compared in terms of, morphology and water CA measurement values. The CA of those materials were studied on electrospun fibres deposited on glass slides. Angles were measured 30 s after the drop of distilled water touched the surface. Three replicates were done for each sample. Table 5.7. shows the results obtained for PCL stock solution fibres and PCL fibres with compound **2.40.**, **2.41.** and **2.42**.

Table 5.7. Contact angle results with standard deviation for PCL stock soln. and PCL fibres with different gelator.

Sample and Specification	1) Angle degrees	2) Angle degrees	3) Angle degrees	Average degrees	STDEV Standard deviation
PCL stock soln.	106.9	109.5	108.61	**108.3**	± 1.32
2.40. 20 mg + 1 mL tol. + 5 mL PCL stock soln.	119.38	116.75	118.54	**118.2**	± 1.34
2.41. 20 mg + 1 mL tol. + 5 mL PCL stock soln.	118.52	125.88	126.26	**123.6**	± 4.36
2.42. 20 mg + 1 mL tol. + 5 mL PCL stock soln.	109.34	108.57	109.66	**109.2**	± 0.56

Table 5.7. shows the results of water CA for PCL fibres and PCL fibres with compounds **2.40.**, **2.41.** and **2.42.** In all the cases, CA > 90° which correspond to low wettability, as expected for a hydrophobic membrane. The most pronounced increase in CA value was obtained for PCL fibres modified by C_{18} gelator **2.41.**, followed by fibres modified by C_{14} gelator **2.40.** Interestingly, the PCL fibres blended with control compound **2.42.** had a very similar CA value to that recorded for the PCL stock solution on its own (shown in Figure 5.15.).
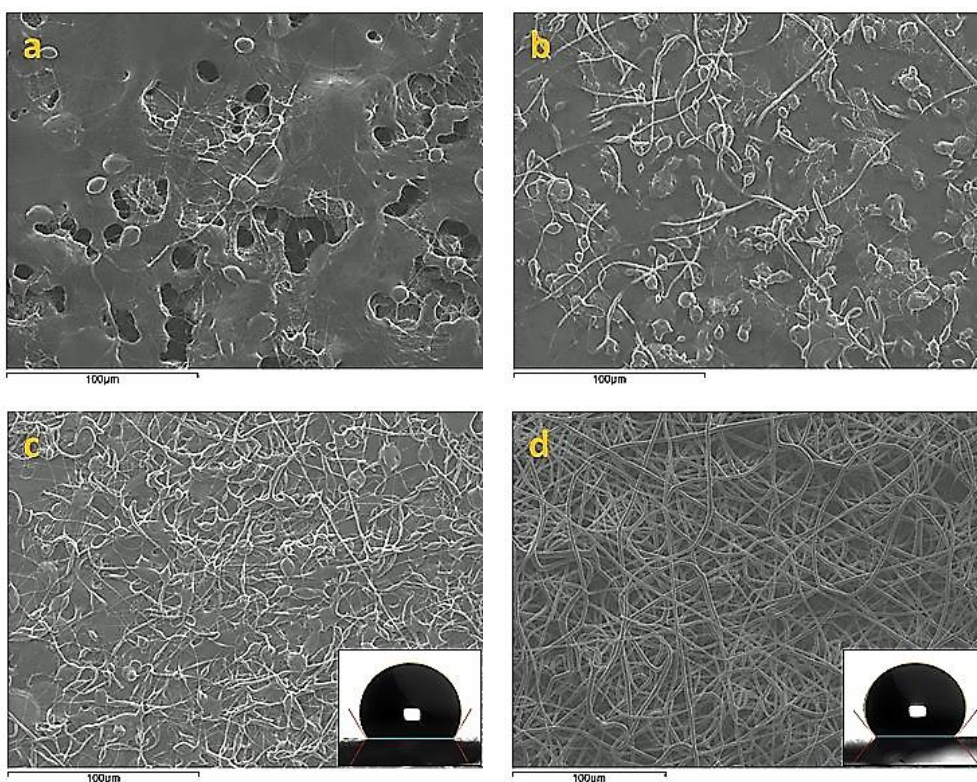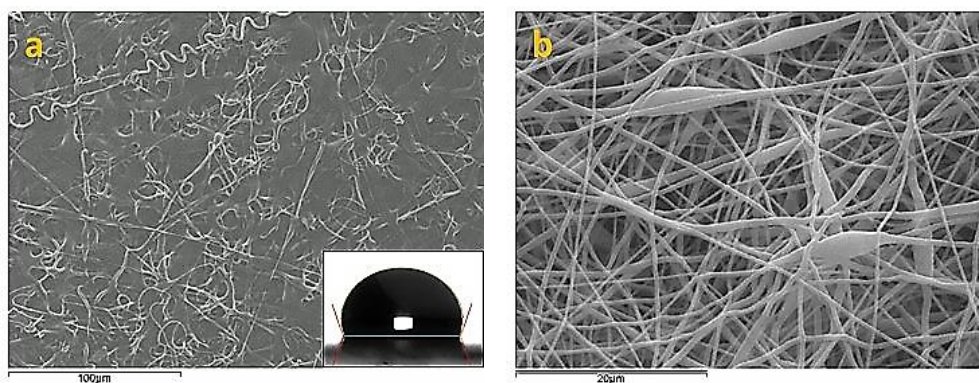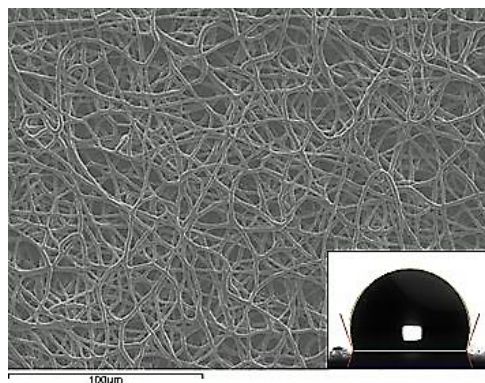
Figure 5.15. SEM images of 1 min. electrospun of PCL stock soln. on a SEM stub at 1 mL/h, 18 G, 13 kV, and a distance of ~ 8 cm. PCL stock soln. (CA included on image). [Scale bar: 100 μm].

5.7.7. ATR-FTIR of PCL Fibres Modified with Lipoamino Acid Gelators

ATR-FTIR spectra give information about the structure of the blend fibres studied. In Figure 5.16., spectra of electrospun samples prepared as: a) Control. 5 mL PCL stock solution + 1 mL toluene; b) PCL stock solution and c) Control. **2.42.**, 20 mg in 1 mL toluene + 5 mL PCL solution blend mats at 600 - 4000 cm^{-1} range are shown. As expected, fibres of PCL solution alone exhibit identical bands to the two controls studied.
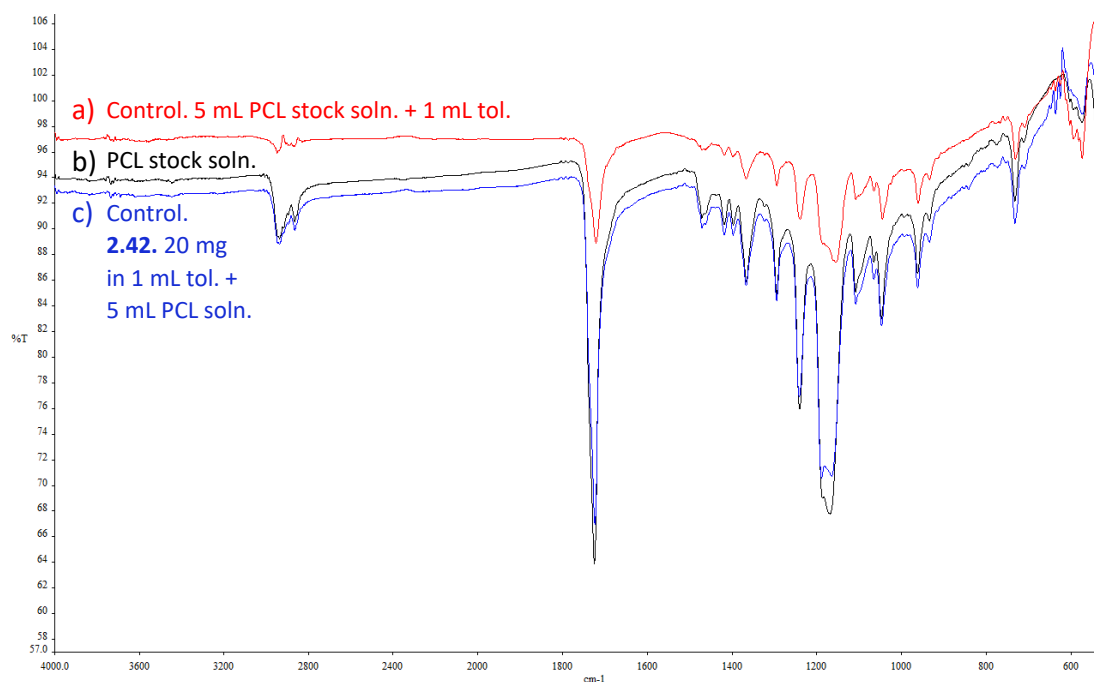
Figure 5.16. Comparison of the ATR-FTIR spectra of dry tissue scaffolds. a) Control. 5 mL PCL stock soln. + 1 mL tol.; b) PCL stock soln. (1 g PCL + 7.5 mL chloroform + 2.5 mL EtOH); c) Control. **2.42.** 20 mg in 1 mL tol. + 5 mL PCL stock soln.

Figure 5.17. compares the spectra of blend dry electrospun PCL fibres prepared as: a) 5 mL PCL solution + **2.38. – 2.41.** (20 mg + 1 mL toluene) on the diamond crystal (ATR-FTIR) and b) FTIR spectra of **2.38. – 2.41.** (solid state, from NaCl film). In all the spectra observed, characteristic PCL peaks can be observed. This result was expected as the PCL concentration was higher than the gelator concentration.
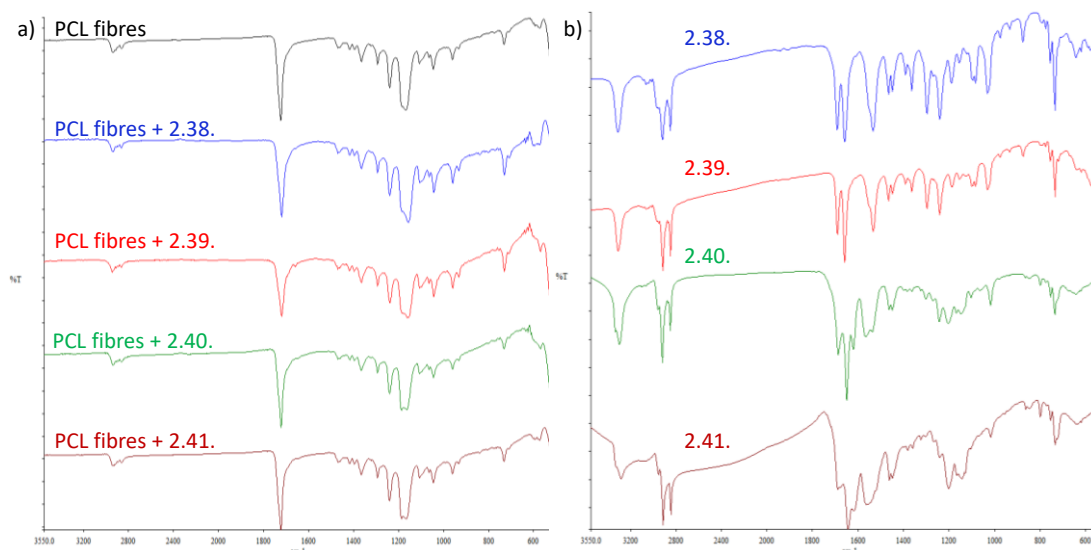
Figure 5.17. Comparison of the ATR-FTIR spectra of dry tissue scaffolds. a) ATR spectra of 5 mL PCL stock soln. + **2.38.** – **2.41.** (20 mg in 1 mL tol.) on the diamond crystal; b) FTIR spectra of **2.38.** – **2.41.** (solid state, from NaCl film).

5.7.8. DSC of PCL Fibres and PCL Fibres Modified with Lipoamino Acid Gelators

DSC analysis of the electrospun fibres was performed to obtain more information about the PCL stock solution fibres and PCL stock solution blend components, which is essential in order to understand the macroscopic and thermal properties of the UFs mats. A single heating cycle between 25 – 120 °C at a constant rate of 5 °C/min was recorded. All the experiments were performed in duplicate and the results were consistent with each other.

Figure 5.18. shows the thermograms of: a) Control. **2.42.** (toluene, 2 w/v %). + 5 mL PCL stock solution; b) Control. 5 mL PCL stock solution + 1 mL toluene and c) PCL stock solution. Comparing with the PCL stock solution, which has a melting point ~ 60 °C [273], with the other two controls, it was observed that the values of the transition melting temperature (T_m) was similar without appreciating significant changes.
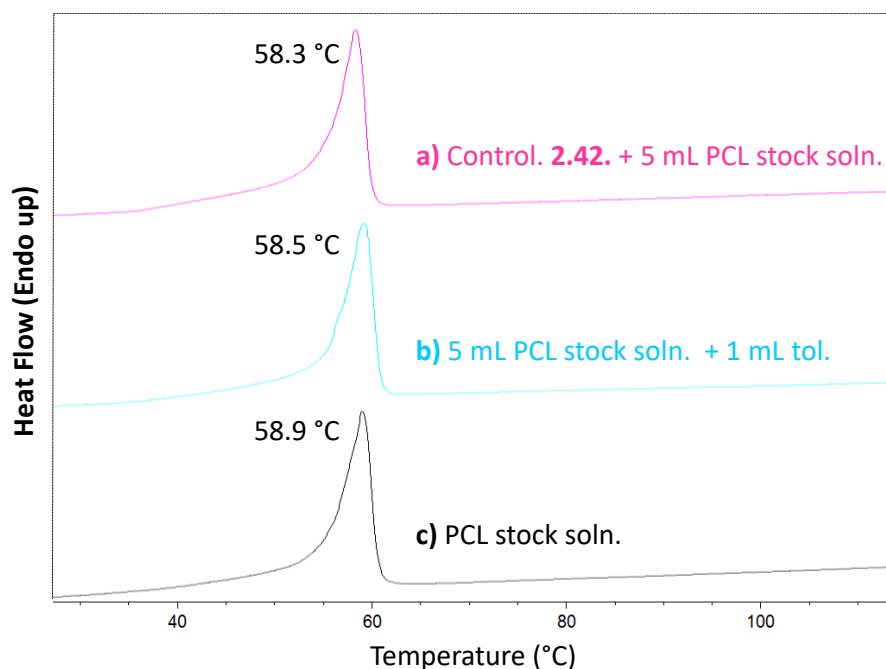
Figure 5.18. DSC thermograms of: a) Control. **2.42.** (tol., 2 w/v %). + 5 mL PCL stock soln.;
b) 5 mL PCL stock soln. + 1 mL tol.; c) PCL stock soln.

Figure 5.19. shows the thermograms of compounds **2.38.**, **2.39.** and **2.42.** from a solution in toluene, 2 w/v %. These compounds did not form a gel in this solvent. The DSC thermograms of xerogels of **2.40.** (toluene, 1.3 w/v %) and **2.41.** (toluene, 1.4 w/v %) are also shown. For compounds **2.38.**, **2.39.** and **2.42.** which cannot form a gel in toluene, similar melting points between 93.4 – 99.9 °C can be observed. In thermograms a) a broad peak can be observed, whereas in thermograms b) two peaks can be observed. The first, at 93.4 °C, can be related to the melting of crystals formed after dissolution in toluene. In thermogram e) a sharp peak can be observed. Comparing thermograms c) and d), multiple melting peaks can be observed, indicating an endothermic process which is characteristic in xerogels due to the melting of 3-D self-assembled xerogel structures. The increase of melting temperature can be explained by the breaking of non-covalent interactions such as H-bonding, dominating the xerogel amorphous structure.[274]
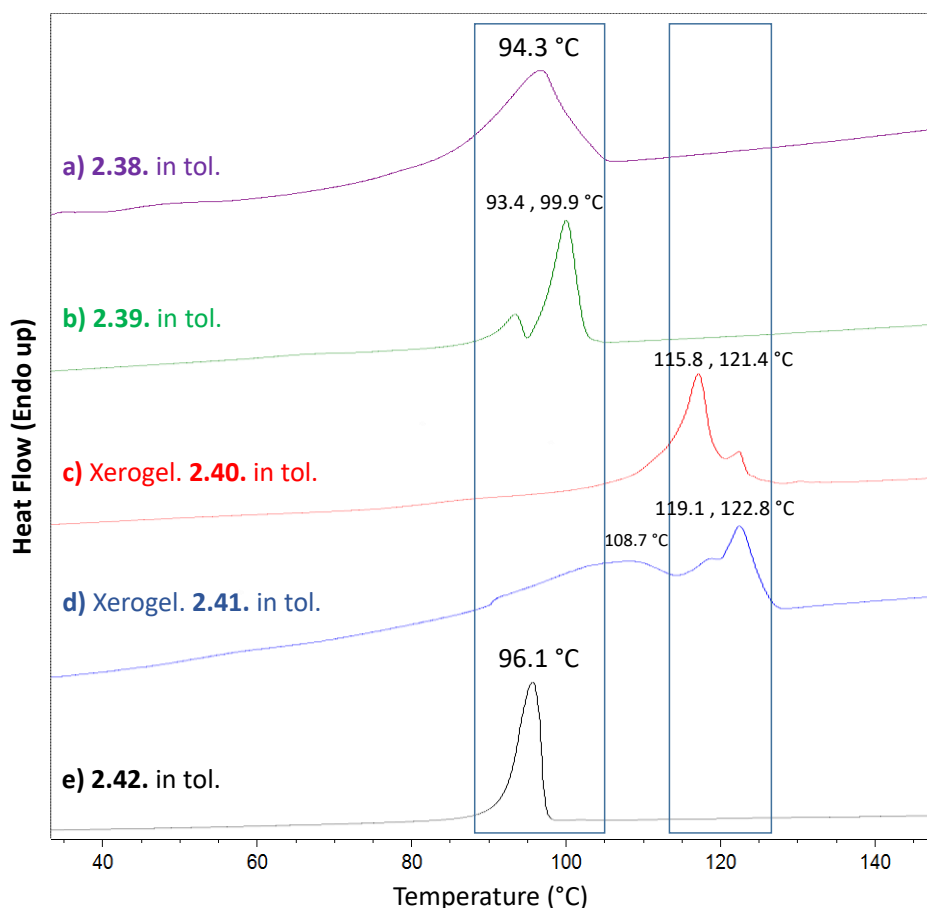
Figure 5.19. DSC thermograms of: a), b) and e) Compounds **2.38.**, **2.39.** and **2.42.** (tol., 2 w/v %). They did not form a gel in this solvent; c) and d) Xerogels of **2.40.** (tol., 1.3 w/v %) and **2.41.** (tol., 1.4 w/v %).

Figure 5.20. shows the thermograms of electrospun fibres modified with: a) **2.38.**; b) **2.39.**; c) **2.40.** and d) **2.41.** (toluene, 2 w/v %). + 5 mL PCL stock soln. and e) PCL stock soln. A single endothermic peak was observed in all the thermograms, which corresponds with the T_m of the polymer at $\sim$ 60 °C. The thermograms from a) to d) were blends of PCL stock solution and a gelator in toluene. A small amount of gelator was sufficient to induce a slight decrease in the fibre T_m. This can be due to the disruption of fibre morphology caused by blending in the conditions described.

The difference in ΔT_m was $\sim$ 1.5 °C between pure PCL [thermogram e)] and thermograms a) and c), whereas the difference in ΔT_m was $\sim$ 0.7 °C between PCL stock solution [thermogram e)] and thermograms b) and d), as could be expected from blending with compounds with longer chains. Thermogram d) **2.41.** (toluene, 2 w/v

%). + 5 mL PCL stock soln. is the closest to T_m of PCL stock solution, which is consistent with the SEM images obtained, [Figure 5.13 d)], revealing smooth and beadless fibres.
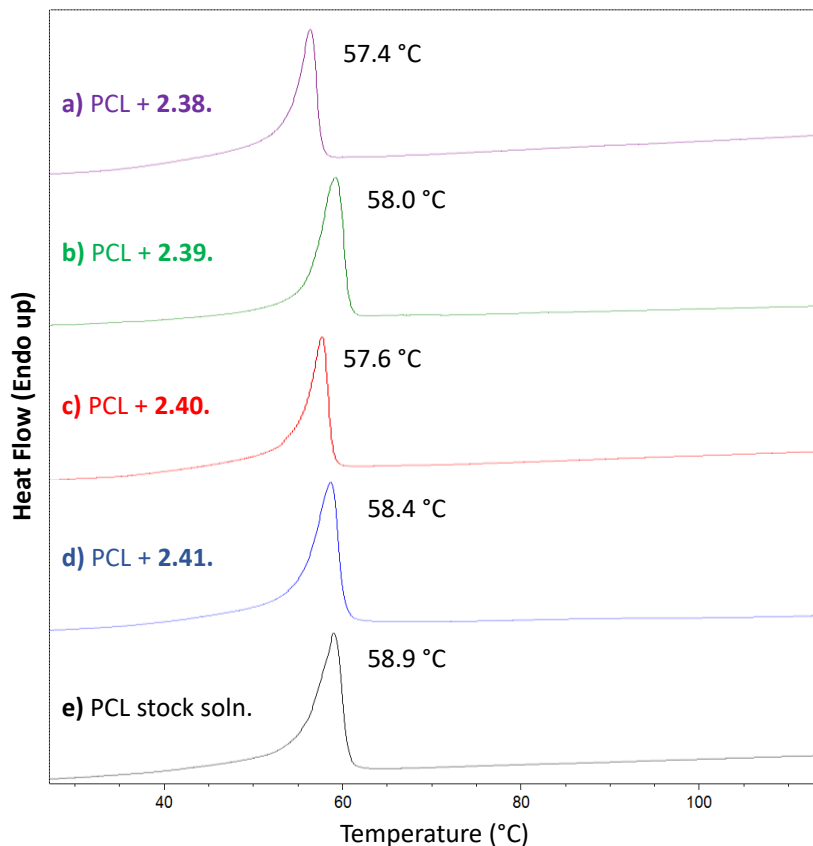
Figure 5.20. DSC thermograms of: a) **2.38.**; b) **2.39.**; c) **2.40.** and d) **2.41.** (tol., 2 w/v %). + 5 mL PCL stock soln.; e) PCL stock soln.

In summary, the experiments described so far indicate that not all the solvents are suitable for the formation of electrospun PCL fibres.[275] In particular, the presence of aromatic solvents, like toluene, prevents the formation of electrospun PCL fibres. The use of toluene gelators like lipoamino acids **2.40.** and **2.41.** which entrap this solvent in the self-assembled gelator matrix allows for effective fibre formation. In addition, the use of the gelators increased significantly the hydrophobicity of the fibres without altering their morphology. These results allow for the expansion of the scope and range of solvents in which blend electrospinning can be carried out, as well as, the use of supramolecular gelators.

5.8. Effect of Galactosyl Based Gelators in PCL Electrospinning

In order to assess if the effects observed when using Fmoc lipoamino acid and gelators in the electrospinning of PCL fibres were also applicable to other supramolecular gelators, similar experiments were performed with galactosyl based gelators (**3.69.** and **4.25.**) described previously in this thesis (Figure 5.21.).

Both compounds share the deprotected galactosyl moieties (free hydroxyl groups) which can give the electrospun mats the hydrophilicity that PCL fibres need to grow cells on them, if used as tissue scaffolds.

3.69.   **4.25.**
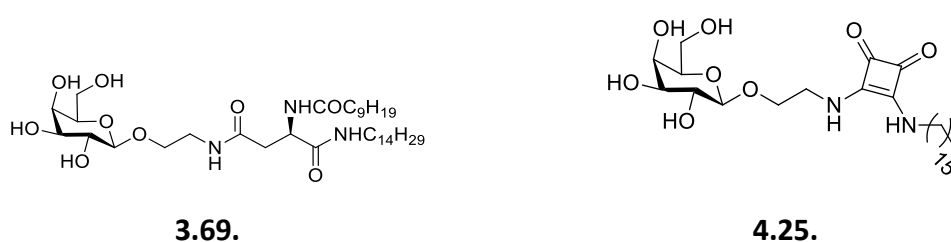
Figure 5.21. Structure of galactosyl based gelators **3.69.** and **4.25.**

However, these two compounds form gels in different solvents. Aspartic acid derivative **3.69.** can form a gel in toluene, while squaramide **4.25.** forms a gel in a mixture of EtOH:H_2O (1:1).

Squaramide derivative **4.25.** was found to gel in a mixture of EtOH:H_2O (1:1) at CGC of 0.1 w/v % as discussed in Chapter 4. Thus, a solution of **4.25.** (20 mg) in 10 mL of EtOH:H_2O was mixed with PCL stock solution at different ratios (1:1), (1:3) and (1:5). Both solutions were difficult to mix at the beginning, with two distinct phases, due to the immiscibility of the solvents. After 24 h stirring in a closed vial, immiscible droplets were still observed in the mixture; however, this did not affect the electrospinning conditions described in previous sections. SEM images were recorded for the electrospun material at different ratios (Figure 5.22.). Comparing images a) – c) (Figure 5.22.), it was observed that electrosprayed material was produced at a ratio (1:1). The appearance of fibres improved with increasing concentration of PCL. Amongst the fibres, some electrosprayed material could be observed at 6 μm magnification for the three images of interest. This could be a

consequence of the immiscible character of the solvents used to prepare the electrospinning solution (Figure 5.22.).
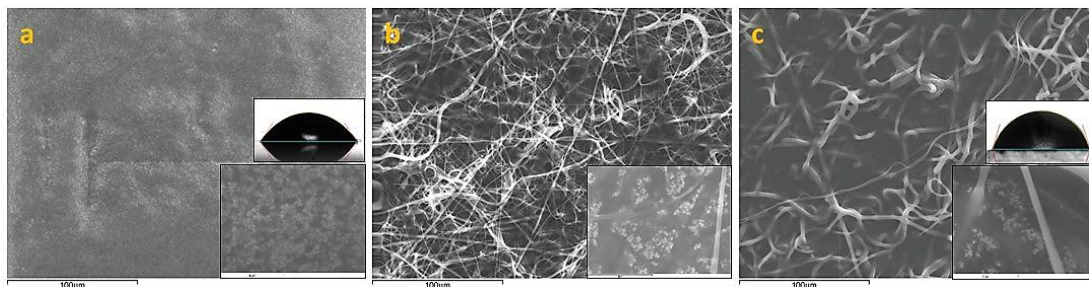
Figure 5.22. SEM images of 1 min. electrospun on a SEM stub at 1 mL/h, 18 G, 13 kV, and a distance of ~ 8 cm. a) **(1:1)** 2 mL **4.25.** (20 mg + 10 mL EtOH:H$_2$O) + 2 mL PCL stock soln.; b) **(1:3)** 1 mL **4.25.** (20 mg + 10 mL EtOH:H$_2$O) + 3 mL PCL stock soln.; c) **(1:5)** 1 mL **4.25.** (20 mg + 10 mL EtOH:H$_2$O) + 5 mL PCL stock soln. [CA included on images a) and c)]. [Scale bar: a) - c) 100 μm].

Some control experiments were carried out for compound **4.25.** (Figure 5.23.). A solution of **4.25.** (20 mg) in 10 mL of EtOH (0.2 w/v %) was prepared as discussed in Chapter 4. **4.25.** was soluble in hot EtOH and it formed aggregates when cooled to rt. This solution was mixed with PCL stock soln. in ratios (1:1) [image a)] and (1:5) [image b)], respectively. Images a) and b) show the formation of very thin fibres with multiple beads. As expected, when the ratio of PCL solution was increased, more fibres with less beads were observed [image b)]. However, the morphology is very different to control b) in Figure 5.14., in which compound **2.40.** (20 mg) was dissolved in 1 mL EtOH with 1 g PCL and 7.5 mL chloroform. In that case, electrospinning of the mixture produced a more uniform fibre formation. This may indicate that the aggregates formed by compound **4.25.** influenced the beading morphology.
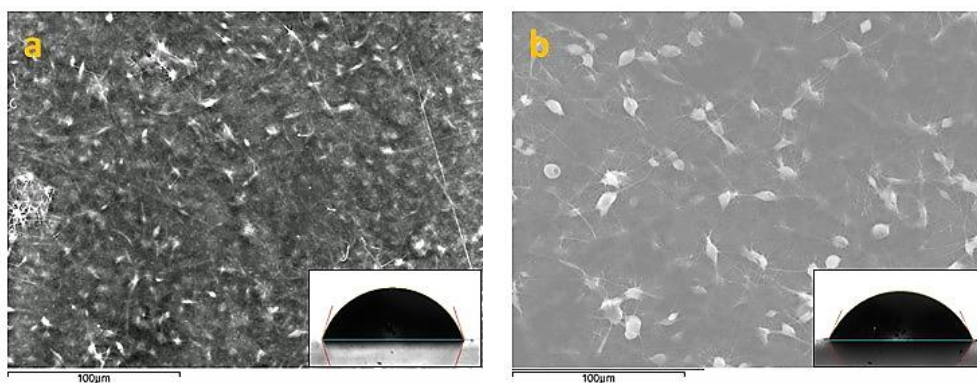
Figure 5.23. SEM images of 1 min. electrospun on a SEM stub at 1 mL/h, 18 G, 13 kV, and a distance of ~ 8 cm. a) **Control 1.** (1:1) 2 mL **4.25.** (20 mg + 10 mL EtOH) + 2 mL PCL stock soln.; b) **Control 2.** (1:5) 1 mL **4.25.** (20 mg + 10 mL EtOH) + 5 mL PCL stock soln. (CA included on images). [Scale bar: a), b) 100 μm].

Aspartic acid derivative compound **3.69.** was found to form a gel in toluene at CGC of 5.5 w/v %, as discussed in Chapter 3. Since the intended use of these materials was as tissue scaffolds, it was decided to use lower concentrations. This would avoid potential undesirable interference with the cells due to the high concentration. Solutions of **3.69.** in toluene at two different concentrations [55 mg **3.69.** + 5 mL tol. (1.1 w/v %) and 27.5 mg **3.69.** + 5 mL tol. (0.55 w/v %)] were investigated when mixed with PCL stock soln. at different ratios (1:1) and (1:5). In this case, the solutions were miscible, showing a homogeneous solution before electrospinning. SEM imaging was recorded for the electrospun materials formed from the mixtures at different ratios and concentrations (Figure 5.24.). The images a) – d) in Figure 5.24. correlate well with the observations discussed for Fmoc lipoamino acid **2.38.** – **2.41.** in Section 5.7.5. Comparing images a) and c) in Figure 5.24., it was observed that a ratio of 1:1 led to the formation of more beads at the higher concentration of compound **3.69.** This was to be expected, as a higher amount of compound was distributed in the solution. When the ratio of PCL was increased, by mixing the PCL stock soln. with the solutions of **3.69.** at both concentrations, better fibre formation can be observed [images b) and d). In Figure 5.24.]. In the images of mixtures with the gelator solution at a lower concentration (0.55 w/v %)] with ratio (1:5), bead formation cannot be observed [image d). Figure 5.24.].
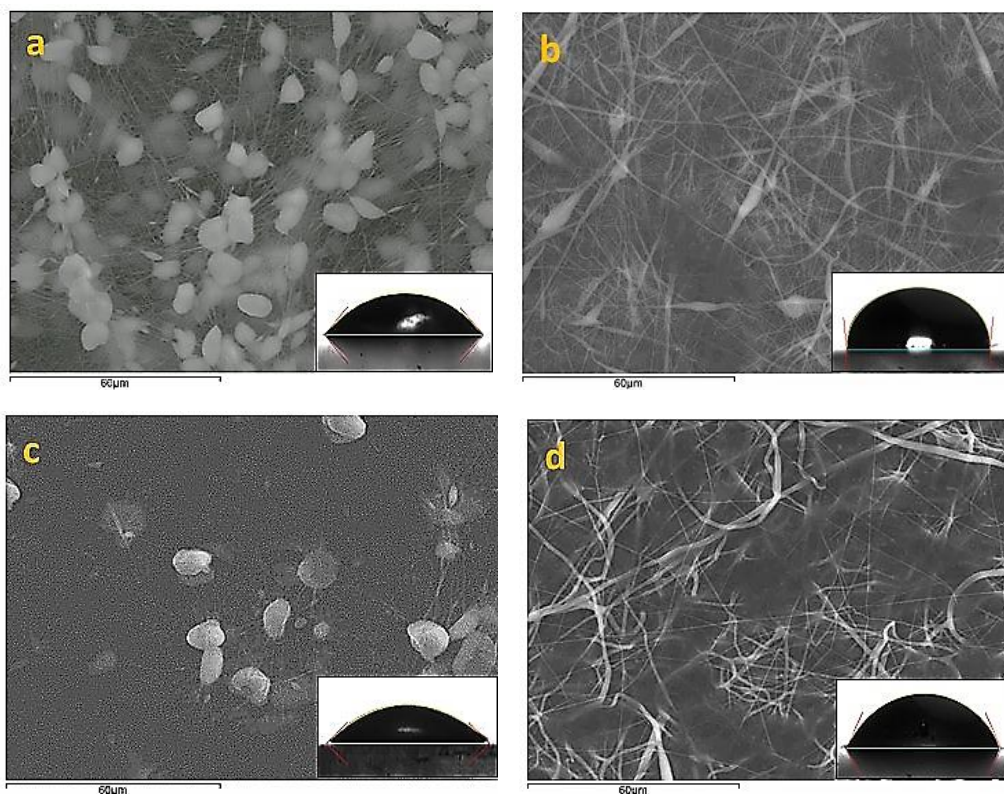
Figure 5.24. SEM images of 1 min. electrospun on a SEM stub at 1 mL/h, 18 G, 13 kV, and a distance of ~ 8 cm. a) **(1:1)** 2 mL **3.69.** (55 mg + 5 mL tol.) + 2 mL PCL stock soln.; b) **(1:5)** 1 mL **3.69.** (55 mg + 5 mL tol.) + 5 mL PCL stock soln.; c) **(1:1)** 2 mL **3.69.** (27.5 mg + 5 mL tol.) + 2 mL PCL stock soln.; d) **(1:5)** 1 mL **3.69.** (27.5 mg + 5 mL tol.) + 5 mL PCL stock soln. (CA included on images). [Scale bar: a) - d) 60 μm].

Glucosamine derivative **5.1.**[276] (Figure 5.25.) which cannot form a gel in toluene was used as a control.
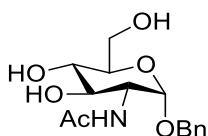
5.1.

Figure 5.25. Structure of compound **5.1.** (phenylmethyl-2-acetylamino-2-deoxy-*α-D*-glucopyranoside) used as control.

A solution of **5.1.** (22 mg in 5 mL of toluene) was prepared and it was mixed with the PCL stock solution. Mixtures at different ratios (1:1) and (1:5) were electrospun and the materials were imaged by SEM (Figure 5.26.). Electrosprayed material was observed in both cases (Figure 5.26.). The increase in PCL solution ratio did not

promote fibre formation. This result supports the previous discussions, relating to how a gelator for a solvent that interferes with the normal formation of UFs, is necessary to avoid fibre destruction.
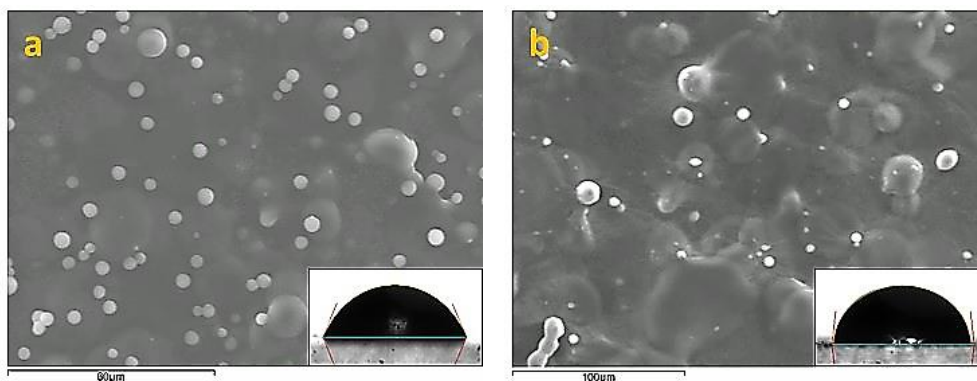
Figure 5.26. SEM images of 1 min. electrospun on a SEM stub at 1 mL/h, 18 G, 13 kV, and a distance of ∼ 8 cm. a) **Control 3.** (1:1) 2 mL **5.1.** (22.6 mg + 5 mL tol.) + 2 mL PCL stock soln.; b) **Control 4.** (1:5) 1 mL **5.1.** (22.6 mg + 5 mL tol.) + 5 mL PCL stock soln. (CA included on images). [Scale bar: a) 80 μm; b) 100 μm].

In summary, these results suggest that even at concentrations lower than CGC, supramolecular gelators can be blended with PCL and UFs can be produced by electrospinning if appropriate ratios and concentrations are used.

5.8.1. Contact Angles Measurements for PCL Fibres Blended with Galactosyl Based Gelators

As discussed in Section 5.7.6. CA measurements give information about the wettability of the surface area of electrospun materials. Small CA (< 90°) correspond to high wettability (hydrophilic character); wetting of the surface is favourable and the fluid will spread over a large area of surface A large CA (> 90°) correspond to low wettability (hydrophobic character); wetting of the surface is unfavourable and the fluid will minimise its contact.[263]

Similarly, as for the CA studies carried out for the PCL electrospun mats with lipoamino acids discussed earlier, the CA values for electrospun materials with galactosyl based gelators were measured on glass slides.

Table 5.8. shows the summary of results obtained for electrospun materials from PCL stock soln., PCL stock soln. blended with compounds **3.69.** and **4.25.** at different ratios [(1:1) or (1:5)], and few controls such as (1:1) or (1:5), of PCL stock soln. with compound **4.25.** or **5.1.** which are commented on in this section.

Table 5.8. Contact angle results with standard deviation for PCL stock soln. and PCL fibres with different gelators.

Entry	Sample and Specification	1) Angle degrees	2) Angle degrees	3) Angle degrees	Average degrees	STDEV Standard deviation
1	**PCL stock soln.**	106.9	109.5	108.61	**108.3**	±1.32
2	**Control 1.** (1:1) 2 mL **4.25.** (20 mg + 10 mL EtOH) + 2 mL PCL soln.	69.32	71.49	71.13	**70.6**	±1.16
3	**Control 2.** (1:5) 1 mL **4.25.** (20 mg + 10 mL EtOH) + 5 mL PCL soln.	62.87	60.57	60.74	**61.4**	±1.28
4	**Control 3.** (1:1) 2 mL **5.1.** (22.63 mg + 10 mL tol.) + 2 mL PCL soln.	64.94	56.34	64.58	**62.0**	±4.86
5	**Control 4.** (1:5) 1 mL **5.1.** (22.63 mg + 10 mL tol.) + 5 mL PCL soln.	97.99	84.72	87.48	**90.1**	±7.00
6	**(1:1)** 2 mL **4.25.** (20 mg + 10 mL EtOH:H_2O) + 2 mL PCL soln.	41.35	43.76	43.96	**43.0**	±1.45
7	**(1:5)** 1 mL **4.25.** (20 mg + 10 mL EtOH:H_2O) + 5 mL PCL soln.	65.26	69.66	72.01	**69.0**	±3.42
8	**(1:1)** 2 mL **3.69.** (55 mg + 5 mL tol.) + 2 mL PCL soln.	12.48	33.95	14.35	**20.3**	±11.89
9	**(1:5)** 1 mL **3.69.** (55 mg + 5 mL tol.) + 5 mL PCL soln.	99.23	98.52	98.02	**98.6**	±0.61
10	**(1:1)** 2 mL **3.69.** (27.5 mg + 5 mL tol.) + 2 mL PCL soln.	8.12	13.15	14.28	**11.9**	±3.28
11	**(1:5)** 1 mL **3.69.** (27.5 mg + 5 mL tol.) + 5 mL PCL soln.	32.89	38.48	33.57	**35.0**	±3.05

These values, in contrast with those obtained for the studies with the lipoamino acid gelators, indicate that the blending of PCL with galactosyl based gelators increases the hydrophilic character of the electrospun materials. The blends with squaramide gelators **4.25.** (Entries 6 and 7) reduced the hydrophobicity of the PCL fibres considerably, even at the higher PCL: gelator, 5:1 ratio (Entry 7).

Interestingly, the blends with the aspartic acid derivative gelator **3.69.,** at the highest ratios (Entries 8 and 10), resulted in the largest reduction of CA, possibly due to the formation of hydrophilic gelator aggregates/beads. Fibre destruction in the absence of gelator molecules could account for the low CA values observed for the four

controls (Entries 2 to 5). Regarding the blend with aspartic acid gelator **3.69.** at higher concentration and higher PCL: gelator ratio, 5:1 (Entry 9) the fibres modified with this gelator were still significantly more hydrophilic than the PCL alone ones (Entry 1). Surprisingly, the blend with aspartic acid gelator **3.69.** at lower concentration and PCL: gelator ratio 5:1, (Entry 11) had the lowest CA value of all the samples at the higher PCL concentrations (5:1 ratios).

5.8.2. ATR-FTIR of Electrospun PCL Blended with Galactosyl Based Gelators

Figure 5.27. compares the ATR-FTIR spectra of blended dry electrospun materials obtained from: a) 1 mL **3.69.** (55 mg + 5 mL toluene) + 5 mL PCL stock soln.; b) 1 mL **4.25.** (20 mg + 10 mL EtOH:H_2O) + 5 mL PCL stock soln. and c) PCL stock soln. As discussed previously, in all the spectra characteristic PCL peaks were observed. However, spectra a) and b) did not have strong absorption bands. The characteristic backbone of the ester group of the PCL at 1726 cm^{-1}, attributed to the carbonyl stretching, decreased in the blended samples. Also, the bands around 2990 and 2940 cm^{-1} displayed decreased intensity and were almost imperceptible peaks. These effects are likely due to the poorer contact of the blended samples with the ATR optics.
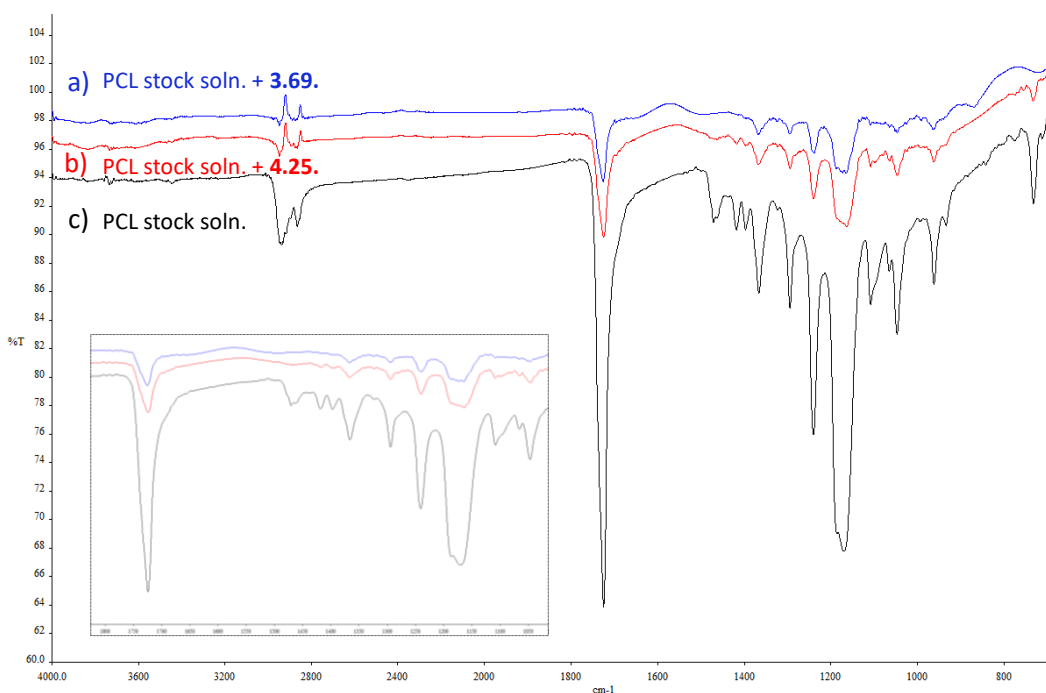
Figure 5.27. Comparison of the ATR-FTIR spectra of dry tissue scaffolds: a) 1 mL **3.69.** (55 mg + 5 mL tol.) + 5 mL PCL stock soln.; b) 1 mL **4.25.** (20 mg + 10 mL EtOH:H_2O) + 5 mL PCL stock soln.; c) PCL stock soln.(1 g PCL + 7.5 mL chloroform + 2.5 mL EtOH).

5.8.3. DSC of PCL Electrospun Fibres Blended with Galactosyl Based Gelators

Figure 5.28. shows the thermograms of electrospun PCL blended with galactosyl based gelators obtained from: a) 1 mL **3.69.** (55 mg + 5 mL tol.) + 5 mL PCL stock soln.; b) 1 mL **4.25.** (20 mg + 10 mL EtOH:H_2O) + 5 mL PCL stock soln. and c) PCL stock soln. A single endothermic peak was observed in all the thermograms, which corresponds with the T_m of the polymer at ~ 60 °C. Thermograms a) and b) were blends of PCL and a gelator in toluene or EtOH:H_2O respectively. The presence of the gelators does not significantly affect the T_m of the polymer.
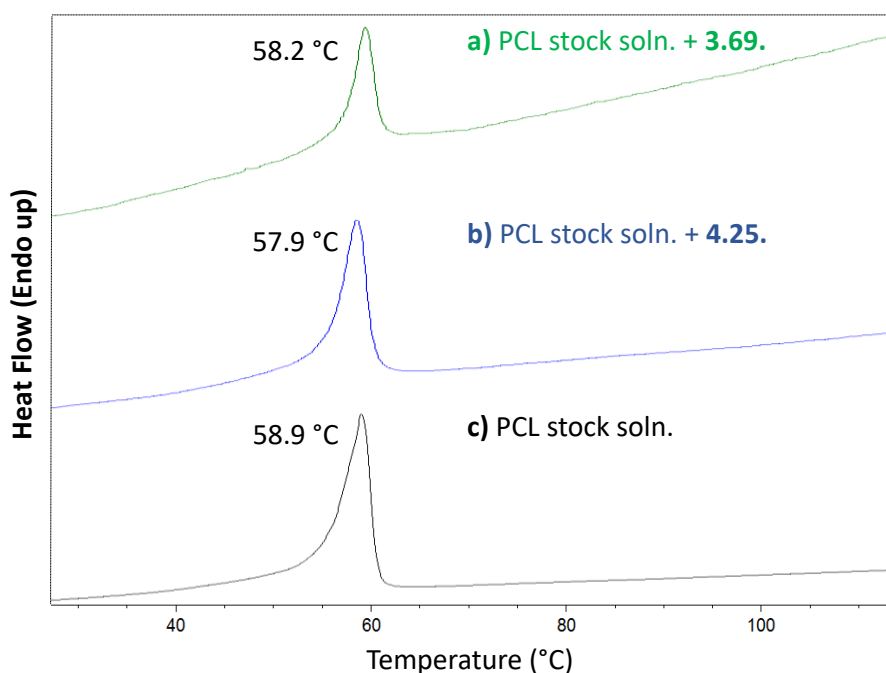
Figure 5.28. DSC thermograms of: a) 1 mL **3.69.** (55 mg + 5 mL tol.) + 5 mL PCL stock soln.; b) 1 mL **4.25.** (20 mg + 10 mL EtOH:H_2O) + 5 mL PCL stock soln.; c) PCL stock soln.

5.8.4. Application of PCL Electrospun Fibres Blended with Galactosyl Based Gelators as Tissue Scaffolds: Preliminary Studies

As discussed earlier, PCL has been widely used in tissue scaffolds to promote cell adhesion. However, normally the PCL UFs need treatment or coating to assist cell growth on them. In a preliminary study in collaboration with Prof. Daniel Kelly (Trinity College Dublin), the application of PCL electrospun fibres blended with galactosyl based gelators **4.25.** and **3.69.** was explored. It is proposed that the functionality of gelators **4.25.** and **3.69.,** both with free hydroxyl groups in the galactose moieties,

may alter the surface of the mats, providing increased hydrophilicity and an improved environment to promote cell growth.

Isolation and expansion of human bone-marrow stem cells (hMSCs) (Figure 5.29.) were carried out by Mr. Tomas Gonzalez-Fernandez and Ms. Dinorath Olvera-Ramos (in Prof. D. Kelly's group). The cells were seeded in:

a) Non-modified PCL electrospun scaffolds (Control 1).

b) Electrospun mats from 1 mL **4.25.** (20 mg + 10 mL EtOH:H_2O, 1:1) + 5 mL PCL stock soln.

c) Electrospun mats from 1 mL **3.69.** (55 mg + 5 mL tol.) + 5 mL PCL stock soln.

d) Electrospun mats from 1 mL **3.69.** (27.5 mg + 5 mL tol.) + 5 mL PCL stock soln.

The following assays were performed:

- Day 3 and 7 DNA quantification (proliferation).

- Day 3 and 7 Alamar Blue (cell metabolic activity).

- Day 3 and 7 Live/dead imaging (cell viability and morphology).
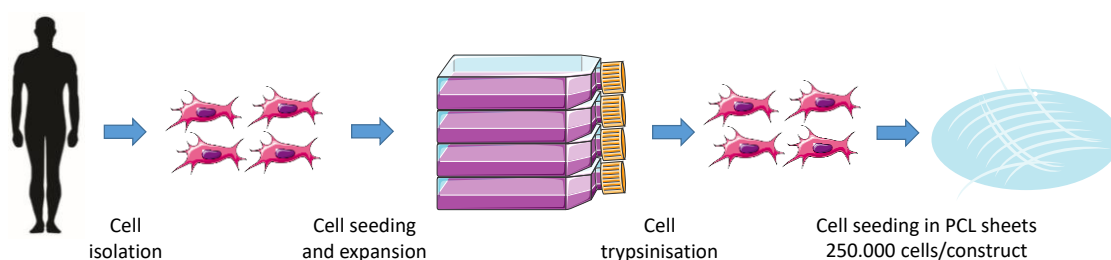
Figure 5.29. Schematic representation of a cell seeding process. (Courtesy of Mr. Tomas Gonzalez-Fernandez, Trinity College Dublin).

The cell viability of the PCL UFs with hMSCs cultured on them were observed under a fluorescent microscope. Briefly, the cells were seeded on the UFs mats and cultured for 3 and 7 days. As it is shown in Figure 5.30., for the four samples studied, significant differences were observed comparing the cell growth and viability between the control PCL stock soln. and the modified scaffolds.

Initially, the modified scaffolds with gelators **4.25.** [sample b)] and **3.69.** [sample d)] showed increased metabolic activity and proliferation than the control. At day 7, the metabolic activity is rather similar for control and sample b) and d), however, the proliferation remains superior for those samples than in the control. Interestingly, sample c) did not perform well in these tests. This could be due to the decreased concentration of gelator **3.69.**, which leads to deficient fibre formation and thus poorer characteristics as a tissue scaffold. Some differences in morphology between the control and the modified scaffolds can be appreciated, however, further studies need to be carried out to assess cell differentiation profiles. These preliminary results are very encouraging regarding the feasibility of using carbohydrate based supramolecular gelators for the development of tissue scaffolds.
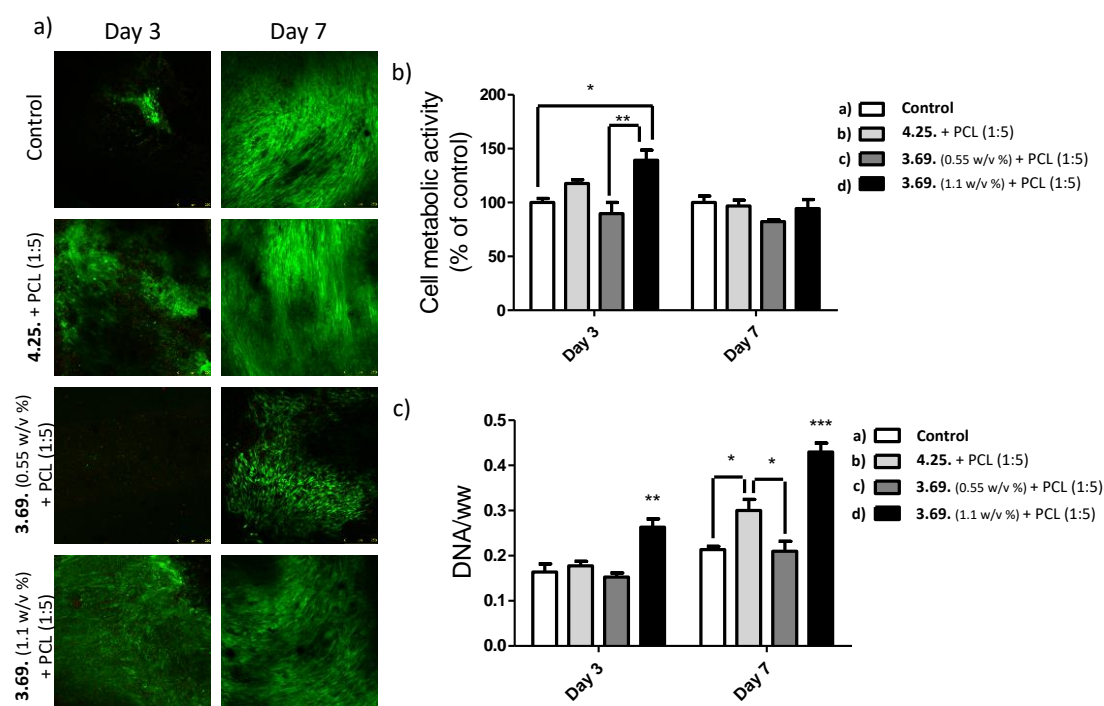
Figure 5.30. a) Cell viability at days 3 and 7 after cell seeding for the four samples studied, green fluorescence indicates viable cells (calcein), and red fluorescence indicates dead cells (ethidium homodimer-1); b) Cell metabolic activity (% of the control) at days 3 and 7 after cell seeding; c) DNA quantification normalised to the wet weight (ww) of the construct at days 3 and 7 after seeding. * denotes significance for $p < 0.05$, ** for $p < 0.01$ and *** for $p < 0.001$. Scale bar = 250 um.

5.8.5. Application of PCL Electrospun Fibres Blended with Lipoamino Acid Gelators for Drug Delivery

Building on the results described in Sections 5.7.4. and 5.7.5., the blending of drugs with PCL to form electrospun fibres for drug delivery was studied in the presence and absence of lipoamino acid gelators.

Fusidic Acid (F.A.), an antibiotic, and Betamethasone Valerate (B.V.), an anti-inflammatory (Figure 5.31.), were provided from Mibe GmbH Arzneimittel (Germany) in a collaboration project to develop new drug delivery systems based on electrospun materials that mimic topic cream formulations. This promising alternative of antibiotic administration has been in development in recent years.[202,277]

a) **5.2.**   b) **5.3.**
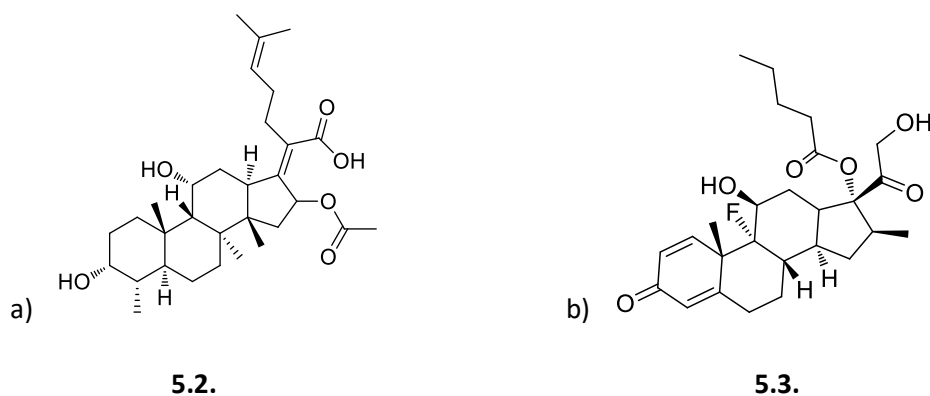
Figure 5.31. Structure of compounds: a) **5.2.** (F.A.) and b) **5.3.** (B.V.) used as controls.

Blends of PCL, drugs and lipoamino acid gelator **2.41.** at the specified concentrations were electrospun directly onto a cellulose membrane (Porafil® RC 0.45 μm) and imaged using SEM (Figure 5.32.). In the absence of lipoamino acid gelator **2.41.,** beading with very poor fibre formation can be clearly appreciated (images a and b). Remarkably, in the presence of a very small amount of gelator **2.41.** (0.15%), beading is suppressed and regular fibre formation with regular morphology is observed (image d).
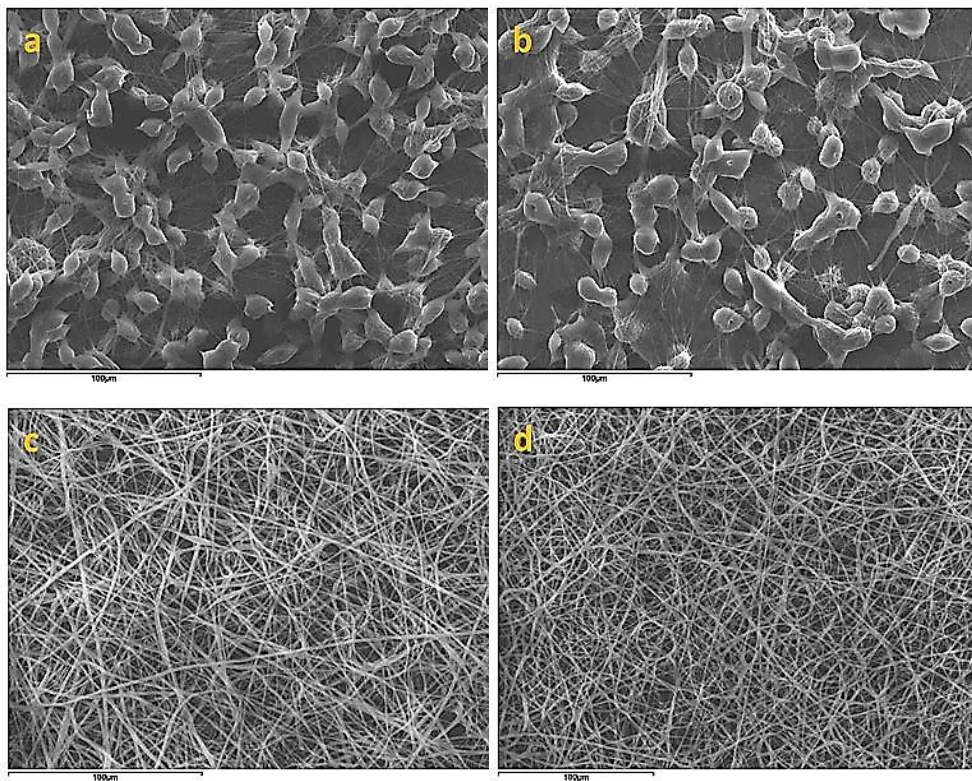
Figure 5.32. SEM images of 1 min. electrospun on a SEM stub at 1 mL/h, 18 G, 13 kV, and a distance of ∼ 8 cm. a) 10 % FA. 0.60 % BV. 89.4 % PCL stock soln.; b) 20 % FA. 1.21 % BV. 78.79 % PCL stock soln.; c) **Control.** 0.15 % **2.41.** 99.85 % PCL stock soln.; d) 20 % FA. 1.21 % BV. 0.15 % **2.41.** 78.64 % PCL stock soln. [Scale bar: a) - d) 100 μm].

Diffusion studies were carried out in Mibe GmbH Arzneimittel (Germany) using a Hanson diffusion cell system, which replicated the process of diffusion of skin – applied medicine as it penetrates the skin for local or systemic action. The results from the diffusion experiments were analysed by HPLC and showed that the presence of lipoamino acid gelator **2.41.** did not significantly modify the release profile of B.V. while slightly reducing the initial amount of F.A. released (Figure 5.33.). These results indicate that the presence of the lipoamino acid gelator improved fibre morphology without affecting the release profile of the material.
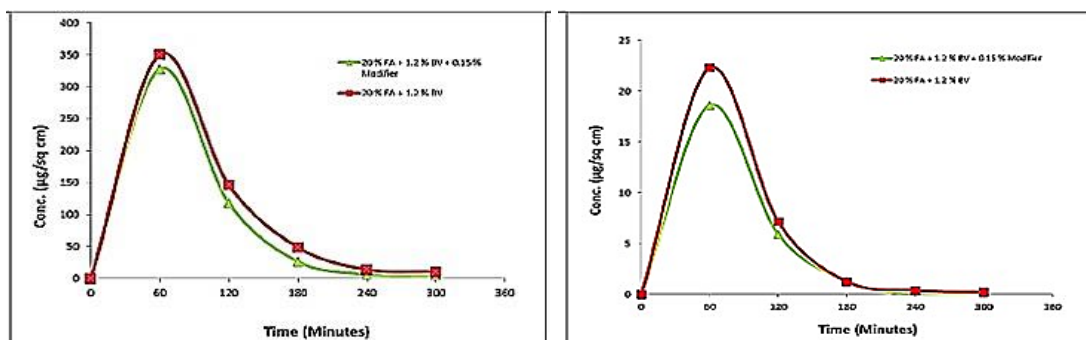
Figure 5.33. Release profile of B.V. (left) and F.A.(right) from mats produced from the electrospinning of 20 % F.A. 1.21 % B.V. 78.79 % PCL stock soln. (red) and 20 % F.A. 1.21 % B.V. 0.15 % **2.41.** 78.64 % PCL stock soln. (green).

Figure 5.34. compares the ATR-FTIR spectra of blend dry electrospun materials of: a) PCL stock soln.; b) **F.A.** (200 mg + 1 mL EtOH) + 5 mL PCL stock soln. and c) **B.V.** (200 mg + 1 mL EtOH) + 5 mL PCL stock soln. As in previous spectra, characteristic PCL peaks were observed. The three samples have a strong absorption bands with differences in absorption possibly due to different contact with the ATR optics. Characteristic bands from the drugs cannot be distinctly appreciated.
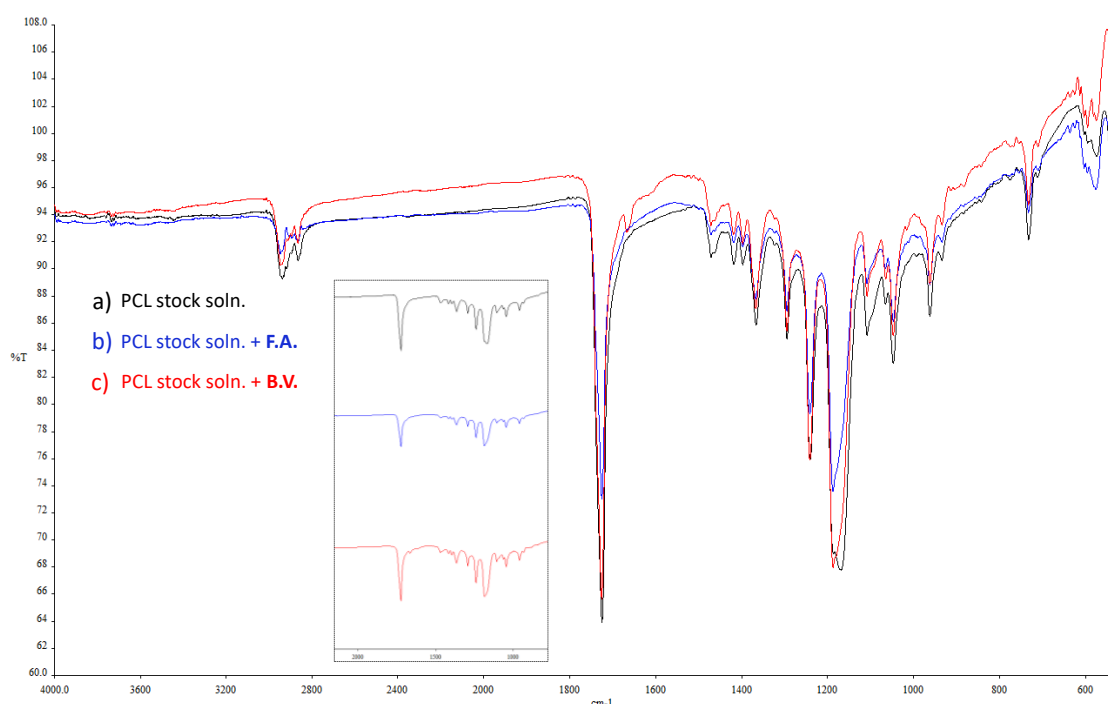
Figure 5.34. Comparison of the ATR-FTIR spectra of dry tissue scaffolds: a) PCL stock soln.; b) **F.A.** (200 mg + 1 mL EtOH) + 5 mL PCL stock soln.; c) **B.V.** (200 mg + 1 mL EtOH) + 5 mL PCL stock soln.

5.9. Conclusion

I.) PCL blended UFs were successfully fabricated via an electrospinning technique.

II.) Parameters such as voltage, needle gauge, solvents and different compounds were optimised for fibre formation and uniformity in the morphology of the fibres.

III.) Blending PCL with supramolecular gelators can also affect the fibre formation and morphology of the fibres. This represents a new approach to modifying the surface of UFs mats which can be designed to modulate the hydrophilicity of PCL electrospun fibres.

IV.) SEM, contact angle measurements, ATR-FTIR and DSC analysis were used to characterise/study the PCL electrospun UFs.

V.) PCL fibres modified with lipoamino acid gelator **2.41.** were investigated as electrospun drug delivery systems for drugs F.A. and B.V. The *in-vitro*-release-profile of the drug substances from the electrospun materials was carried out in collaboration with Mibe GmbH Arzneimittel Company (Germany). The presence of gelator **2.41.** in the blend promotes homogenous fibre formation without significantly affecting the drug release profile.

VI.) Preliminary studies regarding the feasibility of using PCL electrospun fibres blended with galactosyl based gelators **3.69.** and **4.25.** as tissue scaffolds was carried out in collaboration with Prof. D. Kelly (Trinity College Dublin). The results suggest that these materials, which have increased hydrophilic character, may be suitable for this application.

Chapter 6

Conclusions

This thesis focused around the synthesis of different types of scaffolds to form supramolecular self-assembled gels. Chapter 2 was focused on lipoamino acid based gelators. Compounds **2.38.** – **2.42.** were derivatives of *N*-Fmoc-L-serine synthesised and evaluated as LMWGs in a range of organic solvents of different polarity. The gels formed were characterised by determination of their rheological and thermal properties. It was found that subtle structural changes such as replacement of the side chain functional groups of the serine lipoamino acids (from *O-tert*-butyl to hydroxyl) impacted the gelation abilities of these LMWGs. These changes altered their solubility and self-assembly properties. For the shortest chain (C_{14}) derivatives, the structural difference achieved the selective gelation of aliphatic or aromatic solvents. The elongation of the alkyl chain length (C_{18}) improved the physical properties of the gels, however, it reduced the ability to differentiate between aliphatic and aromatic solvent gelation. Distinct self-assembly patterns for *O-tert*-butyl and hydroxyl compound **2.38.** – **2.42.** were proposed according to the morphologies observed in the SEM images of the xerogels. In addition, the lipoamino acids **2.38.** and **2.40.** were also found to be highly effective organogelators of biphasic mixtures and enhanced the removal of organic solvents and toxic dyes such as RhB and MO, from aqueous solutions. Compound **2.40.**, with Fmoc group and compound **2.42.**, the analogue with Cbz group were compared and it was noticed that the presence of Fmoc group in the gelator was necessary for the gel formation.

Chapter 3 was focused on aspartic acid based galactosyl gelators. Core building blocks compounds **3.61.** (D,L) and **3.65.** (L) were synthesised using amide coupling methodologies and their synthesies were optimised as described. In addition, galactosyl compounds **3.66.** – **3.69.** (*O*-glycolipids) and **3.70.** - **3.72.** (*N*-glycolipids) were also synthesised and characterised as LMWGs in a range of solvents with different polarities. It was found that **3.65.** (L) formed gels in a larger range of solvents than the racemic **3.61.** (D,L). The introduction of the galactosyl moiety resulted in a more selective gelation profile for *O*-glycolipid **3.66.** - **3.69.** It was found that the chirality of the α-C strongly influenced the assembly mode of these derivatives and therefore, their gelation properties. It was also observed that the deprotected *O*-glycolipid **3.67.** and **3.69.** formed strong gels in organic non-protic solvents, while the

corresponding acetylated derivatives were able to form gels in a mixture of EtOH:H_2O (1:1). The aspartic acid based *N*-glycolipids **3.71.** and **3.72.** exhibited a weaker ability to form gels than the other derivatives studied. The gels formed [**3.61.** (D,L), **3.65.** (L), **3.67.** (D,L), **3.68.** (L) and **3.69.** (L)] were characterised by study of their rheological and thermal properties. Rheological analysis proved they were gels with different strength and rheological parameters. DSC analysis showed that the gels were thermoreversible. The morphological studies of the xerogels using SEM revealed very different xerogel structures depending on the solvent and gelator. Better defined fibrous structures were observed in the strong gels, while the weak gels revealed compact aggregates and/or multi-lamellar structures. Spectroscopic analysis using NMR and FTIR were carried out to better understand the intermolecular interactions involved in the gelation process. These studies indicated that H-bond formation was involved in the gelation process of the organic non-protic solvents studied. In addition, crystal structures of shorter alkyl chain aspartic acid benzyl ester derivatives of both the pure enantiomer **3.52.** (L) and the racemate **3.56.** (D,L). were obtained. Clear differences in the packing of both structures could be observed.

Chapter 4 was focused on squaramide based gelators. In this case, a novel type of squaramide based LMWGs featuring aminoethyl galactoside derivatives were readily synthesised. These squaramide-carbohydrate conjugates could be obtained in good yield. The gelation ability of the acetyl protected compound **4.24.** and the free-hydroxyl compound **4.25.** were tested in a range of solvents with different polarities. The study of the rheological properties showed that these gels were very strong and had a thixotropic behaviour. DSC analysis showed that the gels were thermoreversible. The morphological studies using SEM revealed very different xerogel structures depending on the solvent. Spectroscopic analysis using NMR and FTIR, indicated that H-bond formation was involved in the gelation process. Unusually, the gel **4.25.** formed in a mixture of EtOH:H_2O (1:1) had a distinct morphology and excellent rheological properties. This opens new possibilities for the use of squaramide-carbohydrate conjugates in materials and biomedical science, other than their classical application in catalysis.

Chapter 5 focused on the modification of electrospun fibres using the LMWGs described in Chapters 2, 3 and 4 for biomedical applications as tissue scaffolds and drug delivery systems. Firstly, PCL blended UFs were successfully fabricated via an electrospinning technique. Parameters such as voltage, needle gauge, solvents and different compounds were optimised for fibre formation and uniformity in the morphology of the fibres. Some solvents, such as toluene, were found to be incompatible with the electrospinning of PCL. However, blending of PCL with the lipoamino acid *N*-Fmoc-L-serine gelators discussed in Chapter 2 which were able to form gels in toluene prevented the destruction of PCL fibers caused by this solvent. This finding expands the scope of solvents that can be used in the electrospinning of PCL fibers and represents a new approach to modifying the surface of UFs mats , which can be designed to modulate their hydrophilicity. SEM, contact angle measurements, ATR-FTIR and DSC analysis were used to characterise/study the PCL electrospun UFs. Subsequently, different blends with galactosyl gelators **3.69.** and **4.25.** both with free hydroxyl groups were investigated. Preliminary studies regarding the feasibility of this approach to develop tissue scaffolds for tissue engineering was carried out in collaboration with Prof. D. Kelly (Trinity College Dublin). The results suggest that these materials, which have increased hydrophilic character, may be suitable for this application. Furthermore, PCL fibres modified with lipoamino acid gelator **2.41.** were investigated as electrospun drug delivery systems for drugs F.A. and B.V in collaboration with Mibe GmbH Arzneimittel Company (Germany). The presence of gelator **2.41.** in the blend promotes homogenous fibre formation without significantly affecting the drug release profile.

Overall, the results discussed in this thesis have lead to the synthesis of novel supramolecular gelators that have been characterised using rheological, thermal and spectroscopic techniques. Preliminary studies to explore different applications of these compounds in materials and biomedical fields have been carried out. The promising results of these studies are encouraging us to further investigate the supramolecular gelators produced in this work.

Chapter 7

Experimental

7.1. General Procedures and Instrumentation

All chemicals purchased were reagent grade and used without further purification, unless stated otherwise. DCM was distilled over CaH_2, THF over Na wire and benzophenone. Anhydrous DMF was purchased from Sigma Aldrich. Molecular sieves (MS) used for glycosylation reactions were 3 Å, 8 - 12 mesh. They were dried in the oven at 100 °C at ambient pressure prior to use. Reactions were monitored using thin layer chromatography (TLC) on Merck Silica Gel F_{254} plates. Detection was effected either by visualisation in UV light and/or charring in a mixture of 5 % sulphuric acid-EtOH or phosphomomolybdic acid-EtOH (12 g in 250 mL). Evaporation under reduced pressure was always effected with the bath temperature kept below 50 °C.

NMR spectra were obtained on a Bruker Ascend 300 and 500 MHz spectrometer operated at 300 or 500 MHz. Residual solvent peak was used as the internal standard. Chemical shits (δ) were reported in ppm. Proton and carbon signals were assigned with the aid of 2-D NMR experiments (COSY, HSQC, HMBC) and DEPT experiments. Flash column chromatography was performed with Merck Silica Gel 60, using adjusted mixtures of Pet Ether/EtOAc, unless otherwise stated.[278] Optical rotations were obtained using an AA-100 polarimeter. $[\alpha]^{25}_D$ values are given in $10^{-1} cm^2 g^{-1}$. The melting points were obtained using a Stuart Scientific SMP1 melting point apparatus and are uncorrected. High resolution mass spectra (HR-MS) were performed on an Agilent-L 1200 Series coupled to a 6210 Agilent Time-of-Flight (TOF) mass spectrometer equipped with both a positive and negative electrospray source both positive and negative (ESI+/-). FT-IR spectra were obtained in the region 4000-400 cm^{-1} on a PerkinElmer precisely (Spectrum 100). SEM was performed using a Hitachi S-3200-N system (Tokyo, Japan) with a tungsten filament. The electrons were accelerated to an energy which was between 5 - 20 keV. If it was necessary, the sample was coated in gold using an Emitech K550x Gold Sputter Coater. Microscope images were taken by an optical microscope on a Leica DMEP DFC-280 and an Olympus BX51M system using Leica application suite and Olympus DP Version 3.2, software, respectively. Gels used for characterisation measurements were prepared in glass vials, specimen tube soda glass 75 x 25 mm, (30 mL). Rheological measurements were performed on a strain-controlled Anton Paar Physica MCR301

rheometer using PP15/Al and a P-PTD 200/TG+H-PTD200 in University of Santiago de Compostela, Spain. DSC analysis was carried out on a PerkinElmer Pyris 6 Differential Scanning Calorimeter. The stainless steel crucibles for DSC were pans: Φ6.7x2.6mm & lids: Φ7x2mm (temperature range: -50~280 °C). UV-Vis spectra were recorded in a PerkinElmer precisely Lambda 35 UV-Vis spectrometer. Contact angle and wetting properties were studied in a contact angle telescope-goniometer FTA1000 drop Shape Analyser. The electrospinning apparatus was equipped with a high-voltage power supply (PLS K007-20. Spraybase. Ireland), using an IVAC P3000 syringe pump.

7.2. Experimental Procedures

7.2.1. Synthetic Experimental Procedures for Chapter 2

N-(9-fluorenylmethyloxycarbonyl)-O-tert-butyl-L-serine tetradecylamide 2.38.
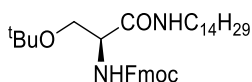
2.38.

DIC (0.3 mL, 1.87 mmol, 1.2 equiv) was added to a solution of Fmoc-*O-tert*-butyl-L-serine (600 mg, 1.56 mmol) in anhydrous DCM (30 mL) under N_2 at rt. The reaction mixture was left to stir for 15 min. Tetradecylamine (400 mg, 1.87 mmol, 1.2 equiv) was then added under N_2 to the reaction mixture and was left to stir for 18 h. The reaction mixture was then washed with 0.5 M HCl (30 mL), saturated aqueous $NaHCO_3$ (20 mL) and brine (20 mL). The organic layer was dried over Na_2SO_4, filtered and the solvent was evaporated under reduced pressure. The crude was purified by column chromatography (Pet Ether:EtOAc, 2:1 to 1:1) to give the product as a white solid (0.85 g, 95%); R_f = 0.94 (Pet Ether:EtOAc, 1:1); $[\alpha]_D$ = + 9 (c 1.0 in $CHCl_3$); ^{1}H NMR (500 MHz, $CDCl_3$): δ 7.76 (d, J = 7.6 Hz, 2 H, H-Ar), 7.60 (d, J = 7.3 Hz, 2 H, H-Ar), 7.39 (at, J = 7.4 Hz, 2 H, H-Ar), 7.31 (at, J = 7.5 Hz, 2 H, H-Ar), 6.59 (bs, 1 H, NHCH$_2$), 5.79 (bs, 1 H, NH-Fmoc), 4.40 (d, J = 6.9 Hz, 2 H, Fmoc-OCH$_2$CH), 4.22 (t, J = 7.1 Hz, 1 H, Fmoc-OCH$_2$CH), 4.16-4.17 (m, 1 H, H-α), 3.81 (dd, J = 3.8 Hz, J = 7.9 Hz, 1 H, H-β), 3.36 (dd, J = 3.8 Hz, J = 7.6 Hz, 1 H, H-β'), 3.27-3.24 (m, 2 H, NHCH_2), 1.50-1.48 (m, 2 H, NHCH$_2$CH_2), 1.29-1.22 (bs, 22 H, NHCH$_2$CH$_2$(CH_2)$_{11}$CH$_3$), 1.20 (s, 9 H, ^{t}Bu), 0.88 (t, J = 6.8 Hz, 3 H, CH$_3$); ^{13}C NMR (125 MHz, $CDCl_3$): δ 169.0 (*C*ONH), 155.1 (*C*O-Fmoc), 142.8,

142.7, 140.3, 140.2 (each C-Ar), 127.7, 126.7, 126.0, 124.1, 124.0, 119.9, 118.9, 118.7 (each CH-Ar), 73.1 ((CH_3)$_3C$), 66.0 (CH_2-β), 60.8 (CH_2-Fmoc), 53.4 (CH-α), 46.2 (CH-Fmoc), 38.5, 30.9 (CH_2), 29.8 ($C(CH_3)_3$), 28.7, 28.64, 28.63, 28.58, 28.53, 28.5, 28.3, 28.2, 26.4, 25.8, 21.7 (each CH_2), 13.1 (CH_3); IR v_{max} (NaCl plate, DCM): 3313.85 (NH), 1691.90 (Fmoc-CO), 1659.78 (NH-CO), cm^{-1}; HRMS m/z (ESI+) calc. for $C_{36}H_{54}N_2O_4$: 578.4083; found 579.4148 [M+H$^+$], 601.3966 [M+Na$^+$].

N-(9-fluorenylmethyloxycarbonyl)-*O*-*tert*-butyl-L-serine octadecylamide 2.39.
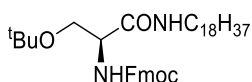
2.39.

DIC (0.3 mL, 1.87 mmol, 1.2 equiv) was added to a solution of Fmoc-*O*-*tert*-butyl-L-serine (600 mg, 1.56 mmol) in anhydrous DCM (30 mL) under N_2 at rt. The reaction mixture was left to stir for 15 min. Octadecylamine (500 mg, 1.87mmol, 1.2 equiv) was then added under N_2 to the reaction mixture and was left to stir for 18 h. The reaction mixture was then washed with 0.5 M HCl (30 mL), saturated aqueous NaHCO$_3$ (20 mL) and brine (20 mL). The organic layer was dried over Na$_2$SO$_4$, filtered and the solvent was evaporated under reduced pressure. The crude was purified by column chromatography (Pet Ether:EtOAc, 2:1 to 1:1) to give the product as a white solid (0.87 g, 88%); R_f = 0.91 (Pet Ether:EtOAc, 1:1); [α]$_D$ = + 9 (c 1.0 CHCl$_3$); ^{1}H NMR (500 MHz, CDCl$_3$): δ 7.76 (d, J = 7.6 Hz, 2 H, H-Ar), 7.60 (d, J = 7.3 Hz, 2 H, H-Ar), 7.40 (at, J = 7.4 Hz, 2 H, H-Ar), 7.31 (at, J = 7.5 Hz, 2 H, H-Ar), 6.58 (s, 1 H, NHCH$_2$), 5.77 (s, 1 H, NH-Fmoc), 4.40 (d, J = 6.9 Hz, 2 H, Fmoc-OCH$_2$CH), 4.22 (t, J = 7.1 Hz, 1 H, Fmoc-OCH$_2$CH), 4.16 (bs,1 H, H-α), 3.81 (dd, J = 3.8 Hz, J = 7.9 Hz, 1H, H-β), 3.35 (dd, J = 3.8 Hz, J = 7.6 Hz, 1 H, H-β'), 3.26-3.24 (m, 2 H, NHCH$_2$), 1.50-1.48 (m, 2 H, NHCH$_2$CH$_2$), 1.28-1.25 (bs, 30 H, NHCH$_2$CH$_2$(CH$_2$)$_{15}$CH$_3$), 1.20 (s, 9 H, t-Bu), 0.88 (t, J = 6.8 Hz, 3 H, CH$_3$); ^{13}C NMR (125 MHz, CDCl$_3$): δ 170.1 (CONH), 156.1 (CO-Fmoc), 143.9, 143.8, 141.3 (each C-Ar), 127.7, 127.1, 125.13, 125.10, 120.0 (each CH-Ar), 74.2 ((CH_3)$_3C$), 67.0 (CH_2-β), 61.9 (CH_2-Fmoc), 54.4 (CH-α), 47.2 (CH-Fmoc), 39.6, 31.9 (CH_2), 29.7 (C(CH_3)$_3$), 29.68, 29.67, 29.66, 29.62, 29.57, 29.5, 29.4, 29.3, 27.5, 26.9, 22.7 (each CH_2), 14.1 (CH_3); IR v_{max} (NaCl plate, DCM): 3311.35 (NH), 1691.41 (Fmoc-CO), 1659.67

(NH-CO) cm^{-1}; HRMS m/z (ESI+) calc. for $C_{40}H_{62}N_2O_4$: 634.4709; found 635.4786 [M+H$^+$], 657.4602 [M+Na$^+$].

N-(9-fluorenylmethyloxycarbonyl)-L-serine tetradecylamide 2.40.[279]

HO—CONHC$_{14}$H$_{29}$ / NHFmoc
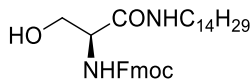
2.40.

TFA (0.9 mL, 11.32 mmol, 15 equiv) was added to a solution of Fmoc-*O-tert*-butyl-L-serine amide **2.38.** (437 mg, 0.76 mmol) in DCM (20 mL) under N_2 at rt. The reaction mixture was stirred for 15 h, diluted with brine (30 mL) and extracted with EtOAc (3 x 30 mL). The combined organic layers were dried over Na_2SO_4, filtered and the solvent was evaporated under reduced pressure. The crude was purified by column chromatography (Pet Ether:EtOAc, 3:1 to 1:1) to give the product as a white solid (641 mg, 85%); R_f = 0.39 (Pet Ether:EtOAc, 1:1); $[\alpha]_D$ = - 6 (c 1.0 CHCl$_3$)); ^{1}H NMR (500 MHz, CDCl$_3$): δ 7.77 (d, *J* = 7.6 Hz, 2 H, H-Ar), 7.58 (d, *J* = 7.5 Hz, 2 H, H-Ar), 7.41 (at, *J* = 7.4 Hz, 2 H, H-Ar), 7.32 (at, *J* = 7.5 Hz, 2 H, H-Ar), 6.49 (s, 1 H, NHCH$_2$), 5.82 (s, 1 H, NH-Fmoc), 4.44 (d, *J* = 6.9 Hz, 2 H, Fmoc-OCH$_2$CH), 4.22 (t, *J* = 6.9 Hz, 1 H, Fmoc-OCH$_2$CH), 4.15 (bs, 1 H, H-α), 3.66 (dd, *J* = 6.3 Hz, *J* = 7 Hz, 1 H, H-β), 3.24 (dd, *J* = 6.3 Hz, *J* = 7.2 Hz, 1 H, H-β'), 3.05-3.03 (m, 2 H, NHCH$_2$), 1.50-1.48 (m, 2 H, NHCH$_2$CH$_2$), 1.25-1.23 (bs, 22 H, NHCH$_2$CH$_2$(CH$_2$)$_{11}$CH$_3$), 0.88 (t, *J* = 6.8 Hz, 3 H, CH$_3$); ^{13}C NMR (125 MHz, CDCl$_3$): δ 175.5 (*C*ONH), 158.4 (*C*O-Fmoc), 143.65, 143.61, 141.3, 136.8 (each *C*-Ar), 127.8, 127.1, 124.9, 120.1 (each *C*H-Ar), 67.3 (*C*H$_2$-β), 62.9 (*C*H$_2$-Fmoc), 54.9 (*C*H-α), 47.1 (*C*H-Fmoc), 39.6, 31.9, 30.9, 29.69, 29.67, 29.65, 29.59, 29.54, 29.4, 29.3, 29.2, 26.8, 22.7 (each *C*H$_2$), 14.1 (*C*H$_3$); IR v_{max} (NaCl plate, DCM): 3300.25 (NH), 1687.57 (Fmoc-CO), 1650.66 (NH-CO) cm^{-1}; HRMS m/z (ESI+) calc. for $C_{32}H_{46}N_2O_4$: 522.3457; found 523.3553 [M+H$^+$], 545.3374 [M+Na$^+$].

This compound has been reported in literature.[279] However, no spectroscopic assignment has been provided.

_N_-(9-fluorenylmethyloxycarbonyl)-L-serine octadecylamide 2.41.
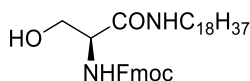
2.41.

TFA (0.7 mL, 8.95 mmol, 15 equiv) was added to a solution of Fmoc-_O-tert_-butyl-L-serine amide **2.39.** (380 mg, 0.59 mmol) in DCM (20 mL) under N_2 at rt. The reaction mixture was stirred for 15 h, diluted with brine (30 mL) and extracted with ethyl acetate (3 x 30 mL). The combined organic layers were dried over Na_2SO_4, filtered and the solvent was evaporated under reduced pressure. The crude was purified by column chromatography (Pet Ether:EtOAc, 3:1 to 1:1) to give the product as a white solid (176 mg, 51%); R_f = 0.42 (Pet Ether:EtOAc, 1:1); $[\alpha]_D$ = - 4 (c 1.03 CHCl$_3$); ^{1}H NMR (500 MHz, CDCl$_3$): δ 7.77 (d, _J_ = 7.6 Hz, 2 H, H-Ar), 7.58 (d, _J_ = 7.5 Hz, 2 H, H-Ar), 7.41 (at, _J_ = 7.5 Hz, 2 H, H-Ar), 7.32 (at, _J_ = 7.3 Hz, 2 H, H-Ar), 6.47 (s, 1 H, NHCH$_2$), 5.80 (s, 1 H, NH-Fmoc), 4.44 (d, _J_ = 6.9 Hz, 2 H, Fmoc-OCH$_2$CH), 4.22 (t, _J_ = 6.9 Hz, 1 H, Fmoc-OCH$_2$CH), 4.15 (bs, 1 H, H-α), 3.66 (dd, _J_ = 6.3 Hz, _J_ = 7.1 Hz, 1 H, H-β), 3.25 (dd, _J_ = 6.2 Hz, _J_ = 7 Hz, 1 H, H-β'), 2.99-2.97 (m, 2 H, NHCH$_2$), 1.50-1.48 (m, 2 H,NHCH$_2$CH$_2$), 1.25-1.23 (bs, 30 H, NHCH$_2$CH$_2$(CH$_2$)$_{15}$CH$_3$), 0.88 (t, _J_ = 6.8 Hz, 3 H, CH$_3$); ^{13}C NMR (125 MHz, CDCl$_3$): δ 170.8 (_C_ONH), 161.1 (_C_O-Fmoc), 143.66, 143.62, 141.3, 134.7 (each _C_-Ar), 127.8, 127.1, 125.0, 120.1 (each _C_H-Ar), 67.3 (_C_H$_2$-β), 62.9 (_C_H$_2$-Fmoc), 55.1 (_C_H-α), 47.1 (_C_H-Fmoc), 41.1, 39.6, 38.2, 36.2, 31.9, 30.4, 29.7, 29.6, 29.58, 29.55, 29.49, 29.4, 29.3, 29.27, 29.25, 29.15, 26.9, 26.8, 22.7 (each _C_H$_2$), 14.1 (_C_H$_3$); IR v$_{max}$ (NaCl plate, DCM): 3286.25 (NH), 1686.13 (Fmoc-CO), 1644.25 (NH-CO) cm^{-1}; HRMS m/z (ESI+) calc. for C$_{36}$H$_{54}$N$_2$O$_4$: 578.4083; found 601.3989 [M+Na$^+$], 617.3723 [M+K$^+$].

_N_-(benzyloxycarbonyl)-L-serine tetradecylamide 2.42.[101]
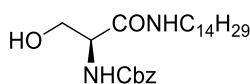
2.42.

DIC (0.2 mL, 1.42 mmol, 1.2 equiv) was added to a solution of _N_-Benzyloxycarbonyl-L-serine (300 mg, 1.18 mmol) in DMF (15 mL) under N_2 at rt. It was left to stir for 15 min. Tetradecylamine (303 mg, 1.43 mmol, 1.2 equiv) was then added under N_2 to the reaction mixture and was left to stir for 18 h. The solvent was removed under

reduced pressure and the residue was then washed with 0.5 M HCl (30 mL), saturated aqueous NaHCO$_3$ (20 mL) and brine (20 mL). The organic layer was dried over Na$_2$SO$_4$ anhydrous, filtered and the solvent was evaporated under reduced pressure. The crude was purified by column chromatography (Pet Ether:EtOAc, 2:1 to 1:1) to give the product as a white solid (0.42 g, 82%); R$_f$ = 0.75 (Pet Ether:EtOAc, 1:1); [α]$_D$ = - 10 (c 1.0 DCM); ^{1}H NMR (500 MHz, CDCl$_3$): δ 7.36-7.33 (m, 5 H, H-Ar), 6.56 (s, 1 H, NHCH$_2$), 5.81 (d, J = 8.0 Hz, 1 H, NH-Cbz), 5.15-5.09 (dd, J = 12 Hz, J = 16.5 Hz, 2 H, PhCH$_2$), 4.38-4.34 (m, 1 H, H-α), 4.04 (dd, J = 1.5 Hz, J = 6.3 Hz, 1 H, H-β), 3.52 (dd, J = 1.5 Hz, J = 4.8 Hz, 1 H, H-β'), 3.24-3.19 (m, 2 H, NHCH$_2$), 1.47-1.46 (m, 2 H, NHCH$_2$CH$_2$), 1.25 (bs, 22 H, NHCH$_2$CH$_2$(CH$_2$)$_{11}$CH$_3$), 0.88 (t, J = 7.0 Hz, 3 H, CH$_3$); ^{13}C NMR (125 MHz, CDCl$_3$): δ 171.1 (CONH), 157.1 (CO-Cbz), 136.0 (C-Ar), 128.6, 128.3, 128.1 (each CH-Ar), 67.3 (CH$_2$-Cbz), 66.6 (CH-α), 58.2 (CH$_2$-β), 42.3 (CH-Cbz), 39.6, 31.9, 29.71, 29.69, 29.67, 29.61, 29.5, 29.4, 29.3, 26.9, 23.5, 22.7, 18.2 (each CH$_2$), 14.1 (CH$_3$); IR v$_{max}$ (NaCl plate, DCM): 3296.62 (NH), 1693.74 (Cbz-CO), 1650.66 (NH-CO) cm^{-1}; HRMS m/z (ESI+) calc. for C$_{25}$H$_{42}$N$_2$O$_4$: 434.3145; found 435.3198 [M+H$^+$].

This compound has been reported in literature.[101] However, no spectroscopic assignment has been provided.

7.2.2. Synthetic Experimental Procedures for Chapter 3

2-Chloroethyl 2,3,4,6-tetra-*O*-acetyl-*β-D*-galactopyranoside 3.45.[134]
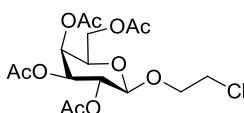
3.45.

A solution of β-D-galactose pentaacetate (4.4 g, 11.27 mmol), 2-chloroethanol (1 mL, 14.92 mmol, 1.3 equiv) in anhydrous DCM (50 mL) with 3 Å molecular sieves (6 g) was stirred under N$_2$ in an ice bath for 15 min. A freshly prepared solution of BF$_3$-Et$_2$O (2.6 mL, 21.06 mmol, 1.9 equiv) in anhydrous DCM (3 mL) was added dropwise over a period of 30 min via cannula. When the addition was completed, the mixture was allowed to reach rt and stirred overnight. The molecular sieves were filtered off with fluted filter paper, the solids were washed with DCM (15 mL) and the filtrate was washed in a separating funnel with a saturated NaHCO$_3$ solution (2 x 20 mL). The

combined aqueous phases were extracted with DCM (20 mL), the combined organic phases were washed with brine (30 mL) and distilled water (30 mL), dried with Na_2SO_4 anhydrous, filtered and concentrated under vacuum. The crude product was obtained as a white solid, which was crystallized from EtOH giving white crystals as pure product. (2.11 g, 45%); R_f = 0.50 (Pet Ether:EtOAc, 1:1); mp: 115-117 °C; $[\alpha]_D$ = - 2.3 (c 1.0 $CHCl_3$); ^{1}H NMR (500 MHz, $CDCl_3$): δ 5.36 (dd, J = 1.0 Hz, J = 3.4 Hz, 1 H, *H*-4), 5.20 (dd, J = 8.1 Hz, J = 10.5 Hz, 1 H, *H*-2), 4.99 (dd, J = 3.4 Hz, J = 10.5 Hz, 1 H, *H*-3), 4.53 (d, J = 8.1 Hz, 1 H, *H*-1), 4.18-4.08 (m, 3 H, *H*-6, *H*-6' and OC*H*), 3.96 (td, J = 1 Hz, J = 6.6 Hz, 1 H, *H*-5), 3.77 (ddd, J = 5.9 Hz, J = 7 Hz, J = 11.2 Hz, 1 H, OC*H*), 3.66-3.63 (m, 2 H, C*H*$_2$Cl), 2.12 (s, 3 H, OAc), 2.02 (s, 3 H, OAc), 2.01 (s, 3 H, OAc), 1.95 (s, 3 H, OAc); ^{13}C NMR (125 MHz, $CDCl_3$): δ 170.2, 170.1, 169.9 169.4 (each *C*O), 101.5 (*C*-1), 70.7 (*C*-3), 70.6 (*C*-5), 69.8 (O*C*H$_2$), 68.5 (*C*-2), 66.9 (*C*-4), 61.2 (*C*-6), 42.5 (*C*H$_2$Cl), 20.7, 20.6, 20.5, 20.4 (each OAc); IR v_{max} (NaCl plate, DCM): 3469.2, 2968.4, 1747.4, 1432.7, 1372.2, 1233.7, 1152.4, 1049.6, 952.5, 914.8, 736.8, 663.8 cm^{-1} ; HRMS m/z (ESI+) calc. for $C_{16}H_{23}ClO_{10}$: 410.1065; found 411.1053 [M+H$^+$]; Anal. Calc. for $C_{16}H_{23}ClO_{10}$: C, 46.78; H, 5.64. Found: C, 47.10; H, 5.55.

The spectroscopic data are in agreement with the literature.[134]

2-Azidoethyl 2,3,4,6-tetra-*O*-acetyl-*β-D*-galactopyranoside 3.46.[135]
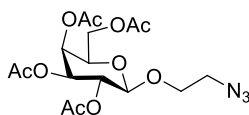
3.46.

A solution of 2-Chloroethyl 2,3,4,6-tetra-*O*-acetyl-β-D-galactopyranoside **3.45.** (500 mg, 1.19 mmol) and NaN_3 (156 mg, 2.39 mmol, 2 equiv) in anhydrous DMF (30 mL) was stirred and heated at 80 °C in a round bottomed flask equipped with a condenser and a $CaCl_2$ drying tube. After 16 h stirring, the solvent was removed under reduced pressure. The crude was dissolved in DCM (30 mL) and washed with distilled water (3 x 15 mL). The organic phase was dried over $MgSO_4$ and concentrated, to give a clear syrup that turned into white crystals upon exposure to high vacuum. It was reacted without further purification. (263 mg, 53%); R_f = 0.53 (Pet Ether:EtOAc, 1:1); mp: 60-64 °C; $[\alpha]_D$ = - 18 (c 1.7 $CHCl_3$); ^{1}H NMR (500 MHz, $CDCl_3$): δ 5.38 (dd, J = 1 Hz, J = 3.4

Hz, 1 H, H-4), 5.21 (dd, J = 8 Hz, J = 10.5 Hz, 1 H, H-2), 5.02 (dd, J = 3.4 Hz, J = 10.5 Hz, 1 H, H-3), 4.54 (d, J = 8 Hz, 1 H, H-1), 4.20-4.11 (m, 2 H, H-6 and H-6'), 4.02 (ddd, J = 3.6 Hz, J = 4.8 Hz, J = 10.6 Hz, 1H, OCH), 3.91 (td, J = 1 Hz, J = 6.6 Hz, J = 6.6 Hz, 1 H, H-5, OCH), 3.67 (ddd, J = 3.4 Hz, J = 8.4 Hz, J = 10.7 Hz, 1H, OCH), 3.47 (ddd, J = 3.5 Hz, J = 8.4 Hz, J = 13.3 Hz, 1H, CHN$_3$), 3.28 (ddd, J = 3.4 Hz, J = 4.6 Hz, J = 13.3 Hz, 1H, CHN$_3$), 2.14 (s, 3 H, OAc), 2.06 (s, 3 H, OAc), 2.04 (s, 3 H, OAc), 1.97 (s, 3 H, OAc); ^{13}C NMR (125 MHz, CDCl$_3$): δ 170.3, 170.1, 170.0, 169.4 (each CO), 101.3 (C-1), 70.9 (C-5), 70.8 (C-3), 68.5 (C-2), 68.3 (OCH_2), 67.1 (C-4), 61.2 (C-6), 50.5 (CH_2N$_3$), 20.7, 20.64, 20.62, 20.5 (each OAc); IR v$_{max}$ (NaCl plate, DCM): 2941.6, 2106.9, 1750.9, 1434.7, 1370.4, 1223.8, 1173.7, 1134.4, 1061.6, 955.6, 899.8 cm^{-1}; HRMS m/z (ESI+) calc. for C$_{16}$H$_{23}$N$_3$O$_{10}$: 417.1463 ; found 440.1476 [M+Na$^+$]; Anal. Calc. for C$_{16}$H$_{23}$N$_3$O$_{10}$: C, 46.04; H, 5.55, N, 10.07. Found: C, 46.12; H, 5.75, N, 10.01.

The spectroscopic data are in agreement with the literature.[135]

2-Aminoethyl 2,3,4,6-tetra-O-acetyl-$β$-D-galactopyranoside 3.47.[131]
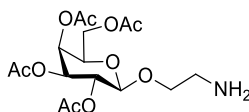
3.47.

To a solution of 2-azidoethyl 2,3,4,6-tetra-O-acetyl-β-D-galactopyranoside **3.46.** (440 mg, 1.05 mmol) in EtOAc (30 mL), Pd/C (50 mg, 10 % w/w) was added. The resulting mixture was stirred at rt under H$_2$ for 4 h. The mixture was then filtered through celite which was washed with EtOAc (50 mL). The filtrate was concentrated under vacuum to afford product **3.47.** as a clear syrup (398 mg, 97%); R$_f$ = 0.0 (Pet Ether:EtOAc, 1:1); [α]$_D$ = - 25 (c 1 CHCl$_3$); ^{1}H NMR (500 MHz, CDCl$_3$): δ 5.37 (d, J = 2.8 Hz, 1 H, H-4), 5.13 (dd, J = 5.8 Hz, J = 10.9 Hz, 1 H, H-2), 5.00 (dd, J = 3.6 Hz, J = 10.5 Hz, 1 H, H-3), 4.51 (d, J = 7.9 Hz, 1 H, H-1), 4.16-4.08 (m, 2 H, H-6 and H-6'), 3.94-3.90 (m, 2 H, overlapping of H-5 and 1 H of OCH_2CH_2NH$_2$), 3.55-3.50 (m, 1 H, 1 H of OCH_2CH$_2$NH$_2$), 3.73-3.39 (m, 2 H, OCH$_2$CH_2NH$_2$), 2.14 (s, 3 H, OAc), 2.06 (s, 3 H, OAc), 2.05 (s, 3 H, OAc), 1.96 (s, 3 H, OAc); ^{13}C NMR (125 MHz, CDCl$_3$): δ 169.5, 169.2, 169.0, 168.8 (each CO), 100.4 (C-1), 69.9 (C-5), 69.7 (C-3), 68.9 (C-2), 68.1 (OCH_2), 67.8 (C-4), 60.5 (C-6), 52.5 (CH_2NH$_2$), 21.7, 21.4, 20.0, 19.9 (each OAc); IR v$_{max}$ (NaCl plate, DCM): 3378.8, 2927.4, 1742.7,

1658.8, 1547.4, 1433.2, 1372.1, 1251.0, 1055.2, 954.4, 915.6, 840.9, 736.4, 703.2, 651.9, 600.9 cm^{-1} ; HRMS m/z (ESI+) calc. for $C_{16}H_{25}NO_{10}$: 391.1458 ; found 414.1351 [M+Na$^+$].

The spectroscopic data are in agreement with the literature.[131]

Azido-2,3,4,6-tetra-*O*-acetyl-*β-D*-galactopyranoside 3.48.[136]
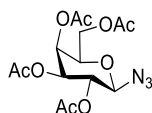
3.48.

TMSN$_3$ (2.5 mL, 19.2 mmol, 2.5 equiv) was added to a solution of β-D-galactose pentaacetate (3 g, 7.68 mmol) in anhydrous DCM (30 mL). SnCl$_4$ 1 M solution in DCM (3.8 mL, 3.84 mmol, 0.5 equiv) was added to this solution and the reaction mixture was stirred for 18 h at rt. Saturated NaHCO$_3$ solution (50 mL) was added and the suspension was extracted with DCM (2 × 50 mL). The combined organic layers were dried over MgSO$_4$, filtered and concentrated in vacuum to afford **3.48.** as a white solid which was used without further purification (2.8 g, 97%); R$_f$ =0.8 (Ether:EtOAc, 1:1); [α]$_D$ = - 23 (c 1 CHCl$_3$); ^{1}H NMR (500 MHz, CDCl$_3$): δ 5.42 (dd, *J* = 0.9 Hz, *J* = 3.4 Hz , 1 H, *H*-4), 5.16 (dd, *J* = 8.8 Hz, *J* = 10.3 Hz, 1 H, *H*-2), 5.03 (dd, *J* = 3.4 Hz , *J* = 10.4 Hz, 1 H, *H*-3), 4.59 (d, *J* = 8.5 Hz, 1 H, *H*-1), 4.19- 4.13 (m, 2 H, *H*-6 and *H*-6'), 4.01 (td, *J* = 6.6 Hz, 1 H, *H*-5), 2.17 (s, 3 H, OAc), 2.09 (s, 3 H, OAc), 2.06 (s, 3 H, OAc), 1.98 (s, 3 H, OAc), ^{13}C NMR (125 MHz, CDCl$_3$): δ 170.2, 170.0, 169.9, 169.3 (each *C*O), 88.2 (*C*-1), 72.8 (*C*-5), 70.6 (*C*-3), 68.5 (*C*-2), 67.2 (*C*-4), 61.2 (*C*-6), 53.5 (*C*H$_2$N$_3$), 20.6, 20.55, 20.51, 20.4 (each OAc); IR v$_{max}$ (NaCl plate, DCM): 3482.5, 2975.9, 2120.3, 1751.9, 1433.9, 1371.3, 1231.3, 1162.6, 1087.9, 1062.9, 1018.5, 955.96, 901.5, 724.1, 627.0, 599.9 cm^{-1}; HRMS m/z (ESI+) calc. for $C_{14}H_{19}N_3O_9$: 373.1121 ; found 396.0992 [M+Na$^+$].

The NMR data is in agreement with the reported values.[136]

Amino-2,3,4,6-tetra-*O*-acetyl-*β*-D-galactopyranoside 3.49.[132]
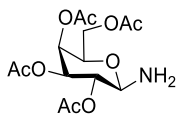
3.49.

H_2 gas was bubbled through a suspension of amino-2,3,4,6-tetra-*O*-acetyl-β-*D*-galactopyranoside **3.48.** (2.6 g, 7.0 mmol) and Pd/C (270 mg, 10 % w/w) in EtOAc (15 mL). It was left to stir for 18 h at rt. The mixture was then filtered through celite which was washed with EtOAc (50 mL). The filtrate was concentrated under vacuum to afford product **3.49.** as a white foamy solid which was used without further purification (2.37 g, 97%); R_f = 0.0 (Pet Ether:EtOAc, 1:1); ^{1}H NMR (500 MHz, CDCl$_3$): δ 5.37 (dd, *J* = 1.0 Hz , *J* = 3.0 Hz, 1 H, *H*-4), 5.07-5.01 (m, 2 H, *H*-2, *H*-3), 4.16 (d, *J* = 8.0 Hz, 1 H, *H*-1), 4.13-4.09 (m, 2 H, *H*-6, *H*-6'), 3.91-3.88 (m, 1 H, *H*-5), 2.15 (s, 3 H, OAc), 2.08 (s, 3 H, OAc), 2.05 (s, 3 H, OAc), 1.99 (s, 3 H, OAc); HRMS m/z (ESI+) calc. for $C_{14}H_{21}NO_9$: 347.1216 ; found 348.1304 [M+H$^+$].

The NMR data is in agreement with the reported values.[132]

Butanoic acid, 4-(propylamino)-3-[[(1,1-dimethylethoxy)-carbonyl]amino]-4-oxo-benzyl ester (3 S/R) 3.50.
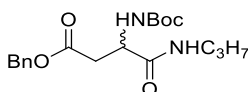
3.50.

HOBt (460 mg, 3.4 mmol, 1.1 equiv), *N*-(tert-Butoxycarbonyl)-*L*-aspartic acid-4-Benzyl ester (1 g, 3.09 mmol), NEt$_3$ (1.3 mL, 9.3 mmol, 3 equiv) and TBTU (1.1 g, 3.4 mmol, 1.1 equiv) were dissolved in DMF (10 mL), under N_2 at rt. The solution was stirred for 15 min and propylamine (0.3 mL, 3.1 mmol, 1 equiv) dissolved in DMF (5 mL) was added. The reaction mixture was stirred for 18 h at rt. The solvent was removed under reduced pressure and the residue was diluted with DCM (30 mL) and washed with 0.5 M HCl (30 mL), saturated aqueous NaHCO$_3$ (20 mL) and brine (20 mL). The organic layer was dried over Na$_2$SO$_4$, filtered and the solvent was evaporated under reduced pressure. The crude was purified by column chromatography (Pet Ether:EtOAc, 1:1) to give the product **3.50.** as a white solid (1.0 g, 89%); R_f = 0.81 (Pet Ether:EtOAc, 1:1);

$[\alpha]_D$ = 0 (c 1.0 DCM); ^{1}H NMR (500 MHz, CDCl$_3$): δ 7.34-7.30 (m, 5 H, Ar), 6.52 (t, *J* = 5.6 Hz, 1 H, N*H*C$_3$H$_7$), 5.71 (d, *J* = 7.5 Hz, 1 H, N*H*COC(CH$_3$)$_3$), 5.11 (q, *J* = 7.5 Hz , 2 H, PhC*H$_2$*), 4.48 (bs, 1 H, *H*-α), 3.21-3.12 (m, 2 H, NHC*H$_2$*C$_2$H$_5$), 2.99 (dd, *J* = 4.5 Hz, *J* = 17.0 Hz, 1 H, *H*-β), 2.71 (dd, *J* =6.0 Hz, *J* = 16.5 Hz, 1 H, *H*-β'), 1.49-1.43 (m, 11 H, overlap of NHCH$_2$C*H$_2$*CH$_3$ and NHCOC(C*H$_3$*)$_3$), 0.87 (t, *J* = 7.5 Hz, 3 H, NHC$_2$H$_4$C*H$_3$*); ^{13}C NMR (125 MHz, CDCl$_3$): δ 171.7, 170.6, 170.5, (each *C*O), 135.4 (Ar*C*), 128.6, 128.5, 128.4, 128.2, 128.0 (each Ar*C*H), 66.8 (Ph*C*H$_2$), 41.3 (NH*C*H$_2$C$_2$H$_5$), 36.2 (NHCH$_2$*C*H$_2$CH$_3$), 28.4, 28.3, 28.1 (COC(*C*H$_3$)$_3$), 22.8, 22.7 (NHCH$_2$*C*H$_2$CH$_3$), 14.1 (NHC$_2$H$_4$*C*H$_3$); IR v_{max} (NaCl plate, DCM): 3319.2, 2968.0, 2934.3, 2876.2, 1717.4, 1664.5, 1530.8, 1456.2, 1390.9, 1366.7, 1250.6, 1168.1, 1080.7, 1051.0, 1026.9, 1001.6, 918.7, 862.6, 780.9, 751.1, 698.0, 579.9 cm^{-1}; HRMS m/z (ESI+) calc. for C$_{19}$H$_{28}$N$_2$O$_5$: 364.1998 ; found 387.1867 [M+Na$^+$].

Butanoic acid, 3-amino-4-oxo-4-propylamino-benzyl ester (3 R/S) 3.51.
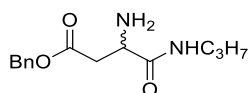
3.51.

A solution of butanoic acid, 4-(propylamino)-3-[[(1,1-dimethylethoxy)-carbonyl]amino]-4-oxo-benzyl ester (3 S/R) **3.50.** (84 mg, 2.3 mmol, 1 equiv) in DCM (20 mL) was cooled in an ice bath and 50 % TFA in DCM (1.8 mL, 23 mmol, 10 equiv) was added dropwise. The reaction mixture was stirred at 0 °C for 30 min and then warmed to rt. The mixture was stirred for a further 4 h. The organic solvent was evaporated under reduced pressure. The residue obtained was diluted with EtOAc (30 mL) and washed with saturated aqueous NaHCO$_3$ (20 mL) and brine (20 mL), dried over MgSO$_4$ and concentrated to yield the corresponding deprotected amine **3.51.** as a white solid which was used without further purification (42 mg, 69%); R$_f$ = 0.0 (Pet Ether:EtOAc, 1:1); $[\alpha]_D$ = 0 (c 1.0 DCM); ^{1}H NMR (500 MHz, CDCl$_3$): δ 7.34-7.26 (m, 5 H, Ar), 5.11 (q, *J* = 8.5 Hz, 2 H, PhC*H$_2$*), 4.4 (bs, 1 H, *H*-α), 3.20-3.13 (m, 2 H, NHC*H$_2$*C$_2$H$_5$), 3.06 (dd, *J* = 6.2 Hz, *J* = 13.1 Hz, 1 H, *H*-β), 2.99 (dd, *J* =5.5 Hz, *J* = 9.4 Hz, 1 H, *H*-β'), 1.44-1.38 (m, 2 H, NHCH$_2$C*H$_2$*CH$_3$), 0.82 (t, *J* = 7.3 Hz, 3 H, NHC$_2$H$_4$C*H$_3$*); ^{13}C NMR (125 MHz, CDCl$_3$): δ 171.9, 171.8 (each *C*O), 135.6 (Ar*C*), 128.6, 128.5, 128.4, 128.3 (each Ar*C*H), 66.7 (Ph*C*H$_2$), 41.5 (NH*C*H$_2$C$_2$H$_5$), 22.8, 22.7, 21.1 (NHCH$_2$*C*H$_2$CH$_3$);

IR v_{max} (NaCl plate, DCM): 3263.7, 3087.9, 2968.4, 1717.8, 1673.4, 1569.3, 1409.9, 1203.3, 1137.2, 998.7, 837.6, 799.6, 722.4, 697.7 cm^{-1}; HRMS m/z (ESI+) calc. for $C_{14}H_{20}N_2O_3$: 264.1474 ; found 265.1550 [M+H$^+$].

Butanoic acid, 4-propylamino-4-oxo-3[(1-oxopropyl)amino]-benzyl ester (3 R/S) 3.52.

3.52.

Propionyl chloride (0.2 mL, 1.9 mmol, 1.2 equiv) was added to a stirring solution of butanoic acid, 3-amino-4-oxo-4-propylamino-benzyl ester (3 R/S) **3.51.** (421 mg, 1.6 mmol) and NEt$_3$ (0.6 mL, 6.2 mmol, 3.3 equiv) dissolved in DMF (20 mL), under N$_2$ at rt. The reaction mixture was stirred for 18 h. The solvent was removed under reduced pressure. The residue was diluted with EtOAc (30 mL), washed with brine (20 mL) and dried over MgSO$_4$, filtered and the solvent was evaporated under reduced pressure. The crude was purified by column chromatography (Pet Ether:EtOAc, 3:1) to give the product **3.52.** as a white solid (339 mg, 67%); R$_f$ = 0.71 (Pet Ether:EtOAc, 1:1);. [α]$_D$ = 0 (c 1.0 DCM); ^{1}H NMR (500 MHz, CDCl$_3$): δ 7.34-7.27 (m, 5 H, Ar), 7.0 (d, J = 7.85 Hz, 1 H, N*H*COC$_2$H$_5$), 6.78 (bs, 1 H, CON*H*C$_3$H$_7$), 5.10 (q, J = 5.0 Hz, 2 H, PhC*H$_2$*), 4.83-4.79 (m, 1 H, *H*-α), 3.15-3.11 (m, 2 H, NHC*H$_2$*C$_2$H$_5$), 2.87 (dd, J = 4.9 Hz, J = 16.7 Hz, 1 H, *H*-β), 2.70 (dd, J = 7.1 Hz, J =16.7 Hz, 1 H, *H*-β'), 2.22-2.17 (m, 2 H, NHCOC*H$_2$*CH$_3$), 1.47-1.42 (m, 2 H, NHCH$_2$C*H$_2$*CH$_3$), 1.09 (t, J = 7.5 Hz, 3 H, NHCOCH$_2$C*H$_3$*), 0.85 (t, J = 7.5 Hz, 3 H, NHCOC$_2$H$_4$C*H$_3$*); ^{13}C NMR (125 MHz, CDCl$_3$): δ 174.1, 171.6, 170.4 (each *C*O), 135.5 (Ar*C*), 128.6, 128.5, 128.4, 128.3, 128.2 (each Ar*C*H), 66.8 (Ph*C*H$_2$), 49.4 (*C*-α), 41.3 (NH*C*H$_2$C$_2$H$_5$), 36.1 (NHCO*C*H$_2$CH$_3$), 30.9 (*C*-β), 22.7, 22.6 (NHCH$_2$*C*H$_2$CH$_3$ and NHCO*C*H$_2$CH$_3$); IR v_{max} (NaCl plate, DCM): 3292.2, 3092.7, 2965.4, 2936.7, 2876.1, 1734.9, 1639.6, 1541.4, 1456.6, 1414.6, 1383.6, 1353.6, 1283.8, 1229.9, 1174.5, 1114.2, 1002.8, 911.1, 735.3, 695.8 cm^{-1}; HRMS m/z (ESI+) calc. for $C_{17}H_{24}N_2O_4$: 320.1736 ; found 321.1814 [M+H$^+$].

Butanoic acid, 4-oxo-3[(1-oxopropyl)amino]-4-propylamino (3 R/S) 3.53.

3.53.

To a solution of Butanoic acid, 4-propylamino-4-oxo-3[(1-oxopropyl)amino]-benzyl ester (3 R/S) **3.52.** (122 mg, 1 mmol) in EtOAc (40 mL), Pd/C (15 mg, 10 % w/w) was added. The resulting mixture was heated to 50 °C and H_2 bubbled through for 4 h. Then the mixture was stirred overnight at rt. The mixture was filtered through celite and washed with warm EtOAc (50 mL). The filtrate was concentrated under vacuum to afford product **3.53.** as a white solid which was used without further purification (84 mg, 96%); $[\alpha]_D$ = 0 (c 1.0 EtOAc); ^{1}H NMR (500 MHz, CDCl$_3$): δ 7.35 (d, J = 8.0 Hz, 1 H, NHCOC$_2$H$_5$), 7.18 (bs, 1 H, CONHC$_3$H$_7$), 4.82-4.78 (m, 1 H, H-α), 3.17-3.13 (m, 2 H, NHCH_2C$_2$H$_5$), 2.81 (dd, J = 5.0 Hz, J = 16.8 Hz, 1 H, H-β), 2.70 (dd, J = 6.7 Hz, J = 16.6 Hz, 1 H, H- β'), 2.28-2.23 (m, 2 H, NHCOCH_2CH$_3$), 1.52-1.44 (m, 2 H, NHCH$_2$CH_2CH$_3$), 1.12 (t, J = 7.6 Hz, 3 H, NHCOCH$_2$CH_3), 0.87 (t, J = 7.4 Hz, 3 H, NHCOC$_2$H$_4$CH_3); ^{13}C NMR (125 MHz, CDCl$_3$): 174.9, 174.3, 171.1 (each CO), 58.3 (C-α), 49.5 (NHCH$_2$C$_2$H$_5$), 48.6 (NHCOCH$_2$CH$_3$), 41.5 (C-β), 29.4, 20.1, 18.2 (NHCH$_2$$CH_2CH_3$ and NHCOCH$_2$CH$_3$); IR ν$_{max}$ (NaCl plate, EtOAc): 3296.5, 3076.9, 2967.4, 2934.1, 1718.6, 1648.1, 1542.1, 1459.6, 1381.5, 1231.8, 1182.5, 1070.0, 916.4 cm^{-1}; HRMS m/z (ESI+) calc. for C$_{10}$H$_{18}$N$_2$O$_4$: 230.1267 ; found 253.1178 [M+Na$^+$].

Butanoic acid, 4-(propylamino)-3-[[(1,1-dimethylethoxy)-carbonyl]amino]-4-oxo-benzyl ester (3 S) 3.54.

3.54.

HOBt (501 mg, 3.7 mmol, 1.2 equiv), N-(tert-Butoxycarbonyl)-L-aspartic acid-4-Benzyl ester (1 g, 3.09 mmol) and DIC (0.6 mL, 3.7 mmol, 1.2 equiv) were dissolved in DMF (10 mL), under N_2 at rt. The solution was stirred for 15 min and propylamine (0.3 mL, 3.1 mmol, 1 equiv) dissolved in DMF (5 mL) was added. The reaction mixture was stirred for 18 h at rt. The solvent was removed under reduced pressure and the

residue was diluted with DCM (30 mL) and washed with 0.5 M HCl (30 mL), saturated aqueous NaHCO$_3$ (20 mL) and brine (20 mL). The organic layer was dried over Na$_2$SO$_4$, filtered and the solvent was evaporated under reduced pressure. The crude was purified by column chromatography (Pet Ether:EtOAc, 1:1) to give the product **3.54.** as a white solid (1.11 g, 98%); R$_f$= 0.78 (Pet Ether:EtOAc, 1:1); [α]$_D$ = + 8.6 (c 1.0 DCM); ^{1}H NMR (500 MHz, CDCl$_3$): δ 7.35-7.29 (m, 5 H, Ar), 6.54 (t, J = 5.7 Hz, 1 H, NHC$_3$H$_7$), 5.72 (d, J = 7.5 Hz, 1 H, NHCOC(CH$_3$)$_3$), 5.11 (q, J = 7.0 Hz, 2 H, PhCH_2), 4.48 (bs, 1 H, H-α), 3.19-3.13 (m, 2 H, NHCH_2C$_2$H$_5$), 2.98 (dd, J = 5.0 Hz, J = 17.0 Hz, 1 H, H-β), 2.71 (dd, J =6.0 Hz, J = 17.0 Hz, 1 H, H-β'), 1.48-1.43 (m, 11 H, overlap of NHCH$_2$CH_2CH$_3$ and NHCOC(CH_3)$_3$), 0.87 (t, J = 7.3 Hz, 3 H, NHC$_2$H$_4$CH_3); ^{13}C NMR (125 MHz, CDCl$_3$): δ 171.7, 170.6, 170.5 (each CO), 135.4 (ArC), 128.6, 128.5, 128.4, 128.2, 128.0 (each ArCH), 66.8 (PhCH$_2$), 41.3 (NHCH$_2$C$_2$H$_5$), 36.2 (NHCH$_2$$CH_2CH_3$), 28.4, 28.3, 28.1 (COC(CH$_3$)$_3$), 22.8, 22.7 (NHCH$_2$$CH_2CH_3$), 14.1 (NHC$_2H_4$$CH_3$); IR v$_{max}$ (NaCl plate, DCM): 3326.1, 3034.2, 2968.6, 2934.8, 2876.4, 1733.9, 1661.7, 1524.4, 1456.5, 1366.7, 1292.2, 1249.9, 1167.6, 1050.8, 995.9, 862.3, 750.6, 697.9 cm^{-1}; HRMS m/z (ESI+) calc. for C$_{19}$H$_{28}$N$_2$O$_5$: 364.1998 ; found 387.1833 [M+Na$^+$].

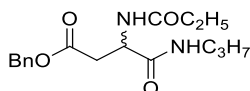**Butanoic acid, 3-amino-4-oxo-4-propylamino-benzyl ester (3 R) 3.55.**

3.55.

A solution of butanoic acid, 4-(propylamino)-3-[[(1,1-dimethylethoxy)-carbonyl]amino]-4-oxo-benzyl ester (3 S) **3.54.** (40 mg, 0.1 mmol, 1 equiv) in DCM (10 mL) was cooled in an ice bath and 50 % TFA in DCM (0.1 mL, 1.1 mmol, 10 equiv) was added dropwise. The reaction mixture was stirred at 0 °C for 30 min and then warmed to rt. The mixture was stirred for a further 4 h. The organic solvent was evaporated under reduced pressure. The residue obtained was diluted with EtOAc (30 mL) and washed with saturated aqueous NaHCO$_3$ (20 mL) and brine (20 mL), dried over MgSO$_4$ and concentrated to yield the corresponding deprotected amine **3.55.** as a white solid which was used without further purification (20 mg, 69%); [α]$_D$ = + 33.3 (c 1.0 DCM); ^{1}H NMR (500 MHz, CDCl$_3$): δ 7.37-7.30 (m, 5 H, Ar), 5.14 (q, J = 5.5 Hz, 2 H, PhCH_2), 3.70 (bs, 1 H, H-α), 3.22-3.18 (m, 2 H, NHCH_2C$_2$H$_5$), 2.99 (dd, J = 3.2 Hz, J = 17.0 Hz, 1

H, *H*-β), 2.68 (dd, *J* = 8.0 Hz, *J* = 16.8 Hz, 1 H, *H*-β'), 1.61-1.44 (m, 2 H, NHCH$_2$C*H*$_2$CH$_3$), 0.91 (t, *J* = 7.4 Hz, 3 H, NHC$_2$H$_4$C*H*$_3$); ^{13}C NMR (125 MHz, CDCl$_3$): δ 171.9, 171.8 (each *C*O), 135.6 (Ar*C*), 128.6, 128.5, 128.4, 128.3 (each Ar*C*H), 66.6 (Ph*C*H$_2$), 40.5 (NH*C*H$_2$C$_2$H$_5$), 22.8, 22.7, 21.0 (NHCH$_2$*C*H$_2$CH$_3$); IR v$_{max}$ (NaCl plate, DCM): 3297.4, 3064.5, 2964.0, 2930.6, 1778.1, 1702.2, 1657.1, 1547.2, 1406.3, 1348.4, 1206.1, 1131.8, 1022.9, 909.9, 800.5, 738.4, 698.6 cm^{-1}; HRMS m/z (ESI+) calc. for C$_{14}$H$_{20}$N$_2$O$_3$: 264.1474 ; found 265.1559 [M+H$^+$].
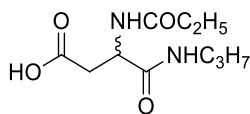
Butanoic acid, 4-propylamino-4-oxo-3[(1-oxopropyl)amino]-benzyl ester (3 R) 3.56.
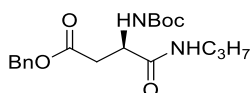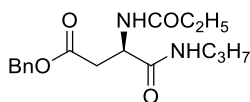

3.56.

Propionyl chloride (0.2 mL, 1.9 mmol, 1.2 equiv) was added to a stirring solution of butanoic acid, 3-amino-4-oxo-4-propylamino-benzyl ester (3 R) **3.55.** (412 mg, 1.5 mmol) and NEt$_3$ (0.5 mL, 5.1 mmol, 3.3 equiv) dissolved in DMF (20 mL), under N$_2$ at rt. The reaction mixture was stirred for 18 h. The solvent was removed under reduced pressure. The residue was diluted with EtOAc (30 mL), washed with brine (20 mL) and dried over MgSO$_4$, filtered and the solvent was evaporated under reduced pressure. The crude was purified by column chromatography (Pet Ether:EtOAc, 3:1) to give the product **3.56.** as a white solid (408 mg, 82%); R$_f$ = 0.74 (Pet Ether:EtOAc, 1:1); [α]$_D$ = - 9.3 (c 1.0 DCM); ^{1}H NMR (500 MHz, CDCl$_3$): δ 7.33-7.29 (m, 5 H, Ar), 6.95 (d, *J* = 8.0 Hz, 1 H, N*H*COC$_2$H$_5$), 6.75 (bs, 1 H, CON*H*C$_3$H$_7$), 5.11 (q, *J* = 5.0 Hz, 2 H, PhC*H*$_2$), 4.82-4.79 (m, 1 H, *H*-α), 3.16-3.12 (m, 2 H, NHC*H*$_2$C$_2$H$_5$), 2.90 (dd, *J* = 5 Hz, *J* = 16.5 Hz, 1 H, *H*- β), 2.70 (dd, *J* = 7 Hz, *J* =17.0 Hz, 1 H, *H*-β'), 2.22-2.14 (m, 2 H, NHCOC*H*$_2$CH$_3$), 1.47-1.43 (m, 2 H, NHCH$_2$C*H*$_2$CH$_3$), 1.10 (t, *J* = 7.5 Hz, 3 H, NHCOCH$_2$C*H*$_3$), 0.85 (t, *J* = 7.5 Hz, 3 H, NHCOC$_2$H$_4$C*H*$_3$); ^{13}C NMR (125 MHz, CDCl$_3$): δ 174.0, 171.7, 170.4 (each *C*O), 135.4 (Ar*C*), 128.6, 128.5, 128.4, 128.3, 128.0 (each Ar*C*H), 66.8 (Ph*C*H$_2$), 49.3 (*C*-α), 41.3 (NH*C*H$_2$C$_2$H$_5$), 36.1 (NHCO*C*H$_2$CH$_3$), 30.9(*C*-β), 22.7, 22.6 (NHCH$_2$*C*H$_2$CH$_3$ and NHCO*C*H$_2$CH$_3$); IR v$_{max}$ (NaCl plate, DCM): 3288.3, 3092.4, 2965.4, 2873.6, 1739.5, 1639.1, 1541.4, 1455.9, 1383.7, 1289.1, 1228.5, 1171.3, 1113.4, 1002.3, 911.6, 735.2, 695.4 cm^{-1}; HRMS m/z (ESI+) calc. for C$_{17}$H$_{24}$N$_2$O$_4$: 320.1736 ; found 321.1809 [M+H$^+$].

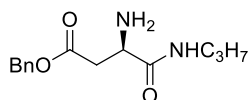**Butanoic acid, 4-oxo-3[(1-oxopropyl)amino]-4-propylamino (3 R) 3.57.**
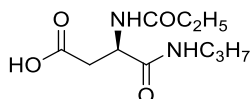
3.57.

To a solution of butanoic acid, 4-oxo-3[(1-oxopropyl)amino]-4-propylamino (3 R) **3.56.** (160 mg, 1 mmol) in EtOAc (40 mL), Pd/C (20 mg, 10 % w/w) was added. The resulting mixture was heated to 50 °C and H_2 bubbled through for 4 h. Then the mixture was stirred overnight at rt. The mixture was filtered through celite and washed with warm EtOAc (50 mL). The filtrate was concentrated under vacuum to afford product **3.57.** as a white solid which was used without further purification (108 mg, 94%); $[\alpha]_D$ = - 30 (c 1.0 EtOAc); ^{1}H NMR (500 MHz, CDCl$_3$): δ 7.25 (d, J = 7.5 Hz, 1 H, NHCOC$_2$H$_5$), 7.11 (bs, 1 H, CONHC$_3$H$_7$), 4.81-4.77 (m, 1 H, H-α), 3.19-3.15 (m, 2 H, NHCH_2C$_2$H$_5$), 2.82 (dd, J = 3.2 Hz, J = 16.9 Hz, 1 H, H-β), 2.68 (dd, J = 6.3 Hz, J = 19.5 Hz, 1 H, H- β'), 2.29-2.26 (m, 2 H, NHCOCH_2CH$_3$), 1.52-1.47 (m, 2 H, NHCH$_2$CH_2CH$_3$), 1.14 (t, J = 7.5 Hz, 3 H, NHCOCH$_2$CH_3), 0.88 (t, J = 7.4 Hz, 3 H, NHCOC$_2$H$_4$CH_3); ^{13}C NMR (125 MHz, CDCl$_3$): δ 173.8, 173.7, 170.1 (each CO), 57.4 (C-α), 48.6 (NHCH_2C$_2$H$_5$), 48.4 (NHCOCH_2CH$_3$), 40.4 (C-β), 28.4, 21.5, 19.9 (NHCH$_2$CH_2CH$_3$ and NHCOCH_2CH$_3$); IR ν$_{max}$ (NaCl plate, EtOAc): 3294.4, 3082.4, 2964.0, 1699.9, 1638.3, 1549.6, 1429.1, 1410.5, 1374.5, 1245.5, 1189.8, 1153.3, 1067.6, 922.2, 705.5 cm^{-1}; HRMS m/z (ESI+) calc. for C$_{10}$H$_{18}$N$_2$O$_4$: 230.1267 ; found 253.1140 [M+Na$^+$].

Butanoic acid, 3-[[(1,1-dimethylethoxy)-carbonyl]amino]-4-oxo-4-(tetradecylamino)-benzyl ester (3 R/S) 3.58.
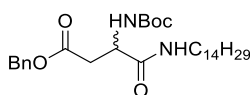
3.58.

HOBt (460 mg, 3.4 mmol, 1.1 equiv), *N*-(tert-Butoxycarbonyl)-*L*-aspartic acid-4-Benzyl ester (1 g, 3.09 mmol) and TBTU (1.1 g, 3.4 mmol, 1.1 equiv) were dissolved in DMF (10 mL), under N$_2$ at rt and NEt$_3$ (1.3 mL, 9.3 mmol, 3 equiv) was added. The solution was stirred for 15 min and tetradecylamine (660 mg, 3.1 mmol, 1 equiv) dissolved in DMF (5 mL) was added. The reaction mixture was stirred for 18 h at rt. The solvent

was removed under reduced pressure and the residue was diluted with DCM (30 mL) and washed with 0.5 M HCl (30 mL), saturated aqueous NaHCO$_3$ (20 mL) and brine (20 mL). The organic layer was dried over Na$_2$SO$_4$, filtered and the solvent was evaporated under reduced pressure. The crude was purified by column chromatography (Pet Ether:EtOAc, 1:1) to give the product **3.58.** as a white solid (1 g, 62%); R$_f$ = 0.93 (Pet Ether:EtOAc, 1:1); [α]$_D$ = 0 (c 1.0 DCM); ^{1}H NMR (500 MHz, CDCl$_3$): δ 7.32-7.28 (m, 5 H, Ar), 6.42 (t, J = 5.5 Hz, 1 H, NHC$_{14}$H$_{29}$), 5.73 (d, J = 8.0 Hz, 1 H, NHCOC(CH$_3$)$_3$), 5.10 (q, J = 5.5 Hz, 2 H, PhCH_2), 4.47 (bs, 1 H, H-α), 3.21-3.15 (m, 2 H, NHCH_2C$_{13}$H$_{27}$), 2.95 (dd, J = 5.0 Hz, J = 17.0 Hz, 1 H, H-β), 2.71 (dd, J = 5.5 Hz, J = 16.5 Hz, 1 H, H-β'), 1.40 (bs, 11 H, overlap of NHCH$_2$CH_2C$_{12}$H$_{25}$ and NHCOC(CH_3)$_3$), 1.29-1.24 (m, 22 H, NHC$_2$H$_4$(CH_2)$_{11}$CH$_3$), 0.86 (t, J = 7.0 Hz, 3 H, NHC$_2$H$_4$(CH$_2$)$_{11}$CH_3); ^{13}C NMR (125 MHz, CDCl$_3$): δ 171.8, 170.4, 169.8 (each CO), 135.4 (ArC), 128.6, 128.5, 128.4, 128.2 (each ArCH), 66.8 (PhCH$_2$), 50.6 (C-α), 39.7 (NHCH$_2$C$_{13}$H$_{27}$), 36.2 (C-β), 31.9, 29.7, 29.68, 29.66, 29.6, 29.5, 29.4, 29.3, 29.2 (NHCH$_2$(CH$_2$)$_{12}$CH$_3$), 28.3 (COC(CH$_3$)$_3$), 26.8, 22.7 (NHCH$_2$(CH$_2$)$_{12}$CH$_3$), 14.1 (NHC$_{13}$H$_{26}$$CH_3$); IR v$_{max}$ (NaCl plate, DCM): 3336.2, 2920.5, 2851.0, 1733.9, 1661.9, 1541.8, 1518.8, 1467.1, 1300.2, 1240.1, 1164.2, 1048.1, 861.5, 753.8 cm^{-1}; HRMS m/z (ESI+) calc. for C$_{30}$H$_{50}$N$_2$O$_5$: 518.372 ; found 541.3603 [M+Na$^+$].

Butanoic acid, 3-amino-4-oxo-4-(tetradecylamino)-benzyl ester (3 R/S) 3.59.

3.59.

A solution of butanoic acid, 3-[[(1,1-dimethylethoxy)-carbonyl]amino]-4-oxo-4-(tetradecylamino)-benzyl ester (3 R/S) **3.58.** (970 mg, 1.7 mmol, 1 equiv) in DCM (30 mL) was cooled in an ice bath and 50 % TFA in DCM (1.3 mL, 16.8 mmol, 10 equiv) was added dropwise. The reaction mixture was stirred at 0 °C for 30 min and then warmed to rt and stirred for a further 4 h. The organic solvent was evaporated under reduced pressure. The residue obtained was diluted with EtOAc (30 mL) and washed with saturated aqueous NaHCO$_3$ (20 mL) and brine (20 mL), dried over MgSO$_4$ and concentrated to yield the corresponding amine **3.59.** as a white solid which was used without further purification (670 mg, 95%); [α]$_D$ = 0 (c 1.2 DCM); ^{1}H NMR (500 MHz,

CDCl$_3$): δ 7.37-7.33 (m, 5 H, Ar), 5.14 (q, J = 5.5 Hz, 2 H, PhCH_2), 3.73 (bs, 1 H, H-α), 3.24-3.19 (m, 2 H, NHCH_2C$_{13}$H$_{27}$), 3.01 (dd, J = 2.2 Hz, J = 16.5 Hz, 1 H, H-β), 2.69 (dd, J = 7.9 Hz, J = 16.8 Hz, 1 H, H-β'), 1.49-1.45 (m, 2 H, NHCH$_2$CH_2C$_{12}$H$_{25}$), 1.28-1.25 (m, 22 H, NHC$_2$H$_4$(CH_2)$_{11}$CH$_3$), 0.88 (t, J = 7.0 Hz, 3 H, NHC$_{13}$H$_{26}$CH_3); ^{13}C NMR (125 MHz, CDCl$_3$): δ 171.9, 171.3 (each CO), 135.6 (ArC), 128.6, 128.4, 128.3 (each ArCH), 66.6 (PhCH$_2$), 50.7 (C-α), 39.4 (NHCH$_2$C$_{13}$H$_{27}$), 36.3 (C-β), 31.9, 29.71, 29.69, 29.67, 29.62, 29.57, 29.55, 29.4, 29.3 (NHCH$_2$(CH$_2$)$_{12}$CH$_3$), 26.9, 22.7 (NHCH$_2$(CH$_2$)$_{12}$CH$_3$), 14.1 (NHC$_{13}$H$_{26}$$CH_3$); IR v$_{max}$ (NaCl plate, DCM): 3307.6, 2918.1, 2849.6, 1718.6, 1633.2, 1523.6, 1470.9, 1361.3, 1261.9, 1183.3, 800.5, 736.5, 696.1 cm^{-1}; HRMS m/z (ESI+) calc. for C$_{25}$H$_{42}$N$_2$O$_3$: 418.3195 ; found 419.3281 [M+H$^+$].

Butanoic acid, 4-oxo-3[(1-oxodecyl)amino]-4-(tetradecylamino)-benzyl ester (3 R/S) 3.60.
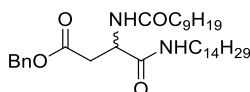
3.60.

HOBt (295 mg, 2.2 mmol, 1.2 equiv) was added to a stirring solution of decanoic acid (388 mg, 2.3 mmol, 1.2 equiv), NEt$_3$ (0.6 mL, 6.1 mmol, 3.3 equiv) and TBTU (724 g, 32.3 mmol, 1.2 equiv) dissolved in DMF (10 mL), under N$_2$ at rt. The mixture was stirred for 10 min and butanoic acid, 3-amino-4-oxo-4-(tetradecylamino)-benzyl ester (3 R/S) **3.59.** (788 mg, 1.9 mmol) was dissolved in DMF (20 mL) and added slowly with a cannula. The reaction mixture was stirred for 18 h. The solvent was removed under reduced pressure. The residue was diluted with EtOAc (30 mL), washed with brine (20 mL) and dried over MgSO$_4$, filtered and the solvent was evaporated under reduced pressure. The crude was purified by column chromatography (Pet Ether:EtOAc, 1:1) to give the product **3.60.** as a white solid (1.05 g, 97%); R$_f$ = 0.83 (Pet Ether:EtOAc, 1:1); [α]$_D$ = 0 (c 1.0 DCM); ^{1}H NMR (500 MHz, CDCl$_3$): δ 7.35-7.33 (m, 5 H, Ar), 6.92 (d, J = 8.0 Hz, 1 H, NHCOC$_9$H$_{19}$), 6.56 (bs, 1 H, CONHC$_{14}$H$_{29}$), 5.13 (q, J = 3.5 Hz, 2 H, PhCH_2), 4.81-4.78 (m, 1 H, H-α), 3.20-3.16 (m, 2 H, NHCH_2C$_{13}$H$_{27}$), 2.92 (dd, J = 4.5 Hz, J = 16.5 Hz, 1 H, H- β), 2.68 (dd, J = 7.5 Hz, J = 17.0 Hz, 1 H, H-β'), 2.19-2.17 (m, 2 H, NHCOCH_2C$_8$H$_{17}$), 1.62-1.58 (m, 2 H, NHCH$_2$CH_2C$_{12}$H$_{25}$), 1.44-1.25 (m, 2 H, NHCOCH$_2$CH_2C$_6$H$_{15}$), 1.29-1.25 (m, 34 H, NHC$_2$H$_4$(CH_2)$_{11}$CH$_3$ and NHCOC$_2$H$_4$(CH_2)$_6$CH$_3$),

0.87 (t, J = 6.5 Hz, 6 H, NHC$_{13}$H$_{26}$CH_3 and NHCOC$_9$H$_{16}$CH_3); ^{13}C NMR (125 MHz, CDCl$_3$): δ 173.5, 171.8, 170.3 (each CO), 135.4 (ArC), 128.6, 128.5, 128.4, 128.2 (each ArCH), 66.8 (PhCH$_2$), 49.2 (C-α), 39.7 (NHCH$_2$C$_{13}$H$_{27}$), 36.5 (NHCOCH$_2$C$_8$H$_{17}$), 35.9 (C-β), 31.9, 31.8, 29.70, 29.69, 29.67, 29.66, 29.62, 29.57, 29.45, 29.36, 29.34, 29.32, 29.28, 29.2, 29.1, 26.9 (NHC$_2$H$_4$(CH$_2$)$_{11}$CH$_3$ and NHCOCH$_2$(CH$_2$)$_7$CH$_3$), 25.6 (NHCH$_2$$CH_2$(CH$_2$)$_{11}CH_3$), 22.69, 22.66 (NHC$_2H_4$($CH_2$)$_{11}CH_3$ and NHCOCH$_2$(CH$_2$)$_7$CH$_3$), 14.1, 14.0 (NHC$_{13}$H$_{26}$$CH_3$ and NHCOC$_8$H$_{16}$$CH_3$); IR ν$_{max}$ (NaCl plate, DCM): 3334.8, 2921.8, 2851.8, 1734.6, 1677.3, 1662.5, 1544.6, 1519.8, 1469.6, 1367.6, 1300.4, 1240.3, 1163.3,1046.7, 1020.6, 860.9, 752.3, 698.1 cm^{-1}; HRMS m/z (ESI+) calc. for C$_{35}$H$_{60}$N$_2$O$_4$: 572.4553 ; found 573.4625 [M+H$^+$].

Butanoic acid, 4-oxo-3[(1-oxodecyl)amino]-4-(tetradecylamino) (3 R/S) 3.61.

3.61.

To a solution of butanoic acid, 4-oxo-3[(1-oxodecyl)amino]-4-(tetradecylamino)-benzyl ester (3 R/S) **3.60.** (236 mg, 0.4 mmol) in EtOAc (25 mL), Pd/C (30 mg, 10 % w/w) was added. The resulting mixture was heated to 50 °C and H$_2$ bubbled through for 4 h. Then the mixture was stirred overnight at rt. The mixture was filtered through celite and washed with warm EtOAc (50 mL). The filtrate was concentrated under vacuum to afford the product **3.61.** as a white solid which was used without further purification (197 mg, 99%); [α]$_D$ = 0 (c 1.0 DCM); ^{1}H NMR (500 MHz, CDCl$_3$): δ 6.98 (d, J = 7.5 Hz, 1 H, NHCOC$_9$H$_{19}$), 6.90 (t, J = 5.8 Hz, 1 H, NHC$_{14}$H$_{29}$), 4.77-4.74 (m, 1 H, H-α), 3.24-3.19 (m, 2 H, NHCH_2C$_{13}$H$_{27}$), 2.91 (dd, J = 3.9 Hz, J = 17.0 Hz, 1 H, H-β), 2.67 (dd, J = 7.3 Hz, J = 17.0 Hz, 1 H, H-β'), 2.26-2.22 (m, 2 H, NHCOCH_2C$_8$H$_{17}$), 1.65-1.59 (m, 2 H, NHCH$_2$CH_2C$_{12}$H$_{25}$), 1.50-1.46 (m, 2 H, NHCOCH$_2$CH_2C$_6$H$_{15}$), 1.29-1.25 (m, 34 H, NHC$_2$H$_4$(CH$_2$)$_{11}$CH$_3$ and NHCOC$_2$H$_4$(CH$_2$)$_6$CH$_3$), 0.88 (t, J = 6.9 Hz, 6 H, NHC$_{13}$H$_{26}$CH_3 and NHCOC$_9$H$_{16}$CH_3); ^{13}C NMR (125 MHz, MeOH): δ 176.8, 174.6, 172.9 (each CO), 51.3 (C-α), 39.4 (NHCH$_2$C$_{13}$H$_{27}$), 39.1 (NHCOCH$_2$C$_8$H$_{17}$), 35.6 (C-β), 31.71, 31.70, 29.44, 29.41, 29.40, 29.36, 29.26, 29.2, 29.14, 29.12, 29.10, 29.03, 29.02, 26.7 (NHC$_2$H$_4$(CH$_2$)$_{11}$CH$_3$ and NHCOCH$_2$(CH$_2$)$_7$CH$_3$), 25.5 (NHCH$_2$$CH_2$(CH$_2$)$_{11}CH_3$), 22.8, 22.4 (NHC$_2H_4$($CH_2$)$_{11}CH_3$ and NHCOCH$_2$(CH$_2$)$_7$CH$_3$), 13.1 (NHC$_{13}$H$_{26}$$CH_3$ and NHCOC$_8$H$_{16}$$CH_3$);

IR v_{max} (NaCl plate, DCM): 3299.7, 2955.0, 2921.0, 2851.1, 1749.7, 1635.8, 1581.6, 1466.8, 1407.5, 1377.5, 1260.4, 1086.7, 801.0, 721.3 cm^{-1}; HRMS m/z (ESI+) calc. for $C_{28}H_{54}N_2O_4$: 482.4084 ; found 505.3977 [M+Na$^+$].

Butanoic acid, 3-[[(1,1-dimethylethoxy)-carbonyl]amino]-4-oxo-4-(tetradecylamino)-benzyl ester (3 R) 3.62.

3.62.

HOBt (501 mg, 3.7 mmol, 1.2 equiv), *N*-(tert-Butoxycarbonyl)-*L*-aspartic acid-4-Benzyl ester (1 g, 3.09 mmol) and DIC (0.6 mL, 3.7 mmol, 1.2 equiv) were dissolved in DMF (10 mL), under N_2 at rt. The solution was stirred for 15 min and tetradecylamine (660 mg, 3.1 mmol, 1 equiv) dissolved in DMF (5 mL) was added. The reaction mixture was stirred for 18 h at rt. The solvent was removed under reduced pressure and the residue was diluted with DCM (30 mL) and washed with 0.5 M HCl (30 mL), saturated aqueous NaHCO$_3$ (20 mL) and brine (20 mL). The organic layer was dried over Na$_2$SO$_4$, filtered and the solvent was evaporated under reduced pressure. The crude was purified by column chromatography (Pet Ether:EtOAc, 1:1) to give the product **3.62.** as a white solid (1.58 g, 98%); R$_f$ = 0.93 (Pet Ether:EtOA, 1:1); [α]$_D$ = + 40 (c 1.0 DCM); ^{1}H NMR (500 MHz, CDCl$_3$): δ 7.34-7.30 (m, 5 H, Ar), 6.49 (t, *J* = 5.5 Hz, 1 H, N*H*C$_{14}$H$_{29}$), 5.70 (d, *J* = 6.5 Hz, 1 H, N*H*COC(CH$_3$)$_3$), 5.11 (q, *J* = 6.5 Hz, 2 H, PhC*H*$_2$), 4.47 (bs, 1 H, *H*-α), 3.23-3.16 (m, 2 H, NHC*H*$_2$C$_{13}$H$_{27}$), 2.99 (dd, *J* = 4.5 Hz, *J* = 17.0 Hz, 1 H, *H*-β), 2.71 (dd, *J* = 6.0 Hz, *J* = 17.0 Hz, 1 H, *H*-β'), 1.43 (bs, 11 H, overlap of NHCH$_2$C*H*$_2$C$_{12}$H$_{25}$ and NHCOC(C*H*$_3$)$_3$), 1.28-1.24 (m, 22 H, NHC$_2$H$_4$(C*H*$_2$)$_{11}$CH$_3$), 0.86 (t, *J* = 7.0 Hz, 3 H, NHC$_2$H$_4$(CH$_2$)$_{11}$C*H*$_3$); ^{13}C NMR (125 MHz, CDCl$_3$): δ 171.8, 170.4, 169.9 (each CO), 135.4 (Ar*C*), 128.6, 128.5, 128.4, 128.2 (each Ar*C*H), 66.8 (Ph*C*H$_2$), 50.6 (*C*-α), 39.7 (NH*C*H$_2$C$_{13}$H$_{27}$), 36.2 (*C*-β), 31.9, 29.70, 29.68, 29.66, 29.60, 29.55, 29.43, 29.3, 29.2 (NHCH$_2$(*C*H$_2$)$_{12}$CH$_3$), 28.3 (COC(*C*H$_3$)$_3$), 26.8, 22.7 (NHCH$_2$(*C*H$_2$)$_{12}$CH$_3$), 14.1 (NHC$_{13}$H$_{26}$*C*H$_3$); IR v_{max} (NaCl plate, DCM): 3336.2, 2921.6, 2851.5, 1734.5, 1676.6, 1662.7, 1544.6, 1519.1, 1467.2, 1667.0, 1300.5, 1241.5, 1165.0, 1048.7, 976.7, 862.8, 753.8 cm^{-1}; HRMS m/z (ESI+) calc. for C$_{30}$H$_{50}$N$_2$O$_5$: 518.372 ; found 541.3602 [M+Na$^+$].

Butanoic acid, 3-amino-4-oxo-4-(tetradecylamino)-benzyl ester (3 R) 3.63.
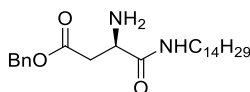

3.63.

A solution of butanoic acid, 3-[[(1,1-dimethylethoxy)-carbonyl]amino]-4-oxo-4-(tetradecylamino)-benzyl ester (3 R) **3.62.** (1.5 g, 2.8 mmol, 1 equiv) in DCM (30 mL) was cooled in an ice bath and 50 % TFA in DCM (2.2 mL, 28.1 mmol, 10 equiv) was added dropwise. The reaction mixture was stirred at 0 °C for 30 min and then warmed to rt and stirred for a further 4 h. The organic solvent was evaporated under reduced pressure. The residue obtained was diluted with EtOAc (30 mL) and washed with saturated aqueous NaHCO$_3$ (20 mL) and brine (20 mL), dried over MgSO$_4$ and concentrated to yield the corresponding amine **3.63.** as a white solid which was used without further purification (1.08 g, 92%); $[\alpha]_D$ = + 21 (c 1.4 DCM); ^{1}H NMR (500 MHz, CDCl$_3$): δ 7.36-7.32 (m, 5 H, Ar), 5.14 (q, J = 5.5 Hz, 2 H, PhCH_2), 3.77 (bs, 1 H, H-α), 3.24-3.18 (m, 2 H, NHCH_2C$_{13}$H$_{27}$), 2.99 (dd, J = 2 Hz, J = 16.9 Hz, 1 H, H-β), 2.71 (dd, J = 7.4 Hz, J = 16.5 Hz, 1 H, H-β'), 1.49-1.46 (m, 2 H, NHCH$_2$CH_2C$_{12}$H$_{25}$), 1.31-1.25 (m, 22 H, NHC$_2$H$_4$(CH_2)$_{11}$CH$_3$), 0.88 (t, J = 7.0 Hz, 3 H, NHC$_{13}$H$_{26}$CH_3); ^{13}C NMR (125 MHz, CDCl$_3$): δ 171.8, 171.6 (each CO), 135.5 (ArC), 128.6, 128.4, 128.3 (each ArCH), 66.7 (PhCH$_2$), 51.3 (C-α), 39.4 (NHCH$_2$C$_{13}$H$_{27}$), 39.1 (C-β), 31.9, 29.71, 29.69, 29.67, 29.62, 29.57, 29.5, 29.4, 29.3 (NHCH$_2$(CH$_2$)$_{12}$CH$_3$), 26.9, 22.7 (NHCH$_2$(CH$_2$)$_{12}$CH$_3$), 14.1 (NHC$_{13}$H$_{26}$$CH_3$); IR v$_{max}$ (NaCl plate, DCM): 3308.8, 2919.6, 2850.6, 1717.4, 1639.2, 1529.8, 1468.7, 1361.3, 1201.7, 800.5, 736.5, 696.1 cm^{-1}; HRMS m/z (ESI+) calc. for C$_{25}$H$_{42}$N$_2$O$_3$: 418.3195 ; found 419.3224 [M+H$^+$].

Butanoic acid, 4-oxo-3[(1-oxodecyl)amino]-4-(tetradecylamino)-benzyl ester (3 R) 3.64.
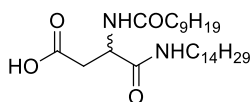

3.64.

HOBt (424 mg, 3.1 mmol, 1.2 equiv) was added to a stirring solution of decanoic acid (558 mg, 3.2 mmol, 1.2 equiv), NEt$_3$ (0.8 mL, 8.8 mmol, 3.3 equiv) and TBTU (1 g, 3.2

mmol, 1.2 equiv) dissolved in DMF (10 mL), under N_2 at rt. The mixture was stirred for 10 min and butanoic acid, 3-amino-4-oxo-4-(tetradecylamino)-benzyl ester (3 R) **3.63.** (1.1 g, 2.7 mmol) was dissolved in DMF (20 mL) and added slowly with a cannula. The reaction mixture was stirred for 18 h. The solvent was removed under reduced pressure. The residue was diluted with EtOAc (30 mL), washed with brine (20 mL) and dried over $MgSO_4$, filtered and the solvent was evaporated under reduced pressure. The crude was purified by column chromatography (Pet Ether:EtOAc, 1:1) to give the product **3.64.** as a white solid (1.53 g, 99%); R_f = 0.89 (Pet Ether:EtOAc, 1:1); $[\alpha]_D$ = 0 (c 1.0 DCM); ^{1}H NMR (500 MHz, CDCl$_3$): δ 7.37-7.34 (m, 5 H, Ar), 6.83 (d, J = 8.0 Hz, 1 H, NHCOC$_9$H$_{19}$), 6.52 (bs, 1 H, CONHC$_{14}$H$_{29}$), 5.15 (q, J = 7.0 Hz, 2 H, PhCH_2), 4.80-4.76 (m, 1 H, H-α), 3.21-3.17 (m, 2 H, NHCH_2C$_{13}$H$_{27}$), 2.98 (dd, J = 4.5 Hz, J = 16.9 Hz, 1 H, H- β), 2.65 (dd, J = 7.1 Hz, J = 17.0 Hz, 1 H, H-β'), 2.21-2.18 (m, 2 H, NHCOCH_2C$_8$H$_{17}$), 1.62-1.59 (m, 2 H, NHCH$_2$CH_2C$_{12}$H$_{25}$), 1.45-1.43 (m, 2 H, NHCOCH$_2$CH_2C$_6$H$_{15}$), 1.29-1.25 (m, 34 H, NHC$_2$H$_4$(CH_2)$_{11}$CH$_3$ and NHCOC$_2$H$_4$(CH_2)$_6$CH$_3$), 0.88 (t, J = 6.8 Hz, 6 H, NHC$_{13}$H$_{26}$CH_3 and NHCOC$_9$H$_{16}$CH_3); ^{13}C NMR (125 MHz, CDCl$_3$): δ 173.4, 172.1, 170.2 (each CO), 135.4 (ArC), 128.6, 128.4, 128.3 (each ArCH), 66.9 (PhCH$_2$), 49.2 (C-α), 39.7 (NHCH$_2$C$_{13}$H$_{27}$), 36.6 (NHCOCH$_2$C$_8$H$_{17}$), 35.8 (C-β), 31.9, 31.8, 29.70, 29.68, 29.65, 29.61, 29.55, 29.49, 29.43, 29.41, 29.38, 29.35, 29.32, 29.26, 29.2, 29.1, 26.8 (NHC$_2$H$_4$(CH$_2$)$_{11}$CH$_3$ and NHCOCH$_2$(CH$_2$)$_7$CH$_3$), 25.6 (NHCH$_2$$CH_2$(CH$_2$)$_{11}CH_3$), 22.7, 22.6 (NHC$_2H_4$($CH_2$)$_{11}CH_3$ and NHCOCH$_2$(CH$_2$)$_7$CH$_3$), 14.1, 14.0 (NHC$_{13}$H$_{26}$$CH_3$ and NHCOC$_8$H$_{16}$$CH_3$); IR v_{max} (NaCl plate, DCM): 3293.4, 2919.9, 2851.2, 1734.5, 1644.0, 1542.9, 1467.3, 1355.1, 1221.6, 739.4 cm^{-1}; HRMS m/z (ESI+) calc. for C$_{35}$H$_{60}$N$_2$O$_4$: 572.4553 ; found 573.4623 [M+H$^+$].

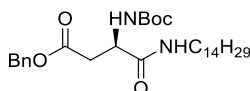**Butanoic acid, 4-oxo-3[(1-oxodecyl)amino]-4-(tetradecylamino) (3 R) 3.65.**
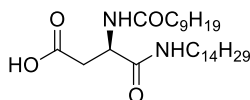
3.65.

To a solution of butanoic acid, 4-oxo-3[(1-oxodecyl)amino]-4-(tetradecylamino)-benzyl ester (3 R) **3.64.** (1.1 g, 1.9 mmol) in EtOAc (50 mL), Pd/C (200 mg, 10 % w/w) was added. The resulting mixture was heated to 50 °C and H$_2$ bubbled through for 4 h. Then the mixture was stirred overnight at rt. The mixture was filtered through

celite and washed with warm EtOAc (50 mL). The filtrate was concentrated under vacuum to afford the product **3.65.** as a white solid which was used without further purification (930 mg, 99%); $[\alpha]_D$ = - 10 (c 1.0 DCM); ^{1}H NMR (500 MHz, CDCl$_3$): δ 7.16 (d, J = 8.0 Hz, 1 H, N*H*COC$_9$H$_{19}$), 7.01 (t, J = 5.5 Hz, 1 H, N*H*C$_{14}$H$_{29}$), 4.82-4.78 (m, 1 H, *H*-α), 3.22-3.18 (m, 2 H, NHC*H$_2$*C$_{13}$H$_{27}$), 2.86 (dd, J = 4.5 Hz, J = 16.5 Hz, 1 H, *H*-β), 2.69 (dd, J = 7.5 Hz, J = 17.0 Hz, 1 H, H-β'), 2.24-2.21 (m, 2 H, NHCOC*H$_2$*C$_8$H$_{17}$), 1.62-1.59 (m, 2 H, NHCH$_2$C*H$_2$*C$_{12}$H$_{25}$), 1.48-1.45 (m, 2 H, NHCOCH$_2$C*H$_2$*C$_6$H$_{15}$), 1.30-1.24 (m, 34 H, NHC$_2$H$_4$(C*H$_2$*)$_{11}$CH$_3$ and NHCOC$_2$H$_4$(C*H$_2$*)$_6$CH$_3$), 0.87 (t, J = 6.8 Hz, 6 H, NHC$_{13}$H$_{26}$C*H$_3$* and NHCOC$_9$H$_{16}$C*H$_3$*); ^{13}C NMR (125 MHz, CDCl$_3$): δ 174.3, 174.1, 170.8 (each *C*O), 49.2 (*C*-α), 39.1 (NH*C*H$_2$C$_{13}$H$_{27}$), 36.5 (NHCO*C*H$_2$C$_8$H$_{17}$), 33.9 (*C*-β), 31.9, 31.8, 29.72, 29.69, 29.67, 29.65, 29.58, 29.52, 29.47, 29.43, 29.37, 29.36, 29.29, 29.25, 29.1, 28.3, 26.7 (NHC$_2$H$_4$(*C*H$_2$)$_{11}$CH$_3$ and NHCOCH$_2$(*C*H$_2$)$_7$CH$_3$), 25.6 (NHCH$_2$*C*H$_2$(CH$_2$)$_{11}$CH$_3$), 22.69, 22.67 (NHC$_2$H$_4$(*C*H$_2$)$_{11}$CH$_3$ and NHCOCH$_2$(*C*H$_2$)$_7$CH$_3$), 14.1, 14.0 (NHC$_{13}$H$_{26}$*C*H$_3$ and NHCOC$_8$H$_{16}$*C*H$_3$); IR v$_{max}$ (NaCl plate, DCM): 3290.5, 2954.3, 2920.0, 2851.6, 2103.8, 1738.9, 1702.1, 1638.1, 1544.6, 1467.2, 1435.8, 1388.4, 1298.4, 1224.8, 1195.4, 1118.0, 951.8, 721.1 cm^{-1}; HRMS m/z (ESI+) calc. for C$_{28}$H$_{54}$N$_2$O$_4$: 482.4084 ; found 483.4159 [M+H$^+$].

N^4-[2-*O*-(2,3,4,6-tetra-*O*-acetyl-*β*-*D*-galactopyranosyl)-ethyl]-*N^2*-decanoyl-L/R-asparagine tetradecylamide 3.66.
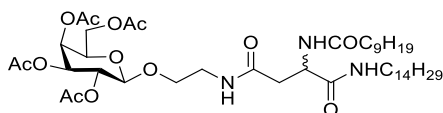
3.66.

HOBt (69 mg, 0.51 mmol, 2 equiv) was added to a stirring solution of butanoic acid, 4-oxo-3[(1-oxodecyl)amino]-4-(tetradecylamino) (3 R/S) **3.61.** (123 mg, 0.26 mmol, 1 equiv) and TBTU (164 mg, 0.51 mmol, 2 equiv) dissolved in DMF (10 mL), under N$_2$ at 30 °C. The mixture was stirred for 10 min and 2-aminoethyl 2,3,4,6-tetra-O-acetyl-β-D-galactopyranoside **3.47.** (400 mg, 1.02 mmol, 4 equiv) was dissolved in DMF (20 mL) and added dropwise with a cannula. The mixture was stirred overnight at rt. The solvent was removed under reduced pressure and the residue was diluted with DCM (30 mL) and washed with 0.5 M HCl (30 mL), saturated aqueous NaHCO$_3$ (20 mL) and brine (20 mL). The organic layer was dried over Na$_2$SO$_4$, filtered and the solvent was

evaporated under reduced pressure. The crude was purified by column chromatography (Pet Ether:EtOAc, 2:1 to 1:1) to give the product **3.66.** as a white solid (160 mg, 73%); R_f = 0.89 (EtOAc); ^{1}H NMR (500 MHz, CDCl$_3$): δ 7.47 (d, J = 7.1 Hz, 1 H, N*H*COC$_9$H$_{19}$), 7.41 (d, J = 7.1 Hz, 1 H, N*H*COC$_9$H$_{19}$), 7.11-7.07 (m, 2 H, CON*H*C$_{14}$CH$_{29}$), 6.51 (t, J = 5.6 Hz, 1 H, CH$_2$CH$_2$N*H*CO), 6.37 (t, J = 5.6 Hz, 1 H, CH$_2$CH$_2$N*H*CO), 5.37 (d, J = 3.3 Hz, 2 H, *H*-4), 5.18-5.13 (m, 2 H, *H*-2), 5.04-5.01 (m, 2 H, *H*-3), 4.67–4.63 (m, 2 H, *H*-α), 4.56 (d, J = 7.9 Hz, 1 H, *H*-1), 4.52 (d, J = 7.9 Hz, 1 H, *H*-1), 4.18–4.08 (m, 4 H, overlap of *H*-6, *H*-6'), 4.04–4.01 (m, 1 H, *H*-5), 3.95–3.92 (m, 1 H, *H*-5), 3.89–3.79 (m, 2 H, OC*H*$_2$CH$_2$NH), 3.75–3.64 (m, 2 H, OC*H*$_2$CH$_2$NH), 3.51–3.36 (m, 4 H, OCH$_2$C*H*$_2$NH), 3.21–3.14 (m, 4 H, NHC*H*$_2$C$_{13}$H$_{27}$), 2.79-2.73 (m, 2 H, H-β), 2.47-2.41 (m, 2 H, H-β'), 2.22–2.19 (m, 2 H, COC*H*$_2$C$_8$H$_{17}$), 2.14, 2.07, 2.03, 1.96 (each s, 3 H x 2, OAc), 1.63–1.57 (m, 4 H, COCH$_2$C*H*$_2$C$_7$H$_{15}$), 1.47–1.42 (m, 4 H, NHCH$_2$C*H*$_2$C$_{12}$H$_{25}$), 1.28-1.20 (m, 34 H x 2, overlap of COC$_2$H$_4$(C*H*$_2$)$_6$CH$_3$, NHC$_2$H$_4$(C*H*$_2$)$_{11}$CH$_3$), 0.85 (t, J = 6.9 Hz, 6 H x 2, overlap of COC$_8$H$_{16}$C*H*$_3$, NHC$_{13}$H$_{26}$C*H*$_3$); ^{13}C NMR (125 MHz, CDCl$_3$): δ 173.6, 171.7, 171.6, 170.6, 170.3, 170.2 (each *C*O), 101.5, 101.3 (*C*-1), 70.9, 70.8, 70.7, 70.6 (*C*-5, *C*-3), 69.0, 68.9 (*C*-2), 68.5, 68.2 (O*C*H$_2$CH$_2$NH) 67.5, 67.2 (*C*-4), 61.7, 61.3 (*C*-6), 49.9, 49.8 (*C*-α), 39.7, 39.6 (OCH$_2$*C*H$_2$NH), 39.3 (NH*C*H$_2$C$_{13}$H$_{27}$), 37.1, 37.0 (*C*-β), 36.6 (*C*OCH$_2$C$_8$H$_{17}$), 31.9, 31.8, 29.7, 29.6, 29.5, 29.4, 29.3, 29.2, 28.3, 26.9, 25.6, 22.7, 22.6 (COC$_2$H$_4$(*C*H$_2$)$_6$CH$_3$, NHC$_2$H$_4$(*C*H$_2$)$_{11}$CH$_3$), 20.8, 20.7, 20.6, 20.5 (OAc), 14.1, 14.0 (COC$_8$H$_{16}$*C*H$_3$, NHC$_{13}$H$_{26}$*C*H$_3$); IR v_{max} (NaCl plate, DCM): 3289.1, 3093.4, 2919.5, 2850.9, 1751.0, 1645.8, 1544.9, 1467.9, 1436.5, 1370.3, 1225.3, 1174.8, 1078.3, 1059.4, 959.8, 902.7, 720.7 cm^{-1}; HRMS m/z (ESI+) calc. for C$_{44}$H$_{77}$N$_3$O$_{13}$: 855.5456 ; found 856.5535 [M+H$^+$].

N^4-[2-O-($β$-D-galactopyranosyl)-ethyl]-N^2-decanoyl-L/R-asparagine tetradecylamide 3.67.
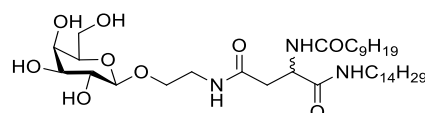
3.67.

NEt$_3$ (0.1 mL, 0.99 mmol, 5.12 equiv) was added to a stirring solution of N^4-[2-O-(2,3,4,6-tetra-O-acetyl-$β$-D-galactopyranosyl)-ethyl]-N^2-decanoyl-L/R-asparagine tetradecylamide **3.66.** (166 mg, 0.19 mmol, 1 equiv) dissolved in DCM / MeOH / H$_2$O

(3 mL / 6 mL / 3 mL). The mixture was stirred for 18 h at 40 °C. The reaction mixture was concentrated under reduced pressure to afford product **3.67.** as a white solid (106 mg, 79%); ^{1}H NMR (500 MHz, d_5-Pyr): δ 9.00-8.98 (m, 2 H, N*H*COC$_9$H$_{19}$), 8.92-8.89 (m, 2 H, CH$_2$CH$_2$N*H*CO), 8.58-8.54 (m, 2 H, CON*H*C$_{14}$CH$_{29}$), 5.57–5.51 (m, 2 H, *H*-α), 4.79 (d, *J* = 7.7 Hz, 2 H, *H*-1), 4.52–4.39 (m, 8 H, overlap of *H*-2, *H*-4, *H*-6, *H*-6'), 4.18–4.15 (m, 4 H, overlap of *H*-3, *H*-5), 4.11-4.07 (m, 2 H, OC*H*$_2$CH$_2$NH), 3.98–3.96 (m, 2 H, OC*H*$_2$CH$_2$NH), 3.81–3.78 (m, 2 H, OCH$_2$C*H*$_2$NH), 3.68–3.65 (m, 2 H, OCH$_2$C*H*$_2$NH), 3.48–3.38 (m, 4 H, NHC*H*$_2$C$_{13}$H$_{27}$), 3.23-3.12 (m, 4 H, overlap of *H*-β, *H*-β'), 2.38-2.34 (m, 2 H, COC*H*$_2$C$_8$H$_{17}$), 1.77–1.71 (m, 4 H, COCH$_2$C*H*$_2$C$_7$H$_{15}$), 1.57–1.53 (m, 4 H, NHCH$_2$C*H*$_2$C$_{12}$H$_{25}$), 1.27-1.16 (m, 34 H x 2, overlap of COC$_2$H$_4$(C*H*$_2$)$_6$CH$_3$, NHC$_2$H$_4$(C*H*$_2$)$_{11}$CH$_3$), 0.88-0.83 (m, 6 H x 2, overlap of COC$_8$H$_{16}$C*H*$_3$, NHC$_{13}$H$_{26}$C*H*$_3$); ^{13}C NMR (125 MHz, d_5-Pyr): δ 173.2, 171.7, 170.9 (each *C*O), 105.5, 105.4 (*C*-1), 76.8, 76.5, 75.1, 74.3, 74.0, 72.3, 71.9, 70.1 (*C*-2, *C*-4, *C*-3, *C*-5), 69.5 (O*C*H$_2$CH$_2$NH), 62.4, 62.3 (*C*-6), 51.1, 51.0 (*C*-α), 40.8, 40.7 (each O*C*H$_2$CH$_2$NH), 40.4, 40.3 (NH*C*H$_2$C$_{13}$H$_{27}$), 40.2, 40.1 (*C*-β), 39.6, 38.5, 36.3, 31.9, 31.8, 29.9, 29.7, 29.6, 29.5, 29.4, 29.3, 29.2, 27.0, 25.9 (each *C*H$_2$), 22.7 (COC$_8$H$_{16}$*C*H$_3$), 14.1 (NHC$_{13}$H$_{26}$*C*H$_3$); IR v_{max} (NaCl plate, CHCl$_3$): 3339.7, 3282.9, 2963.6, 2919.0, 2850.11, 1686.7, 1625.9, 1570.2, 1464.9, 1381.8, 1362.2, 1247.8, 1169.7, 1057.1, 1032.7 cm^{-1}; HRMS m/z (ESI+) calc. for C$_{36}$H$_{69}$N$_3$O$_9$: 687.5034; found 688.5092 [M+H$^+$].

N^4-[2-*O*-(2,3,4,6-tetra-*O*-acetyl-*β-D*-galactopyranosyl)-ethyl]-N^2-decanoyl-L-asparagine tetradecylamide 3.68.[130]
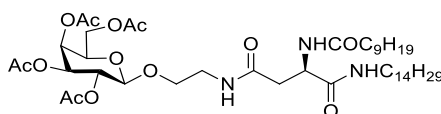
3.68.

HOBt (100 mg, 0.74 mmol, 2 equiv) was added to a stirring solution of butanoic acid, 4-oxo-3[(1-oxodecyl)amino]-4-(tetradecylamino) (3 R) **3.65.** (178 mg, 0.37 mmol, 1 equiv) and TBTU (237 mg, 0.74 mmol, 2 equiv) dissolved in DMF (10 mL), under N$_2$ at 30 °C. The mixture was stirred for 10 min and 2-aminoethyl 2,3,4,6-tetra-O-acetyl-β-D-galactopyranoside **3.47.** (578 mg, 1.47 mmol, 4 equiv) was dissolved in DMF (20 mL) and added dropwise with a cannula. The mixture was stirred overnight at rt. The solvent was removed under reduced pressure and the residue was diluted with DCM

(30 mL) and washed with 0.5 M HCl (30 mL), saturated aqueous NaHCO$_3$ (20 mL) and brine (20 mL). The organic layer was dried over Na$_2$SO$_4$, filtered and the solvent was evaporated under reduced pressure. The crude was purified by column chromatography (Pet Ether:EtOAc, 2:1 to 1:1) to give product **3.68.** as a white solid (238 mg, 75%); R$_f$ = 0.91 (EtOAc); [α]$_D$ = - 12.5 (c 1.0 DCM); ^{1}H NMR (500 MHz, CDCl$_3$): δ 7.41 (d, J = 7.0 Hz, 1 H, N*H*COC$_9$H$_{19}$), 7.09 (t, J = 5.4 Hz, 1 H, CON*H*C$_{14}$CH$_{29}$), 6.35 (t, J = 5.4 Hz, 1 H, CH$_2$CH$_2$N*H*CO), 5.38 (d, J = 3.3 Hz, 1 H, *H*-4), 5.16 (dd, J = 8.1 Hz, J = 10.3 Hz, 1 H, *H*-2), 5.03 (dd, J = 3.3 Hz, J = 10.4 Hz, 1 H, *H*-3), 4.68–4.64 (m, 1 H, *H*-α), 4.52 (d, J = 7.9 Hz, 1 H, *H*-1), 4.19–4.09 (m, 2 H, overlap of *H*-6, *H*-6'), 3.95–3.92 (m, 1 H, *H*-5), 3.88–3.84 (m, 1 H, OC*H*$_2$CH$_2$NH), 3.69–3.65 (m, 1 H, OC*H*$_2$CH$_2$NH), 3.51–3.40 (m, 2 H, OCH$_2$C*H*$_2$NH), 3.20–3.16 (m, 2 H, NHC*H*$_2$C$_{13}$H$_{27}$), *2*.76 (dd, J = 3.4 Hz, J = 15.4 Hz, 1 H, H-β), 2.45 (dd, J = 6.8 Hz, J = 15.3 Hz, 1 H, H-β'), 2.25–2.18 (m, 2 H, COC*H*$_2$C$_8$H$_{17}$), *2*.15, 2.08, 2.03, 1.97 (each s, 3 H, OAc), 1.64–1.58 (m, 2 H, COCH$_2$C*H*$_2$C$_7$H$_{15}$), 1.48–1.42 (m, 2 H, NHCH$_2$C*H*$_2$C$_{12}$H$_{25}$), 1.28-1.22 (m, 34 H, overlap of COC$_2$H$_4$(C*H*$_2$)$_6$CH$_3$, NHC$_2$H$_4$(C*H*$_2$)$_{11}$CH$_3$), 0.86 (t, J = 6.8 Hz, 6 H, overlap of COC$_8$H$_{16}$C*H*$_3$, NHC$_{13}$H$_{26}$C*H*$_3$); ^{13}C NMR (125 MHz, CDCl$_3$): δ 173.6, 171.7, 170.6, 170.4, 170.2, 170.1, 169.9 (each *C*O), 101.3 (*C*-1), 70.8, 70.7 (*C*-5, *C*-3), 69.0 (*C*-2), 68.5 (O*C*H$_2$CH$_2$NH) 67.0 (*C*-4), 61.3 (*C*-6), 49.8 (*C*-α), 39.7 (OCH$_2$*C*H$_2$NH), 39.3 (NH*C*H$_2$C$_{13}$H$_{27}$), 37.0 (*C*-β), 36.6 (CO*C*H$_2$C$_8$H$_{17}$), 31.9, 31.8, 29.7, 29.6, 29.5, 29.4, 29.3, 28.3, 26.9, 25.6, 22.7, 22.6 (COC$_2$H$_4$(*C*H$_2$)$_6$CH$_3$, NHC$_2$H$_4$(*C*H$_2$)$_{11}$CH$_3$), 20.8, 20.7, 20.6, 20.5 (OAc), 14.1, 14.0 (COC$_8$H$_{16}$*C*H$_3$, NHC$_{13}$H$_{26}$*C*H$_3$); IR ν$_{max}$ (NaCl plate, DCM): 3289.7, 3096.6, 2919.3, 2850.8, 1751.4, 1646.5, 1542.2, 1467.4, 1369.7, 1224.0, 1174.9, 1057.9, 906.7, 720.9 cm^{-1}; HRMS m/z (ESI+) calc. for C$_{44}$H$_{77}$N$_3$O$_{13}$: 855.5456 ; found 856.5419 [M+H$^+$].

The spectroscopic data are in agreement with the literature.[130]

N^4-[2-O-($β$-D-galactopyranosyl)-ethyl]-N^2-decanoyl-L-asparagine   tetradecylamide 3.69.[130]
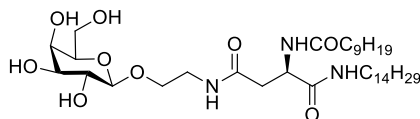
3.69.

NEt_3 (0.4 mL, 2.83 mmol, 5.12 equiv) was added to a stirring solution of N^4-[2-O-(2,3,4,6-tetra-O-acetyl-$β$-D-galactopyranosyl)-ethyl]-N^2-decanoyl-L-asparagine tetradecylamide **3.68.** (473 mg, 0.55 mmol, 1 equiv) dissolved in DCM /MeOH /H_2O (4 mL / 8 mL / 4 mL). The mixture was stirred for 18 h at 40 °C. The reaction mixture was concentrated under reduced pressure to afford product **3.69.** as a white solid (288 mg, 76%); $[α]_D$ = - 6.1 (c 1.0 EtOAc); ^{1}H NMR (500 MHz, d_5-Pyr): δ 8.99 (d, J = 8.1 Hz, 1 H, NHCOC$_9$H$_{19}$), 8.89 (t, J = 5.5 Hz, 1 H, CH$_2$CH$_2$NHCO), 8.57 (t, J = 5.7 Hz, 1 H, CONHC$_{14}$CH$_{29}$), 5.56–5.52 (m, 1 H, H-α), 4.78 (d, J = 7.7 Hz, 1 H, H-1), 4.50–4.36 (m, 4 H, overlap of H-2, H-4, H-6, H-6'), 4.17–4.13 (m, 2 H, overlap of H-3, H-5), 4.09 (t, J = 5.9 Hz, 1 H of OCH_2CH$_2$NH), 3.98–3.94 (m, 1 H, 1 H of OCH_2CH$_2$NH), 3.82–3.74 (m, 1 H, OCH$_2$CH_2NH), 3.68–3.58 (m, 1 H, OCH$_2$CH_2NH), 3.48–3.35 (m, 2 H, NHCH_2C$_{13}$H$_{27}$), 3.16 (td, J = 7.0 Hz, J = 14.9 Hz, 2 H, overlap of H-β, H-β'), 2.39-2.33 (m, 2 H, COCH_2C$_8$H$_{17}$), 1.77–1.70 (m, 2 H, COCH$_2$CH_2C$_7$H$_{15}$), 1.58–1.50 (m, 2 H, NHCH$_2$CH_2C$_{12}$H$_{25}$), 1.32-1.15 (m, 34 H, overlap of COC$_2$H$_4$(CH_2)$_6$CH$_3$, NHC$_2$H$_4$(CH_2)$_{11}$CH$_3$), 0.87-0.82 (m, 6 H, overlap of COC$_8$H$_{16}$CH_3, NHC$_{13}$H$_{26}$CH_3); ^{13}C NMR (125 MHz, d_5-Pyr): δ 174.4, 172.9, 171.9 (each CO), 106.6 (C-1), 77.9, 76.2, 73.5, 71.2 (C-2, C-4, C-3, C-5), 70.6 (OCH$_2$CH$_2$NH), 63.5 (C-6), 53.8 (C-α), 52.2 (OCH$_2$$CH_2$NH), 41.4 (NH$CH_2C_{13}H_{27}$), 40.7 ($C$-β), 39.6, 37.4, 33.0, 32.9, 31.2, 30.9, 30.8, 30.6, 30.5, 30.4, 28.2, 27.0 (each CH$_2$), 23.8 (COC$_8$H$_{16}$$CH_3$), 15.2 (NHC$_{13}H_{26}$$CH_3$); IR v$_{max}$ (NaCl plate, EtOAc): 3303.3, 3065.9, 2922.1, 2852.4, 1693.1, 1654.0, 1539.8, 1466.7, 1450.8, 1391.2, 1363.8, 1296.6, 1242.7, 1194.5, 1157.5, 1085.7, 1032.7, 935.12, 879.5, 800.2, 756.2, 737.7, 670.3 cm^{-1}; HRMS m/z (ESI+) calc. for C$_{36}$H$_{69}$N$_3$O$_9$: 687.5034; found 688.5132 [M+H$^+$].

The spectroscopic data are in agreement with the literature.[130]

N^4-(2,3,4,6-Tetra-*O*-acetyl-*β*-*D*-galactopyranosyl)-*N²*-decanosyl-L/R-aspargine tetradecylamide 3.70.


3.70.

DMTMM (153 mg, 0.55 mmol, 2 equiv) was added to a stirring solution of butanoic acid, 4-oxo-3[(1-oxodecyl)amino]-4-(tetradecylamino) (3 R/S) **3.61.** (133 mg, 0.28 mmol, 1 equiv) dissolved in DMF (10 mL), under N_2 at rt. The mixture was stirred for 10 min and amino-2,3,4,6-tetra-*O*-acetyl-*β*-D-galactopyranoside **3.49.** (115 mg, 0.33 mmol, 1.2 equiv) was dissolved in DMF (20 mL) and added dropwise with a cannula. The mixture was stirred overnight at rt. The solvent was removed under reduced pressure and the residue was diluted with DCM (30 mL) and washed with 0.5 M HCl (30 mL), saturated aqueous $NaHCO_3$ (20 mL) and brine (20 mL). The organic layer was dried over Na_2SO_4, filtered and the solvent was evaporated under reduced pressure. The crude product was purified by column chromatography (Pet Ether:EtOAc; 1:1) to give the product **3.70.** as the four isomeric products (0.4 α-L, 0.9 α-R, 0.9 β-L, 0.4 β-R) (107 mg, 48%); R_f = 0.87 (Pet Ether:EtOAc); ^{1}H NMR (500 MHz, CDCl₃): δ 7.83 (d, *J* = 8.2 Hz, 1 H, N*H*COC₉H₁₉), 7.55 (d, *J* = 7.7 Hz, 1 H, N*H*COC₉H₁₉), 7.46 (d, *J* = 7.2 Hz, 1 H, N*H*COC₉H₁₉), 7.30 (d, *J* = 7.4 Hz, 1 H, N*H*COC₉H₁₉), 6.89 (d, *J* = 7.2 Hz, 1 H, CH₂CH₂N*H*CO), 6.84 (d, *J* = 8.8 Hz, 1 H, CH₂CH₂N*H*CO), 6.79-6.75 (m, 1 H, CON*H*C₁₄CH₂₉ x 2), 5.95-5.93 (m, 1 H, *H*-α (α-L)), 5.88-5.86 (m, 1 H, *H*-α (α-R)), 5.43 (m, 1 H, *H*-4), 5.31-5.29 (m, 1 H, *H*-3), 5.18-5.09 (m, 2 H, overlap of *H*-2, *H*-1), 4.71-4.64 (m, 1 H, *H*-α (β-L and β-R)), 4.16-3.98 (m, 3 H, overlap of *H*-5, *H*-6, *H*-6'), 3.22-3.10 (m, 2 H, OC*H*₂CH₂NH), *2.67* (dd, *J* = 3.5 Hz, *J* = 15.6 Hz, 1 H, H-β x 2), 2.43 (dd, *J* = 5.6 Hz, *J* = 15.6 Hz, 1 H, H-β' x 2), 2.24–2.19 (m, 2 H, COC*H*₂C₈H₁₇), *2.15*, 2.13, 2.02, 1.98 (each s, 3 H, OAc), 1.62–1.58 (m, 2 H, COCH₂C*H*₂C₇H₁₅), 1.47-1.42 (m, 2 H, NHCH₂C*H*₂C₁₂H₂₅), 1.29-1.20 (m, 34 H, overlap of COC₂H₄(C*H*₂)₆CH₃, NHC₂H₄(C*H*₂)₁₁CH₃), 0.87 (t, *J* = 6.9 Hz, 6 H, overlap of COC₈H₁₆C*H*₃, NHC₁₃H₂₆C*H*₃); IR v$_{max}$ (NaCl plate, DCM): 3290.9, 3071.1, 2933.4, 2854.0, 2120.6, 1742.1, 1659.1, 1547.1, 1466.9, 1374.5, 1246.3, 1062.1, 956.5, 909.7, 721.3, 600.6 cm^{-1}; HRMS m/z (ESI+) calc. for C₄₂H₇₃N₃O₁₂: 811.5194 ; found 812.5265 [M+H⁺].

N[4]-(2,3,4,6-Tetra-*O*-acetyl-*β*-*D*-galactopyranosyl)-*N*[2]-decanosyl-L-aspargine tetradecylamide 3.71.[130]

3.71.

HOBt (738 mg, 5.47 mmol, 2 equiv) was added to a stirring solution of butanoic acid, 4-oxo-3[(1-oxodecyl)amino]-4-(tetradecylamino) (3 R) **3.65.** (1.3 g, 2.73 mmol, 1 equiv) and TBTU (1.8 g, 5.47 mmol, 2 equiv) dissolved in DMF (10 mL), under N_2 at 30 °C. The mixture was stirred for 10 min and amino-2,3,4,6-tetra-*O*-acetyl-*β*-D-galactopyranoside **3.49.** (1.7 g, 5.02 mmol, 1.8 equiv) was dissolved in DMF (30 mL) and added dropwise with a cannula. The mixture was stirred overnight at rt. The solvent was removed under reduced pressure and the residue was diluted with DCM (30 mL) and washed with 0.5 M HCl (30 mL), saturated aqueous $NaHCO_3$ (20 mL) and brine (20 mL). The organic layer was dried over Na_2SO_4, filtered and the solvent was evaporated under reduced pressure. The crude product was purified by column chromatography (Tolu:Pet Ether:EtOAc; 1:1:3 to 1:1:2) to give product **3.71.** as a white solid (977 mg, 44%); R_f = 0.47 (Tolu:Pet Ether:EtOAc); $[\alpha]_D$ = + 10 (c 1.0 DCM); ^{1}H NMR (500 MHz, $CDCl_3$): δ 7.55 (d, *J* = 7.7 Hz, 1 H, N*H*COC$_9$H$_{19}$), 6.81 (d, *J* = 8.7 Hz, 1 H, CH$_2$CH$_2$N*H*CO), 6.75 (t, *J* = 5.5 Hz, 1 H, CON*H*C$_{14}$CH$_{29}$), 5.42 (d, *J* = 1.8 Hz, 1 H, *H*-4), 5.23-5.19 (m, 1 H, *H*-1), 5.15-5.09 (m, 2 H, overlap of *H*-2, *H*-3), 4.69–4.66 (m, 1 H, *H*-α), 4.12–3.98 (m, 3 H, overlap of *H*-5, *H*-6, *H*-6'), 3.14–3.10 (m, 2 H, NHC*H*$_2$C$_{13}$H$_{27}$), *2*.66 (dd, *J* = 3.4 Hz, *J* = 15.6 Hz, 1 H, H-β), 2.42 (dd, *J* = 5.7 Hz, *J* = 15.6 Hz, 1 H, H-β'), 2.21–2.17 (m, 2 H, COC*H*$_2$C$_8$H$_{17}$), *2*.13, 2.11, 2.01, 1.97 (each s, 3 H, OAc), 1.62–1.57 (m, 2 H, COCH$_2$C*H*$_2$C$_7$H$_{15}$), 1.44-1.39 (m, 2 H, NHCH$_2$C*H*$_2$C$_{12}$H$_{25}$), 1.28-1.22 (m, 34 H, overlap of COC$_2$H$_4$(C*H*$_2$)$_6$CH$_3$, NHC$_2$H$_4$(C*H*$_2$)$_{11}$CH$_3$), 0.85 (t, *J* = 6.9 Hz, 6 H, overlap of COC$_8$H$_{16}$C*H*$_3$, NHC$_{13}$H$_{26}$C*H*$_3$); ^{13}C NMR (125 MHz, $CDCl_3$): δ 173.7, 172.9, 172.0, 170.4, 170.3, 169.9, 169.8 (each *C*O), 88.2 (*C*-1), 71.1 (*C*-5), 70.8 (*C*-3), 68.7, (*C*-2), 67.2 (*C*-4), 61.4 (*C*-6), 49.7 (*C*-α), 39.6 (NH*C*H$_2$C$_{13}$H$_{27}$), 38.7 (*C*-β), 36.6 (CO*C*H$_2$C$_8$H$_{17}$), 31.9, 31.8, 30.4, 29.7, 29.6, 29.5, 29.4, 29.3, 29.2, 28.9, 26.9, 25.6, 23.7, 22.9, 22.7, 22.6 (COC$_2$H$_4$(*C*H$_2$)$_6$CH$_3$, NHC$_2$H$_4$(*C*H$_2$)$_{11}$CH$_3$), 20.9, 20.8, 20.6, 20.5 (OAc), 14.1, 14.0 (COC$_8$H$_{16}$*C*H$_3$, NHC$_{13}$H$_{26}$*C*H$_3$); IR v$_{max}$ (NaCl plate, DCM): 3281.5, 3078.6, 2924.5,

2854.0, 1751.8, 1640.0, 1546.2, 1466.6, 1437.6, 1370.9, 1228.2, 1121.1, 1085.5, 1055.7, 956.9, 909.6, 721.2, 600.4 cm^{-1}; HRMS m/z (ESI+) calc. for $C_{42}H_{73}N_3O_{12}$: 811.5194 ; found 812.5269 [M+H$^+$].

The spectroscopic data are in agreement with the literature.[130]

N^4-($β$-D-galactopyranosyl)-N^2-decanosyl-L-aspargine tetradecylamide 3.72.[130]

3.72.

NEt$_3$ (0.2 mL, 1.24 mmol, 5.12 equiv) was added to a stirring solution of N^4-(2,3,4,6-Tetra-O-acetyl-$β$-D-galactopyranosyl)-N^2-decanosyl-L-aspargine tetradecylamide **3.71.** (197 mg, 0.24 mmol, 1 equiv) dissolved in DCM / MeOH / H$_2$O (4 mL / 8 mL / 4 mL). The mixture was stirred for 18 h at 40 °C. The reaction mixture was concentrated under reduced pressure to afford product **3.72.** as a white solid (108 mg, 69%); [α]$_D$ = - 3.5 (c 1.0 EtOAc); ^{1}H NMR (500 MHz, d_5-Pyr): δ 10.14 (d, J = 9.0 Hz, 1 H, NHCOCH$_2$), 9.67 (d, J = 8.6 Hz, 1 H, NHCOC$_9$H$_{19}$), 8.62 (t, J = 5.6 Hz, 1 H, CONHC$_{14}$H$_{29}$), 5.43 (d, J = 1.2 Hz, 1 H, H-1), 5.39–5.36 (m, 1 H, H-α), 5.15-5.11 (m, 1 H, H-4), 4.45-4.40 (m, 1 H, H-2), 4.11-4.08 (m, 2 H, H-6, H-6'), 4.02-3.86 (m, 1 H, H-3), 3.74-3.63 (m, 1 H, H-5), 3.20-3.15 (m, 2 H of NHCH_2C$_{13}$H$_{27}$), 2.97-2.78 (m, 2 H, overlap of H-β, H-β'), 1.93-1.90 (m, 2 H of COCH_2C$_8$H$_{17}$), 1.29-1.23 (m, 1 H, COCH$_2$CH_2C$_7$H$_{15}$), 1.10-1.05 (m, 1 H, COCH$_2$CH_2C$_7$H$_{15}$), 0.96-0.91 (m, 2 H, NHCH$_2$CH_2C$_{12}$H$_{25}$), 0.76-0.66 (m, 34 H, overlap of COC$_2$H$_4$(CH_2)$_6$CH$_3$, NHC$_2$H$_4$(CH_2)$_{11}$CH$_3$), 0.38-0.36 (m, 6 H, overlap of COC$_8$H$_{16}$CH_3, NHC$_{13}$H$_{26}$CH_3); ^{13}C NMR (125 MHz, d_5-Pyr): δ 173.4, 171.9, 171.6 (each CO), 81.7 (C-1), 78.2 (C-5), 76.9 (C-3), 71.6 (C-2), 70.3 (C-4), 62.5 (C-6), 54.9 (C-α), 52.8 (NHCH$_2$C$_{13}$H$_{27}$), 51.2 (C-β), 39.7, 38.9, 36.3, 31.8, 29.8, 29.7, 29.6, 29.5, 29.4, 29.3, 29.2, 27.1, 25.9, 25.8 (each CH$_2$), 22.7 (COC$_8$H$_{16}$$CH_3$), 14.0 (NHC$_{13}H_{26}$$CH_3$); IR ν$_{max}$ (NaCl plate, DCM): 3287.8, 2920.2, 2851.2, 1643.7, 1589.3, 1466.0, 1363.4, 1205.3, 1117.5, 1083.7, 811.6 cm^{-1}; HRMS m/z (ESI+) calc. for $C_{34}H_{65}N_3O_8$: 643.4844; found 644.4844 [M+H$^+$].

The spectroscopic data are in agreement with the literature.[130]

7.2.3. Synthetic Experimental Procedures for Chapter 4

3-Ethoxy-4-hexadecylamino-3-cyclobutene-1,2-dione 4.23.[152]

4.23.

Hexadecylamine (1.4 g, 5.9 mmol, 1 equiv) was dissolved in EtOH (10 mL) and added to a stirring solution of 3,4-diethoxy-3-cyclobutene-1,2-dione (0.9 mL, 5.88 mmol) dissolved in EtOH (5 mL). The mixture was stirred overnight at rt. The precipitate formed was filtered and washed with EtOH (30 mL) and diethyl ether (30 mL) to afford product **4.23.** as a white solid which was fully dried under high vacuum (1 g, 49%); R_f = 0.67 (Pet Ether:EtOAc); $[\alpha]_D$ = - 11.8 (c 1.0 DCM); ^{1}H NMR (500 MHz, DMSO): 8.69-8.66 (bs, 1 H, NHCH$_2$), 4.67-4.62 (m, 2 H, OCH_2CH$_3$), 4.34 (s, 2 H, NHCH_2), 3.46-3.42 (m, 6 H, NHCH_2CH_2 CH_2), 1.51-1.48 (m, 2 H, NHCH_2), 1.36 (t, J = 7.0 Hz, 3 H, CH$_2$CH_3); 1.27-1.19 (m, 26 H, NHC$_2$H$_4$(CH_2)$_{13}$CH$_3$), 1.09-1.01 (m, 5 H, NH(CH$_2$)$_{14}$C$_2$$H_5$), 0.85 (t, J = 6.3 Hz, 3 H, CH_3); ^{13}C NMR (125 MHz, DMSO): δ 182.4, 177.1 (each CO), 173.1, 165.5 (each C=C), 69.2 (OCH$_2$CH$_3$), 56.5 (CNH), 44.2 (NHCH$_2$C$_{15}$H$_{31}$), 43.9 (NHCH$_2$$CH_2C_{14}H_{30}$), 31.8, 30.3, 29.5, 29.2, 26.2, 22.6, 19.0 (NHC$_2$H$_4$(CH$_2$)$_{13}$CH$_3$), 16.1 (OCH$_2$$CH_3$), 14.4 (NHC$_{15}H_{30}$$CH_3$); IR v_{max} (KBr disk): 3254.3, 3232.8, 3059.5, 2916.9, 2849.7, 1815.3, 1690.7, 1647.5, 1589.9, 1540.5, 1470.4, 1419.3, 1374.7, 1344.4, 1144.4, 1111.3, 1003.4, 942.4, 903.2, 863.9, 833.2, 821.8, 718.7, 653.3, 601.9, 593.8 cm^{-1}; HRMS m/z (ESI+) calc. for C$_{22}$H$_{39}$NO$_3$: 365.2930 ; found 366.3015 [M+H$^+$].

N^4-[2-O-(2,3,4,6-tetra-O-acetyl-β-D-galactopyranosyl)-ethyl]-N^2-3-4-dioxocyclobut-1-en-1-yl-hexadecylamino 4.24.

4.24.

2-aminoethyl 2,3,4,6-tetra-*O*-acetyl-*β*-*D*-galactopyranoside **3.20.** (463 mg, 1.18 mmol, 2 equiv) was dissolved in EtOH (10 mL) and added to a stirring solution of 3-ethoxy-4-hexadecylamino-3-cyclobutene-1,2-dione **4.23.** (216 mg, 0.59 mmol) in EtOH (10 mL). The reaction mixture was heated until it became a solution and then NEt$_3$ (0.5 mL, 3.55 mmol, 6 equiv) was added. The mixture was stirred overnight at rt. The solvent was removed under reduced pressure. The residue was purified by column chromatography (DCM:MeOH; 95:5) to give product **4.24.** as a white solid (388 mg, 92%); R$_f$ = 0.77 (DCM:MeOH; 95:5); [α]$_D$ = - 6.6 (c 1.0 DCM); ^{1}H NMR (500 MHz, CDCl$_3$): 7.29 (s, 2 H, C*H*$_2$CH$_2$N*H* and N*H*CH$_2$), 5.38 (d, *J* = 2.8 Hz, 1 H, *H*-4), 5.17-5.12 (m, 1 H, *H*-2), 5.01 (dd, *J* = 3.4 Hz, *J* = 10.5 Hz, 1 H, *H*-3), 4.56 (d, *J* = 7.9 Hz, 1 H, *H*-1), 4.18–4.09 (m, 2 H, overlap of *H*-6, *H*-6'), 4.01-3.99 (m, 1 H, OC*H*$_2$CH$_2$NH), 3.95–3.92 (m, 1 H, *H*-5), 3.87–3.76 (m, 3 H, OC*H*$_2$C*H*$_2$NH), 3.66-3.62 (m, 2 H, NH C*H*$_2$), 2.13, 2.03, 2.00, 1.95 (each s, 3 H, OAc), 1.64–1.58 (m, 2 H, NHCH$_2$C*H*$_2$), 1.37-1.23 (m, 26 H, NHC$_2$H$_4$(C*H*$_2$)$_{13}$CH$_3$), 0.85 (t, *J* = 6.9 Hz, 3 H, C*H*$_3$); ^{13}C NMR (125 MHz, CDCl$_3$): δ 182.8, 182.4, 170.5, 170.4, 170.1, 169.9 (each *C*O), 168.1, 167.8 (each *C*=*C*), 101.4 (*C*-1), 70.9, 70.8 (*C*-5, *C*-3), 69.2 (*C*-2), 68.9 (O*C*H$_2$CH$_2$NH) 67.0 (*C*-4), 61.3 (*C*-6), 44.7 (OCH$_2$*C*H$_2$NH), 43.8 (NH*C*H$_2$C$_{15}$H$_{31}$), 31.9, 31.3, 31.2, 29.7, 29.6, 29.5, 29.4, 29.3, 29.2, 26.6, 26.3, 23.2, 22.7 (NHC$_2$H$_4$(*C*H$_2$)$_{13}$CH$_3$), 20.8, 20.7, 20.6, 20.5 (OAc), 14.1 (NHC$_{15}$H$_{30}$*C*H$_3$); IR ν$_{max}$ (NaCl plate, DCM): 3173.9, 2955.8, 2917.1, 2849.9, 2117.1, 1801.0, 1751.6, 1649.1, 1578.5, 1470.5, 1437.1, 1370.6, 1227.2, 1175.5, 1133.5, 1059.4, 956.9, 906.7, 736.6 cm^{-1}; HRMS m/z (ESI+) calc. for C$_{36}$H$_{58}$N$_2$O$_{12}$: 710.4063; found 711.4083 [M+H$^+$].

N^4-[2-O-($β$-D-galactopyranosyl)-ethyl]-N^2-3-4-dioxocyclobut-1-en-1-yl-hexadecylamino 4.25.

4.25.

NEt$_3$ (0.3 mL, 2 mmol, 5.12 equiv) was added to a stirring solution of N^4-[2-O-(2,3,4,6-tetra-O-acetyl-$β$-D-galactopyranosyl)-ethyl]-N^2-3-4-dioxocyclobut-1-en-1-yl-hexadecylamino **4.24.** (335 mg, 0.39 mmol, 1 equiv) dissolved in DCM / MeOH / H$_2$O (3 mL / 6 mL /3 mL). The mixture was stirred for 18 h at 40 °C. The reaction mixture was concentrated under reduced pressure to afford product **4.25.** as a white solid (288 mg, 98%); [α]$_D$ = 0 (c 1.0 EtOH); ^{1}H NMR (500 MHz, DMSO): 7.50 (s, 2 H, overlap of CH_2CH_2NH and NHCH$_2$), 4.82 (d, J = 4.1 Hz, 1 H, OH), 4.74 (d, J = 5.0 Hz, 1 H, OH), 4.68-4.64 (m, 1 H, OH), 4.39 (d, J = 4.3 Hz, 1 H, OH), 4.13 (d, J = 7.4 Hz, 1 H, H-1), 3.84–3.79 (m, 1 H, OCH_2CH$_2$NH), 3.73-3.62 (m, 4 H, overlap of OCH_2CH_2NH and H-5), 3.54-3.44 (m, 4 H, overlap of NHCH_2, H-6 and H-6'), 3.40-3.25 (m, overlap of H$_2$O signals, H-2, H-3 and H-4), 1.51-1.48 (m, 2 H, NHCH$_2$CH_2), 1.26-1.23 (m, 26 H, NHC$_2$H$_4$(CH_2)$_{13}$CH$_3$), 0.85 (t, J = 7.1 Hz, 3 H, CH_3); ^{13}C NMR (125 MHz, DMSO): δ 182.9, 182.8 (each CO), 172.4, 168.0 (each C=C), 104.4 (C-1), 75.8, 73.8, 70.9 (C-4, C-3, C-2), 69.4 (OCH$_2$CH$_2$NH) 68.6 (C-5), 60.9 (C-6), 44.1 (OCH$_2$$CH_2$NH), 43.7 (NH$CH_2C_{15}H_{31}$), 31.7, 31.3, 31.2, 29.7, 29.6, 29.5, 29.4, 29.3, 29.2, 29.1, 26.6, 26.3, 22.6 (NHC$_2$H$_4$(CH$_2$)$_{13}$CH$_3$), 14.4 (NHC$_{15}$H$_{30}$$CH_3$); IR v$_{max}$ (KBr disk): 3449.2, 3232.5, 2917.8, 2850.7, 1796.9, 1641.4, 1570.9, 1470.5, 1425.2, 1349.7, 1171.2, 1077.8, 899.8, 779.6, 718.9, 603.6 cm^{-1}; HRMS m/z (ESI+) calc. for C$_{28}$H$_{50}$N$_2$O$_8$: 542.3567 ; found 543.3646 [M+H$^+$].
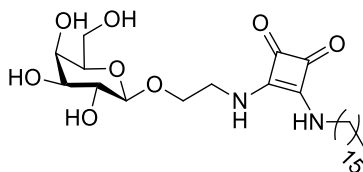
7.3. Experimental Procedures for Preparation and Gel Characterisation Measurements

7.3.1. Preparation of the Gels

The gelator (20 mg, unless otherwise specified) was mixed with the required solvent (1 mL) in a glass vial with a lid (specimen tube soda glass 75 x 25 mm. 30 mL). The

mixture was heated slowly (under the boiling point of the solvent to prevent build-up of pressure inside the vial or solvent evaporation) and/or sonicated for 1 min until the gelator was completely dissolved. The vial was then placed horizontally and was allowed to cool to rt. After 2 h, the gelation was checked visually by inversion of the vial (inverted test tube method)[55]. Gel formation was considered to have occurred if no flow was observed upon vial inversion.

7.3.2. Determination of Critical Gel Concentration (CGC)

The minimal gel concentration required for the gelator to entrap the required solvent was defined as CGC, which was determined as follows: to a solution of gelator (20 mg) in a given solvent (1 mL), 0.2 mL aliquots of the solvent were added. For each aliquot the sample was heated and/or sonicated, then allowed to cool to rt. The gelation was then evaluated by the inverted test tube method to ascertain if the solvent was flowing freely. This process was repeated until partial gelation occurred or until the inverted test tube method showed free flowing solvent. In the latter case, the CGC was calculated by dividing 20 mg by the volume of solvent used to form the gel. The units used to express this CGC value was w/v %.

7.3.3. Determination of the Transition Temperature from Gel to Solution Phase (T_{gs})

The transition temperature from gel to solution (T_{gs}) was determined by heating the gel sample and monitoring the temperature of the melting process. The gel at the CGC was formed in a vial (specimen tube soda glass 75 x 25 mm. 30 mL) which was left 96 h at rt to allow for stabilisation of the three dimensional network prior to tests. A water bath between 0 – 5 °C (temperature determined by the freezing point of the required solvent) was heated and stirred on a hot plate. The vial containing the formed gel was placed in the water, without touching the bottom of the bath (Figure 7.1.). The temperature range at which free flow of solvent was first observed until all the gel was in the solution phase was recorded.
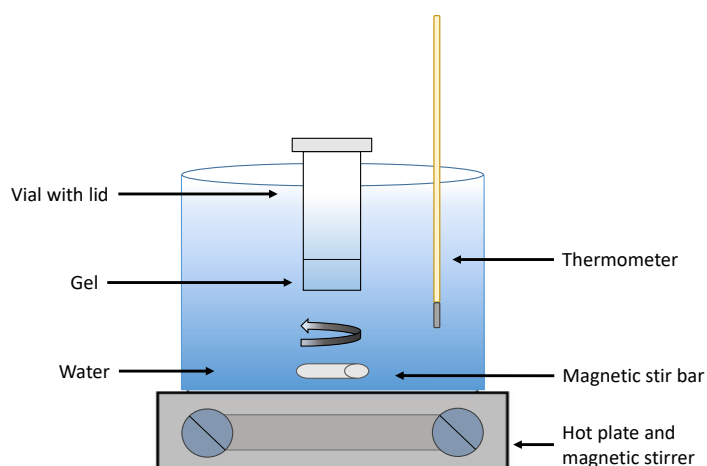
Figure 7.1. Schematic representation of the T_{gs} determination set-up.

7.3.4. Rheological Evaluation

Rheological characterisation was carried out using a controlled stress rheometer (MCR 301, Anton Paar, Austria) with parallel plates (15 mm diameter, 0.5 mm gap) at selected temperature always between 10 – 15 °C under the T_{gs} ($\pm$ 0.1 °C). Gels to be tested were placed between the plates and the excess volume of sample was trimmed and the edge was coated with paraffin (Figure 7.2.) to prevent solvent evaporation during the measurement. A rest time of 15 min was applied to all samples prior to any measurements.
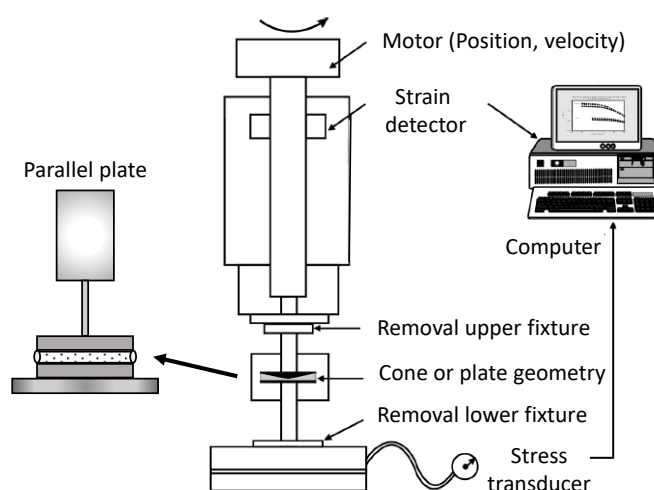
Figure 7.2. Schematic representation of a modern controlled strain rheometer with parallel plate geometry.[31]

The linear viscoelastic region (LVER) was determined by means of a strain sweep (γ, 0.01 – 1 %) at a frequency of 1 Hz. The mechanical spectra of gels were obtained by frequency sweep test or SAOS from 0.1 to 100 rad/s of angular frequency (ω) at 0.1 % strain (inside the LVER of the samples) to determine the storage, G' (Pa) and loss, G'' (Pa) modulus and the loss tangent (tan δ = G''/G').

7.3.5. Gel Thermoreverisibility Evaluation by Differential Scanning Calorimetry (DSC) Measurements.

The thermal reversibility of gels were investigated by DSC under a nitrogen atmosphere. DSC traces were recorded for heating / cooling cycles to identify melting and the formation temperature of the gel in a reversible process. The temperature ranges for the experiments were decided based on the previously calculated T_{gs} and the boiling point of the solvent. Temperature cycles were at a constant rate of 2 °C/min. Stainless steel pans of medium pressure were used for the gels tested. A small quantity of the gel (20 – 40 mg) made at the CGC in a closed vial was transferred with a spatula to the pan which was closed under pressure. A reference pan was filled with the gelation solvent alone.

7.3.6. Preparation of Xerogels for X-Ray Powder Diffraction, DSC and SEM Analysis

7.3.6.1. X-Ray Powder Diffraction Analysis of Xerogels

Xerogels for X-Ray diffraction (XRD) analysis were prepared by forming the gels at CGC with the required solvent in a closed vial. The solvent was allowed to evaporate slowly at rt until the xerogel was formed, without preventing shrinkage.

7.3.6.2. DSC Analysis of Xerogels

Xerogels were prepared before being scanned as described in the above section 7.3.6.1. Then they were placed in aluminium pans and DSC traces were measured under a nitrogen atmosphere. DSC traces were recorded between 25 – 150 °C at a constant rate of 5 °C/min.

7.3.6.3. SEM Imaging of Xerogels

The morphologies of the xerogels were characterised using SEM. A small quantity of the gel made at the CGC with the required solvent in a closed vial was transferred with a spatula to the metal stub (previously prepared with a double-sided adhesive

tape which was a conductive carbon tab). The xerogel was formed on the stub by allowing evaporation of the solvent.

7.4. Spectroscopic Analysis of the Gelation Process

7.4.1. ^{1}H-NMR Spectroscopic Analysis

^{1}H NMR spectra were recorded at increasing concentrations of the gelator in the relevant deuterated solvent or at a fixed concentration and variable temperature as specified in each experiment. The comparable increments in chemical shift ($\Delta\delta$) observed following changes in gelator concentration or temperature suggested the formation or destruction of intermolecular H-bonding.[47]

7.4.2. FTIR Spectroscopic Analysis

FT-IR was recorded at different sample states (from solution to gel) and at increasing time from 0 min (when the gelator was in a warm solution at CGC in the required solvent) and X-end min (when the gel was formed and subsequently allowed to cool). Measurements were recorded between T_{gs} and rt every 5 min until no further changes could be observed as specified in each experiment. Experiments were carried out in a closed cell or in an universal attenuated total reflection (ATR) accessory (diamond crystal) for liquids. The sample handling techniques were chosen depending on the solvent to prevent evaporation during the gelation process. Spectra were recorded between 4000 and 400 cm^{-1} from warm solution (gelator totally soluble in the solvent) to rt.

7.5. Removal of Toxic Dyes by Biphasic Gelation

UV-Vis absorption spectra were recorded using 1 cm quartz cuvettes. Calibration curves for the cationic dye RhB and the anionic dye Methyl orange were calculated prior to starting experiments.

7.6. Preparation of Electrospun Materials

Commercially available PCL [Sigma - Aldrich. M_n 70.000 – 90.000 (CAS: 24980-41-4)] was dissolved in CHCl$_3$:EtOH (75:25) to prepare a 10 w/v % stock solution. The polymer pellets (1 g) were dissolved in chloroform (7.5 mL). The solution was stirred

overnight at rt in a closed vial. EtOH (2.5 mL) was added to the CHCl$_3$ solution and the mixture was stirred for further 1 - 2 h until a clear viscous solution was obtained.[280]

The electrospinning set up utilised in this thesis consisted of a syringe (10 mL) and a blunt-end stainless steel needle (18 Ga. 51 mm / pst3. HAMILTON), a syringe pump (IVAC P3000) with a flow rate from 1 to 6 mL/h, a ground electrode and a high voltage supply (0 - 20 kV) (Figure 7.3.).
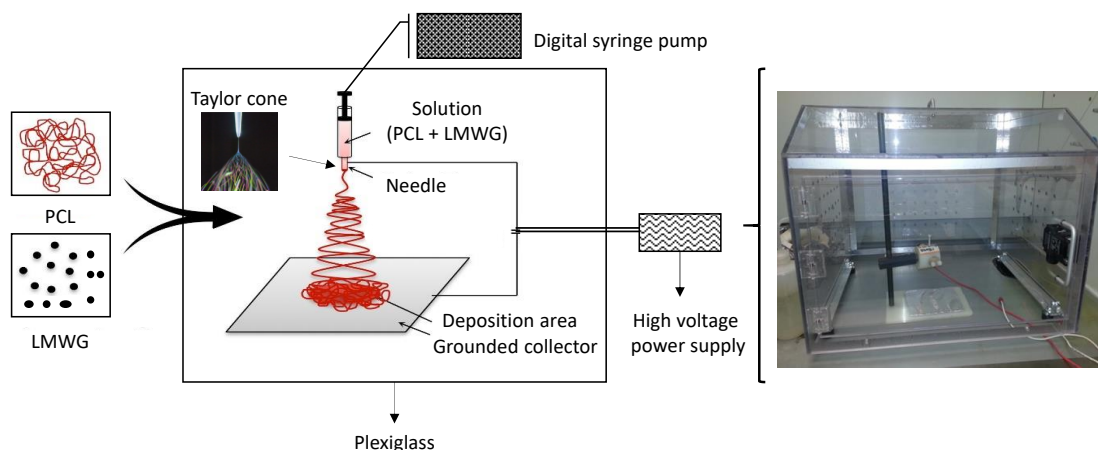
Figure 7.3. Schematic diagram of the electrospinning set-up.

Solutions were placed in a 10 mL syringe connected to the needle through a plastic tube. The syringe pump was used to control the flow rate of the solution through the needle spinneret. The flow rate was set between 1 to 6 mL/h, as specified in each experiment. The steel needle was connected to an electrode of a high voltage power supply and a grounded copper plate covered with aluminium foil as the collector. The collector was placed at a distance of 6 cm from the needle tip to collect the microfibres or ultrafine fibres. The positive voltage applied to the polymer solutions varied between 13 and 18 kV depending on the experiment. All the experiments were carried out at rt. After electrospinning the samples were dried in a vacuum desiccator at 833.3 mbar for 24 h.

7.6.1. Preparation of Electrospun Samples for DSC, SEM, Optical Microscope, Contact Angle and ATR Analysis

7.6.1.1. DSC Analysis

A small quantity of the sample, between 10 - 20 mg was placed in an aluminium pan and closed with a lid under pressure. An empty aluminium pan was used as a

reference. DSC traces were recorded under a nitrogen atmosphere in a heating cycle between 25 - 120 °C at a constant rate of 5 °C/min.

7.6.1.2. SEM Imaging

The morphology of the electrospun fibres was characterised using SEM. Samples were spun directly onto a SEM metal stub covered with a double-sided adhesive tape which was a conductive carbon tab. After electrospinning the samples were dried in a vacuum desiccator at 833.3 mbar for 24 h before analysis. If required, the samples were sputter-coated with a layer of gold.

7.6.1.3. Optical Microscope Imaging

The diameters of the electrospun fibres were estimated using an optical microscope. Samples were spun directly onto a glass slide. After electrospinning the samples were allowed to dry in a vacuum desiccator at 833.3 mbar for 24 h before analysis.

7.6.1.4. Contact Angle Analysis

The surface wettability of ultrafine electrospun fibres was determined by contact angle measurements. Samples were electrospun on a glass slide and allowed to dry in a vacuum desiccator at 833.3 mbar for 24 h before analysis. FTA1000 Drop Shape Analyser was equipped with a USB camera and fixed zoom optics and a simple manual stage and fluid dispenser. A drop of deionised water was deposited from a needle (diameter used was 0.047 in / 1.194 mm), provided by Kahnetics stainless steel, on the sample and a picture of the drop was taken 30 sec after the drop set onto the sample. The contact angle could be calculated by analysing the shape of the drop with "FTA32" software. Three replicates per sample were expressed as mean ± standard error.

7.6.1.5. ATR Analysis

The FT-IR spectra of ultrafine electrospun fibres were obtained with a Perkin Elmer Precisely (Spectrum 100) using a universal attenuated total reflection (ATR) accessory (diamond crystal) for polymers. Spectra were recorded between 4000 and 600 cm^{-1} at rt. The matt of fibres was placed on the diamond crystal, closed and scanned.

7.7. Crystallography

Crystals for X-Ray crystallographic analysis were prepared as follows: A small quantity of the compound was placed in a clean vial with a rubber lid which had a needle (specimen tube soda glass 50 x 10 mm. 2 mL). The compound was fully dissolved in the minimum amount of solvent (EtOAc). The mixture was heated and sonicated. This vial was placed inside a larger vial (specimen tube soda glass 75 x 25 mm. 30 mL) containing a solvent in which the compound was insoluble (Diethyl ether). After adding the solvent the vial was fully sealed with a lid and parafilm. Both vials were placed horizontally and not disturbed. After a week the crystals began to appear. They were taken for X-Ray analysis in the mother liquor. This technique is known as vapour diffusion (Figure 7.4.).
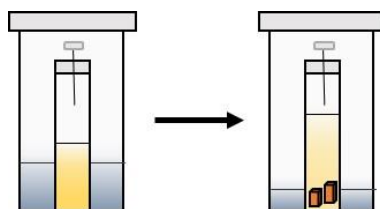
Figure 7.4. Schematic representation of the vapour diffusion set-up for growing crystals.

Bibliography

Bibliography

(1)   Miravet, J. F.; Escuder, B. *Supramol. Syst. Biomed. Fields,* **2013**, 331-354.

(2)   Steed, J. W. *Chem. Commun. (Cambridge, England),* **2011**, *47*, 1379-1383.

(3)   Yan, J.; Wong, B. S.; Kang, L. *Soft Fibrillar Mater.: Fabr. and Appl. (Chapter 4),* **2013**, 129-162.

(4)   Marr, P. C.; Marr, A. C. *Green Chem.,* **2015**, 105-128.

(5)   Sangeetha, N. M.; Maitra, U. *Chem. Soc. Rev.,* **2005**, *34*, 821-836.

(6)   Roy, S.; Chakraborty, A.; Chattopadhyay, B.; Bhattacharya, A.; Mukherjee, A. K.; Ghosh, R. *Tetrahedron,* **2010**, *66*, 8512-8521.

(7)   Pal, A.; Mahapatra, R. D.; Dey, J. *Langmuir,* **2014**, *30*, 13791-13798.

(8)   Lipowitz, V. *Ann. Chem. Pharm.,* **1841**, *38*, 348-355.

(9)   Hirst, A. R.; Escuder, B.; Miravet, J. F.; Smith, D. K. *Angew. Chem. Int. Ed.,* **2008**, *47*, 8002-8018.

(10)   Aida, T.; Meijer, E. W.; Stupp, S. I. *Science,* **2012**, *335*, 813-817.

(11)   Yoshii, T.; Onogi, S.; Shigemitsu, H.; Hamachi, I. *J. Am. Chem. Soc.,* **2015**, 3360-3365.

(12)   Duan, P.; Yanai, N.; Nagatomi, H.; Kimizuka, N. *J. Am. Chem. Soc.,* **2015**, *137*, 1887-1894.

(13)   Zhang, X.; Lee, S.; Liu, Y.; Lee, M.; Yin, J.; Sessler, J. L.; Yoon, J. *Sci. Rep.,* **2014**, *4*, 1-8.

(14)   Yao, X.; Wu, S.; Chen, L.; Ju, J.; Gu, Z.; Liu, M.; Wang, J.; Jiang, L. *Angew. Chem.,* **2015**, *127*, 9103-9107.

(15)   Okesola, B. O.; Suravaram, S. K.; Parkin, A.; Smith, D. K. *Angew. Chem. Int. Ed.,* **2015**, *54*, 1-6.

(16)   Skilling, K. J.; Citossi, F.; Bradshaw, T. D.; Ashford, M.; Kellam, B.; Marlow, M. *Soft Matter,* **2014**, *10*, 237-256.

(17)   Afrasiabi, R.; Kraatz, H.-B. *Chem. Eur. J.,* **2015**, *21*, 1-7.

(18)   Yu, H.; Lü, Y.; Chen, X.; Liu, K.; Fang, Y. *Soft matter,* **2014**, *10*, 9159-9166.

(19)   Yan, X.; Wang, F.; Zheng, B.; Huang, F. *Chem. Soc. Rev.,* **2012**, *41*, 6042-6065.

(20)   Aggeli, A.; Nyrkova, I. A.; Bell, M.; Harding, R.; Carrick, L.; McLeish, T. C. B.; Semenov, A. N.; Boden, N. *Proc. Natl. Acad. Sci.,* **2001**, *98*, 11857-11862.

(21)   Jang, K.; Ranasinghe, A. D.; Heske, C.; Lee, D. C. *Langmuir,* **2010**, *26*, 13630-13636.

(22)   Yu, G.; Yan, X.; Han, C.; Huang, F. *Chem. Soc. Rev.,* **2013**, *42*, 6697-6722.

(23)   Piepenbrock, M. O. M.; Lloyd, G. O.; Clarke, N.; Steed, J. W. *Chem. Rev.,* **2010**, *110*, 1960-2004.

(24)   Jung, J. H.; John, G.; Masuda, M.; Yoshida, K.; Shinkai, S.; Shimizu, T. *Langmuir,* **2001**, *17*, 7229-7232.

(25)   Zhao, X.; Wang, X. Z.; Jiang, X. K.; Chen, Y. Q.; Li, Z. T.; Chen, G. J. *J. Am. Chem. Soc.,* **2003**, *125*, 15128-15139.

(26)   Sengupta, S.; Mondal, R. *RSC Adv.,* **2016**, *6*, 14009-14015.

(27)   Sahoo, P.; Sankolli, R.; Lee, H. Y.; Raghavan, S. R.; Dastidar, P. *Chem. Eur. J.,* **2012**, *18*, 8057-8063.

(28)   Rajkamal, R.; Chatterjee, D.; Paul, A.; Banerjee, S.; Yadav, S. *Chem. Commun.,* **2014**, *50*, 12131-12134.

(29)   Yuan, J.; Fang, X.; Zhang, L.; Hong, G.; Lin, Y.; Zheng, Q.; Xu, Y.; Ruan, Y.; Weng, W.; Xia, H.; Chen, G. *J. Mater. Chem.,* **2012**, *22*, 11515-11522.

(30)   Yuan, D.; Du, X.; Shi, J.; Zhou, N.; Zhou, J.; Xu, B. *Angew. Chem. Int. Ed.,* **2015**, *54*, 5705-5708.

(31)   Picout, D. R.; Ross-Murphy, S. B. *Sci. World J.,* **2003**, *3*, 105-121.

(32)   Tadros, T. F. *Chapter 7. Rheol. Dispersion. Wiley-VCH Verlag GmbH & Co. KGaA,* **2010**, 149–167.

(33)   B., W.; Pyda, M. *J. Reinf. Plast. Comp.,* **1999**, *18*, 487-498.

(34)   Ghini, G.; Lascialfari, L.; Vinattieri, C.; Cicchi, S.; Brandi, A.; Berti, D.; Betti, F.; Baglioni, P.; Mannini, M. *Soft Matter,* **2009**, *5*, 1863-1869.

(35)   Lascialfari, L.; Pescitelli, G.; Brandi, A.; Mannini, M.; Berti, D.; Cicchi, S. *Soft Matter,* **2015**, *11*, 8333-8341.

(36)   Bairi, P.; Chakraborty, P.; Mondal, S.; Roy, B.; Nandi, A. K. *Soft Matter,* **2014**, *10*, 5114-5120.

(37)   Mitchell, G. R.; Windle, A. H. *Polym.,* **1984**, *25*, 906-920.

(38)   Park, T.; Zimmerman, S. C.; Nakashima, S. *J. Am. Chem. Soc.,* **2005**, *127*, 6520-6521.

(39)   Ding, W.; Wada, M.; Minamikawa, H.; Kameta, N.; Masuda, M.; Shimizu, T. *Chem. Commun. (Cambridge, England),* **2012**, *48*, 8625-8627.

(40)   Park, T.; Zimmerman, S. C. *J. Am. Chem. Soc.,* **2006**, *128*, 13986-13987.

(41)   Kölbel, M.; Menger, F. M. *Langmuir,* **2001**, *17*, 4490-4492.

(42)   Cheng Wang; Deqing Zhang, a.; Daoben Zhu* *J. Am. Chem. Soc. Commun.,* **2005**, *127*, 16372-16373.

(43)   Wang, C.; Zhang, D.; Zhu, D. *Langmuir,* **2007**, *23*, 1478-1482.

(44)   Shen, J.-S.; Mao, G.-J.; Zhou, Y.-H.; Jiang, Y.-B.; Zhang, H.-W. *Dalton Trans.,* **2010**, *39*, 7054-7058.

(45)   Rodriguez-Llansola, F.; Hermida-Merino, D.; Nieto-Ortega, B. n.; Ramirez, F. J.; Navarrete, J. T. L. p.; Casado, J.; Hamley, I. W.; Escuder, B.; Hayes, W.; Miravet, J. F. *Chem. Eur. J.,* **2012**, *18*, 14725-14731.

(46)   Smith, D. K. *Supramol. Chem.,* **2012**, 1-22.

(47)   Liu, Y.; Wang, Y.; Jin, L.; Chen, T.; Yin, B. *Soft Matter,* **2016**, *12*, 934-945.

(48)   Shapiro, Y. E. *Progr. Polym. Sci. (Oxford),* **2011**, *36*, 1184-1253.

(49)   Escuder, B.; Llusar, M.; Miravet, J. F. *J. Org. Chem.,* **2006**, *71*, 7747-7752.

(50)   Hirst, A. R.; Coates, I. A.; Boucheteau, T. R.; Miravet, J. F.; Escuder, B.; Castelletto, V.; Hamley, I. W.; Smith, D. K. *J. Am. Chem. Soc.,* **2008**, *130*, 9113-9121.

(51)   Simon, F.-X.; Nguyen, T. T. T.; Díaz, N.; Schmutz, M.; Demé, B.; Jestin, J.; Combet, J.; Mésini, P. J. *Soft Matter,* **2013**, *9*, 8483-8493.

(52)   Bastiat, G.; Leroux, J.-C. *J. Mater. Chem.,* **2009**, *19*, 3867-3877.

(53)   Suzuki, M.; Yumoto, M.; Shirai, H.; Hanabusa, K. *Chem. Eur. J.,* **2008**, *14*, 2133-2144.

(54)   Nebot, V. J.; Armengol, J.; Smets, J.; Prieto, S. F.; Escuder, B.; Miravet, J. F. *Chem. Eur. J.,* **2012**, *18*, 4063-4072.

(55)   Tanigami, T.; Suzuki, H.; Yamaura, K.; Matsuzawa, S. *Macromol.,* **1985**, *18*, 2595-2600.

(56)   Zurcher, D. M.; McNeil, A. J. *J. Org. Chem.,* **2015**, *80*, 2473-2478.

(57)   Tomasini, C.; Castellucci, N. *Chem. Soc. Rev.,* **2013**, 156-172.

(58)   Duan, P.; Cao, H.; Zhang, L.; Liu, M. *Soft Matter,* **2014**, *10*, 5428-5448.

(59)   Ahmed, S.; Mondal, J. H.; Behera, N.; Das, D. *Langmuir,* **2013**, *29*, 14274-14283.

(60)   Hartgerink, J. D.; Beniash, E.; Stupp, S. I. *Science,* **2001**, *294*, 1684-1688.

(61)   Ghosh, A.; Dey, J. *Langmuir,* **2009**, *25*, 8466-8472.

(62)   Mallia, V. A.; George, M.; Blair, D. L.; Weiss, R. G. *Langmuir,* **2009**, *25*, 8615-8625.

(63)   Zhang, M.; Selvakumar, S.; Zhang, X.; Sibi, M. P.; Weiss, R. G. *Chem. Eur. J.,* **2015**, *21*, 8530-8543.

(64)   Das, A. K.; Collins, R.; Ulijn, R. V. *Small,* **2008**, *4*, 279-287.

(65)   Jayawarna, V.; Richardson, S. M.; Hirst, A. R.; Hodson, N. W.; Saiani, A.; Gough, J. E.; Ulijn, R. V. *Acta Biomater.,* **2009**, *5*, 934-943.

(66)   Jayawarna, V.; Smith, A.; Gough, J. E.; Ulijn, R. V. *Biochem. Soc. Trans.,* **2007**, *35*, 535-537.

(67)   Li, X.; Li, J.; Gao, Y.; Kuang, Y.; Shi, J.; Xu, B. *J. Am. Chem. Soc.,* **2010**, *132*, 17707-17709.

(68)   Kuang, Y.; Gao, Y.; Zhang, Y.; Gao, P.; Xu, B. *J. Am. Chem. Soc.,* **2010**, *132*, 2719-2728.

(69)   Yan, X.; Zhu, P.; Li, J. *Chem. Soc. Rev.,* **2010**, *39*, 1877-1890.

(70)   Reddy, S. M. M.; Shanmugam, G.; Duraipandy, N.; Kiran, M. S.; Mandal, A. B. *Soft Matter,* **2015**, *11*, 8126-8140.

(71)   Raeburn, J.; Pont, G.; Chen, L.; Cesbron, Y.; Lévy, R.; Adams, D. J. *Soft Matter,* **2012**, *8*, 1168-1174.

(72)   Draper, E. R.; Morris, K. L.; Little, M. a.; Raeburn, J.; Colquhoun, C.; Cross, E. R.; McDonald, T. O.; Serpell, L. C.; Adams, D. J. *CrystEngComm,* **2015**, *17*, 8047-8057.

(73)   Reches, M.; Gazit, E. *Isr. J. Chem.,* **2005**, *45*, 363-371.

(74)   Mahler, A.; Reches, M.; Rechter, M.; Cohen, S.; Gazit, E. *Adv. Mater.,* **2006**, *18*, 1365-1370.

(75)   Mishra, A.; Clark, J. *Chapter 1: Green Mater. Sustain. Water Rem. Treat.,* **2013**, 1-10.

(76)   Readman, J. W. *Intro. Pollut. Sci.,* **2006**, 77-121.

(77)   Babel, S.; Kurniawan, T. A. *J. hazard. Mater.,* **2003**, *97*, 219-243.

(78)   Gupta, V. K.; Suhas *J. Environ. Manage.,* **2009**, *90*, 2313-2342.

(79)   Ohsedo, Y. *Polym. Adv. Technol.,* **2016**, *27*, 704-711.

(80)   Yu, X.; Chen, L.; Zhang, M.; Yi, T. *Chem. Soc. Rev.,* **2014**, *43*, 5346-5371.

(81)   Mukherjee, S.; Shang, C.; Chen, X.; Chang, X.; Liu, K.; Yu, C.; Fang, Y. *Chem. Commun.,* **2014**, *50*, 13940-13943.

(82)   Moreno, R.; Jover, L.; Diez, C.; Sardà, F.; Sanpera, C. *PLOS ONE,* **2013**, *8*, 1-10.

(83)   Ghaly, A. E.; Dave, D. *Am. J. Environ. Sci.,* **2011**, *7*, 423-440.

(84)   Prendergast, D. P.; Gschwend, P. M. *Assess. perform. cost oil spill remed. technol,* **2014**, *78*, 233-242.

(85)   Liu, K.; He, P.; Fang, Y. *Sci. China Chem.,* **2011**, *54*, 575-586.

(86)   Okesola, B. O.; Smith, D. K. *Chem. Soc. Rev.,* **2016**, 4226-4251.

(87)   *USEPA-Water qual. offi. Gelling crude oils reduc. mar. pollut. tanker oil spills. Water pollut. control res. ser. 15080DJN 1/71, U.S. govern. pr. office, Washington D.C. 20402,* **1971**.

(88)   Saito, T.; Matsuzawa, Y.; Ninagawa, S.; Honna, M.; Takesada, M.; Takehara, M. *Patent. U.S. 3969087,* **1976**.

(89)   Bhattacharya, S.; Krishnan-Ghosh, Y. *Chem. Commun.,* **2001**, 185-186.

(90)   Hai, F. I.; Yamamoto, K.; Fukushi, K.; Hai, F. I. *Crit. Rev. Env. Sci. Technol.,* **2007**, *37*, 315-377.

(91)   Zweep, N.; van Esch, J. H. *Funct. Mol. Gels,* **2014**, 1-29.

(92)   zhang, y.; Ma, Y.; Deng, M.; shang, h.; Liang, C.; Jiang, S. *Soft Matter,* **2015**, *11*, 5095-5100.

(93)   Wang, Y.; Liu, Y.; Jin, L.; Yin, B. *Soft Matter,* **2016**, *12*, 6373-6384.

(94)   Babu, S. S.; Praveen, V. K.; Ajayaghosh, A. *Chem. Rev.,* **2014**, *114*, 1973-2129.

(95)   Fleming, S.; Ulijn, R. V. *Chem. Soc. Rev.,* **2014**, *43*, 8150-8177.

(96)   Xie, Y.; Wang, X.; Huang, R.; Qi, W.; Wang, Y.; Su, R.; He, Z. *Langmuir,* **2015**, *31*, 2885-2894.

(97)   Han, S. Y.; Kim, Y. A. *Tetrahedron,* **2004**, *60*, 2447-2467.

(98)   Han, S.-Y. K., Y.-A. *Pol. J. Chem.,* **1982**, *56*, 1067-1070.

(99)   Kar, T.; Mandal, S. K.; Das, P. K. *Chem. Eur. J.,* **2011**, *17*, 14952-14961.

(100)   Bonnet, J.; Suissa, G.; Raynal, M.; Bouteiller, L. *Soft Matter,* **2015**, *11*, 2308-2312.

(101)   Fukunaga, K.; Yoshida, M.; Nakajima, F.; Uematsu, R.; Hara, M.; Inoue, S.; Kondo, H.; Nishimura, S. I. *Bioorg. Med. Chem. Lett.,* **2003**, *13*, 813-815.

(102)   Yang, L.; Brazier, J. B.; Hubbard, T. A.; Rogers, D. M.; Cockroft, S. L. *Angew. Chem. Int. Ed.,* **2016**, *55*, 912-916.

(103)   Starkova, O.; Aniskevich, A. *Mech. Time-Depend. Mat.,* **2007**, *11*, 111-126.

(104)   Bourne, M. C. *Elsevier Science & Technology Books,* **2002**, 1-423.

(105)   Dahan, E.; Sundararajan, P. R. *Langmuir,* **2013**, *29*, 8452-8458.

(106)   Terech, P.; Weiss, R. G. *Chem. Rev.,* **1997**, *97*, 3133-3160.

(107)   Wang, G.; Hamilton, A. D. *Chem. Eur. J.,* **2002**, *8*, 1954-1961.

(108)   González-Rodríguez, D.; Schenning, A. P. H. J. *Chem. Mater.,* **2011**, *23*, 310-325.

(109)   Cao, H.; Yuan, Q.; Zhu, X.; Zhao, Y. P.; Liu, M. *Langmuir,* **2012**, *28*, 15410-15417.

(110)   Serrano, V.; Liu, W.; Franzen, S. *Biophys. J.,* **2007**, *93*, 2429-2435.

(111)   Pal, A.; Dey, J. *J. Phys. Chem.,* **2014**, *118*, 12112-12120.

(112)   Jadhav, S. R.; Vemula, P. K.; Kumar, R.; Raghavan, S. R.; John, G. *Angew. Chem. Int. Ed.,* **2010**, *49*, 7695-7698.

(113)   Debnath, S.; Shome, A.; Dutta, S.; Das, P. K. *Chem. (Weinheim an der Bergstrasse, Germany),* **2008**, *14*, 6870-6881.

(114)   Zhou, M.; Smith, A. M.; Das, A. K.; Hodson, N. W.; Collins, R. F.; Ulijn, R. V.; Gough, J. E. *Biomater.,* **2009**, *30*, 2523-2530.

(115)   Zhang, X.; Song, J.; Ji, W.; Xu, N.; Gao, N.; Zhang, X.; Yu, H. *J. Mater. Chem. A,* **2015**, *3*, 18953-18962.

(116)   Cheng, N.; Hu, Q.; Guo, Y.; Wang, Y.; Yu, L. *ACS Appl. Mater. Interfaces,* **2015**, *7*, 10258-10265.

(117)   Jalil, A. A.; Triwahyono, S.; Adam, S. H.; Rahim, N. D.; Aziz, M. A. A.; Hairom, N. H. H.; Razali, N. A. M.; Abidin, M. A. Z.; Mohamadiah, M. K. A. *J. Hazard. Mater.,* **2010**, *181*, 755-762.

(118)   Bhattacharya, S.; Srivastava, A.; Pal, A. *Angew. Chem. Int. Ed.,* **2006**, *45*, 2934-2937.

(119)   Ohtsubo, K.; Marth, J. D. *Cell,* **2006**, *126*, 855-867.

(120)   Datta, S.; Bhattacharya, S. *Chem. Soc. Rev.,* **2015**, *44*, 5596-5637.

(121)   Kiyonaka, S.; Sugiyasu, K.; Shinkai, S.; Hamachi, I. *J. Am. Chem. Soc.,* **2002**, *124*, 10954-10955.

(122)   Zhou, S. L.; Matsumoto, S.; Tian, H. D.; Yamane, H.; Ojida, A.; Kiyonaka, S.; Hamachi, I. *Chem. Eur. J.,* **2005**, *11*, 1130-1136.

(123)   Wang, G.; Cheuk, S.; Yang, H.; Goyal, N.; Narasimha Reddy, P. V.; Hopkinson, B. *Langmuir,* **2009**, *25*, 8696-8705.

(124)   Wang, G.; Cheuk, S.; Williams, K.; Sharma, V.; Dakessian, L.; Thorton, Z. *Carbohydr. Res.,* **2006**, *341*, 705-716.

(125)   Nie, X.; Wang, G. *J. Org. Chem.,* **2006**, *71*, 4734-4741.

(126)   Clemente, M. J.; Fitremann, J.; Mauzac, M.; Serrano, J. L.; Oriol, L. *Langmuir,* **2011**, *27*, 15236-15247.

(127)   Imae, T.; Takahashi, Y.; Muramatsu, H. *J. Am. Chem. Soc.,* **1992**, *114*, 3414-3419.

(128)   Imae, T.; Hayashi, N.; Matsumoto, T.; Tada, T.; Furusaka, M. *J. Colloid Interface Sci.,* **2000**, *225*, 285-290.

(129)   Hamachi, I.; Kiyonaka, S.; Shinkai, S. *Chem. Commun.,* **2000**, 1281-1282.

(130)   Velasco-Torrijos, T.; Abbey, L.; O'Flaherty, R. *Molecules,* **2012**, *17*, 11346-11362.

(131)   More, S. V.; Chang, T. T.; Chiao, Y. P.; Jao, S. C.; Lu, C. K.; Li, W. S. *Eur. J. Med. Chem.,* **2013**, *64*, 169-178.

(132)   Ross, B. P.; Au, C. H. *Patent. U.S. 7312194 B2,* **2007**, 743-749.

(133)   Reddy, A., Ramos, J., Abbey, L., Ziegler, T., Velasco-Torrijos, T., Vogel C., Murphy P. *Chapter 25. Carbohydr. Chem.: Proven Synth. Methods,* **2017**, *4*, 201-208.

(134)   Xue, J. L.; Cecioni, S.; He, L.; Vidal, S.; Praly, J. P. *Carbohydr. Res.,* **2009**, *344*, 1646-1653.

(135)   Chernyak, A. Y.; Sharma, G. V. M.; Kononov, L. O.; Krishna, P. R.; Levinsky, A. B.; Kochetkov, N. K.; Rama Rao, A. V. *Carbohydr. Res.,* **1992**, *223*, 303-309.

(136)   Bertho, A. *Liebigs. Ann.,* **1949**, *562*, 229–239.

(137)   Kunishima, M.; Kawachi, C.; Morita, J.; Terao, K.; Iwasaki, F.; Tani, S. *Tetrahedron,* **1999**, *55*, 13159-13170.

(138)   Brizard, A.; Oda, R.; Huc, I. *Top. Curr. Chem.,* **2005**, *256*, 167-218.

(139)   Makarević, J.; Jokić, M.; Raza, Z.; Štefanić, Z.; Kojić-Prodić, B.; Žinić, M. *Chem. Eur. J.,* **2003**, *9*, 5567-5580.

(140)   Čaplar, V.; Žinić, M.; Pozzo, J. L.; Fages, F.; Mieden-Gundert, G.; Vögtle, F. *Eur. J. Org. Chem.,* **2004**, 4048-4059.

(141)   Becerril, J.; Escuder, B.; Miravet, J. F.; Gavara, R.; Luis, S. V. *Eur. J. Org. Chem.,* **2005**, 481-485.

(142)   Fleming, S.; Frederix, P. W. J. M.; Ramos Sasselli, I. n.; Hunt, N. T.; Ulijn, R. V.; Tuttle, T. *Langmuir,* **2013**, *29*, 9510-9515.

(143)   Cohen, S.; Cohen, S. G. *J. Am Chem. Soc.,* **1966**, *88*, 1533-1536.

(144)   Yu, Y., et.al., *Bioorg. Med. Chem. Lett.,* **2008**, *18*, 1318-1322.

(145)   Storer, R. I.; Aciro, C.; Jones, L. H. *Chem. Soc. Rev.,* **2011**, *40*, 2330-2346.

(146)   Soberats, B.; Martínez, L.; Sanna, E.; Sampedro, A.; Rotger, C.; Costa, A. *Chem. Eur. J.,* **2012**, *18*, 7533-7542.

(147)   Lopez, C.; Sanna, E.; Carreras, L.; Vega, M.; Rotger, C.; Costa, A. *Chem. Asian J.,* **2013**, *8*, 84-87.

(148)   Alemán, J.; Parra, A.; Jiang, H.; Jørgensen, K. A. *Chem. Eur. J.,* **2011**, *17*, 6890-6899.

(149)   Alegre-Requena, J. V. *Synlett.,* **2014**, *25*, 298-299.

(150)   Chauhan, P.; Mahajan, S.; Kaya, U.; Hack, D.; Enders, D. *Adv. Synth. Catal.,* **2015**, *357*, 253-281.

(151)   Dong, Z.; Jin, X.; Wang, P.; Min, C.; Zhang, J.; Chen, Z.; Zhou, H. B.; Dong, C. *Arkivoc,* **2011**, *2011*, 367-380.

(152)   Bobcheva, Z.; Zhiryakova, D.; Guncheva, M. *J. Enzyme Inhib. Med. Chem.,* **2011**, *26*, 587-591.

(153)   Wurm, F. R.; Klok, H.-A. *Chem. Soc. Rev.,* **2013**, *42*, 8220-8236.

(154)   Prohens, R.; Portell, A.; Puigjaner, C.; Barbas, R.; Alcobé, X.; Font-Bardia, M.; Tomàs, S. *CrystEngComm,* **2012**, *14*, 5745-5748.

(155)   Portell, A.; Prohens, R. *Powder Diffr.,* **2009**, *28*, 470-480.

(156)   Portell, A.; Font-Bardia, M.; Prohens, R. *Cryst. Growth Des.,* **2013**, *13*, 4200-4203.

(157)   Schiller, J.; Alegre-Requena, J. V.; Marqués-López, E.; Herrera, R. P.; Casanovas, J.; Alemán, C.; Díaz Díaz, D. *Soft Matter,* **2016**, *12*, 4361-4374.

(158)   Quinonero, D.; Frontera, A.; Tomas, S.; Suner, G. A.; Morey, J.; Costa, A.; Ballester, P.; Deya, P. M. *Theor. Chem. Acc.,* **2000**, *104*, 50-66.

(159)   Frontera, A.; Orell, M.; Garau, C.; Quiñonero, D.; Molins, E.; Mata, I.; Morey, J. *Org. Lett.,* **2005**, *7*, 1437-1440.

(160)   Portell, A.; Barbas, R.; Braga, D.; Polito, M.; Puigjaner, C.; Prohens, R. *CrystEngComm,* **2009**, *11*, 52-54.

(161)   Ambrosi, G.; Formica, M.; Fusi, V.; Giorgi, L.; Guerri, A.; Micheloni, M.; Paoli, P.; Pontellini, R.; Rossi, P. *Chem.-Eur. J.,* **2007**, *13*, 702-712.

(162)   Ohsedo, Y.; Miyamoto, M.; Tanaka, A.; Watanabe, H. *New J. Chem.,* **2013**, *37*, 2874-2880.

(163)   Alegre-Requena, J. V.; Marques-Lopez, E.; Herrera, R. P. *RSC Adv.,* **2015**, *5*, 33450-33462.

(164)   López, C.; Ximenis, M.; Orvay, F.; Rotger, C.; Costa, A. *Chem. Eur. J.,* **2017**, *23*, 7590-7594.

(165)   Rotger, C.; Piña, M. N.; Vega, M.; Ballester, P.; Deyà, P. M.; Costa, A. *Angew. Chem. Int. Ed.,* **2006**, *45*, 6844-6848.

(166)   Rotger, M. C.; Piña, M. N.; Frontera, A.; Martorell, G.; Ballester, P.; Deyà, P. M.; Costa, A. *J. Org. Chem.,* **2004**, *69*, 2302-2308.

(167)   Lalitha, K.; Prasad, Y. S.; Sridharan, V.; Maheswari, C. U.; John, G.; Nagarajan, S. *RSC Adv.,* **2015**, *5*, 77589-77594.

(168)   Mukhopadhyay, P.; Fujita, N.; Takada, A.; Kishida, T.; Shirakawa, M.; Shinkai, S. *Angew. Chem. Int. Ed.,* **2010**, *49*, 6338-6342.

(169)   Kirilov, P.; Gauffre, F.; Franceschi-Messant, S.; Perez, E.; Rico-Lattes, I. *J. Phys. Chem. B,* **2009**, *113*, 11101-11108.

(170)   Formhals, A. *Process and apparatus for preparing artificial threads. US, patent 1975504,* **1934**.

(171)   Reneker, D. H.; Chun, I. *Nanotechnol.,* **1996**, *7*, 216-223.

(172)   Gopal, R.; Kaur, S.; Feng, C. Y.; Chan, C.; Ramakrishna, S.; Tabe, S.; Matsuura, T. *J. Membr. Sci.,* **2007**, *289*, 210-219.

(173)   Aussawasathien, D.; Teerawattananon, C.; Vongachariya, A. *J. Membr. Sci.,* **2008**, *315*, 11-19.

(174)   Lee, S.; Obendorf, S. K. *Text. Res. J.,* **2007**, *77*, 696-702.

(175)   Gorji, M.; Karimi, M.; Nasheroahkam, S. *J. Ind. Text.,* **2016**, 1-19.

(176)   Schiffman, K. A. R. N. P. B. J. D. *J. Mater. Chem. B,* **2013**, *1*, 4531–4541.

(177)   Elzatahry, A. A.; Al-Enizi, A. M.; Elsayed, E. A.; Butorac, R. R.; Al-Deyab, S. S.; Wadaan, M. A. M.; Cowley, A. H. *Int. J. Nanomed.,* **2012**, *7*, 2829-2832.

(178)   Lala, N. L.; Thavasi, V.; Ramakrishna, S. *Sensors,* **2009**, *9*, 86-101.

(179)   Liu, A. *Biosens. Bioelectron.,* **2008**, *24*, 167-177.

(180)   Pinto, N. J. *J. Phys. Conf. Ser.,* **2013**, *421*, 1-6.

(181)   Fathy, M.; Kashyout, A. B.; El Nady, J.; Ebrahim, S.; Soliman, M. B. *Alexandria Eng. J.,* **2016**, *55*, 1737-1743.

(182)   Kim, J. U.; Park, S. H.; Choi, H. J.; Lee, W. K.; Lee, J. K.; Kim, M. R. *Sol. Energy Mater. Sol. Cells,* **2009**, *93*, 803-807.

(183)   Dong, Z.; Kennedy, S. J.; Wu, Y. *J. Power Sources,* **2011**, *196*, 4886-4904.

(184)   Chou, S. F.; Carson, D.; Woodrow, K. A. *J. Controlled Release,* **2015**, *220*, 584-591.

(185)   Pillay, V.; Dott, C.; Choonara, Y. E.; Tyagi, C.; Tomar, L.; Kumar, P.; Toit, L. C.; Ndesendo, V. M. K. *J. Nanomater.,* **2013**, *2013*, 1-22.

(186)   He, C. L.; Nie, W.; Feng, W. *J. Mater. Chem. B,* **2014**, *2*, 7828-7848.

(187)   Ren, X.; Feng, Y.; Guo, J.; Wang, H.; Li, Q.; Yang, J.; Hao, X.; Lv, J.; Ma, N.; Li, W. *Chem. Soc. Rev.,* **2015**, *44*, 5680-5742.

(188)   Saracino, G. a. a.; Cigognini, D.; Silva, D.; Caprini, A.; Gelain, F. *Chem. Soc. Rev.,* **2012**, 225-262.

(189)   Nagarajan, S.; Soussan, L.; Bechelany, M.; Teyssier, C.; Cavaillès, V.; Pochat-Bohatier, C.; Miele, P.; Kalkura, N.; Janot, J.-M.; Balme, S. *J. Mater. Chem. B,* **2016**, *4*, 1134-1141.

(190)   Li, D.; Xia, Y. *Adv. Mater.,* **2004**, *16*, 1151-1170.

(191)   Taylor, G. *Proc. R. Soc. Lond. A,* **1969**, *313*, 453-475.

(192)   Martins, a.; Reis, R. L.; Neves, N. M. *Int. Mater. Rev.,* **2008**, *53*, 257-274.

(193)   Sahay, R.; Thavasi, V.; Ramakrishna, S. *J. Nanomater.,* **2011**, *2011*, 1-17.

(194)   Megelski, S.; Stephens, J. S.; Bruce Chase, D.; Rabolt, J. F. *Macromol.,* **2002**, *35*, 8456-8466.

(195)   Deitzel, J. M.; Kleinmeyer, J.; Harris, D.; Beck Tan, N. C. *Polym.,* **2001**, *42*, 261-272.

(196)   Katsogiannis, K. A. G.; Vladisavljevi, G. T.; Georgiadou, S. *Eur. Polym. J.,* **2015**, *69*, 284-295.

(197)   Nezarati, R. M.; Eifert, M. B.; Cosgriff-Hernandez, E. *Tissue Eng. Part C: Methods,* **2013**, *19*, 810-819.

(198)   Balaji, A.; Vellayappan, M. V.; John, A. A.; Subramanian, A. P.; Jaganathan, S. K.; Supriyanto, E.; Razak, S. I. A. *RSC Adv.,* **2015**, *5*, 57984-58004.

(199)   Grafahrend, D.; Heffels, K.-H.; Beer, M. V.; Gasteier, P.; Möller, M.; Boehm, G.; Dalton, P. D.; Groll, J. *Nat. Mater.,* **2010**, *10*, 67-73.

(200)   Ulery, B. D.; Nair, L. S.; Laurencin, C. T. *J. Polym. Sci., Part B: Polym. Phys.,* **2011**, *49*, 832-864.

(201)   Liang, D.; Hsiao, B. S.; Chu, B. *Adv. Drug Deliv. Rev.,* **2007**, *59*, 1392-1412.

(202)   Gilchrist, S. E.; Lange, D.; Letchford, K.; Bach, H.; Fazli, L.; Burt, H. M. *J. Controlled Release,* **2013**, *170*, 64-73.

(203)   Zhang, Y. Z.; Wang, X.; Feng, Y.; Li, J.; Lim, C. T.; Ramakrishna, S. *Biomacromol.,* **2006**, *7*, 1049-1057.

(204)   Liang, D.; Luu, Y. K.; Kim, K.; Hsiao, B. S.; Hadjiargyrou, M.; Chu, B. *Nucleic Acids Res.,* **2005**, *33*, 1-10.

(205)   Jayasinghe, S. N. *Analyst,* **2013**, *138*, 2215-2223.

(206)   Ahn, S.; Kim, G. *J. Mater. Chem. B,* **2015**, *3*, 9132-9139.

(207)   He, C. L.; Huang, Z. M.; Han, X. J.; Liu, L.; Zhang, H. S.; Chen, L. S. *J. Macromol. Sci. Part B,* **2006**, *45*, 515-524.

(208)   Wang, L.; Wang, M.; Topham, P. D.; Huang, Y. *RSC Adv.,* **2012**, *2*, 2433-2438.

(209)   Manuel, C. B. J.; Jesús, V. G. L.; Aracely, S. M. *Chapter 7. Electrospinning - Mater., Techniq. & Biomed. Applic.,* **2016**.

(210)   Weldon CB, T. J., Shankarappa SA, et al. *J Control Release,* **2012**, *161*, 903-909.

(211)   Seitz, J. M.; Durisin, M.; Goldman, J.; Drelich, J. W. *Adv. Healthc. Mater.,* **2015**, *4*, 1915-1936.

(212)   Lee, J. E.; Park, S.; Park, M.; Kim, M. H.; Park, C. G.; Lee, S. H.; Choi, S. Y.; Kim, B. H.; Park, H. J.; Park, J. H.; Heo, C. Y.; Choy, Y. B. *Acta Biomater,* **2013**, *9*, 8318-8327.

(213)   Kashiwabuchi, F.; Parikh, K. S.; Omiadze, R.; Zhang, S.; Luo, L.; Patel, H. V.; Xu, Q.; Ensign, L. M.; Mao, H.-Q.; Hanes, J.; McDonnell, P. J. *Transl. Vis. Sci. Technol.,* **2017**, *6*, 1-8.

(214)   Langer, R.; Vacanti, J. P. *Science (New York, N.Y.),* **1993**, *260*, 920-926.

(215)   Hassan, M. I.; Sultana, N.; Hamdan, S. *J. Nanomater.,* **2014**, *2014*, 1-6.

(216)   Pignatello, R. *InTech,* **2011**.

(217)   Zafar, M.; Najeeb, S.; Khurshid, Z.; Vazirzadeh, M.; Zohaib, S.; Najeeb, B.; Sefat, F. *Mater.,* **2016**, *9*, 1-21.

(218)   Jinjun Shi, A. R. V., Omid C. Farokhzad, and Robert Langer *Nano Lett.,* **2010**, *10*, 3223-3230.

(219)   Murugan, R.; Ramakrishna, S. *Tissue Eng.,* **2006**, *12*, 435-447.

(220)   Pant, H. R.; Neupane, M. P.; Pant, B.; Panthi, G.; Oh, H. J.; Lee, M. H.; Kim, H. Y. *Colloids Surf. B: Biointerfaces,* **2011**, *88*, 587-592.

(221)   Bikiaris, D. N.; Papageorgiou, G. Z.; Achilias, D. S.; Pavlidou, E.; Stergiou, A. *Eur. Polym. J.,* **2007**, *43*, 2491-2503.

(222)   Dhandayuthapani, B.; Yoshida, Y.; Maekawa, T.; Kumar, D. S. *Int. J. Polym. Sci.,* **2011**, *2011*, 1-19.

(223)   Azimi, B.; Nourpanah, P.; Rabiee, M.; Arbab, S. *J. Eng. Fiber Fabr.,* **2014**, *9*, 74-90.

(224)   Al-Omair, M. A. *Polymers,* **2015**, *7*, 1464-1475.

(225)   Kim, S.-e.; Wang, J.; Jordan, A. M.; Korley, L. T. J.; Baer, E.; Pokorski, J. K. *ACS Macro Lett.,* **2014**, *3*, 585-589.

(226)   Beachley, V.; Wen, X. *Progr. Polym. Sci. (Oxford),* **2010**, *35*, 868-892.

(227)   Koh, H. S.; Yong, T.; Chan, C. K.; Ramakrishna, S. *Biomater.,* **2008**, *29*, 3574-3582.

(228)   Recek, N.; Resnik, M.; Motaln, H.; Lah-Turnšek, T.; Augustine, R.; Kalarikkal, N.; Thomas, S.; Mozetič, M. *Int. J. Polym. Sci.,* **2016**, *2016*, 1-9.

(229)   Gancarz, M. B. I. *Chapter 7. Membr. Modification. Technol. and Appl.,* **2012**, 179-214.

(230)   Yue, M.; Zhou, B.; Jiao, K.; Qian, X.; Xu, Z.; Teng, K.; Zhao, L.; Wang, J.; Jiao, Y. *Appl. Surf. Sci.,* **2015**, *327*, 93-99.

(231)   Chen, J.; Yan, C.; Zhu, M.; Yao, Q.; Shao, C.; Lu, W.; Wang, J.; Mo, X.; Gu, P.; Fu, Y.; Fan, X. *Int. J. Nanomed.,* **2015**, *10*, 3337-3350.

(232)   Ma, Z.; Kotaki, M.; Inai, R.; Ramakrishna, S. *Tissue Eng.,* **2005**, *11*, 101-109.

(233)   Mashhadikhan, M.; Soleimani, M.; Parivar, K.; Yaghmaei, P. *Avicenna J. Med. Biotechnol.,* **2015**, *7*, 32-38.

(234)   Zander, N. E.; Beebe, T. P. *Biointerphases,* **2014**, *9*, 1-9.

(235) Lv, J.; Chen, L.; Zhu, Y.; Hou, L.; Liu, Y. *ACS Appl. Mater. Interfaces,* **2014**, *6*, 4954-4964.

(236) Yu, H. S.; Jang, J. H.; Kim, T. I.; Lee, H. H.; Kim, H. W. *J. Biomed. Mater. Res. Part A,* **2009**, *88*, 747-754.

(237) Patel, S.; Kurpinski, K.; Quigley, R.; Gao, H.; Hsiao, B. S.; Poo, M. M.; Li, S. *Nano Lett.,* **2007**, *7*, 2122-2128.

(238) Kim, T. G.; Park, T. G. *Tissue Eng.,* **2006**, *12*, 221-233.

(239) Li, W.; Guo, Y.; Wang, H.; Shi, D.; Liang, C.; Ye, Z.; Qing, F.; Gong, J. *J. Mater. Sci. Mater. Med.,* **2008**, *19*, 847-854.

(240) Zhang, M.; Wang, Z.; Wang, Z.; Feng, S.; Xu, H.; Zhao, Q.; Wang, S.; Fang, J.; Qiao, M.; Kong, D. *Colloids Surf. B: Biointerfaces,* **2011**, *85*, 32-39.

(241) Kolb, H. C.; Finn, M. G.; Sharpless, K. B. *Angew. Chem. Int. Ed.,* **2001**, *40*, 2004-2021.

(242) Jordan, A. M.; Viswanath, V.; Kim, S.-E.; Pokorski, J. K.; Korley, L. T. J. *J. Mater. Chem. B,* **2016**, *4*, 5958-5974.

(243) Tayi, A. S.; Pashuck, E. T.; Newcomb, C. J.; McClendon, M. T.; Stupp, S. I. *Biomacromol.,* **2014**, *15*, 1323-1327.

(244) Maleki, M.; Natalello, A.; Pugliese, R.; Gelain, F. *Acta Biomater.,* **2017**, *51*, 268-278.

(245) Doshi, J.; Reneker, D. H. *J. Electrost.,* **1993**, *35*, 151-160.

(246) Reneker, D. H.; Yarin, A. L.; Fong, H.; Koombhongse, S. *J. Appl. Phys.,* **2000**, *87*, 4531-4547.

(247) Shin, Y. M.; Hohman, M. M.; Brenner, M. P.; Rutledge, G. C. *Appl. Phys. Lett.,* **2001**, *78*, 1149-1151.

(248) Liu, W.; Adanur, S. *Text. Res. J.,* **2009**, *80*, 124-134.

(249) Zong, X.; Kim, K.; Fang, D.; Ran, S.; Hsiao, B. S.; Chu, B. *Polym.,* **2002**, *43*, 4403-4412.

(250) Leach, M. K.; Feng, Z.-Q.; Tuck, S. J.; Corey, J. M. *JoVE,* **2011**, 1-5.

(251) Subbiah, T.; Bhat, G. S.; Tock, R. W.; Parameswaran, S.; Ramkumar, S. S. *J. Appl. Polym. Sci.,* **2005**, *96*, 557-569.

(252) Huang, F.; Wei, Q.; Cai, Y.; Wu, N. *Int. J. Polym. Anal. Charact.,* **2008**, *13*, 292-301.

(253) Hoque, M. E.; San, W. Y.; Wei, F.; Li, S.; Huang, M.-H.; Vert, M.; Hutmacher, D. W. *Tissue Eng. Part A,* **2009**, *15*, 3013-3024.

(254) Zahedi, P.; Rafie, A.; Wojczak, E. *Indian J. Fibre Text. Res.,* **2016**, *41*, 13-18.

(255) Liu, H.; Hsieh, Y. L. *J. Polym. Sci. Part B: Polym. Phy.,* **2002**, *40*, 2119-2129.

(256) Patel, H. N.; Thai, K. N.; Chowdhury, S.; Singh, R.; Vohra, Y. K.; Thomas, V. *Prog. Biomater.,* **2015**, *4*, 67-76.

(257) Savoji, H.; Maire, M.; Lequoy, P.; Liberelle, B.; De Crescenzo, G.; Ajji, A.; Wertheimer, M. R.; Lerouge, S. *Biomacromol.,* **2017**, *18*, 303-310.

(258) Wan, J. C.; Jun, H. K.; Se, H. O.; Hyun, H. N.; Jin, M. K.; Lee, J. H. *J. Biomed. Mater. Res. Part A,* **2009**, *91*, 400-407.

(259) Song, W.; Markel, D. C.; Wang, S.; Shi, T.; Mao, G.; Ren, W. *Nanotechnol.,* **2012**, *23*, 1-15.

(260) Wang, L. N.; Xin, C. Z.; Liu, W. T.; Xia, X. L.; He, S. Q.; Liu, H.; Zhu, C. S. *Arab. J. Sci. Eng.,* **2015**, *40*, 2889-2895.

(261) Chen, L.; Bai, Y.; Liao, G.; Peng, E.; Wu, B.; Wang, Y.; Zeng, X.; Xie, X. *PLoS ONE,* **2013**, *8*, 14-16.

(262)   Kurusu, R. S.; Demarquette, N. R. *Langmuir,* **2015**, *31*, 5495-5503.

(263)   Yuan, Y.; Lee, T. R. *Chapter 1. Contact Angle Wetting Prop.,* **2013**, *51*, 1-34.

(264)   Kumar, G.; Prabhu, K. N. *Adv. Colloid Interface Sci.,* **2007**, *133*, 61-89.

(265)   Mohammadmoradi, P.; Kantzas, A. *SPE-181309-MS,* **2016**, 1-22.

(266)   Sakai, M.; Yanagisawa, T.; Nakajima, A.; Kameshima, Y.; Okada, K. *Langmuir,* **2009**, *25*, 13-16.

(267)   Park, J.; Han, H.-S.; Kim, Y.-C.; Ahn, J.-P.; Ok, M.-R.; Lee, K. E.; Lee, J.-W.; Cha, P.-R.; Seok, H.-K.; Jeon, H. *Sci. Rep.,* **2016**, *5*, 1-12.

(268)   Yang, H.; Jiang, P. *Langmuir,* **2010**, *26*, 12598-12604.

(269)   Koch, K.; Bhushan, B.; Jung, Y. C.; Barthlott, W. *Soft Matter,* **2009**, *5*, 1386-1393.

(270)   Herminghaus, S.; Brinkmann, M.; Seemann, R. *Annu. Rev. Mater. Res.,* **2008**, *38*, 101-121.

(271)   Keshavarz-Motamed, Z.; Kadem, L.; Dolatabadi, A. *Microfluid. Nanofluidics,* **2010**, *8*, 47-56.

(272)   Nanayakkara, Y. S.; Perera, S.; Bindiganavale, S.; Wanigasekara, E.; Moon, H.; Armstrong, D. W. *Anal. Chem.,* **2010**, *82*, 3146-3154.

(273)   Kelnar, I.; Kratochvíl, J.; Kaprálková, L. *J. of Therm. Anal. and Calori.,* **2016**, *124*, 799-805.

(274)   Fathi, E.; Atyabi, N.; Imani, M.; Alinejad, Z. *Carb. Pol.,* **2011**, *84*, 145-152.

(275)   Lee, K. H.; Kim, H. Y.; Khil, M. S.; Ra, Y. M.; Lee, D. R. *Polym.,* **2003**, *44*, 1287-1294.

(276)   Autar, R.; Liskamp, R. M. J.; Pieters, R. J. *Carbohydr. Res.,* **2005**, *340*, 2436-2442.

(277)   Said, S. S.; Aloufy, A. K.; El-Halfawy, O. M.; Boraei, N. A.; El-Khordagui, L. K. *Eur. J. of Pharm. and Biopharm.,* **2011**, *79*, 108-118.

(278)   W. C. Still, M. K., A. Mitra, *J. Org. Chem.,* **1978**, *43*, 2923-2925.

(279)   Clary, L.; Greiner, J.; Santaella, C.; Vierling, P. *Tetrahedron Lett.,* **1995**, *36*, 539-542.

(280)   Dea, S. O. *Spraybase,* **2011**, 1-4.

Appendix

Publication List

Ramos, J.; Arufe, S.; O'Flaherty, R.; Rooney, D.; Moreira, R.; Velasco-Torrijos, T. Selective aliphatic/aromatic organogelation controlled by the side chain of serine amphiphiles. *RSC Adv.* **2016**, *6*, 108093-108104.

Reddy, A., Ramos, J., Abbey, L., Ziegler, T., Velasco-Torrijos, T. 2-Chloroethyl and 2-Azidoethyl 2, 3, 4, 6 – Tetra–*O*-acetyl-*α*-D-gluco- and α-D-galactopyranosides. *Carbohydrate Chemistry: Proven Synthetic Methods, Volume 4*, Murphy PV, Voguel C (Eds.). CRC Press, Taylor and Francis group, **2017**.

Oral Presentations

Ramos, J., *Selective aliphatic/aromatic organogelation controlled by the side-chain protection of serine amphiphiles*, 68th Irish Universities Chemistry Research Colloquium, **University College Cork**, June 2016.

Poster Presentations

Ramos, J.; Velasco-Torrijos, T. *Gelation of aromatic solvents induced by π-gelators. Applications in electrospinning*, Postgraduate Research Day, **Maynooth University**, (September 2014).

Ramos, J.; Velasco-Torrijos, T. *Gelation of aromatic solvents induced by π-gelators. Applications in electrospinning*, Supramolecular Chemistry Ireland (SCI) symposium, **Maynooth University**, (July 2015).

Ramos, J.; Velasco-Torrijos, T. *Gelation of aromatic solvents induced by π-gelators. Applications in electrospinning*, Publications festival, **Maynooth University**, (January 2016).

Ramos, J.; Arufe, S.; O'Flaherty, R.; Rooney, D.; Moreira, R.; Velasco-Torrijos, T. *Selective aliphatic/aromatic organogelation controlled by the side-chain protection of serine amphiphiles*, 69th Irish Universities Chemistry Research Colloquium, **Dublin City University**, (June 2017).

Ramos, J.; Arufe, S.; O'Flaherty, R.; Rooney, D.; Moreira, R.; Velasco-Torrijos, T. *Selective aliphatic/aromatic organogelation controlled by the side-chain protection of serine amphiphiles*, Supramolecular Chemistry Ireland (SCI) symposium, **Maynooth University**, (June 2017).

Ramos, J.; Velasco-Torrijos, T.; Elmes, R.; Arufe, S.; Moreira, R. *Glycolipid conjugates of aspartic acid and Squaramide: Application as LMWGs and in electrospun scaffolds for tissue engineering*, 19th European Carbohydrate Symposium, **Institut Químic de Sarrià, University Ramon Llull, under the auspices of the European Carbohydrate Organisation**, (July 2017).

Graduate Modules

Chemistry Specific Modules:

CH801 = Core skills and research techniques in Chemistry.

CH803 = Teaching skills in Chemistry.

CH804 = Thesis plan.

CH806 = Research training workshops in Chemistry.

CH807 = Review of research papers.

CH808 = Research supervision training.

Generic / Transferable Modules:

GSE2 = Innovation and research commercialization.

CTL1 = Professional certificate in postgraduate teaching and learning: Tutors and demonstrators.

GST5 = Creative thinking and problem solving.

Table A.1. X-Ray powder diffraction data for compounds **2.38.** – **2.39.** in hexane and **2.40.** – **2.41.** in toluene.

COMPOUND	Pos. [°2θ]	Height [cts]	d-spacing [Å]
2.38. Fmoc-O^{t}Bu-C$_{14}$ in hexane	5.7921 7.9787 9.8863 11.7469 19.6256 22.0194 24.8500	276.37 235.35 217.03 203.09 859.11 454.30 143.42	15.25875 11.08129 8.94702 7.53370 4.52348 4.03685 3.58306
2.39. Fmoc-O^{t}Bu-C$_{18}$ in hexane	5.8640 7.6652 9.6154 11.0213 11.8769 13.4607 15.4309 18.1315 18.4252 19.4491 21.1840 22.7050 32.4392 36.8439	564.19 160.33 449.27 1342.51 1887.84 1055.18 457.12 1604.68 2145.43 3222.15 6405.38 3118.04 134.80 118.76	15.07187 11.53381 9.19847 8.02799 7.45154 6.57813 5.74240 4.89273 4.81540 4.56413 4.19412 3.91648 2.76005 2.43958
2.40. Fmoc-OH-C$_{14}$ in toluene	7.1011 16.4940 18.6558 19.7234 22.0602 25.8604 37.2761	250.78 240.28 1581.75 2119.41 2902.67 649.17 95.71	12.44870 5.37461 4.75638 4.50128 4.02947 3.44531 2.41228
2.41. Fmoc-OH-C$_{18}$ in toluene	6.0324 6.6278 8.0820 9.5361 10.3283 13.1938 14.2830 15.3025 18.5337 19.5468 21.2237 22.1244 23.1675 25.5548 36.8617	967.71 751.25 202.15 324.25 376.78 845.99 270.24 537.51 835.77 1426.98 3626.88 3390.39 1703.51 676.16 76.55	14.65158 13.33652 10.93983 9.27472 8.56507 6.71060 6.20121 5.79031 4.78745 4.54155 4.18636 4.01792 3.83933 3.48582 2.43844

Crystal Structure Report for 3.50. Dissolved in Ethyl acetate. Diethyl Ether was the solvent used for diffusion to grow the crystal.

A specimen of $C_{17}H_{24}N_2O_4$, approximate dimensions 0.030 mm x 0.110 mm x 0.600 mm, was used for the X-ray crystallographic analysis. The X-ray intensity data were measured at 100(2)K using an Oxford Cryosystems low temperature device using a MiTeGen micromount. See Table 1 for collection parameters and exposure time. Bruker APEX software was used to correct for Lorentz and polarization effects.

A total of 3815 frames were collected. The total exposure time was 17.97 hours. The frames were integrated with the Bruker SAINT software package using a narrow-frame algorithm. The integration of the data using a monoclinic unit cell yielded a total of 19887 reflections to a maximum θ angle of 68.37° (0.83 Å resolution), of which 6047 were independent (average redundancy 3.289, completeness = 99.1%, R_{int} = 5.09%, R_{sig} = 5.53%) and 5727 (94.71%) were greater than $2\sigma(F^2)$. The final cell constants of <u>a</u> = 17.6267(6) Å, <u>b</u> = 5.0402(2) Å, <u>c</u> = 38.3753(13) Å, β = 94.6099(18)°, volume = 3398.3(2) Å^3, are based upon the refinement of the XYZ-centroids of 9880 reflections above 20 σ(I) with 4.620° < 2θ < 136.4°. Data were corrected for absorption effects using the Multi-Scan method (SADABS). The ratio of minimum to maximum apparent transmission was 0.781. The calculated minimum and maximum transmission coefficients (based on crystal size) are 0.5882 and 0.7531.

The structure was solved using the Bruker APEX Software Package and refined with XL in Olex2, using the space group C_2, with Z = 8 for the formula unit, $C_{17}H_{24}N_2O_4$. The final anisotropic full-matrix least-squares refinement on F^2 with 447 variables converged at R1 = 5.21%, for the observed data and wR2 = 13.95% for all data. The goodness-of-fit was 1.047. The largest peak in the final difference electron density synthesis was 0.442 e$^-$/Å^3 and the largest hole was -0.269 e$^-$/Å^3 with an RMS deviation of 0.051 e$^-$/Å^3. On the basis of the final model, the calculated density was 1.252 g/cm^3 and F(000), 1376 e$^-$.

Refinement Note: One CH_3CH_2NH chain (N38-C41) is disordered in two positions with 50% occupancy and refined with restraints (SADI) and constraints (EADP).

References: see CIF.

Table 1: Data collection details for TCD722b.

Axis	dx/mm	2θ/°	ω/°	φ/°	χ/°	Width/°	Frames	Time/s	Wavelength/Å	Voltage/kV	Current/mA	Temperature/K
Omega	50.020	109.14	95.23	264.00	-54.74	1.00	135	20.00	1.54184	45	0.6	100
Omega	50.020	109.14	95.23	24.00	-54.74	1.00	135	20.00	1.54184	45	0.6	100
Omega	50.020	-49.54	189.42	160.00	54.74	1.00	135	10.00	1.54184	45	0.6	100
Omega	50.020	109.14	95.23	120.00	-54.74	1.00	135	20.00	1.54184	45	0.6	100
Omega	50.020	-49.54	189.42	96.00	54.74	1.00	135	10.00	1.54184	45	0.6	100
Omega	50.020	-49.54	298.02	224.00	-64.50	1.00	117	10.00	1.54184	45	0.6	100
Omega	50.020	109.14	95.23	0.00	-54.74	1.00	135	20.00	1.54184	45	0.6	100
Omega	50.020	109.14	342.65	48.00	64.50	1.00	139	20.00	1.54184	45	0.6	100
Phi	50.020	94.30	80.73	0.00	-57.00	1.00	360	20.00	1.54184	45	0.6	100
Omega	50.020	-49.54	189.42	32.00	54.74	1.00	135	10.00	1.54184	45	0.6	100
Omega	50.020	109.14	95.23	240.00	-54.74	1.00	135	20.00	1.54184	45	0.6	100
Omega	50.020	109.14	95.23	144.00	-54.74	1.00	135	20.00	1.54184	45	0.6	100
Omega	50.020	-11.07	227.89	360.00	54.74	1.00	135	10.00	1.54184	45	0.6	100
Omega	50.020	-49.54	298.02	96.00	-64.50	1.00	117	10.00	1.54184	45	0.6	100
Phi	50.020	79.30	65.73	360.00	-57.00	1.00	360	20.00	1.54184	45	0.6	100
Phi	50.020	109.30	95.73	360.00	-57.00	1.00	360	20.00	1.54184	45	0.6	100
Omega	50.020	109.14	95.23	288.00	-54.74	1.00	135	20.00	1.54184	45	0.6	100
Omega	50.020	-49.54	189.42	360.00	54.74	1.00	135	10.00	1.54184	45	0.6	100
Omega	50.020	109.14	342.65	24.00	64.50	1.00	139	20.00	1.54184	45	0.6	100
Omega	50.020	-49.54	189.42	64.00	54.74	1.00	135	10.00	1.54184	45	0.6	100
Omega	50.020	-11.07	227.89	255.00	54.74	1.00	135	20.00	1.54184	45	0.6	100
Omega	50.020	-49.54	298.02	160.00	-64.50	1.00	117	10.00	1.54184	45	0.6	100
Phi	50.020	109.30	4.12	236.00	23.00	1.00	216	20.00	1.54184	45	0.6	100

Table 2. Crystal data and structure refinement for tcd722b.

Identification code	tcd722b
Empirical formula	$C_{17}H_{24}N_2O_4$
Formula weight	320.38
Temperature	100(2) K
Wavelength	1.54178 Å
Crystal system	Monoclinic
Space group	C_2
Unit cell dimensions	a = 17.6267(6) Å α= 90°.
	b = 5.0402(2) Å β= 94.6099(18)°.
	c = 38.3753(13) Å γ = 90°.
Volume	3398.3(2) Å^3
Z	8
Density (calculated)	1.252 Mg/m^3
Absorption coefficient	0.731 mm^{-1}
F(000)	1376
Crystal size	0.6 x 0.11 x 0.03 mm^3
Theta range for data collection	2.310 to 68.373°.
Index ranges	-21≤h≤21, -5≤k≤6, -45≤l≤46
Reflections collected	19887
Independent reflections	6047 [R(int) = 0.0509]
Completeness to theta = 67.679°	99.4 %
Absorption correction	Semi-empirical from equivalents
Max. and min. transmission	0.7531 and 0.5882
Refinement method	Full-matrix least-squares on F^2
Data / restraints / parameters	6047 / 8 / 447
Goodness-of-fit on F^2	1.047
Final R indices [I>2σ(I)]	R1 = 0.0521, wR2 = 0.1374
R indices (all data)	R1 = 0.0544, wR2 = 0.1395
Absolute structure parameter	0.03(11)
Largest diff. peak and hole	0.442 and -0.269 e.Å^{-3}

Table 3. Atomic coordinates (x 10^4) and equivalent isotropic displacement parameters (Å^{2}x 10^3) for tcd722b. U(eq) is defined as one third of the trace of the orthogonalized U^{ij} tensor.

	x	y	z	U(eq)
C(24)	6778(2)	5732(8)	2263(1)	31(1)
C(25)	6964(2)	7610(8)	2020(1)	32(1)
C(26)	6455(2)	8264(8)	1740(1)	34(1)
C(27)	5751(2)	7017(9)	1709(1)	37(1)
C(28)	5556(2)	5161(9)	1953(1)	35(1)
C(29)	6068(2)	4498(7)	2235(1)	27(1)
C(30)	5848(2)	2439(8)	2490(1)	31(1)
O(31)	6283(1)	2961(6)	2822(1)	31(1)
C(32)	6229(2)	1126(8)	3072(1)	29(1)
O(33)	5865(2)	-871(6)	3037(1)	38(1)
C(34)	6718(2)	1944(7)	3396(1)	29(1)
C(35)	6687(2)	-31(8)	3693(1)	30(1)
C(36)	7354(2)	389(9)	3969(1)	35(1)
O(37)	7631(2)	2595(7)	4031(1)	44(1)
N(38A)	7640(10)	-1562(19)	4181(3)	30(2)
N(38)	7538(10)	-2068(18)	4094(3)	30(2)
C(39)	8177(5)	-2220(20)	4363(2)	30(2)
C(39A)	8223(6)	-1300(20)	4471(2)	30(2)
C(40A)	8042(4)	-2969(18)	4775(2)	34(1)
C(40)	7970(5)	-1381(18)	4720(2)	34(1)
C(41)	8570(20)	-2150(100)	5020(10)	51(3)
C(41A)	8640(20)	-2400(100)	5082(9)	51(3)
N(42)	5978(2)	251(6)	3863(1)	26(1)
C(43)	5586(2)	-1867(8)	3966(1)	27(1)
O(44)	5801(2)	-4158(5)	3930(1)	34(1)
C(45)	4863(2)	-1237(8)	4137(1)	30(1)
C(46)	4890(2)	-2424(10)	4502(1)	40(1)
C(1)	3148(2)	4470(8)	2826(1)	29(1)
C(2)	2978(2)	2612(8)	3075(1)	31(1)
C(3)	3514(2)	1941(8)	3343(1)	34(1)
C(4)	4224(2)	3148(9)	3357(1)	40(1)
C(5)	4395(2)	4980(9)	3107(1)	36(1)
C(6)	3860(2)	5645(7)	2838(1)	27(1)

C(7)	4063(2)	7686(8)	2574(1)	29(1)
O(8)	3598(1)	7207(5)	2250(1)	29(1)
C(9)	3670(2)	8984(8)	1992(1)	28(1)
O(10)	4078(2)	10851(6)	2018(1)	37(1)
C(11)	3154(2)	8236(7)	1673(1)	29(1)
C(12)	3228(2)	10201(7)	1378(1)	27(1)
C(13)	3982(2)	9885(7)	1213(1)	26(1)
O(14)	4224(1)	7646(5)	1154(1)	31(1)
N(15)	4330(2)	12083(7)	1128(1)	29(1)
C(16)	5013(2)	12030(8)	936(1)	34(1)
C(17)	4846(3)	11356(10)	555(1)	51(1)
C(18)	4354(3)	13373(12)	360(1)	61(1)
N(19)	2616(2)	9827(6)	1102(1)	27(1)
C(20)	2291(2)	11886(8)	923(1)	28(1)
O(21)	2461(2)	14202(5)	991(1)	35(1)
C(22)	1695(2)	11187(8)	633(1)	36(1)
C(23)	1853(3)	12566(12)	295(1)	57(1)

Table 4. Bond lengths [Å] and angles [°] for tcd722b.

_____

C(24)-H(24)	0.9500	C(39A)-C(40A)	1.495(10)
C(24)-C(25)	1.387(5)	C(40A)-H(40A)	0.9900
C(24)-C(29)	1.394(5)	C(40A)-H(40B)	0.9900
C(25)-H(25)	0.9500	C(40A)-C(41A)	1.543(15)
C(25)-C(26)	1.383(5)	C(40)-H(40C)	0.9900
C(26)-H(26)	0.9500	C(40)-H(40D)	0.9900
C(26)-C(27)	1.388(5)	C(40)-C(41)	1.547(15)
C(27)-H(27)	0.9500	C(41)-H(41A)	0.9800
C(27)-C(28)	1.386(6)	C(41)-H(41B)	0.9800
C(28)-H(28)	0.9500	C(41)-H(41C)	0.9800
C(28)-C(29)	1.392(5)	C(41A)-H(41D)	0.9800
C(29)-C(30)	1.501(5)	C(41A)-H(41E)	0.9800
C(30)-H(30A)	0.9900	C(41A)-H(41F)	0.9800
C(30)-H(30B)	0.9900	N(42)-C(43)	1.348(5)
C(30)-O(31)	1.457(4)	N(42)-H(42)	0.887(14)
O(31)-C(32)	1.342(5)	C(43)-O(44)	1.226(5)
C(32)-O(33)	1.196(5)	C(43)-C(45)	1.513(5)
C(32)-C(34)	1.510(5)	C(45)-H(45A)	0.9900
C(34)-H(34A)	0.9900	C(45)-H(45B)	0.9900
C(34)-H(34B)	0.9900	C(45)-C(46)	1.520(5)
C(34)-C(35)	1.518(5)	C(46)-H(46A)	0.9800
C(35)-H(35)	1.0000	C(46)-H(46B)	0.9800
C(35)-C(36)	1.531(5)	C(46)-H(46C)	0.9800
C(35)-N(42)	1.463(4)	C(1)-H(1)	0.9500
C(36)-O(37)	1.230(6)	C(1)-C(2)	1.390(5)
C(36)-N(38A)	1.349(9)	C(1)-C(6)	1.385(5)
C(36)-N(38)	1.358(9)	C(2)-H(2)	0.9500
N(38A)-H(38A)	0.8800	C(2)-C(3)	1.381(5)
N(38A)-C(39A)	1.456(9)	C(3)-H(3)	0.9500
N(38)-H(38)	0.8782	C(3)-C(4)	1.389(5)
N(38)-C(39)	1.468(9)	C(4)-H(4)	0.9500
C(39)-H(39A)	0.9900	C(4)-C(5)	1.382(6)
C(39)-H(39B)	0.9900	C(5)-H(5)	0.9500
C(39)-C(40)	1.507(9)	C(5)-C(6)	1.384(5)
C(39A)-H(39C)	0.9900	C(6)-C(7)	1.507(5)
C(39A)-H(39D)	0.9900	C(7)-H(7A)	0.9900

C(7)-H(7B)	0.9900	C(24)-C(25)-H(25)	119.6
C(7)-O(8)	1.454(4)	C(26)-C(25)-C(24)	120.7(3)
O(8)-C(9)	1.347(4)	C(26)-C(25)-H(25)	119.6
C(9)-O(10)	1.184(5)	C(25)-C(26)-H(26)	120.7
C(9)-C(11)	1.513(5)	C(25)-C(26)-C(27)	118.7(4)
C(11)-H(11A)	0.9900	C(27)-C(26)-H(26)	120.7
C(11)-H(11B)	0.9900	C(26)-C(27)-H(27)	119.5
C(11)-C(12)	1.517(5)	C(28)-C(27)-C(26)	121.0(4)
C(12)-H(12)	1.0000	C(28)-C(27)-H(27)	119.5
C(12)-C(13)	1.528(5)	C(27)-C(28)-H(28)	119.8
C(12)-N(19)	1.463(4)	C(27)-C(28)-C(29)	120.4(3)
C(13)-O(14)	1.234(5)	C(29)-C(28)-H(28)	119.8
C(13)-N(15)	1.319(5)	C(24)-C(29)-C(30)	122.3(3)
N(15)-C(16)	1.461(4)	C(28)-C(29)-C(24)	118.4(3)
N(15)-H(15)	0.887(14)	C(28)-C(29)-C(30)	119.3(3)
C(16)-H(16A)	0.9900	C(29)-C(30)-H(30A)	110.2
C(16)-H(16B)	0.9900	C(29)-C(30)-H(30B)	110.2
C(16)-C(17)	1.508(6)	H(30A)-C(30)-H(30B)	108.5
C(17)-H(17A)	0.9900	O(31)-C(30)-C(29)	107.6(3)
C(17)-H(17B)	0.9900	O(31)-C(30)-H(30A)	110.2
C(17)-C(18)	1.497(7)	O(31)-C(30)-H(30B)	110.2
C(18)-H(18A)	0.9800	C(32)-O(31)-C(30)	116.0(3)
C(18)-H(18B)	0.9800	O(31)-C(32)-C(34)	109.3(3)
C(18)-H(18C)	0.9800	O(33)-C(32)-O(31)	124.6(3)
N(19)-C(20)	1.347(5)	O(33)-C(32)-C(34)	126.0(3)
N(19)-H(19)	0.890(14)	C(32)-C(34)-H(34A)	109.1
C(20)-O(21)	1.228(5)	C(32)-C(34)-H(34B)	109.1
C(20)-C(22)	1.508(5)	C(32)-C(34)-C(35)	112.7(3)
C(22)-H(22A)	0.9900	H(34A)-C(34)-H(34B)	107.8
C(22)-H(22B)	0.9900	C(35)-C(34)-H(34A)	109.1
C(22)-C(23)	1.518(6)	C(35)-C(34)-H(34B)	109.1
C(23)-H(23A)	0.9800	C(34)-C(35)-H(35)	108.9
C(23)-H(23B)	0.9800	C(34)-C(35)-C(36)	110.9(3)
C(23)-H(23C)	0.9800	C(36)-C(35)-H(35)	108.9
		N(42)-C(35)-C(34)	110.7(3)
C(25)-C(24)-H(24)	119.6	N(42)-C(35)-H(35)	108.9
C(25)-C(24)-C(29)	120.8(3)	N(42)-C(35)-C(36)	108.3(3)
C(29)-C(24)-H(24)	119.6	O(37)-C(36)-C(35)	122.0(4)

O(37)-C(36)-N(38A)	114.7(6)	H(41A)-C(41)-H(41C)	109.5
O(37)-C(36)-N(38)	132.5(6)	H(41B)-C(41)-H(41C)	109.5
N(38A)-C(36)-C(35)	123.1(6)	C(40A)-C(41A)-H(41D)	109.5
N(38)-C(36)-C(35)	105.5(5)	C(40A)-C(41A)-H(41E)	109.5
C(36)-N(38A)-H(38A)	116.5	C(40A)-C(41A)-H(41F)	109.5
C(36)-N(38A)-C(39A)	126.9(10)	H(41D)-C(41A)-H(41E)	109.5
C(39A)-N(38A)-H(38A)	116.5	H(41D)-C(41A)-H(41F)	109.5
C(36)-N(38)-H(38)	111.8	H(41E)-C(41A)-H(41F)	109.5
C(36)-N(38)-C(39)	116.3(10)	C(35)-N(42)-H(42)	119(4)
C(39)-N(38)-H(38)	111.4	C(43)-N(42)-C(35)	122.0(3)
N(38)-C(39)-H(39A)	108.9	C(43)-N(42)-H(42)	119(4)
N(38)-C(39)-H(39B)	108.9	N(42)-C(43)-C(45)	115.5(3)
N(38)-C(39)-C(40)	113.3(9)	O(44)-C(43)-N(42)	122.9(3)
H(39A)-C(39)-H(39B)	107.7	O(44)-C(43)-C(45)	121.7(3)
C(40)-C(39)-H(39A)	108.9	C(43)-C(45)-H(45A)	109.5
C(40)-C(39)-H(39B)	108.9	C(43)-C(45)-H(45B)	109.5
N(38A)-C(39A)-H(39C)	109.4	C(43)-C(45)-C(46)	110.6(3)
N(38A)-C(39A)-H(39D)	109.4	H(45A)-C(45)-H(45B)	108.1
N(38A)-C(39A)-C(40A)	111.3(9)	C(46)-C(45)-H(45A)	109.5
H(39C)-C(39A)-H(39D)	108.0	C(46)-C(45)-H(45B)	109.5
C(40A)-C(39A)-H(39C)	109.4	C(45)-C(46)-H(46A)	109.5
C(40A)-C(39A)-H(39D)	109.4	C(45)-C(46)-H(46B)	109.5
C(39A)-C(40A)-H(40A)	110.0	C(45)-C(46)-H(46C)	109.5
C(39A)-C(40A)-H(40B)	110.0	H(46A)-C(46)-H(46B)	109.5
C(39A)-C(40A)-C(41A)	108(2)	H(46A)-C(46)-H(46C)	109.5
H(40A)-C(40A)-H(40B)	108.4	H(46B)-C(46)-H(46C)	109.5
C(41A)-C(40A)-H(40A)	110.0	C(2)-C(1)-H(1)	119.7
C(41A)-C(40A)-H(40B)	110.0	C(6)-C(1)-H(1)	119.7
C(39)-C(40)-H(40C)	108.8	C(6)-C(1)-C(2)	120.6(3)
C(39)-C(40)-H(40D)	108.8	C(1)-C(2)-H(2)	119.8
C(39)-C(40)-C(41)	114(2)	C(3)-C(2)-C(1)	120.4(3)
H(40C)-C(40)-H(40D)	107.7	C(3)-C(2)-H(2)	119.8
C(41)-C(40)-H(40C)	108.8	C(2)-C(3)-H(3)	120.6
C(41)-C(40)-H(40D)	108.8	C(2)-C(3)-C(4)	118.8(4)
C(40)-C(41)-H(41A)	109.5	C(4)-C(3)-H(3)	120.6
C(40)-C(41)-H(41B)	109.5	C(3)-C(4)-H(4)	119.6
C(40)-C(41)-H(41C)	109.5	C(5)-C(4)-C(3)	120.8(4)
H(41A)-C(41)-H(41B)	109.5	C(5)-C(4)-H(4)	119.6

C(4)-C(5)-H(5)	119.8	N(15)-C(16)-H(16B)	109.0
C(4)-C(5)-C(6)	120.4(4)	N(15)-C(16)-C(17)	112.8(3)
C(6)-C(5)-H(5)	119.8	H(16A)-C(16)-H(16B)	107.8
C(1)-C(6)-C(7)	122.2(3)	C(17)-C(16)-H(16A)	109.0
C(5)-C(6)-C(1)	118.9(3)	C(17)-C(16)-H(16B)	109.0
C(5)-C(6)-C(7)	118.9(3)	C(16)-C(17)-H(17A)	109.0
C(6)-C(7)-H(7A)	110.0	C(16)-C(17)-H(17B)	109.0
C(6)-C(7)-H(7B)	110.0	H(17A)-C(17)-H(17B)	107.8
H(7A)-C(7)-H(7B)	108.4	C(18)-C(17)-C(16)	113.1(4)
O(8)-C(7)-C(6)	108.3(3)	C(18)-C(17)-H(17A)	109.0
O(8)-C(7)-H(7A)	110.0	C(18)-C(17)-H(17B)	109.0
O(8)-C(7)-H(7B)	110.0	C(17)-C(18)-H(18A)	109.5
C(9)-O(8)-C(7)	115.9(3)	C(17)-C(18)-H(18B)	109.5
O(8)-C(9)-C(11)	110.0(3)	C(17)-C(18)-H(18C)	109.5
O(10)-C(9)-O(8)	124.2(3)	H(18A)-C(18)-H(18B)	109.5
O(10)-C(9)-C(11)	125.9(3)	H(18A)-C(18)-H(18C)	109.5
C(9)-C(11)-H(11A)	109.4	H(18B)-C(18)-H(18C)	109.5
C(9)-C(11)-H(11B)	109.4	C(12)-N(19)-H(19)	117(4)
C(9)-C(11)-C(12)	111.0(3)	C(20)-N(19)-C(12)	122.0(3)
H(11A)-C(11)-H(11B)	108.0	C(20)-N(19)-H(19)	121(4)
C(12)-C(11)-H(11A)	109.4	N(19)-C(20)-C(22)	116.0(3)
C(12)-C(11)-H(11B)	109.4	O(21)-C(20)-N(19)	122.5(3)
C(11)-C(12)-H(12)	108.9	O(21)-C(20)-C(22)	121.5(3)
C(11)-C(12)-C(13)	111.8(3)	C(20)-C(22)-H(22A)	109.4
C(13)-C(12)-H(12)	108.9	C(20)-C(22)-H(22B)	109.4
N(19)-C(12)-C(11)	110.7(3)	C(20)-C(22)-C(23)	111.0(3)
N(19)-C(12)-H(12)	108.9	H(22A)-C(22)-H(22B)	108.0
N(19)-C(12)-C(13)	107.5(3)	C(23)-C(22)-H(22A)	109.4
O(14)-C(13)-C(12)	119.8(3)	C(23)-C(22)-H(22B)	109.4
O(14)-C(13)-N(15)	123.3(3)	C(22)-C(23)-H(23A)	109.5
N(15)-C(13)-C(12)	116.9(3)	C(22)-C(23)-H(23B)	109.5
C(13)-N(15)-C(16)	121.8(3)	C(22)-C(23)-H(23C)	109.5
C(13)-N(15)-H(15)	121(4)	H(23A)-C(23)-H(23B)	109.5
C(16)-N(15)-H(15)	117(4)	H(23A)-C(23)-H(23C)	109.5
N(15)-C(16)-H(16A)	109.0	H(23B)-C(23)-H(23C)	109.5

_____

Table 5. Anisotropic displacement parameters (Å^2x 10^3) for tcd722b. The anisotropic displacement factor exponent takes the form: $-2\pi^2[\,h^2\,a^{*2}U^{11} + ... + 2\,h\,k\,a^*\,b^*\,U^{12}\,]$

	U^{11}	U^{22}	U^{33}	U^{23}	U^{13}	U^{12}
C(24)	29(2)	34(2)	30(2)	3(2)	5(1)	-2(2)
C(25)	26(2)	35(2)	35(2)	0(2)	8(1)	-5(2)
C(26)	38(2)	35(2)	30(2)	1(2)	11(2)	-1(2)
C(27)	35(2)	40(2)	36(2)	6(2)	-2(2)	-1(2)
C(28)	28(2)	38(2)	39(2)	-2(2)	2(2)	-6(2)
C(29)	28(2)	25(2)	29(2)	-2(1)	7(1)	-1(1)
C(30)	28(2)	33(2)	31(2)	-1(2)	6(1)	-5(2)
O(31)	34(1)	30(1)	30(1)	2(1)	6(1)	-8(1)
C(32)	28(2)	29(2)	32(2)	0(1)	13(1)	1(2)
O(33)	44(2)	28(2)	44(2)	2(1)	8(1)	-13(1)
C(34)	32(2)	22(2)	34(2)	1(1)	10(1)	-2(2)
C(35)	36(2)	20(2)	34(2)	4(1)	13(1)	5(2)
C(36)	25(2)	43(3)	38(2)	10(2)	15(2)	10(2)
O(37)	36(1)	45(2)	50(2)	7(1)	-2(1)	-2(1)
N(38A)	23(4)	42(4)	25(6)	5(4)	-4(3)	2(4)
N(38)	23(4)	42(4)	25(6)	5(4)	-4(3)	2(4)
C(39)	24(4)	30(6)	35(6)	-8(4)	0(4)	-4(4)
C(39A)	26(4)	38(6)	25(5)	-2(4)	-4(4)	3(4)
C(40A)	36(3)	32(4)	36(3)	3(3)	1(2)	7(3)
C(40)	36(3)	32(4)	36(3)	3(3)	1(2)	7(3)
C(41)	36(6)	61(9)	54(10)	-13(7)	-8(4)	-1(5)
C(41A)	36(6)	61(9)	54(10)	-13(7)	-8(4)	-1(5)
N(42)	30(2)	19(2)	32(1)	1(1)	8(1)	2(1)
C(43)	30(2)	24(2)	28(2)	2(1)	5(1)	6(1)
O(44)	39(1)	22(2)	44(2)	2(1)	15(1)	2(1)
C(45)	27(2)	25(2)	40(2)	1(1)	7(1)	4(1)
C(46)	32(2)	47(3)	43(2)	4(2)	13(2)	-5(2)
C(1)	26(2)	30(2)	32(2)	1(1)	5(1)	2(2)
C(2)	26(2)	34(2)	34(2)	1(2)	10(1)	-3(2)
C(3)	39(2)	28(2)	33(2)	6(2)	7(2)	1(2)
C(4)	37(2)	46(3)	38(2)	13(2)	-5(2)	-7(2)
C(5)	28(2)	40(2)	41(2)	6(2)	2(2)	-7(2)
C(6)	28(2)	23(2)	31(2)	-1(1)	9(1)	-1(1)

C(7)	28(2)	29(2)	31(2)	-2(2)	4(1)	-6(2)
O(8)	34(1)	25(1)	29(1)	4(1)	5(1)	-5(1)
C(9)	29(2)	25(2)	31(2)	2(1)	9(1)	0(2)
O(10)	41(2)	34(2)	36(1)	4(1)	3(1)	-14(1)
C(11)	34(2)	24(2)	31(2)	0(1)	8(1)	-6(2)
C(12)	30(2)	24(2)	28(2)	-1(1)	4(1)	-4(1)
C(13)	26(2)	24(2)	26(2)	2(1)	0(1)	-1(1)
O(14)	32(1)	20(1)	42(1)	1(1)	5(1)	-2(1)
N(15)	29(2)	27(2)	33(2)	0(1)	10(1)	-3(1)
C(16)	29(2)	28(2)	46(2)	4(2)	13(2)	-1(2)
C(17)	50(2)	52(3)	52(3)	2(2)	19(2)	3(2)
C(18)	65(3)	74(4)	47(3)	2(2)	18(2)	11(3)
N(19)	28(2)	20(2)	33(2)	-1(1)	5(1)	-5(1)
C(20)	26(2)	26(2)	34(2)	-1(1)	8(1)	-2(1)
O(21)	43(2)	22(2)	40(1)	1(1)	1(1)	-3(1)
C(22)	33(2)	24(2)	52(2)	-1(2)	-3(2)	-4(2)
C(23)	66(3)	61(3)	41(2)	2(2)	-11(2)	-9(3)

_____

Appendix

Table 6. Hydrogen coordinates (x 10^4) and isotropic displacement parameters ($Å^2$x 10 ^{3}) for tcd722b.

_____

	x	y	z	U(eq)
_____

H(24)	7139	5281	2451	37
H(25)	7447	8457	2046	38
H(26)	6584	9542	1573	41
H(27)	5397	7441	1517	45
H(28)	5070	4336	1928	42
H(30A)	5296	2542	2519	37
H(30B)	5965	642	2405	37
H(34A)	6546	3699	3475	35
H(34B)	7252	2129	3337	35
H(35)	6716	-1869	3597	35
H(38A)	7455	-3164	4141	36
H(38)	7591	-3208	3925	36
H(39A)	8595	-1068	4293	36
H(39B)	8370	-4062	4376	36
H(39C)	8261	582	4544	36
H(39D)	8721	-1844	4392	36
H(40A)	8054	-4871	4711	41
H(40B)	7526	-2541	4843	41
H(40C)	7476	-2198	4764	41
H(40D)	7902	569	4722	41
H(41A)	8433	-1329	5238	76
H(41B)	9071	-1537	4965	76
H(41C)	8575	-4088	5047	76
H(41D)	9134	-3107	5028	76
H(41E)	8482	-3248	5295	76
H(41F)	8681	-479	5119	76
H(45A)	4420	-1962	3993	36
H(45B)	4800	711	4151	36
H(46A)	4970	-4344	4488	60
H(46B)	4408	-2073	4604	60
H(46C)	5309	-1620	4649	60
H(1)	2772	4940	2645	35

H(2)	2490	1798	3062	37
H(3)	3399	675	3515	40
H(4)	4596	2710	3541	49
H(5)	4884	5788	3121	44
H(7A)	3967	9492	2661	35
H(7B)	4609	7543	2533	35
H(11A)	2620	8195	1735	35
H(11B)	3288	6438	1594	35
H(12)	3197	12043	1473	32
H(16A)	5373	10704	1045	41
H(16B)	5263	13788	956	41
H(17A)	5332	11202	444	61
H(17B)	4589	9608	536	61
H(18A)	4214	12729	122	92
H(18B)	4635	15045	348	92
H(18C)	3893	13664	481	92
H(22A)	1187	11723	702	44
H(22B)	1690	9243	597	44
H(23A)	1427	12256	119	85
H(23B)	2322	11857	211	85
H(23C)	1910	14477	337	85
H(19)	2500(30)	8160(50)	1042(15)	85
H(15)	4170(30)	13660(60)	1193(16)	85
H(42)	5800(30)	1860(60)	3899(16)	85

_____

Table 7. Torsion angles [°] for tcd722b.

_____

C(24)-C(25)-C(26)-C(27)	0.5(6)	N(42)-C(35)-C(36)-N(38)	92.2(10)
C(24)-C(29)-C(30)-O(31)	27.2(5)	N(42)-C(43)-C(45)-C(46)	-122.5(4)
C(25)-C(24)-C(29)-C(28)	1.2(6)	O(44)-C(43)-C(45)-C(46)	56.7(5)
C(25)-C(24)-C(29)-C(30)	179.4(3)	C(1)-C(2)-C(3)-C(4)	-0.2(6)
C(25)-C(26)-C(27)-C(28)	0.3(6)	C(1)-C(6)-C(7)-O(8)	-27.3(5)
C(26)-C(27)-C(28)-C(29)	-0.4(6)	C(2)-C(1)-C(6)-C(5)	-1.4(6)
C(27)-C(28)-C(29)-C(24)	-0.4(6)	C(2)-C(1)-C(6)-C(7)	-179.4(3)
C(27)-C(28)-C(29)-C(30)	-178.7(4)	C(2)-C(3)-C(4)-C(5)	-0.3(6)
C(28)-C(29)-C(30)-O(31)	-154.5(3)	C(3)-C(4)-C(5)-C(6)	0.0(7)
C(29)-C(24)-C(25)-C(26)	-1.2(6)	C(4)-C(5)-C(6)-C(1)	0.8(6)
C(29)-C(30)-O(31)-C(32)	-172.3(3)	C(4)-C(5)-C(6)-C(7)	179.0(4)
C(30)-O(31)-C(32)-O(33)	1.2(5)	C(5)-C(6)-C(7)-O(8)	154.7(3)
C(30)-O(31)-C(32)-C(34)	179.3(3)	C(6)-C(1)-C(2)-C(3)	1.1(6)
O(31)-C(32)-C(34)-C(35)	179.9(3)	C(6)-C(7)-O(8)-C(9)	175.4(3)
C(32)-C(34)-C(35)-C(36)	162.8(3)	C(7)-O(8)-C(9)-O(10)	-0.2(5)
C(32)-C(34)-C(35)-N(42)	-76.9(4)	C(7)-O(8)-C(9)-C(11)	-180.0(3)
O(33)-C(32)-C(34)-C(35)	-2.0(5)	O(8)-C(9)-C(11)-C(12)	-179.7(3)
C(34)-C(35)-C(36)-O(37)	31.8(5)	C(9)-C(11)-C(12)-C(13)	72.8(4)
C(34)-C(35)-C(36)-N(38A)	-154.0(10)	C(9)-C(11)-C(12)-N(19)	-167.4(3)
C(34)-C(35)-C(36)-N(38)	-146.0(9)	O(10)-C(9)-C(11)-C(12)	0.6(5)
C(34)-C(35)-N(42)-C(43)	139.5(3)	C(11)-C(12)-C(13)-O(14)	42.5(4)
C(35)-C(36)-N(38A)-C(39A)	-174.0(12)	C(11)-C(12)-C(13)-N(15)	-139.9(3)
C(35)-C(36)-N(38)-C(39)	179.2(11)	C(11)-C(12)-N(19)-C(20)	143.4(3)
C(35)-N(42)-C(43)-O(44)	1.0(5)	C(12)-C(13)-N(15)-C(16)	-173.8(3)
C(35)-N(42)-C(43)-C(45)	-179.9(3)	C(12)-N(19)-C(20)-O(21)	-3.5(5)
C(36)-C(35)-N(42)-C(43)	-98.6(4)	C(12)-N(19)-C(20)-C(22)	177.0(3)
C(36)-N(38A)-C(39A)-C(40A)	140.2(16)	C(13)-C(12)-N(19)-C(20)	-94.1(4)
C(36)-N(38)-C(39)-C(40)	77.5(18)	C(13)-N(15)-C(16)-C(17)	74.3(5)
O(37)-C(36)-N(38A)-C(39A)	1(2)	O(14)-C(13)-N(15)-C(16)	3.7(5)
O(37)-C(36)-N(38)-C(39)	2(2)	N(15)-C(16)-C(17)-C(18)	63.4(5)
N(38A)-C(39A)-C(40A)-C(41A)	-175(2)	N(19)-C(12)-C(13)-O(14)	-79.3(4)
N(38)-C(39)-C(40)-C(41)	166(2)	N(19)-C(12)-C(13)-N(15)	98.3(4)
N(42)-C(35)-C(36)-O(37)	-89.9(4)	N(19)-C(20)-C(22)-C(23)	-129.3(4)
N(42)-C(35)-C(36)-N(38A)	84.3(11)	O(21)-C(20)-C(22)-C(23)	51.2(5)

_____

Table 8. Hydrogen bonds for tcd722b [Å and °].

D-H...A	d(D-H)	d(H...A)	d(D...A)	<(DHA)
C(34)-H(34A)...O(44)#1	0.99	2.51	3.348(4)	141.8
N(38A)-H(38A)...O(37)#2	0.88	2.21	3.001(10)	150.1
N(38)-H(38)...O(37)#2	0.88	2.15	2.707(10)	120.4
C(39)-H(39B)...O(37)#2	0.99	2.45	3.032(11)	117.0

Symmetry transformations used to generate equivalent atoms:

#1 x,y+1,z   #2 x,y-1,z

Crystal Structure Report for 3.56. Dissolved in Ethyl acetate. Diethyl Ether was the solvent used for diffusion to grow the crystal.

A specimen of $C_{17}H_{24}N_2O_4$, approximate dimensions 0.060 mm x 0.060 mm x 0.570 mm, was used for the X-ray crystallographic analysis. The X-ray intensity data were measured at 100(2)K using an Oxford Cryosystems low temperature device using a MiTeGen micromount. See Table 1 for collection parameters and exposure time. Bruker APEX software was used to correct for Lorentz and polarization effects.

A total of 3214 frames were collected. The total exposure time was 37.52 hours. The integration of the data using a triclinic unit cell yielded a total of 9553 reflections to a maximum θ angle of 68.34° (0.83 Å resolution), of which 3040 were independent (average redundancy 3.142, completeness = 98.8%, R_{int} = 4.24%, R_{sig} = 4.53%) and 2630 (86.51%) were greater than $2\sigma(F^2)$. The final cell constants of $\underline{a}$ = 5.0625(2) Å, $\underline{b}$ = 9.7762(4) Å, $\underline{c}$ = 17.7883(7) Å, α = 76.791(2)°, β = 88.028(2)°, γ = 79.244(2)°, volume = 842.00(6) $Å^3$, are based upon the refinement of the XYZ-centroids of reflections above 20 σ(I). Data were corrected for absorption effects using the Multi-Scan method (SADABS). The ratio of minimum to maximum apparent transmission was 0.885. The calculated minimum and maximum transmission coefficients (based on crystal size) are 0.6241 and 0.7531.

The structure was solved using the Bruker APEX Software Package and refined with XL in Olex2, using the space group P$\overline{1}$, with Z = 2 for the formula unit, $C_{17}H_{24}N_2O_4$. The final anisotropic full-matrix least-squares refinement on F^2 with 218 variables converged at R1 = 5.21%, for the observed data and wR2 = 14.79% for all data. The goodness-of-fit was 1.063. The largest peak in the final difference electron density synthesis was 0.325 $e^-/Å^3$ and the largest hole was -0.212 $e^-/Å^3$ with an RMS deviation of 0.056 $e^-/Å^3$. On the basis of the final model, the calculated density was 1.264 g/cm^3 and F(000), 344 e^-.

Refinement Note: Donor NH hydrogen atoms refined with restraints (DFIX).

References: see CIF.

Table 1: Data collection details for TCD715.

Axis	dx/mm	2θ/°	ω/°	φ/°	χ/°	Width/°	Frames	Time/s	Wavelength/Å	Voltage/kV	Current/mA	Temperature/K
Omega	55.000	110.58	339.09	120.00	64.50	1.10	134	55.00	1.54184	45	0.6	100
Omega	55.000	111.00	353.94	252.34	72.96	1.10	70	55.00	1.54184	45	0.6	100
Phi	55.000	110.89	0.81	360.00	23.00	1.10	327	55.00	1.54184	45	0.6	100
Phi	55.000	-53.29	347.95	360.00	23.00	1.10	327	20.00	1.54184	45	0.6	100
Omega	55.000	101.26	152.14	120.02	-81.96	1.10	85	55.00	1.54184	45	0.6	100
Omega	55.000	110.58	93.59	48.00	-54.74	1.10	130	55.00	1.54184	45	0.6	100
Omega	55.000	-55.62	288.52	0.00	-64.50	1.10	115	20.00	1.54184	45	0.6	100
Omega	55.000	110.58	93.59	0.00	-54.74	1.10	130	55.00	1.54184	45	0.6	100
Omega	55.000	-55.62	288.52	224.00	-64.50	1.10	115	20.00	1.54184	45	0.6	100
Omega	55.000	110.58	93.59	240.00	-54.74	1.10	130	55.00	1.54184	45	0.6	100
Omega	55.000	-0.33	234.42	288.00	54.74	1.10	130	20.00	1.54184	45	0.6	100
Omega	55.000	110.58	339.10	360.00	64.50	1.10	134	55.00	1.54184	45	0.6	100
Omega	55.000	-55.62	179.12	224.00	54.74	1.10	130	20.00	1.54184	45	0.6	100
Omega	55.000	110.58	93.59	168.00	-54.74	1.10	130	55.00	1.54184	45	0.6	100
Omega	55.000	-55.62	179.12	128.00	54.74	1.10	130	20.00	1.54184	45	0.6	100
Omega	55.000	110.58	93.59	264.00	-54.74	1.10	130	55.00	1.54184	45	0.6	100
Omega	55.000	110.58	93.59	336.00	-54.74	1.10	130	55.00	1.54184	45	0.6	100
Omega	50.000	109.30	96.19	120.00	-54.74	1.10	122	55.00	1.54184	45	0.6	100
Omega	50.000	109.30	342.11	216.00	64.50	1.10	127	55.00	1.54184	45	0.6	100
Omega	50.000	-49.30	190.47	180.00	54.74	1.10	122	20.00	1.54184	45	0.6	100
Omega	50.000	109.30	96.19	72.00	-54.74	1.10	122	55.00	1.54184	45	0.6	100
Omega	50.000	-57.74	182.02	360.00	54.74	1.10	122	20.00	1.54184	45	0.6	100
Omega	50.000	109.30	96.19	24.00	-54.74	1.10	122	55.00	1.54184	45	0.6	100

Table 2. Crystal data and structure refinement for tcd715.

Identification code	tcd715
Empirical formula	$C_{17}H_{24}N_2O_4$
Formula weight	320.38
Temperature	100(2) K
Wavelength	1.54178 Å
Crystal system	Triclinic
Space group	$P\overline{1}$
Unit cell dimensions	a = 5.0625(2) Å α= 76.791(2)°.
	b = 9.7762(4) Å β= 88.028(2)°.
	c = 17.7883(7) Å γ = 79.244(2)°.
Volume	842.00(6) Å^3
Z	2
Density (calculated)	1.264 Mg/m^3
Absorption coefficient	0.738 mm^{-1}
F(000)	344
Crystal size	0.57 x 0.06 x 0.06 mm^3
Theta range for data collection	2.551 to 68.339°.
Index ranges	-6≤h≤5, -11≤k≤11, -21≤l≤21
Reflections collected	9553
Independent reflections	3040 [R(int) = 0.0424]
Completeness to theta = 67.679°	99.0 %
Absorption correction	Semi-empirical from equivalents
Max. and min. transmission	0.7531 and 0.6665
Refinement method	Full-matrix least-squares on F^2
Data / restraints / parameters	3040 / 2 / 218
Goodness-of-fit on F^2	1.063
Final R indices [I>2σ(I)]	R1 = 0.0521, wR2 = 0.1404
R indices (all data)	R1 = 0.0594, wR2 = 0.1479
Largest diff. peak and hole	0.325 and -0.212 e.Å^{-3}

Crystal Data for $C_{17}H_{24}N_2O_4$ (*M* =320.38 g/mol): triclinic, space group $P\overline{1}$ (no. 2), *a* = 5.0625(2) Å, *b* = 9.7762(4) Å, *c* = 17.7883(7) Å, *α* = 76.791(2)°, *β* = 88.028(2)°, *γ* = 79.244(2)°, *V* = 842.00(6) Å^3, Z = 2, *T* = 100(2) K, μ(CuKα) = 0.738 mm^{-1}, *Dcalc* = 1.264 g/cm^3, 9553 reflections measured (5.102° ≤ 2Θ ≤ 136.678°), 3040 unique (R_{int} = 0.0424, R$_{sigma}$ = 0.0453) which were used in all calculations. The final R_1 was 0.0521 (I > 2σ(I)) and *wR$_2$* was 0.1479 (all data).

Appendix

Table 3. Atomic coordinates (x 10^4) and equivalent isotropic displacement parameters (Å^2x 10^3) for tcd715. U(eq) is defined as one third of the trace of the orthogonalized U^{ij} tensor.

	x	y	z	U(eq)
C(1)	617(4)	1251(2)	5632(1)	30(1)
C(2)	-1177(4)	617(2)	6144(1)	32(1)
C(3)	-2392(4)	1272(2)	6712(1)	32(1)
C(4)	-1802(4)	2584(2)	6766(1)	31(1)
C(5)	-4(4)	3216(2)	6258(1)	29(1)
C(6)	1207(4)	2568(2)	5683(1)	26(1)
C(7)	3153(4)	3289(2)	5144(1)	28(1)
O(8)	3510(3)	2661(1)	4477(1)	28(1)
C(9)	5327(3)	3108(2)	3961(1)	25(1)
O(10)	6653(3)	3979(2)	4020(1)	34(1)
C(11)	5463(3)	2348(2)	3310(1)	26(1)
C(12)	7364(3)	2877(2)	2673(1)	24(1)
N(13)	7495(3)	2031(2)	2089(1)	25(1)
C(14)	9789(3)	1617(2)	1739(1)	24(1)
O(15)	11950(2)	1910(1)	1884(1)	30(1)
C(16)	9545(4)	770(2)	1135(1)	30(1)
C(17)	12229(4)	-50(2)	942(1)	33(1)
C(18)	6398(3)	4455(2)	2282(1)	24(1)
O(19)	3986(2)	4948(1)	2178(1)	30(1)
N(20)	8355(3)	5190(2)	2044(1)	27(1)
C(21)	7817(4)	6678(2)	1621(1)	30(1)
C(22)	8642(4)	6853(2)	778(1)	35(1)
C(23)	7001(5)	6178(2)	313(1)	41(1)

Table 4. Bond lengths [Å] and angles [°] for tcd715.

_____

C(1)-H(1)	0.9500	N(20)-C(21)	1.457(2)
C(1)-C(2)	1.390(3)	N(20)-H(20)	0.877(16)
C(1)-C(6)	1.398(2)	C(21)-H(21A)	0.9900
C(2)-H(2)	0.9500	C(21)-H(21B)	0.9900
C(2)-C(3)	1.384(3)	C(21)-C(22)	1.523(3)
C(3)-H(3)	0.9500	C(22)-H(22A)	0.9900
C(3)-C(4)	1.395(3)	C(22)-H(22B)	0.9900
C(4)-H(4)	0.9500	C(22)-C(23)	1.520(3)
C(4)-C(5)	1.387(3)	C(23)-H(23A)	0.9800
C(5)-H(5)	0.9500	C(23)-H(23B)	0.9800
C(5)-C(6)	1.389(3)	C(23)-H(23C)	0.9800
C(6)-C(7)	1.507(2)		
C(7)-H(7A)	0.9900	C(2)-C(1)-H(1)	119.9
C(7)-H(7B)	0.9900	C(2)-C(1)-C(6)	120.22(17)
C(7)-O(8)	1.448(2)	C(6)-C(1)-H(1)	119.9
O(8)-C(9)	1.336(2)	C(1)-C(2)-H(2)	119.6
C(9)-O(10)	1.203(2)	C(3)-C(2)-C(1)	120.71(17)
C(9)-C(11)	1.506(2)	C(3)-C(2)-H(2)	119.6
C(11)-H(11A)	0.9900	C(2)-C(3)-H(3)	120.4
C(11)-H(11B)	0.9900	C(2)-C(3)-C(4)	119.27(17)
C(11)-C(12)	1.523(2)	C(4)-C(3)-H(3)	120.4
C(12)-H(12)	1.0000	C(3)-C(4)-H(4)	119.9
C(12)-N(13)	1.461(2)	C(5)-C(4)-C(3)	120.12(17)
C(12)-C(18)	1.534(2)	C(5)-C(4)-H(4)	119.9
N(13)-C(14)	1.338(2)	C(4)-C(5)-H(5)	119.6
N(13)-H(13)	0.872(16)	C(4)-C(5)-C(6)	120.89(17)
C(14)-O(15)	1.232(2)	C(6)-C(5)-H(5)	119.6
C(14)-C(16)	1.519(2)	C(1)-C(6)-C(7)	121.98(16)
C(16)-H(16A)	0.9900	C(5)-C(6)-C(1)	118.79(17)
C(16)-H(16B)	0.9900	C(5)-C(6)-C(7)	119.22(15)
C(16)-C(17)	1.514(3)	C(6)-C(7)-H(7A)	110.0
C(17)-H(17A)	0.9800	C(6)-C(7)-H(7B)	110.0
C(17)-H(17B)	0.9800	H(7A)-C(7)-H(7B)	108.4
C(17)-H(17C)	0.9800	O(8)-C(7)-C(6)	108.50(13)
C(18)-O(19)	1.230(2)	O(8)-C(7)-H(7A)	110.0
C(18)-N(20)	1.332(2)	O(8)-C(7)-H(7B)	110.0

C(9)-O(8)-C(7)	116.51(13)	C(16)-C(17)-H(17B)	109.5
O(8)-C(9)-C(11)	109.80(14)	C(16)-C(17)-H(17C)	109.5
O(10)-C(9)-O(8)	124.45(16)	H(17A)-C(17)-H(17B)	109.5
O(10)-C(9)-C(11)	125.75(16)	H(17A)-C(17)-H(17C)	109.5
C(9)-C(11)-H(11A)	109.1	H(17B)-C(17)-H(17C)	109.5
C(9)-C(11)-H(11B)	109.1	O(19)-C(18)-C(12)	120.73(15)
C(9)-C(11)-C(12)	112.64(13)	O(19)-C(18)-N(20)	124.37(16)
H(11A)-C(11)-H(11B)	107.8	N(20)-C(18)-C(12)	114.84(15)
C(12)-C(11)-H(11A)	109.1	C(18)-N(20)-C(21)	122.44(15)
C(12)-C(11)-H(11B)	109.1	C(18)-N(20)-H(20)	120.3(15)
C(11)-C(12)-H(12)	109.3	C(21)-N(20)-H(20)	117.3(15)
C(11)-C(12)-C(18)	111.60(14)	N(20)-C(21)-H(21A)	109.1
N(13)-C(12)-C(11)	109.01(13)	N(20)-C(21)-H(21B)	109.1
N(13)-C(12)-H(12)	109.3	N(20)-C(21)-C(22)	112.35(15)
N(13)-C(12)-C(18)	108.44(13)	H(21A)-C(21)-H(21B)	107.9
C(18)-C(12)-H(12)	109.3	C(22)-C(21)-H(21A)	109.1
C(12)-N(13)-H(13)	114.4(16)	C(22)-C(21)-H(21B)	109.1
C(14)-N(13)-C(12)	122.38(14)	C(21)-C(22)-H(22A)	108.8
C(14)-N(13)-H(13)	123.1(16)	C(21)-C(22)-H(22B)	108.8
N(13)-C(14)-C(16)	115.32(14)	H(22A)-C(22)-H(22B)	107.7
O(15)-C(14)-N(13)	122.84(16)	C(23)-C(22)-C(21)	113.63(16)
O(15)-C(14)-C(16)	121.84(16)	C(23)-C(22)-H(22A)	108.8
C(14)-C(16)-H(16A)	109.1	C(23)-C(22)-H(22B)	108.8
C(14)-C(16)-H(16B)	109.1	C(22)-C(23)-H(23A)	109.5
H(16A)-C(16)-H(16B)	107.8	C(22)-C(23)-H(23B)	109.5
C(17)-C(16)-C(14)	112.64(15)	C(22)-C(23)-H(23C)	109.5
C(17)-C(16)-H(16A)	109.1	H(23A)-C(23)-H(23B)	109.5
C(17)-C(16)-H(16B)	109.1	H(23A)-C(23)-H(23C)	109.5
C(16)-C(17)-H(17A)	109.5	H(23B)-C(23)-H(23C)	109.5

_____

Table 5. Anisotropic displacement parameters ($\mathring{A}^2$x 10^3) for tcd715. The anisotropic displacement factor exponent takes the form: $-2\pi^2[\,h^2\,a^{*2}U^{11} + ... + 2\,h\,k\,a^*\,b^*\,U^{12}\,]$

	U^{11}	U^{22}	U^{33}	U^{23}	U^{13}	U^{12}
C(1)	32(1)	31(1)	31(1)	-11(1)	2(1)	-9(1)
C(2)	35(1)	30(1)	35(1)	-7(1)	1(1)	-12(1)
C(3)	28(1)	36(1)	30(1)	-3(1)	2(1)	-11(1)
C(4)	28(1)	37(1)	28(1)	-10(1)	1(1)	-6(1)
C(5)	29(1)	31(1)	30(1)	-10(1)	-1(1)	-9(1)
C(6)	24(1)	29(1)	26(1)	-6(1)	-2(1)	-8(1)
C(7)	30(1)	30(1)	27(1)	-10(1)	2(1)	-11(1)
O(8)	28(1)	34(1)	30(1)	-14(1)	5(1)	-14(1)
C(9)	20(1)	27(1)	28(1)	-5(1)	-1(1)	-5(1)
O(10)	36(1)	40(1)	34(1)	-15(1)	7(1)	-21(1)
C(11)	22(1)	28(1)	31(1)	-9(1)	2(1)	-9(1)
C(12)	18(1)	27(1)	29(1)	-11(1)	1(1)	-7(1)
N(13)	20(1)	28(1)	31(1)	-11(1)	1(1)	-8(1)
C(14)	21(1)	25(1)	28(1)	-5(1)	1(1)	-7(1)
O(15)	21(1)	38(1)	36(1)	-16(1)	3(1)	-10(1)
C(16)	25(1)	37(1)	33(1)	-15(1)	2(1)	-10(1)
C(17)	29(1)	37(1)	35(1)	-16(1)	-1(1)	-3(1)
C(18)	20(1)	29(1)	25(1)	-12(1)	1(1)	-6(1)
O(19)	19(1)	30(1)	41(1)	-11(1)	-1(1)	-6(1)
N(20)	19(1)	28(1)	33(1)	-6(1)	-1(1)	-6(1)
C(21)	27(1)	28(1)	36(1)	-6(1)	-3(1)	-7(1)
C(22)	30(1)	37(1)	37(1)	-2(1)	-1(1)	-12(1)
C(23)	42(1)	47(1)	36(1)	-10(1)	0(1)	-15(1)

Appendix

Table 6. Hydrogen coordinates (x 10^4) and isotropic displacement parameters (Å^2x 10 ^{3}) for tcd715.

_____

	x	y	z	U(eq)
H(1)	1445	788	5247	36
H(2)	-1573	-276	6103	39
H(3)	-3614	833	7060	38
H(4)	-2633	3045	7152	37
H(5)	404	4103	6304	34
H(7A)	2441	4327	4981	33
H(7B)	4901	3155	5410	33
H(11A)	3639	2491	3087	31
H(11B)	6070	1311	3517	31
H(12)	9198	2757	2898	29
H(16A)	8320	89	1327	36
H(16B)	8738	1434	659	36
H(17A)	11961	-586	557	50
H(17B)	13031	-715	1411	50
H(17C)	13430	622	734	50
H(21A)	8808	7240	1871	36
H(21B)	5873	7065	1647	36
H(22A)	8451	7885	537	42
H(22B)	10564	6417	755	42
H(23A)	7643	6320	-221	61
H(23B)	5102	6628	317	61
H(23C)	7200	5153	542	61
H(20)	10040(30)	4780(20)	2130(13)	31(6)
H(13)	5940(40)	1880(30)	1964(14)	38(6)

_____

Table 7. Torsion angles [°] for tcd715.

_____

C(1)-C(2)-C(3)-C(4)	0.1(3)
C(1)-C(6)-C(7)-O(8)	17.9(2)
C(2)-C(1)-C(6)-C(5)	0.8(3)
C(2)-C(1)-C(6)-C(7)	179.59(17)
C(2)-C(3)-C(4)-C(5)	-0.4(3)
C(3)-C(4)-C(5)-C(6)	0.8(3)
C(4)-C(5)-C(6)-C(1)	-1.0(3)
C(4)-C(5)-C(6)-C(7)	-179.88(16)
C(5)-C(6)-C(7)-O(8)	-163.24(15)
C(6)-C(1)-C(2)-C(3)	-0.3(3)
C(6)-C(7)-O(8)-C(9)	-175.47(14)
C(7)-O(8)-C(9)-O(10)	0.1(3)
C(7)-O(8)-C(9)-C(11)	179.63(14)
O(8)-C(9)-C(11)-C(12)	176.22(14)
C(9)-C(11)-C(12)-N(13)	176.72(14)
C(9)-C(11)-C(12)-C(18)	-63.53(18)
O(10)-C(9)-C(11)-C(12)	-4.3(3)
C(11)-C(12)-N(13)-C(14)	-140.90(16)
C(11)-C(12)-C(18)-O(19)	-36.4(2)
C(11)-C(12)-C(18)-N(20)	146.41(15)
C(12)-N(13)-C(14)-O(15)	0.4(3)
C(12)-N(13)-C(14)-C(16)	-178.76(15)
C(12)-C(18)-N(20)-C(21)	176.37(15)
N(13)-C(12)-C(18)-O(19)	83.70(19)
N(13)-C(12)-C(18)-N(20)	-93.51(17)
N(13)-C(14)-C(16)-C(17)	-162.13(16)
O(15)-C(14)-C(16)-C(17)	18.7(2)
C(18)-C(12)-N(13)-C(14)	97.41(18)
C(18)-N(20)-C(21)-C(22)	-109.33(19)
O(19)-C(18)-N(20)-C(21)	-0.7(3)
N(20)-C(21)-C(22)-C(23)	65.7(2)

Table 8. Hydrogen bonds for tcd715 [Å and °].

_____

D-H...A	d(D-H)	d(H...A)	d(D...A)	<(DHA)
C(11)-H(11A)...O(15)#1	0.99	2.55	3.296(2)	132
N(20)-H(20)...O(19)#2	0.877(16)	2.040(18)	2.8300(19)	149(2)
N(13)-H(13)...O(15)#1	0.872(16)	2.025(17)	2.8710(19)	163(2)

_____

Symmetry transformations used to generate equivalent atoms:

#1 x-1,y,z   #2 x+1,y,z

¹H-NMR Spectra Expanded Region. Chapter 3
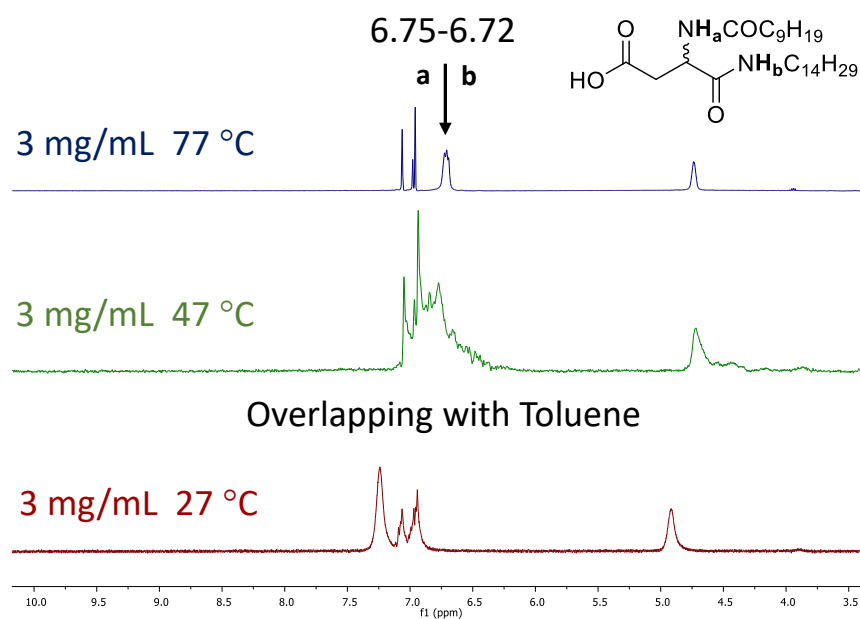
Expanded region. ¹H NMR spectra **3.61.** in (D$_8$)-toluene at 3 mg/mL at different temperature.
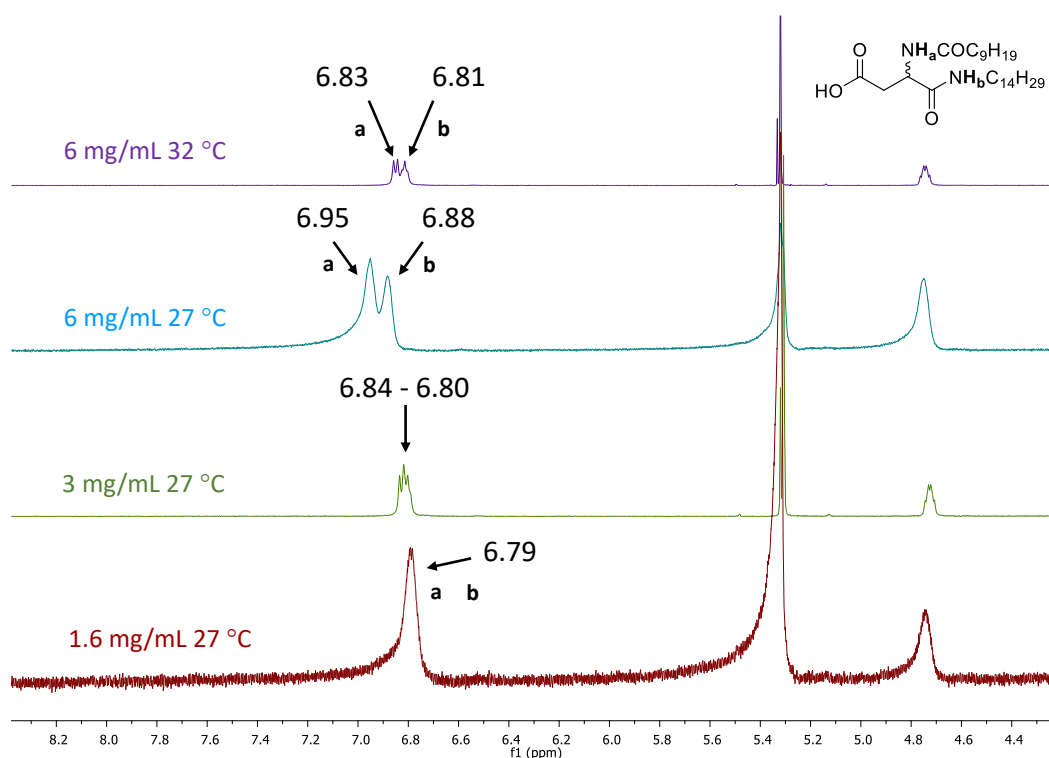
Expanded region. ¹H NMR spectra **3.61.** in (D$_2$)-DCM at different concentrations and temperature.
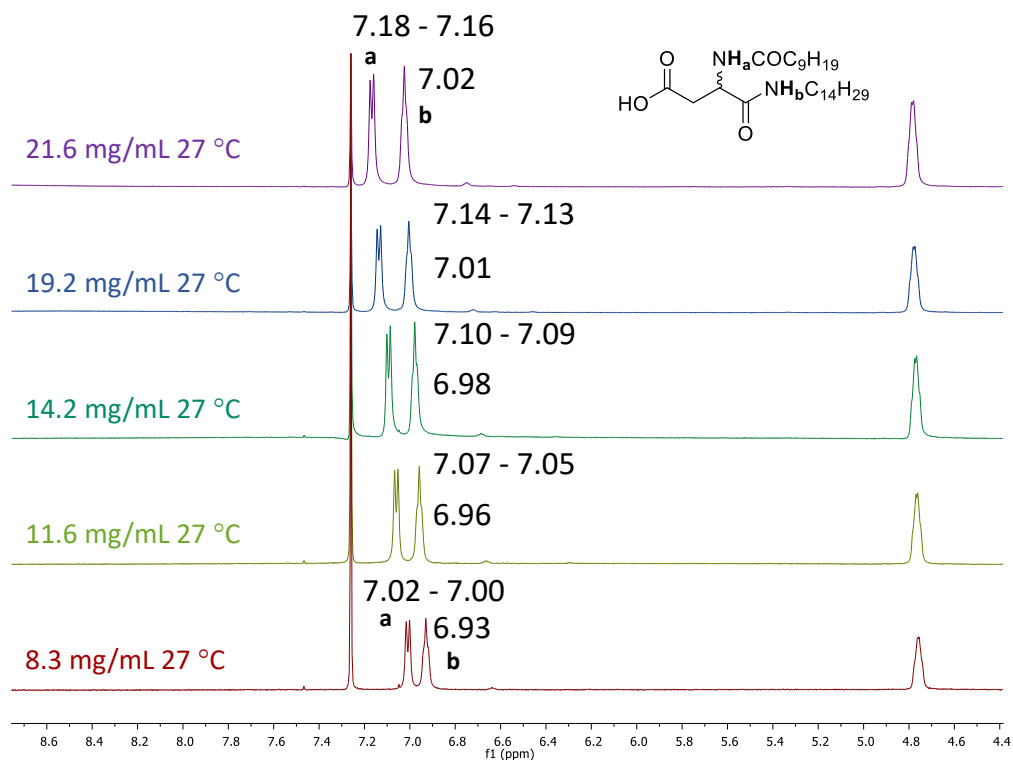
Expanded region. ^{1}H NMR spectra **3.61.** in (D)-chloroform at different concentrations.
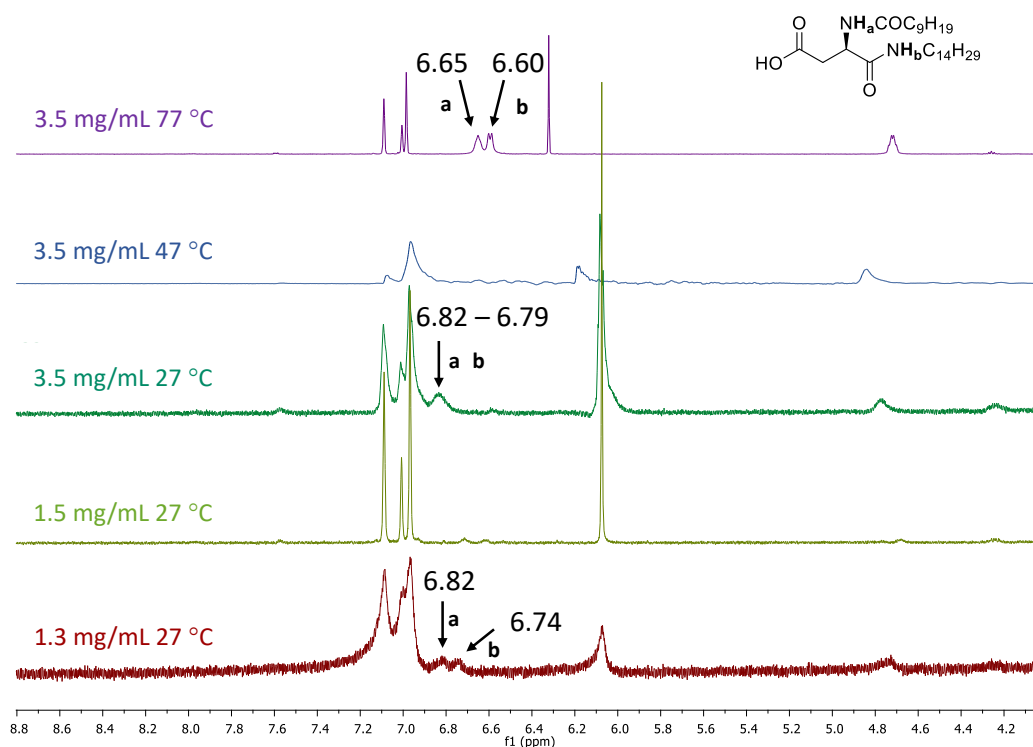
Expanded region. ^{1}H NMR spectra **3.65.** in (D$_8$)-toluene at different concentrations and temperature.
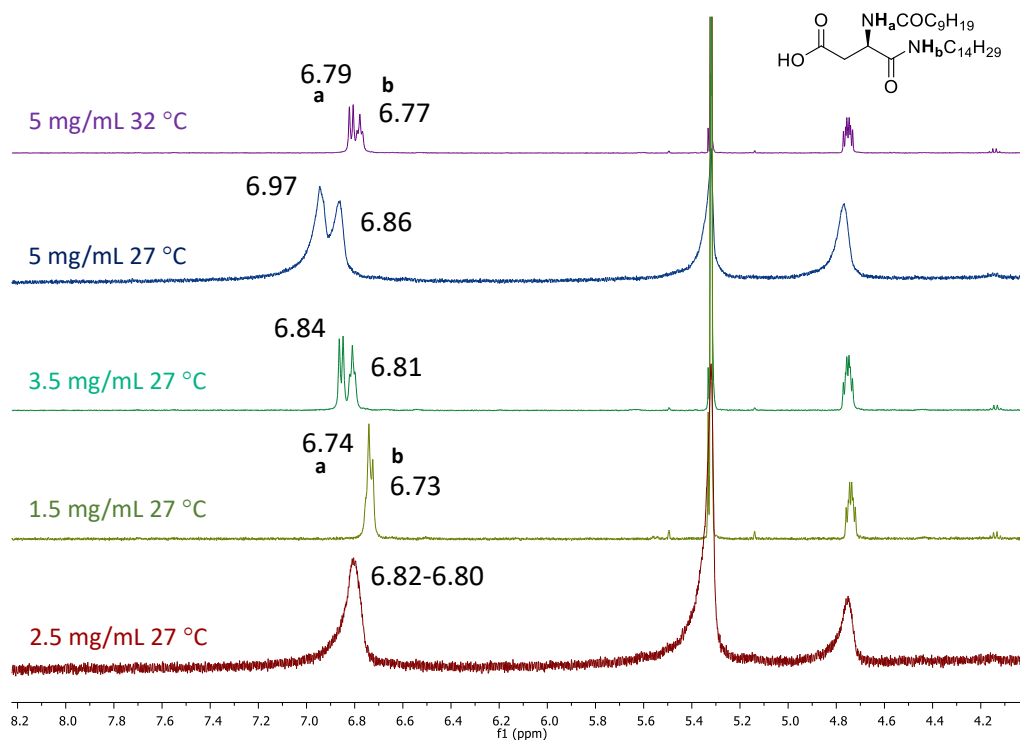
Expanded region. ^{1}H NMR spectra **3.65.** in (D$_2$)-DCM at different concentrations and temperature.
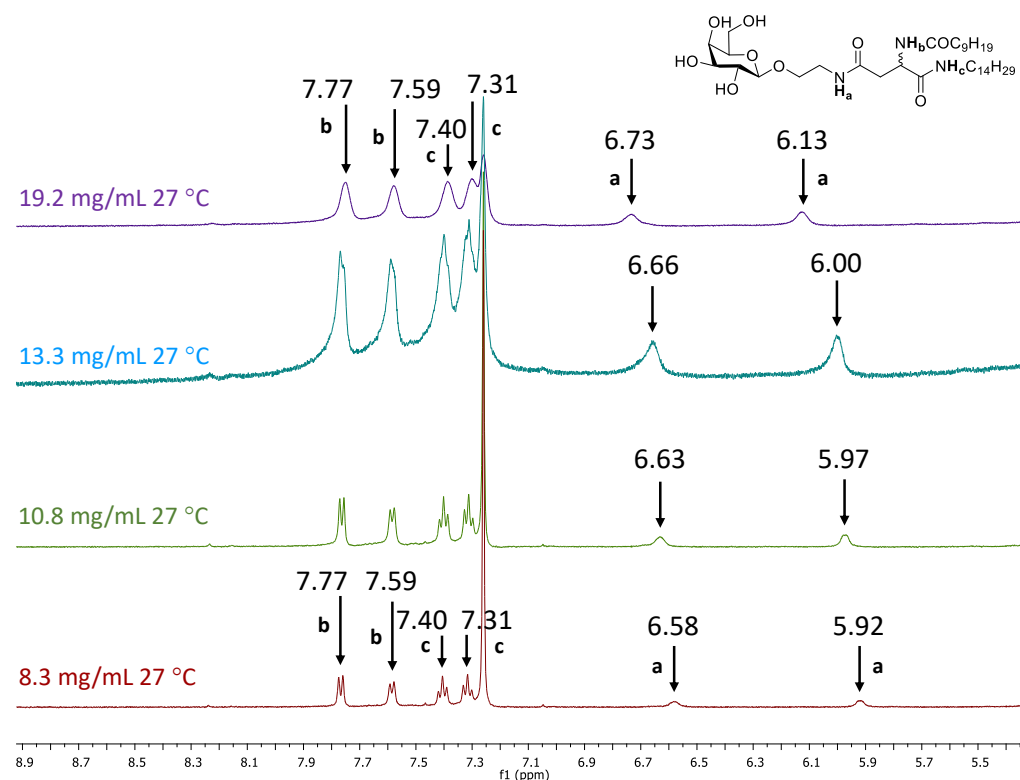
Expanded region. ^{1}H NMR spectra **3.67.** in (D)-chloroform at different concentrations.

Appendix
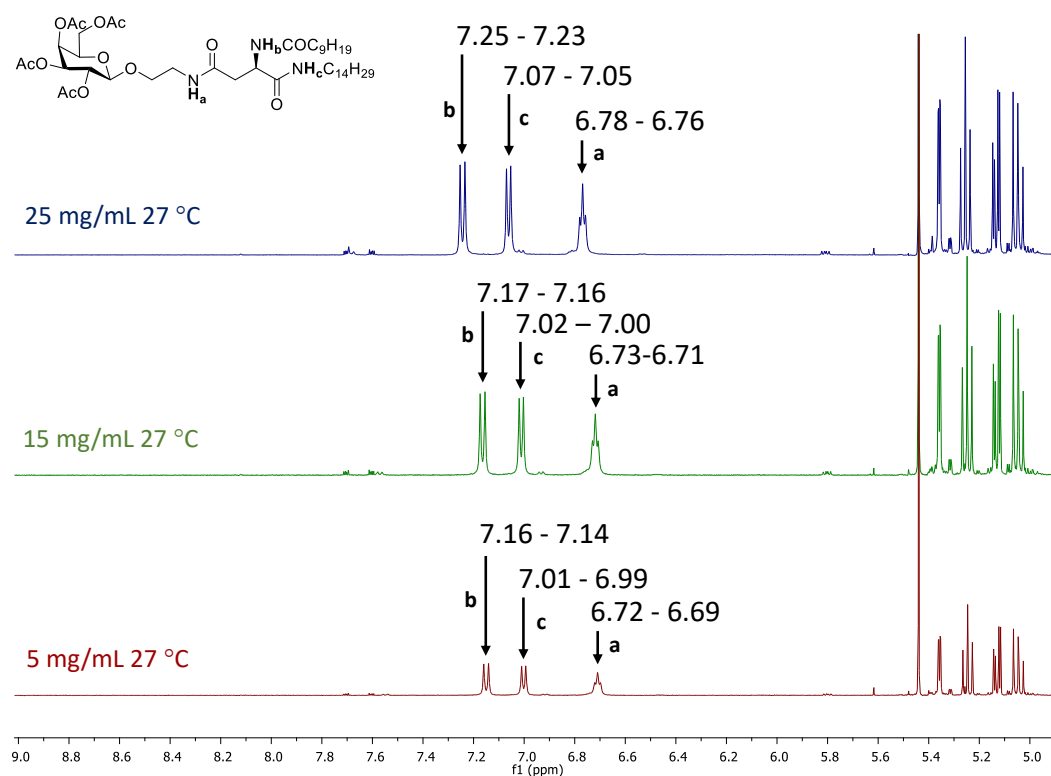
Expanded region. ^{1}H NMR spectra **3.68.** in (D$_3$)-MeCN at different concentrations.

FTIR of Different Solvents Used

Toluene

Toluene, Cell.sp

Cyclohexane

Cyclohexane.sp

Appendix

Chloroform

Chloroform.sp

EtOAc

EtOAc.sp

Appendix

MeCN

Acetonitrile.sp

DCM

DCM.sp
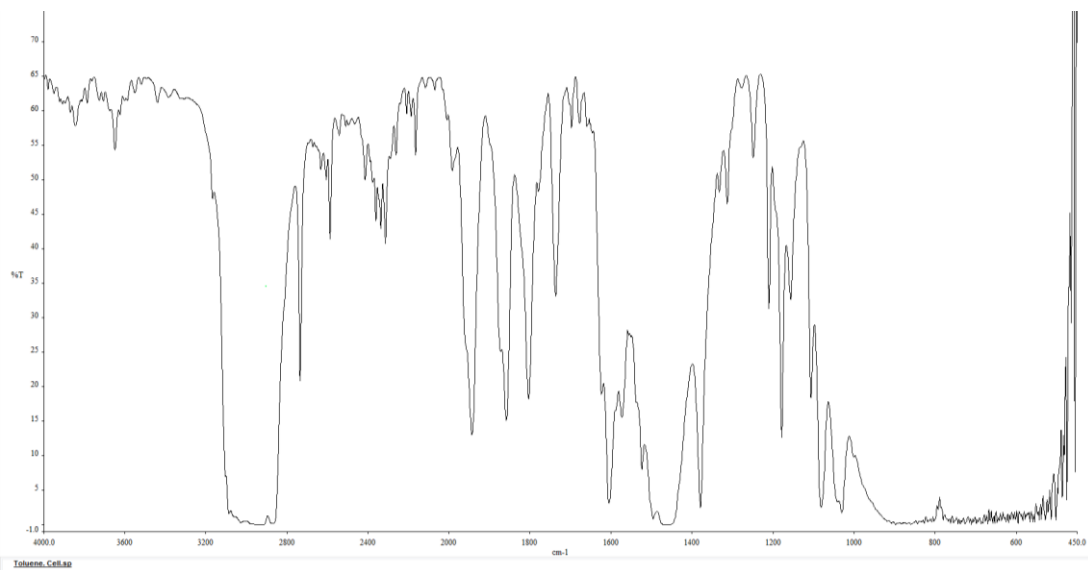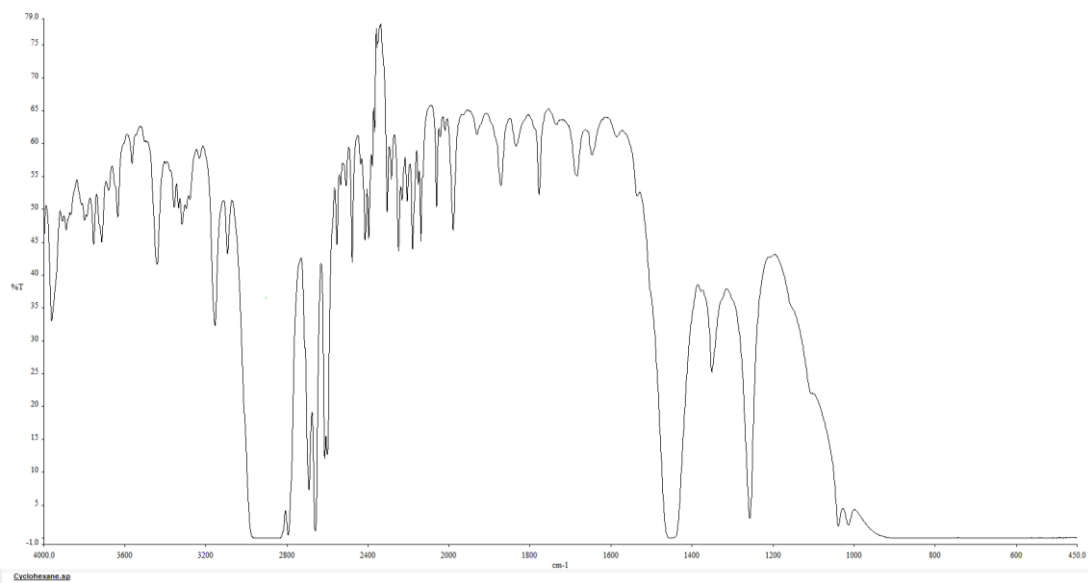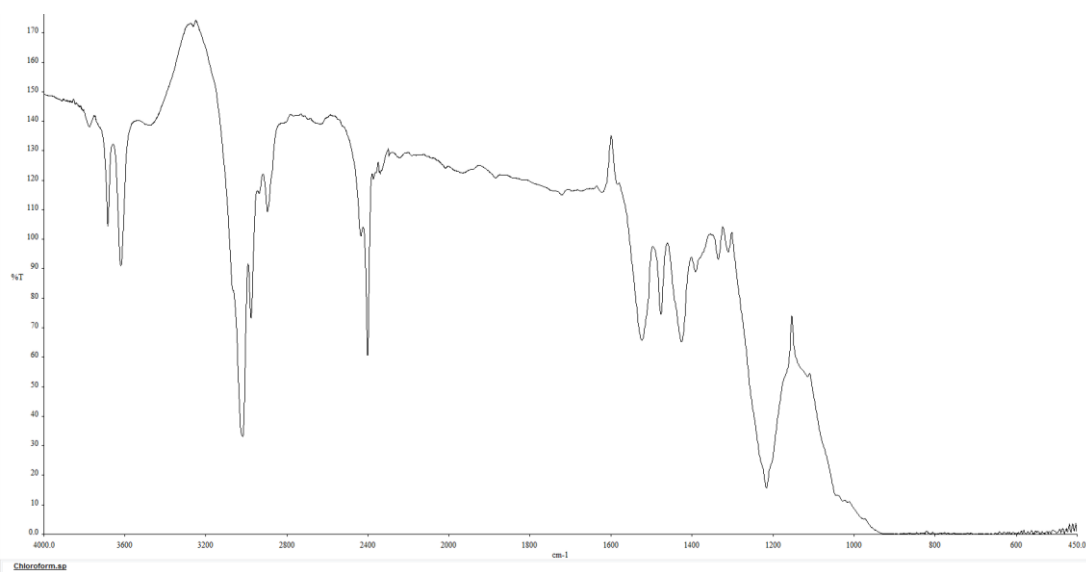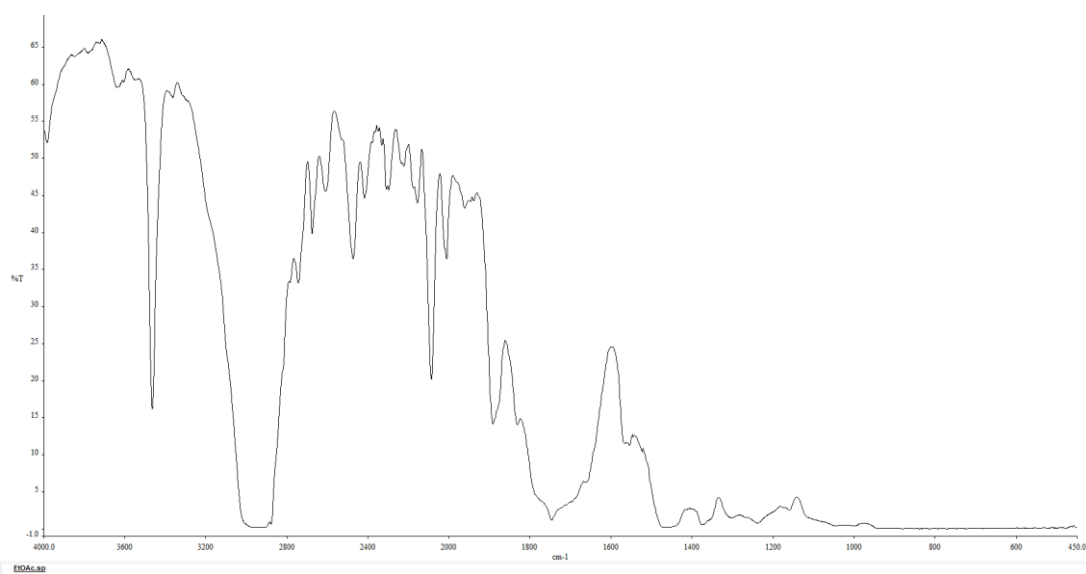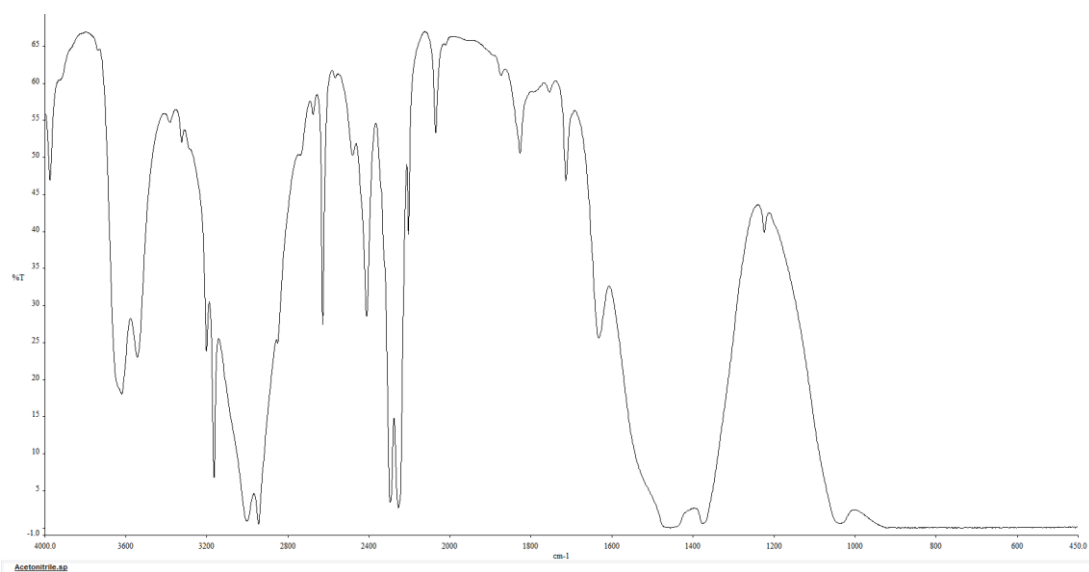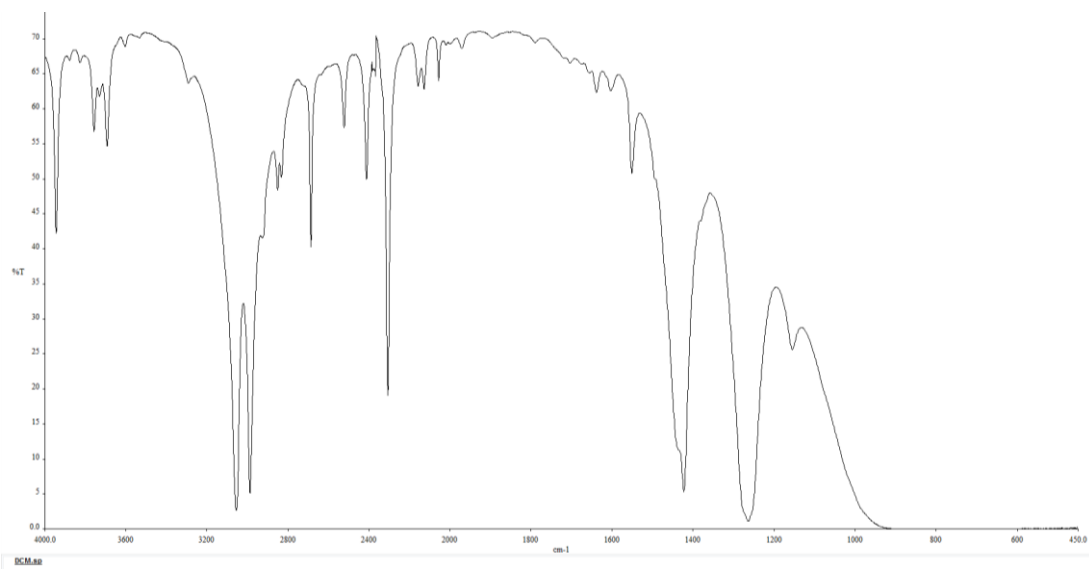
Appendix

EtOH:H$_2$O (1:1)

H2O-EtOH (1-1).sp
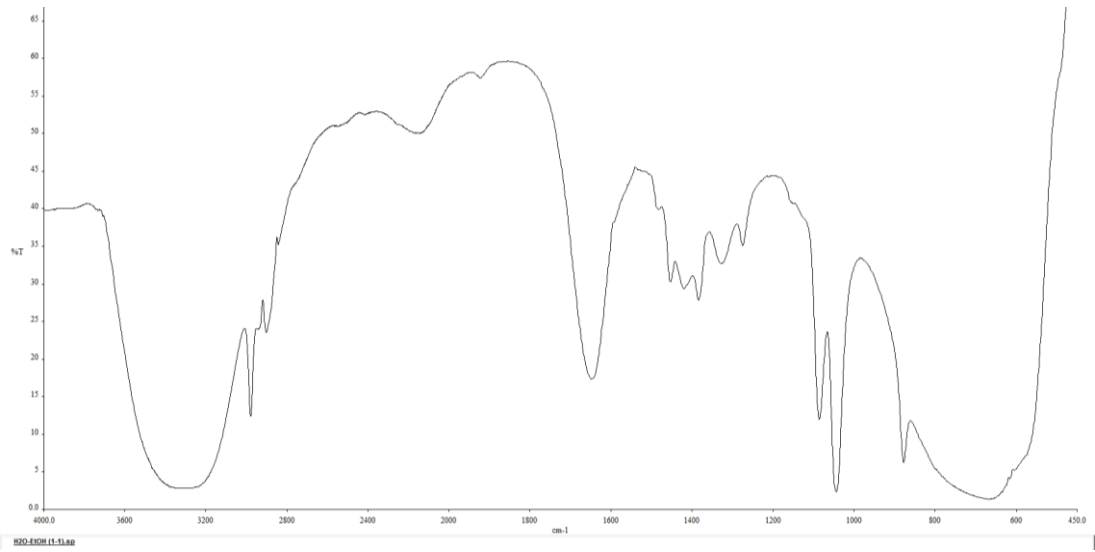
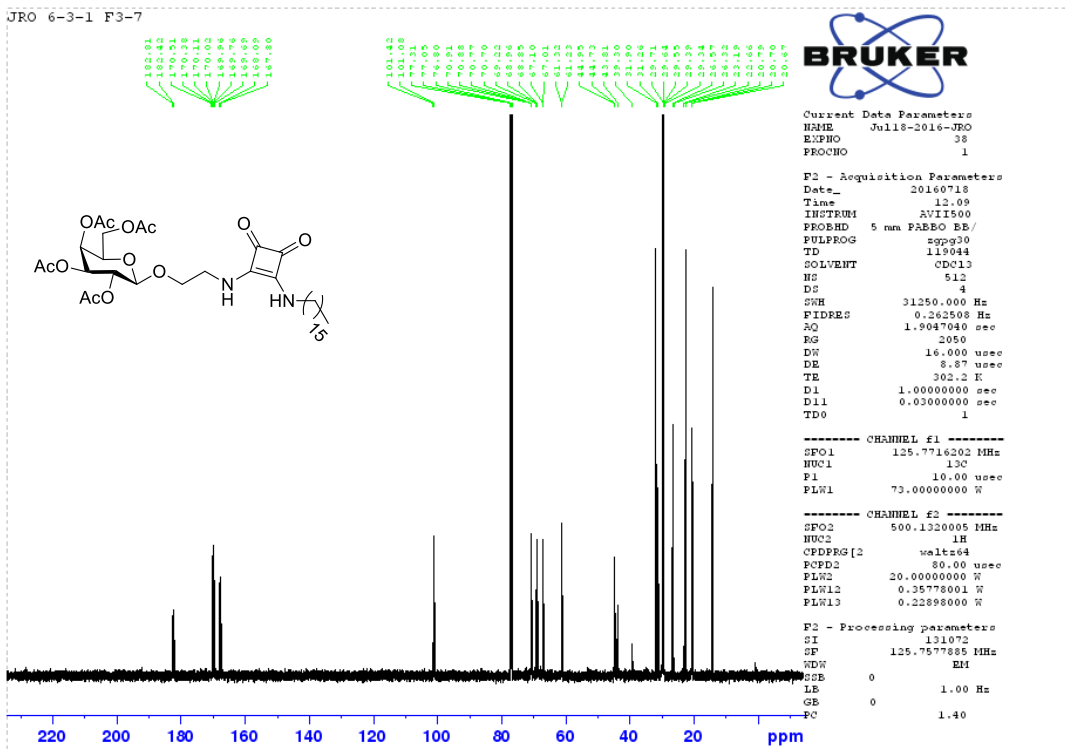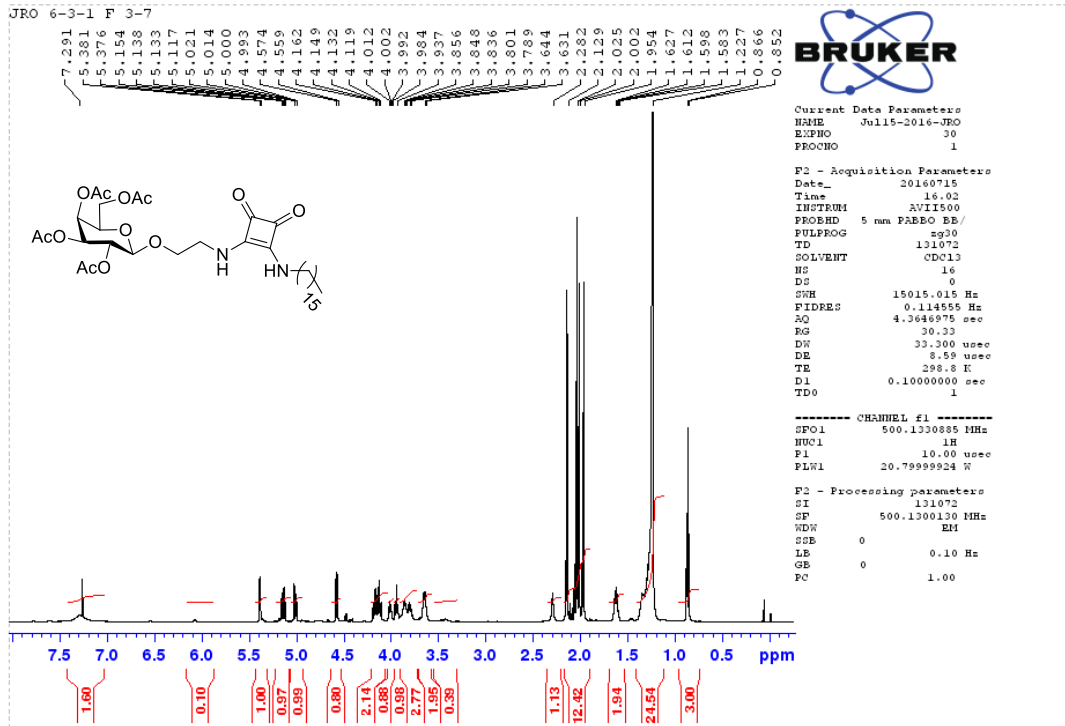# ¹H and ¹³C NMR Spectra for compounds 4.23.; 4.24. and 4.25.

Appendix